ECMWF COPERNICUS REPORT

Copernicus Atmosphere Monitoring Service

Validation report of the CAMS near-real time global atmospheric composition service

December 2018 – February 2019

Issued by: KNMI

Date: 6 June 2019

Ref: CAMS84_2018SC1_D1.1.1_DJF2019_v1

IMPLEMENTED BY ECMWF

Validation report of the CAMS near-real-time global atmospheric composition service. Period December 2018 - February 2019

EDITORS:
M. Schulz (MetNo), Y. Christophe (BIRA-IASB), M. Ramonet (LSCE),
A. Wagner (MPG), H.J. Eskes (KNMI)

AUTHORS:
S. Basart (BSC), A. Benedictow (MetNo), Y. Bennouna (CNRS-LA),
A.-M. Blechschmidt (IUP-UB), S. Chabrillat (BIRA-IASB), E. Cuevas (AEMET),
A. El-Yazidi (LSCE), H. Flentje (DWD), K. M. Hansen (AU), U. Im (AU),
J. Kapsomenakis (AA), B. Langerock (BIRA-IASB), A. Richter (IUP-UB),
N. Sudarchikova (MPG), V. Thouret (CNRS-LA), T. Warneke (UBC),
C. Zerefos (AA)

REPORT OF THE COPERNICUS ATMOSPHERE MONITORING SERVICE, VALIDATION SUBPROJECT.

AVAILABLE AT:
http://atmosphere.copernicus.eu/quarterly_validation_reports

CITATION:
Schulz, M., Y. Christophe, M. Ramonet, Wagner, A., H.J. Eskes, S. Basart, A. Benedictow, Y. Bennouna, A.-M. Blechschmidt, S. Chabrillat, E. Cuevas, A. El-Yazidi, H. Flentje, K.M. Hansen, U. Im, J. Kapsomenakis, B. Langerock, A. Richter, N. Sudarchikova, V. Thouret, T. Warneke, C. Zerefos, Validation report of the CAMS near-real-time global atmospheric composition service: Period December 2018 -February 2019, Copernicus Atmosphere Monitoring Service (CAMS) report, CAMS84_2018SC1_D1.1.1_DJF2019_v1.pdf, June 2019, doi:10.24380/7th6-tk72.

STATUS:
Version 1, Final

DATE:
6 June 2019

Executive Summary

The Copernicus Atmosphere Monitoring Service (http://atmosphere.copernicus.eu, CAMS) is a component of the European Earth Observation programme Copernicus. The CAMS global near-real time (NRT) service provides daily analyses and forecasts of reactive trace gases, greenhouse gases and aerosol concentrations. This document presents the validation statistics and system evolution of the CAMS NRT service for the period up to 1 March 2019. Updates of this document appear every 3 months. The previous report for SON-2018 is Wagner et al. (2019).

This summary is split according to service themes as introduced on the CAMS website: air quality & atmospheric composition, climate forcing, ozone layer and UV. Specific attention is given to the ability of the CAMS system to capture recent events. We focus on the 'o-suite' composition fields, which are the daily analyses and forecasts produced by the IFS (Integrated Forecast System) modelling system at ECMWF, using the available meteorological and atmospheric composition observations which are ingested in the ECMWF 4D-Var assimilation system. The model and assimilation configurations are summarised in section 2. We furthermore assess the impact of the composition observations by comparing the validation results from the 'o-suite' to a 'control' configuration without assimilation. Also, the pre-operational delayed-mode analyses and high-resolution forecasts of CO_2 and CH_4 are assessed in this report.

The o-suite data delivery for the period December-February 2019 (DJF-2019) was good, with an availability of 98.85% at 10 and 22 UTC (two forecasts per day). There were two delays.

Air quality and atmospheric composition

Tropospheric ozone (O_3)

CAMS o-suite ozone is validated with surface and free tropospheric ozone observations from the GAW and ESRL networks, IAGOS airborne data, ozone sondes and IASI tropospheric ozone retrievals. For free tropospheric ozone against ozone sondes the o-suite modified normalized mean biases (MNMBs) are on average small, ±10% over the Northern Hemisphere (NH), between ±30% for stations in the Tropics, and ±15% for the Arctic in more recent years (Fig. S.1). Over Antarctica o-suite biases are observed between 0% and +20% for recent years, whereas the control run shows negative biases. For DJF 2018/2019 good agreement is found over the NH mid latitudes in the free troposphere, which is confirmed with IAGOS evaluations over Frankfurt and IASI observations worldwide. Ozone is well represented throughout the profiles except for the UTLS region where ozone is generally overestimated by the o-suite and partly better represented by the control run.

In comparison with surface observations we find a steady improvement of the o-suite over the past 5 years over European GAW stations. Biases are generally around ±10%, and within ±20% (the Arctic is discussed below). The o-suite slightly overestimates surface ozone for Europe during December to February 2019 with MNMBs up to 10%. Both runs overestimate O_3 observations for Asia with MNMBs up to 13% for the o-suite and up to 21% for the control run. For the tropics, surface ozone is overestimated with MNMBs within 30%. Both runs can reproduce Antarctic surface observations with MNMBs within ±3%.

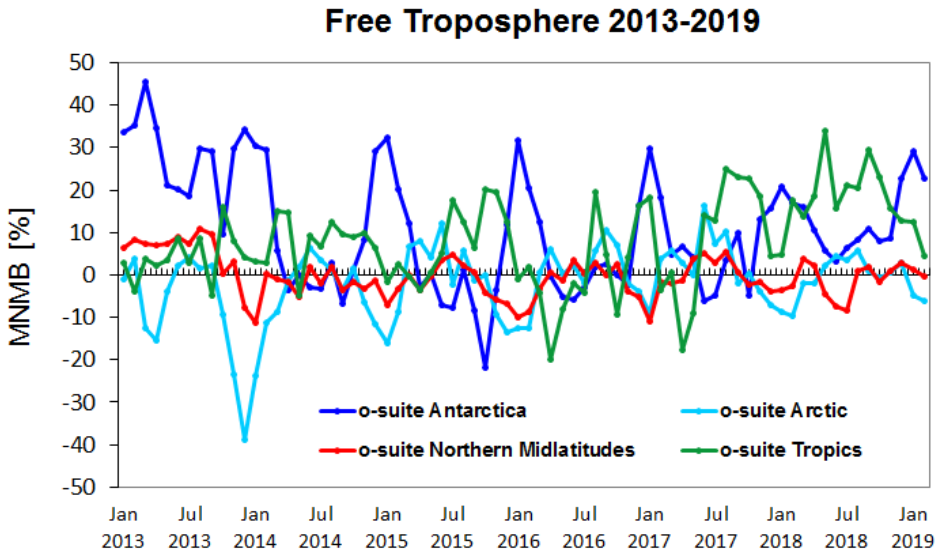

Figure S.1: Time series of MNMB of ozone in the o-suite, compared against ozone sondes, averaged over different latitude bands. The free troposphere is defined here as the layer between 750 and 300 hPa.

Tropospheric Nitrogen dioxide (NO_2)

Model validation, with respect to SCIAMACHY/Envisat NO_2 data before April 2012 and GOME-2/MetOp-A NO_2 data afterwards, shows that tropospheric NO_2 columns are well reproduced by the NRT model runs, indicating that emission patterns and NO_x photochemistry are generally well represented, although modelled shipping signals are more pronounced than in the satellite retrievals. Tropospheric NO_2 columns over some local emission hotspots (e.g. Moscow, and Red Basin in China) are overestimated, while wintertime and springtime values over Europe around Benelux are underestimated. Since December 2014, the agreement between satellite retrievals and model results for time series over East-Asia and Europe is better than for previous years (Fig. S.2), as observed columns of NO_2 decreased recently, likely associated with reduced emissions, and (in contrast to the observations) simulated values show an increase over the whole timeseries available. Mainly in summer and autumn the models regularly show an overestimation over several regions with fire activity (e.g. Western Australia).

Tropospheric Carbon Monoxide (CO)

Model validation with respect to GAW network surface observations, IAGOS airborne data, FTIR observations (NDACC and TCCON) and MOPITT / IASI satellite retrievals reveals that the absolute values, latitude dependence and seasonality, as well as day-to-day variability of CO can be reproduced well by the CAMS-global analyses and forecasts. Biases are between -2% and -30% for European GAW stations, and up to -6% in Asia.

For stations in the southern hemisphere the comparison with NDACC (Fig. S.3) and GAW measurements shows that data assimilation efficiently reduces the large positive MNMBs observed in the control run. The o-suite compared with the TCCON CO observations shows basically no

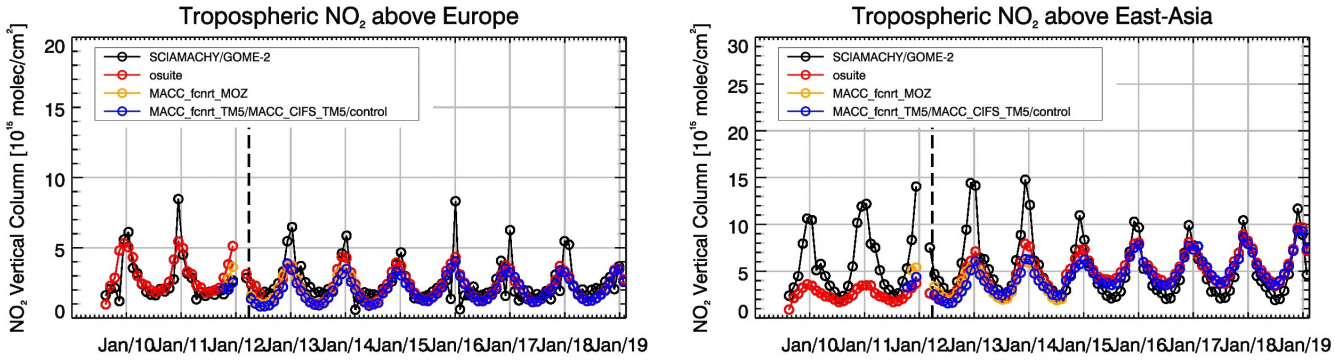

Figure S.2: Time series of tropospheric NO_2 columns from SCIAMACHY (up to March 2012) and GOME-2 (from April 2012 onwards) compared to model results for Europe and East-Asia. The o-suite is in red, control is in blue (the model run without data assimilation is termed control since Sep 2014).

latitude dependence. Overall, there seems to be a small positive bias of < 5% with TCCON. Similar results are obtained when comparing to the NDACC FTIR measurements, but now with a small negative bias of a few % for the tropospheric CO column. A small seasonal cycle is observed in the biases, but this stays within 5%.

The comparisons with MOPITT and IASI confirm these findings. The day 0 o-suite forecast shows differences within 10% regionally compared to MOPITT, with little latitude dependence of the bias. Regionally these biases increase during the 4-day forecast. A general reduction of CO emissions from the year 2015 to the year 2018 can be seen over Europe, the US and East Asian regions. Due to the stability of the (small) bias this trend is well reproduced by the o-suite.

Formaldehyde

Model validation, with respect to SCIAMACHY/Envisat HCHO data before April 2012 and GOME-2/MetOp-A HCHO data afterwards (Fig. S.4), shows that modelled monthly HCHO columns represent well the magnitude of oceanic and continental background values and the overall spatial distribution in comparison with mean satellite HCHO columns. Compared to GOME-2 satellite retrievals, an overestimation of values regularly occurs over Australia and Central Africa, which could be both related to biogenic emissions or fire emissions. For time series over East-Asia and the Eastern US, both regions where HCHO columns are probably dominated by biogenic emissions, models and retrievals agree rather well. However, the yearly cycle over East-Asia is underestimated by the models.

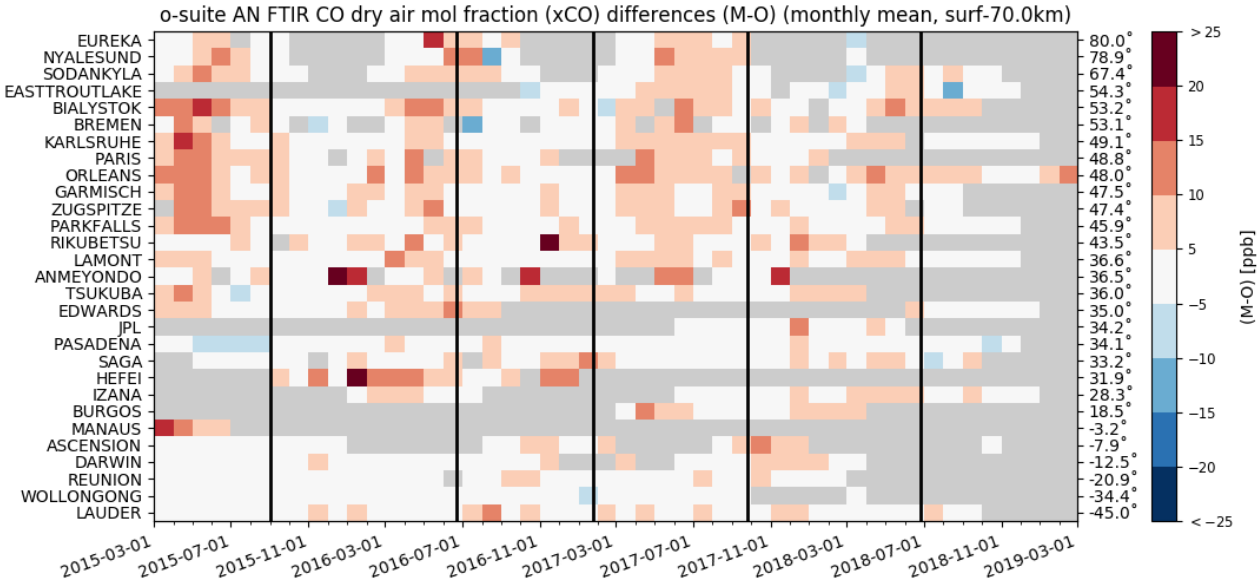

Figure S.3: Monthly mean relative CO bias (o-suite – observation)/observation for the last 4 years. Comparisons are made against TCCON FTIR CO remote sensing observations. Model upgrades are indicated with the black lines. The stations are sorted with decreasing latitude (northern to southern hemisphere). A similar plot for the control run shows biases up to 40% in the southern hemisphere.

Aerosol

We estimate that the o-suite aerosol optical depth showed an average positive bias in the latest three months of +18%, measured as modified normalized mean bias against daily Aeronet (V3 level 1.5) sun photometer data. The +3 day forecasted aerosol distribution shows 15% less aerosol optical depth (AOD) than that from the initial forecast day, as shown in Fig. S.5-a. The spatio-temporal correlation, shown in Fig. S.5-b, shows month-to-month variation in DJF 2018/19 similar to winter 2018/19, indicating the simulation reproduces approximately 55% of the day to day AOD variability across all Aeronet stations. We find a high AOD bias in Southern Latitudes. The o-suite forecast at +3 days shows slightly lower correlation, as a consequence of imperfect forecasted meteorology and fading impact of the initial assimilation of MODIS AOD and MODIS fire info on model performance. The o-suite forecast running each day at 12UTC shows almost identical performance as the forecast starting at 00UTC.

The AOD performance of the o-suite with respect to the AERONET data exhibits no pronounced seasonal cycle but somewhat less correlation in late summer. Since October 2017, global AOD is dominated by organics and sea salt. Sea salt AOD increased further due to the latest model upgrade in June 2018 with the new sea salt emission scheme activated, while dust AOD became lower compared to earlier years.

The aerosol Ångström exponent (AE) contains information about the size distribution of the aerosol, and implicitly about composition. In the last 6 months the o-suite AE became more positive indicating a change to slightly more fine particles since the latest model upgrade to version 45R1 in June 2018.

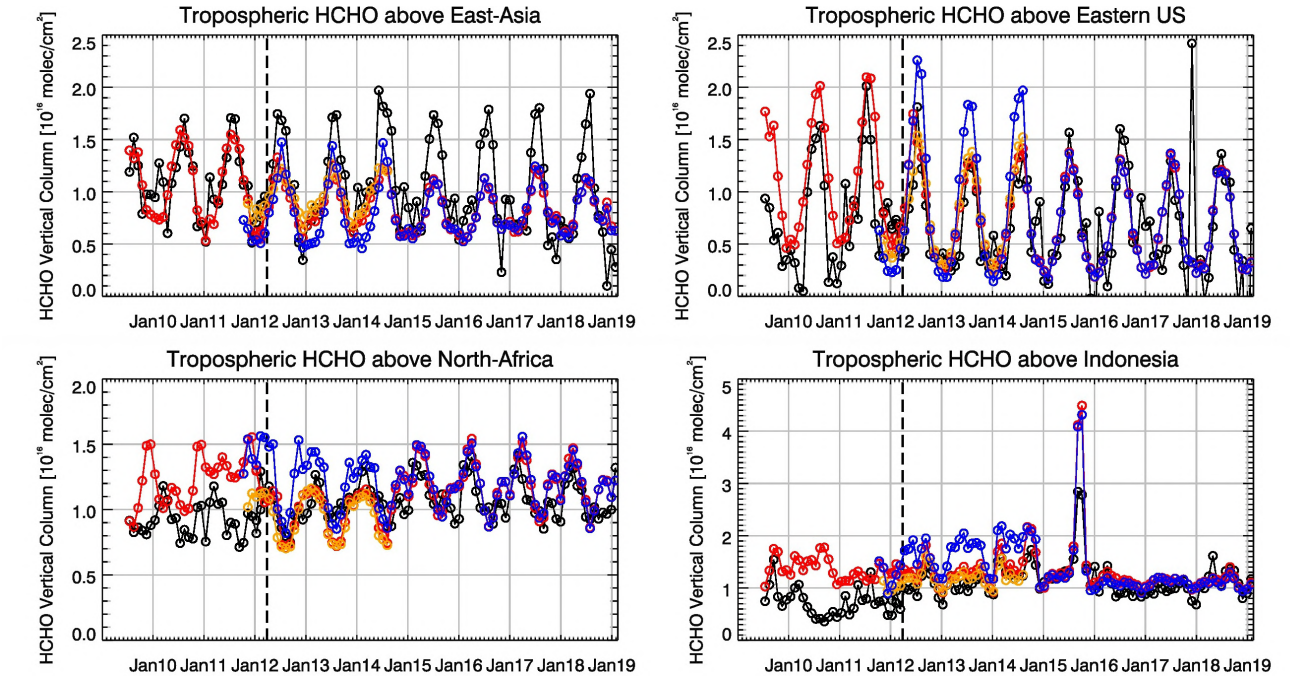

Figure S.4: Time series of average tropospheric HCHO columns [10^{16} molec cm^{-2}] from SCIAMACHY (up to March 2012) and GOME-2 (from April 2012 onwards) compared to model results for different regions. The blue line shows CAMS control results including older configurations from the MACC project before September 2014. The regions are: East-Asia (25-40°N, 110-125°E), Eastern US (30-40°N, 75-90°W), Northern Africa (0-15°N, 15°W-25°E) and Indonesia (5°S-5°N, 100-120°E). Vertical dashed black lines mark the change from SCIAMACHY to GOME-2 based comparisons in April 2012.

PM data are evaluated as defined by the IFS aerosol model. An evaluation of these PM10 and PM25 surface concentrations against an average from data in the period 2000-2009 at 160 background sites in North America and Europe indicate that PM10 concentrations exhibit on average in the latest period an underestimation with MNMB bias of -56% in Europe and overestimation of 8% in North America. PM25 concentrations are underestimated -35% in Europe and overestimated 41% in North America. A higher positive bias is also found for AOD in North America than in Europe. The fraction of data within a factor 2 of observed values has increased for PM10 and decreased for PM25 compared to earlier years.

For winter, both CAMS experiments simulate well the main areas of dust activity in the North Africa in comparison with MODIS. The o-suite and control show generally lower season values (seasonal DOD up to 0.3). The o-suite shows lower values in the Sahara region than control and the SDS-WAS multi-median product, in particular over the Bodélé. Neither both CAMS experiments, nor the SDS-WAS multi-model product are capturing the maximum AOD values observed in the Arabian Peninsula and the Red Sea, indicating missing dust emissions in all the experiments. For December to February, the o-suite reproduces the daily variability of AERONET observations with a correlation coefficient of 0.74, averaged over all the AERONET sites in comparison with the control experiments (0.65). These results are slightly lower than those obtained by the SDS-WAS Multi-model product (0.78). Regarding mean bias (MB), both CAMS experiments (o-suite and control), as well as the SDS-WAS Multi-model ensemble underestimate the AERONET observations resulting in an MB of -0.05 for control, -0.07 for o-suite and -0.06 the SDS-WAS multi-model.

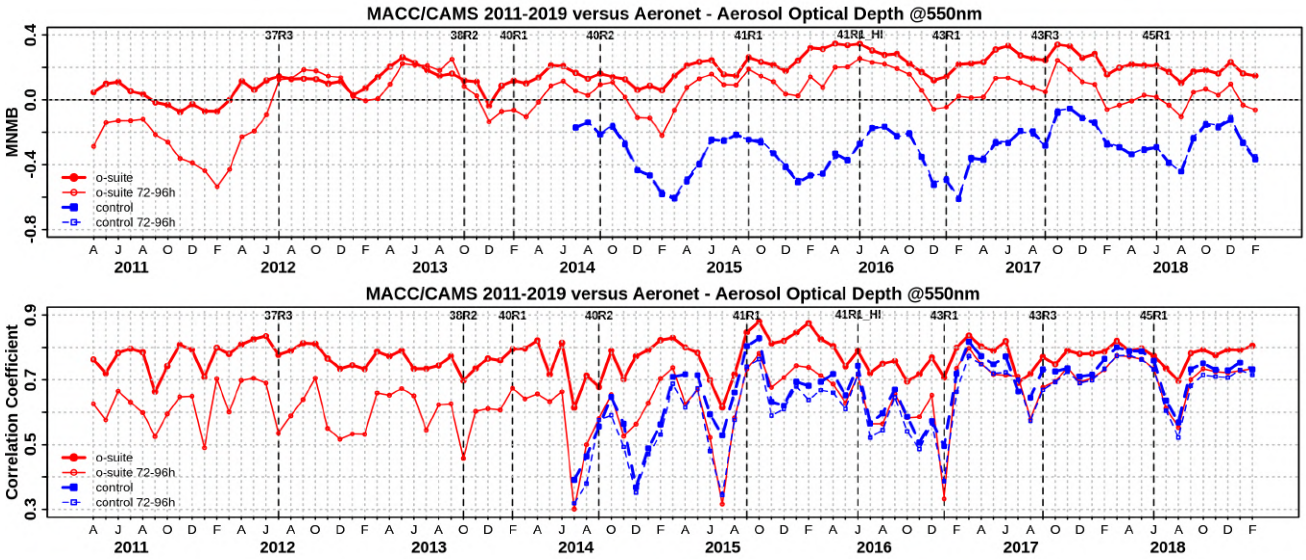

Figure S.5. Aerosol optical depth at 550nm in IFS 00Z model simulations for April 2011 – February 2019 against daily matching Aeronet Version3 level 1.5 data. a) Modified normalized mean bias (MNMB); o-suite (thick red curve); o-suite at last forecast day (light red curve); Control (blue dashed); Control at last forecast day (light blue dashed); b) Corresponding correlation coefficient. Model version changes are marked as vertical bars.

In the Middle East, the o-suite reproduces the daily variability better than the control run (with correlation coefficient of 0.86 for o-suite and 0.84 for control) and the SDS-WAS Multi-model presents lower correlations (0.73). Underestimations are observed in both CAMS experiments (MB of -0.05 for control and -0.07 for o-suite). Over the Sahara both CAMS experiments show closer results with a correlation coefficient of 0.67 for control and 0.75 for o-suite although o-suite shows slightly higher overestimation (MB of 0.02) than the control experiment which tends to overestimate the AERONET observations (MB of 0.04). The o-suite shows better results than the SDS-WAS Median Multi-model that shows a correlation coefficient of 0.73 for the Sahara, although it underestimates the observations with an MB of -0.10. On the contrary, in the Sahel, the o-suite shows strong underestimations (MB of -0.31, slightly higher than control with MB of -0.28) although the o-suite reproduces the observed daily variability better (with a correlation value of 0.69 for o-suite in comparison of for control that has a correlation of 0.45). The underestimations observed in o-suite in the Sahel are also spread to the Tropical North Atlantic. Lower skills in North-Western Maghreb is associated with the low AOD values observed as well as the low number of observations during this season due to the presence of clouds.

Otherwise, the comparison of the 48h and 72h forecasts for both CAMS experiments shows that the prediction is stable during the first 3-days of the forecast with correlation coefficients 0.74 (0.65), 0.70 (0.65), and 0.67 (0.64) for the 24, 48 and 72h forecasts respectively for 24, 48 and 72h forecasts for all the sites for o-suite (control). In North Western Maghreb, the correlation coefficient (r) for control increases from 0.65 to 0.73 in going from the 48h to 72h forecast.

Backscatter coefficients are biased low in the planetary boundary layer (PBL). Possible reasons are missing of ammonia and nitrate in the model (foreseen to be activated soon), assumption of too high particle densities (for pure compact materials) in the mass to backscatter conversion, and the lack of a vertical transport barrier at the top of the PBL, causing dilution with free troposphere air.

Against this, free troposphere (FT) background backscatter coefficients are biased high, probably due to the assimilation re-distributing between PBL and FT. The backscatter bias on a specific level thus depends on its relative position with respect to the BLH. Generally, monthly average vertical backscatter profiles to some extent follow the annual cycle of the observations, but they are smoother. The reason for the discrepancy between results with two different forward operators is not resolved yet. The summary monthly Taylor plots over 21 German stations indicate that daily averages of correlation coefficients cluster around 0.4-0.6, too large variability in winter, often due to overestimated layers of sea-salt, and that this causes a less consistent day-to-day performance in winter as compared to summer.

System performance in the Arctic

The CAMS model runs are evaluated using surface ozone measurements from 6 sites within the IASOA networks and ozone concentrations in the free troposphere and the stratosphere are evaluated using ozone soundings.

For the period from December 2014 to February 2019 the simulations of the surface ozone concentrations are on average in good agreement with the observations apart from ozone depletion events in spring (March to June). During December 2018 – February 2019 there is generally an underestimation of the surface ozone concentrations in the Arctic apart from Summit and Barrow, central Greenland for the o-suite (NMB = -12% to 14%) and an overestimation for the control run (NMB = -1% to 24%). The o-suite performs better with higher correlation coefficients (r = 0.20 – 0.80 for the o-suite compared to r = 0.10 – 0.75 for the control run).

Ozone concentrations in the free troposphere are in good agreement with observations with low relative bias (-6% - 3% for the o-suite and -6%-6% for the control run). In the UTLS, the o-suite has a higher positive bias for the Arctic sites (15-20%). Ozone concentrations in the stratosphere are in good agreement with observations with low relative bias (-1% - 10% for the o-suite). The vertical distribution of stratospheric ozone is well represented in the Arctic.

System performance in the Mediterranean

The model is compared to surface O_3 observations from the AirBase network. Our analysis shows that model MNMBs vary between -50% and 20% depending on the station. Temporal correlation coefficients between simulated and observed surface ozone for both the o-suite and control runs are highly significant over the entire Mediterranean from Gibraltar to Cyprus.

The CAMS o-suite reproduces the daily variability of AERONET AOD observations (with correlation coefficients of 0.68, 0.48 and 0.55, respectively for Western, Central and Eastern Mediterranean). Underestimations observed in the Mediterranean Basin in control (MB of -0.02, -0.02 and 0 for Western, Central and Eastern Mediterranean regions respectively) are corrected in the o-suite, introducing overestimations in the Basin (MB of 0.01, 0.02 and 0.03 for Western, Central and Eastern Mediterranean regions respectively), particularly in Central Mediterranean. Dust activity was low during the DJF season and the most important events were observed in the Eastern Mediterranean. The CAMS product tends to overestimate the PM10 and PM2.5 EIONET-Airbase observations in north-western Mediterranean sites, but meanwhile tends to underestimate the

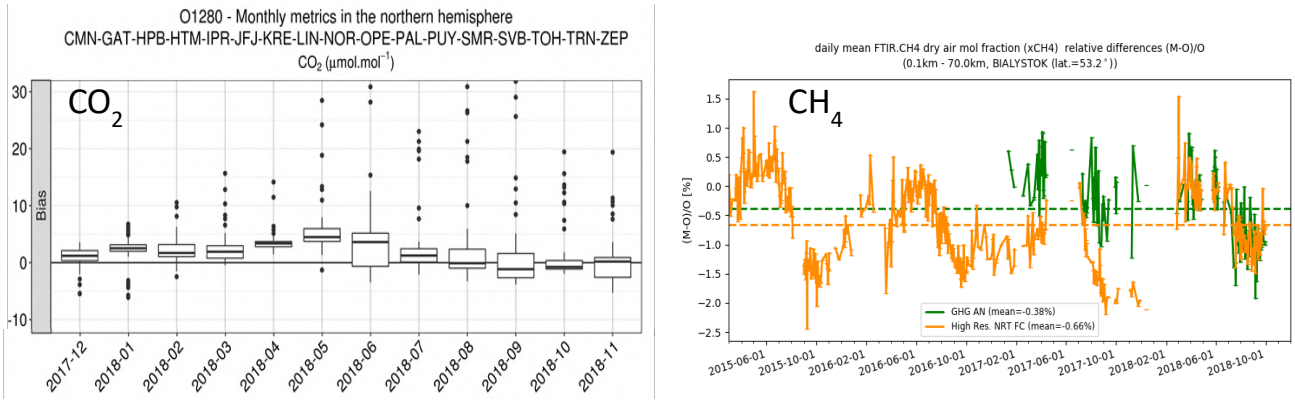

Figure S.6. Left: CO_2 monthly differences (in ppm) of the high-resolution model with ICOS surface observations for a composite of 17 European sites (Dec.2017-Dec.2018). Right: CH_4 differences (in %) of the high-resolution model (orange) and the analysis (green) with TCCON total column measurements at Bialystok, Poland (2015-2018).

PM10 and PM2.5 observed values at Spanish sites. Overestimations (above 50 µg/m^3) at north-western Mediterranean sites are linked to the overestimation of the CAMS model in mid-January and end-February.

Climate forcing

Greenhouse gases

CO_2 and CH_4 surface concentrations from ICOS network, and total or partial columns from TCCON and NDACC stations have been used to validate the analysis and high-resolution forecast experiments (Fig. S.6).

The surface and total column measurements indicate an overestimation of the amplitude of the CO_2 seasonal cycle in the northern hemisphere by ±1%. The drought anomaly in spring/summer 2018 has an additional effect on the comparison with surface sites from May to July 2018, with an overestimated impact of the drought on the CO_2 concentrations. The TCCON site of Orléans shows a higher positive bias in 2018/2019, compared to previous years

For CH4 we observe a systematic positive bias of 20 to 50 ppb at the Nordic stations, turning to a negative bias in Southern France and Italy.

Only small differences appear between the analysis and the high-resolution models. However, for CH_4 the correlation coefficients of the analysis time series are slightly larger for most sites, compared to the high-resolution model both for total column and surface measurements.

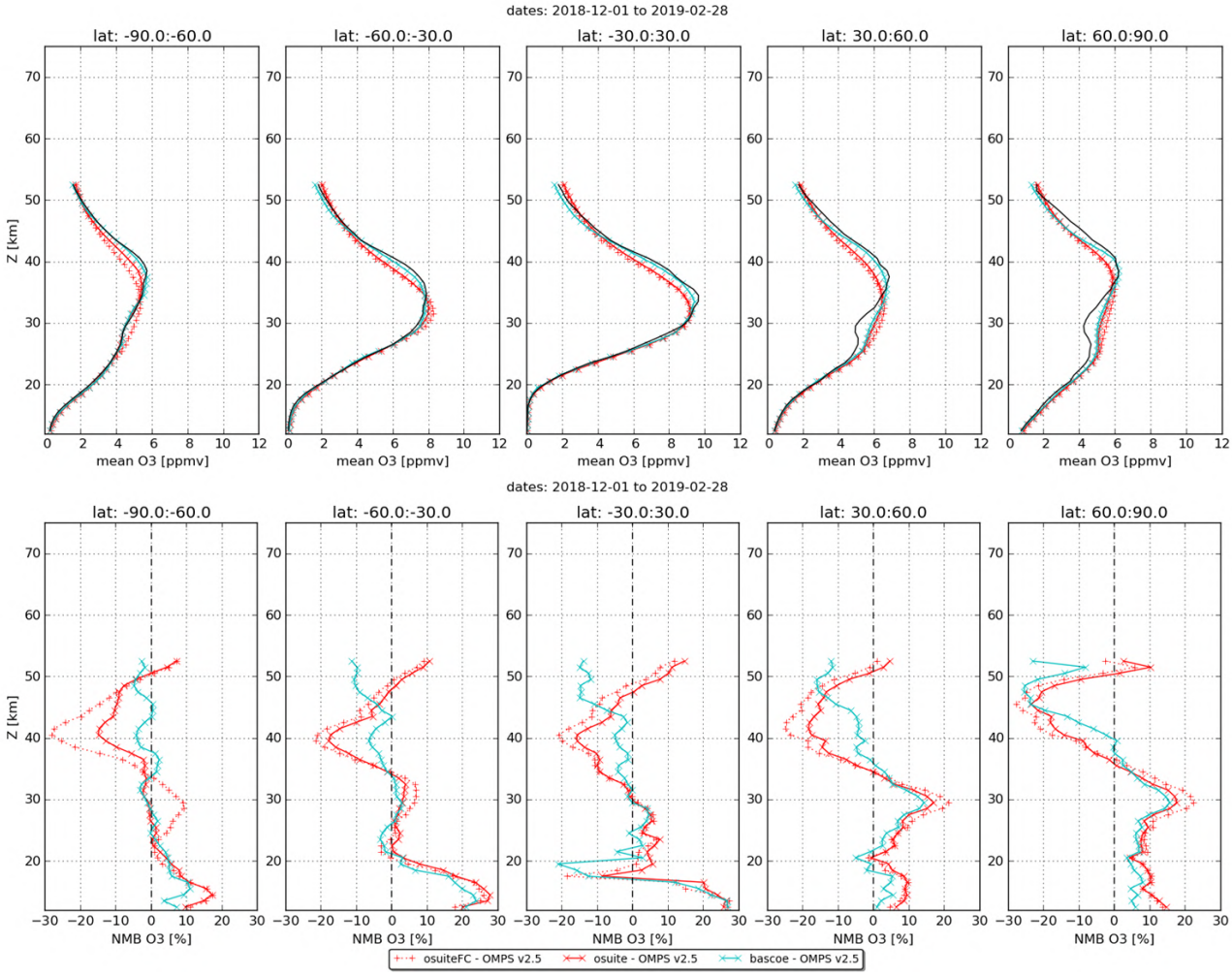

Figure S.7: Mean value (top) and normalized mean bias (bottom) of the ozone profile between o-suite analyses (red, solid), o-suite forecasts 4th day (red, dotted) and BASCOE (cyan line) with OMPS-LP v2.5 observations for the period December 2018 to February 2019.

Ozone layer and UV

Ozone partial columns and vertical profiles

Ozone columns and profiles have been compared with the following observations: vertical profiles from balloon-borne ozone sondes; ground-based remote-sensing observations from the NDACC (Network for the Detection of Atmospheric Composition Change, http://www.ndacc.org); and satellite observations by two instrument (OMPS-LP, ACE-FTS). Furthermore, the o-suite analyses are compared with those delivered by the independent assimilation system BASCOE.

Compared to ozone sondes the model O_3 partial pressures are slightly overestimated in all latitude bands (MNMB between 4 and +12%) except above the Antarctic.

Comparisons with the NDACC network include 16 stations for UVVIS and FTIR stratospheric columns, microwave profiles for Ny Alesund (78.9°N) and Bern (47°N) and LIDAR profiles at Hohenpeissenberg (47.8°N) and Observatoire Haute Provence (OHP), France (43°N). The comparison with the UVVIS stations are generally in agreement with the o-suite, while it indicates a

latitudinal dependence of the biases for the control run. The result from MWR and LIDAR comparisons for the current period are in line with those of previous reports.

The comparison with independent satellite observations (Fig. S.7) is generally in good agreement for the considered period: for ACE-FTS, the NMB is mainly within 10% between 5km and 40km, and mostly within 5% between 15km and 35km except in the tropics. OMPS-LP has less regular profiles, but the NMB still remain within 15% for most parts of the 20-40 km range.

Other stratospheric trace gases

Due to the lack of stratospheric chemistry in the C-IFS-CB05 scheme, the only useful product in the stratosphere is ozone. Other species, like NO_2, have also been evaluated but the results are only indicative.

Events

Dusty Eastern Mediterranean during 24-27 January 2019: In second half of January 2019, Saharan dust was heading for the central and eastern Mediterranean including Greece, Turkey and Cyprus. The comparison with the MODIS satellite instrument shows how the model predicts a large band of dust with AOD up to 1.2 over Libya and Crete, consistent with the observations on the 25th of January. The o-suite dust plume is extending into the cloudy region over Europe where observations are not available from MODIS.

Table of Contents

1. Introduction

The Copernicus Atmosphere Monitoring Service (CAMS, http://atmosphere.copernicus.eu/) is a component of the European Earth Observation programme Copernicus. The CAMS global near-real time (NRT) service provides daily analyses and forecasts of trace gas and aerosol concentrations. The CAMS near-real time services consist of daily analysis and forecasts with the ECMWF IFS system with data assimilation of trace gas concentrations and aerosol properties. This document presents the system evolution and the validation statistics of the CAMS NRT global atmospheric composition analyses and forecasts. The validation methodology and measurement datasets are discussed in Eskes et al. (2015).

In this report the performance of the system is assessed in two ways: both the longer-term mean performance (seasonality) as well as its ability to capture recent events are documented. Table 1.1 provides an overview of the trace gas species and aerosol aspects discussed in this CAMS near-real time validation report. This document is updated every 3 months to report the recent status of the near-real time service. The report covers results for a period of at least one year to document the seasonality of the biases. Sometimes reference is made to other model versions or the reanalysis to highlight aspects of the near-real time products.

This validation report is accompanied by the "Observations characterization and validation methods" report, Eskes et al. (2018a), which describes the observations used in the comparisons, and the validation methodology. This report can also be found on the global validation page, http://atmosphere.copernicus.eu/user-support/validation/verification-global-services.

Key CAMS NRT products and their users are: Boundary conditions for regional air quality models (e.g. AQMEII, air quality models not participating in CAMS); Long range transport of air pollution (e.g. LRTAP); Stratospheric ozone column and UV (e.g. WMO, DWD); 3D ozone fields (e.g. SPARC). As outlined in the MACC-II Atmospheric Service Validation Protocol (2013) and MACC O-INT document (2011), relevant user requirements are quick looks of validation scores, and quality flags and uncertainty information along with the actual data. This is further stimulated by QA4EO (Quality Assurance Framework for Earth Observation, http://www.qa4eo.org) who write that “all earth observation data and derived products is associated with it a documented and fully traceable quality indicator (QI)”. It is our long-term aim to provide such background information. The user is seen as the driver for any specific quality requirements and should assess if any supplied information, as characterised by its associated QI, are "fit for purpose" (QA4EO task team, 2010).

CAMS data are made available to users as data products (grib or netcdf files) and graphical products from ECMWF, accessible through the catalogue on http://atmosphere.copernicus.eu/.

A summary of the system and its recent changes is given in section 2. Subsequent sections gives an overview of the performance of the system for various species, and during recent events. Routine validation results can be found online via regularly updated verification pages, http://atmosphere.copernicus.eu/user-support/validation/verification-global-services. Table 1.2 lists all specific validation websites that can also be found through this link.

Table 1.1: Overview of the trace gas species and aerosol aspects discussed in this CAMS near-real time validation report. Shown are the datasets assimilated in the CAMS analysis (second column) and the datasets used for validation, as shown in this report (third column). Green colours indicate that substantial data is available to either constrain the species in the analysis, or substantial data is available to assess the quality of the analysis. Yellow boxes indicate that measurements are available, but that the impact on the analysis is not very strong or indirect (second column), or that only certain aspects are validated (third column).

Species, vertical range	Assimilation	Validation
Aerosol, optical properties	MODIS Aqua/Terra AOD PMAp AOD	AOD, Ångström: AERONET, GAW, Skynet, MISR, OMI, lidar, ceilometer
Aerosol mass (PM10, PM2.5)	MODIS Aqua/Terra	European AirBase stations
O_3, stratosphere	MLS, GOME-2A, GOME-2B, OMI, SBUV-2, OMPS	Sonde, lidar, MWR, FTIR, OMPS, ACE-FTS, OSIRIS, BASCOE and MSR analyses
O_3, UT/LS	MLS	IAGOS, ozone sonde
O_3, free troposphere	Indirectly constrained by limb and nadir sounders	IAGOS, ozone sonde, IASI
O_3, PBL / surface		Surface ozone: WMO/GAW, NOAA/ESRL-GMD, AIRBASE
CO, UT/LS	IASI, MOPITT	IAGOS
CO, free troposphere	IASI, MOPITT	IAGOS, MOPITT, IASI, TCCON
CO, PBL / surface	IASI, MOPITT	Surface CO: WMO/GAW, NOAA/ESRL
NO_2, troposphere	OMI, GOME-2, partially constrained due to short lifetime	SCIAMACHY, GOME-2, MAX-DOAS
HCHO		GOME-2, MAX-DOAS
SO_2	GOME-2A, GOME-2B (Volcanic eruptions)	
Stratosphere, other than O_3		NO_2 column only: SCIAMACHY, GOME-2
CO_2, surface, PBL		ICOS
CO_2, column	GOSAT	TCCON
CH_4, surface, PBL		ICOS
CH_4, column	GOSAT, IASI	TCCON

Table 1.2: Overview of quick-look validation websites of the CAMS system.

Reactive gases – Troposphere
IAGOS tropospheric ozone and carbon monoxide: http://www.iagos.fr/cams/ Surface ozone from EMEP (Europe) and NOAA-ESRL (USA): http://www.academyofathens.gr/cams Tropospheric nitrogen dioxide and formaldehyde columns against satellite retrievals: http://www.doas-bremen.de/macc/macc_veri_iup_home.html Tropospheric CO columns against satellite retrievals: http://www.mpimet-cams.de GAW surface ozone and carbon monoxide: https://atmosphere.copernicus.eu/charts/cams_gaw_ver/v0d_gaw_oper_operfc_nrt_sites?facets=undefined&time=2018060100,0,2018060100&fieldpair=CO&site=cmn644n00
Reactive gases - Stratosphere
Stratospheric composition: http://www.copernicus-stratosphere.eu NDACC evaluation in stratosphere and troposphere (the NORS server) http://nors-server.aeronomie.be
Aerosol
Evaluation against Aeronet stations: http://aerocom.met.no/cams-aerocom-evaluation/ More in-depth evaluations are available from the Aerocom website. WMO Sand and Dust Storm Warning Advisory and Assessment System (SDS-WAS) model intercomparison and evaluation: http://sds-was.aemet.es/forecast-products/models Aeronet verification of CAMS NRT forecasts: https://atmosphere.copernicus.eu/charts/cams_aeronet_ver/?facets=undefined&time=2019020100,0,2019020100&site=ARM_Graciosa
Satellite data monitoring
Monitoring of satellite data usage in the Near-Real-Time production: https://atmosphere.copernicus.eu/charts/cams/cams_satmon?facets=undefined&time=2016071800&Parameter=AURA_MLS_profile_Ozone_1_GLOBE

Naming and color-coding conventions in this report follow the scheme as given in Table 1.3.

Table 1.3. Naming and colour conventions as adopted in this report.

Name in figs	experiment	Colour
{obs name}	{obs}	black
o-suite D+0 FC	0001	red
control	gsyg	blue
GHG high-resolution run	gqpe / ghqy	orange
GHG global analysis	gqiq	green

2. System summary and model background information

The specifics of the different CAMS model versions are given below (section 2.1) including an overview of model changes. Other systems used in CAMS are listed in section 2.2. An overview of products derived from this system is given in section 2.3. Timeliness and availability of the CAMS products is given in section 2.4.

2.1 System based on the ECMWF IFS model (the o-suite and control run)

Key model information is given on the CAMS data-assimilation and forecast run o-suite and its control experiment, used to assess the performance of the assimilation. The forecast products are listed in Table 2.1. Table 2.2 provides information on the satellite data used in the o-suite. Further details on the different model runs and their data usage can be found at http://atmosphere.copernicus.eu/documentation-global-systems.

Table 2.1: Overview of model runs assessed in this validation report.

Forecast system	Exp. ID	Brief description	Upgrades (e-suite ID)
o-suite	0001	Operational CAMS DA/FC run	20180626-present 20170926-20180625 20170124-20170926 20160621-20170124 20150903-20160620 20140918-20150902
Control	gzhy gsyg gnhb gjjh geuh g4o2	control FC run without DA	20180626-present (gzhy) 20170926-20180625 (gsyg) 20170124-20170926 (gnhb) 20160621-20170124 (gjjh) 20150901-20160620 (geuh) 20140701-20150902 (g4o2)
GHG run	ghqy gf39	High resolution T1279, NRT CO_2 and CH_4 without DA	20160301-20170621 (ghqy) 20150101-20160229 (gf39)
	gqpe	High resolution Tco1279 (~9km) NRT CO_2, CH_4 and linCO forecast, initialized from GHG analysis gqiq and CAMS operational CO analysis	20170101-present
	gqiq	GHG analysis Tco399 (~25km)	20170101-present

Table 2.2: Satellite retrievals of reactive gases and aerosol optical depth that are actively assimilated in the o-suite.

Instrument	Satellite	Provider	Version	Type	Status
MLS	AURA	NASA	V4	O3 Profiles	20130107 -
OMI	AURA	NASA	V883	O3 Total column	20090901 -
GOME-2A	Metop-A	Eumetsat	GDP 4.8	O3 Total column	20131007 - 20181231
GOME-2B	Metop-B	Eumetsat	GDP 4.8	O3 Total column	20140512 -
SBUV-2	NOAA-19	NOAA	V8	O3 21 layer profiles	20121007 -
OMPS	Suomi-NPP	NOAA / EUMETSAT		O3 Profiles	20170124 -
IASI	MetOp-A	LATMOS/ULB Eumetsat	-	CO Total column	20090901 - 20180621 20180622 -
IASI	MetOp-B	LATMOS/ULB Eumetsat	-	CO Total column	20140918 - 20180621 20180622 -
MOPITT	TERRA	NCAR	V5-TIR V7-TIR V7-TIR Lance	CO Total column	20130129 - 20160124 - 20180626 20180626
OMI	AURA	KNMI	DOMINO V2.0	NO2 Tropospheric column	20120705 -
GOME-2A/2B	METOP A/B	Eumetsat	GDP 4.8	NO2 Tropospheric column	20180626 -
OMI	AURA	NASA	v003	SO2 Tropospheric column	20120705-20150901
GOME-2A/2B	METOP A/B	Eumetsat	GDP 4.8	SO2 Tropospheric column	20150902 -
MODIS	AQUA / TERRA	NASA	Col. 5 Deep Blue Col. 6, 6.1	Aerosol total optical depth, fire radiative power	20090901 - 20150902 - 20170124 -
PMAp	METOP-A METOP-B	EUMETSAT		AOD	20170124 - 20170926 -

2.1.1 o-suite

The o-suite consists of the IFS-CB05 chemistry combined with the CAMS bulk aerosol model. The chemistry is described in Flemming et al. (2015) and Flemming et al. (2017), aerosol is described in Morcrette et al. (2009). The forecast length is 120 h. The o-suite data is stored under **expver '0001'** of **class 'MC'**. On 21 June 2016 the model resolution has seen an upgrade from T255 to T511, and forecasts are produced twice per day. The latest upgrade of the system is based on IFS version cy45r1_CAMS (https://confluence.ecmwf.int/display/COPSRV/Current+global+production+suites) and took place on 26 June 2018. The validation for this upgrade is described in Eskes et al., 2018b/2018c. The update relevant for this report (for SON-2018) is this 26 June 2018 upgrade. A short summary of the main specifications:

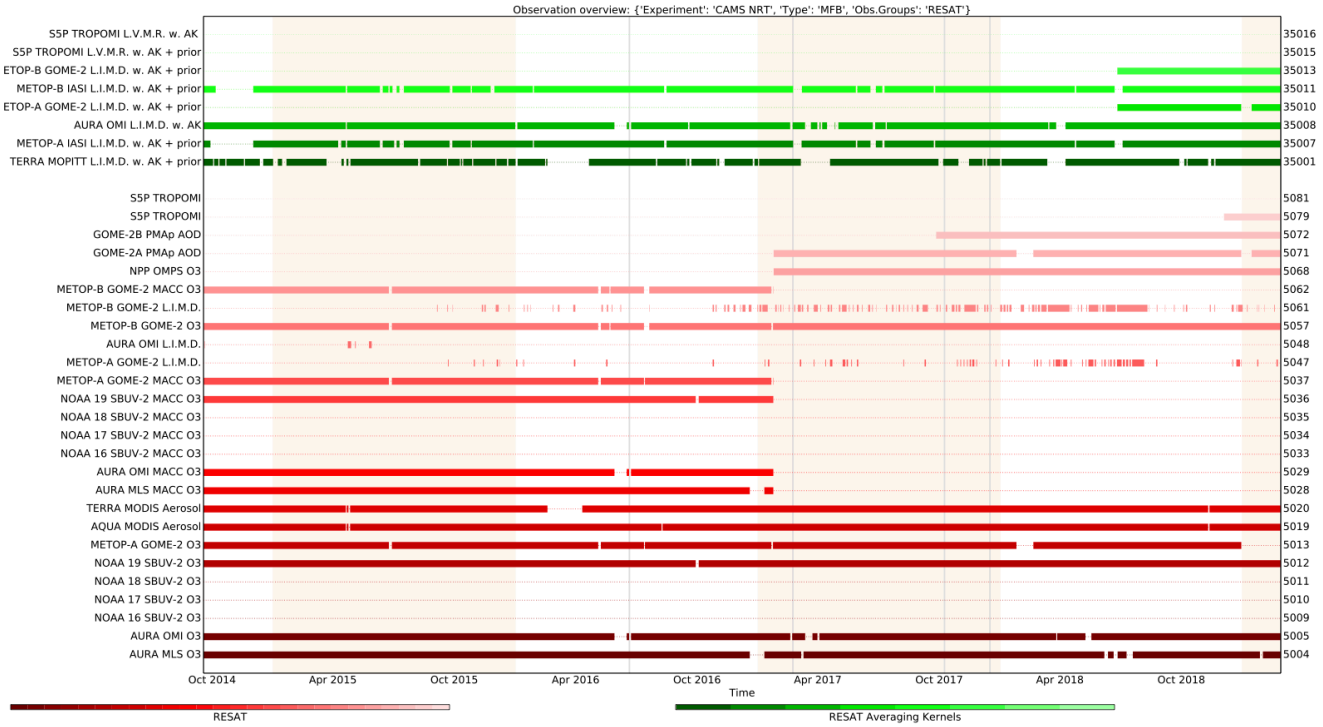

Figure 2.1: Satellite observation usage in the real-time analysis, for ozone, CO, aerosol AOD, from October 2014 onwards. Top eight rows: products assimilated using averaging kernels. New assimilated products since the 24 January 2017 upgrade are the PMaP AOD including GOME-2B and OMPS ozone profile observations. Sentinel-5P TROPOMI ozone is assimilated since Dec. 2018 (5079=O_3) and other products are monitored (35016=NO_2, 35015=CO, 5081=SO_2). Note that the lines mentioning "MACC O3" should be discarded.

- The modified CB05 tropospheric chemistry is used (Williams et al., 2013), originally taken from the TM5 chemistry transport model (Huijnen et al., 2010)
- Stratospheric ozone during the forecast is computed from the Cariolle scheme (Cariolle and Teyssèdre, 2007) as already available in IFS, while stratospheric NOx is constrained through a climatological ratio of HNO_3/O_3 at 10 hPa.
- Monthly mean dry deposition velocities are based on the SUMO model provided by the MOCAGE team.
- Data assimilation is described in Inness et al. (2015) and Benedetti et al. (2009) for chemical trace gases and aerosol, respectively. Satellite data assimilated is listed in Table 2.2 and Fig. 2.1.
- Anthropogenic and biogenic emissions are based on MACCity (Granier et al., 2011) and a climatology of the MEGAN-MACC emission inventories (Sindelarova et al., 2014)
- NRT fire emissions are taken from GFASv1.2 (Kaiser et al. 2012).

The aerosol model includes 12 prognostic variables, which are 3 bins for sea salt and desert dust, hydrophobic and hydrophilic organic matter and black carbon, sulphate aerosols and its precursor trace gas SO_2 (Morcrette et al., 2009). Aerosol total mass is constrained by the assimilation of MODIS AOD (Benedetti et al. 2009). A variational bias correction for the MODIS AOD is in place based on the approach used also elsewhere in the IFS (Dee and Uppala, 2009).

New source scheme for Secondary Organic Aerosols (part of the Organic Matter), based on scaled CO emissions. This is a change from the current AEROCOM-based emissions. The impact is an increase of organic matter aerosol concentrations. The upgrade of 24 January 2017 introduced the following adjustments: 1. Reduced dust emissions over Taklamakan desert and India. 2. Dust emissions adjusted towards more larger particles. 3. Reduction in sulphate aerosol. 4. Mass fixer for aerosols.

A history of updates of the o-suite is given in Table 2.4, and is documented in earlier MACC-VAL reports: https://atmosphere.copernicus.eu/node/326. This includes a list with changes concerning the assimilation system.

The CAMS o-suite system is upgraded regularly, following updates to the ECMWF meteorological model as well as CAMS-specific updates such as changes in chemical data assimilation. These changes are documented in e-suite validation reports, as can be found from the link above. Essential model upgrades are also documented in Table 2.4.

On 26 June 2018 the system has been upgraded to cy45r1. A validation report for this upgrade (Eskes et al., 2018b) is available: https://atmosphere.copernicus.eu/sites/default/files/2018-06/CAMS84_2015SC2_D84.3.1.5_201802_esuite_v1_0.pdf The addendum to this document is called CAMS84_2015SC3_D84.3.1.5_201802_esuite_addendum.pdf (Eskes et al., 2018c).

2.1.2 Control

The control run (relevant expver = **gzhy,** since 26/06/2018) applies the same settings as the respective o-suites, based on the coupled IFS-CB05 system with CAMS aerosol for cy54r1, except that data assimilation is not switched on. The only two exceptions with regard to this setup are:

- at the start of every forecast the ECMWF operational system is used to initialise *stratospheric* ozone, considering that stratospheric ozone, as well as other stratospheric species are not considered to be a useful product of this run. The reason for doing so is that this ensures reasonable stratospheric ozone as boundary conditions necessary for the tropospheric chemistry.
- The full meteorology in the control run is also initialized from the ECMWF operational NWP analyses. Note that this is different from the o-suite, which uses its own data assimilation setup for meteorology. This can cause slight differences in meteorological fields between o-suite and control, e.g. as seen in evaluations of upper stratospheric temperatures.

2.1.3 High-resolution CO_2 and CH_4 forecasts and delayed-mode analyses

The pre-operational forecasts of CO_2 and CH_4 use an independent setup of the IFS as the o-suite, at a resolution of TL1279, i.e. ~16 km horizontal, and with 137 levels. This system runs in NRT, and does not apply data assimilation for the greenhouse gases.

The land vegetation fluxes for CO_2 are modelled on-line by the CTESSEL carbon module (Boussetta et al., 2013). A biogenic flux adjustment scheme is used in order to reduce large-scale biases in the net ecosystem fluxes (Agusti-Panareda, 2015). The anthropogenic fluxes are based on the annual mean EDGARv4.2 inventory using the most recent year available (i.e. 2008) with estimated and climatological trends to extrapolate to the current year. The fire fluxes are from GFAS (Kaiser et al., 2012). Methane fluxes are prescribed in the IFS using inventory and climatological data sets,

Table 2.4: Long-term o-suite system updates.

Date	o-suite update
2009.08.01	Start of first NRT experiment f7kn with coupled MOZART chemistry, without aerosol. Also without data assimilation.
2009.09.01	Start of first MACC NRT experiment f93i, based on meteo cy36r1, MOZART v3.0 chemistry, MACC aerosol model, RETRO/REAS and GFEDv2 climatological emissions, T159L60 (IFS) and 1.875°×1.875° (MOZART) resolution.
2012.07.05	Update to experiment fnyp: based on meteo cy37r3, MOZART v3.5 chemistry, where changes mostly affect the stratosphere, MACCity (gas-phase), GFASv1 emissions (gas phase and aerosol), T255L60 (IFS) and 1.125°×1.125° (MOZART) resolution. Rebalancing aerosol model, affecting dust.
2013.10.07	Update of experiment fnyp from e-suite experiment fwu0: based on meteo cy38r2, no changes to chemistry, but significant rebalancing aerosol model. Assimilation of 21 layer SBUV/2 ozone product
2014.02.24	Update of experiment fnyp from e-suite experiment fzpr: based on meteo cy40r1. No significant changes to chemistry and aerosol models.
2014.09.18	Update to experiment g4e2: based on meteo cy40r2. In this model version IFS-CB05 is introduced to model atmospheric chemistry.
2015.09.03	Update to experiment g9rr: based on meteo cy41r1.
2016.06.21	Update to experiment 0067: based on meteo cy41r1, but a resolution increase from T255 to T511, and two production runs per day
2017.01.24	Update to cycle 43R1_CAMS, T511L60
2017.09.26	Update to cycle 43R3_CAMS, T511L60
2018.06.26	Update to cycle 45R1_CAMS, T511L60

consistent with those used as prior information in the CH_4 flux inversions from Bergamaschi et al. (2009). The anthropogenic fluxes are from the EDGAR 4.2 database (Janssens-Maenhout et al, 2012) valid for the year 2008. The biomass burning emissions are from GFAS v1.2 (Kaiser et al., 2012). The high-resolution forecast experiments also included a linear CO scheme (Massart et al., 2015).

The experiments analysed in this report are:

- "**ghqy**" from March 2016. The initial conditions used in ghqy on 1st of March 2016 are from the GHG analysis (experiment gg5m). Furthermore, the meteorological analysis used to initialize the ghqy forecast changed resolution and model grid in March 2016. Note that the CO_2, CH_4 and linear CO tracers are free-running.
- "**gqpe**" from January 2017 to present. It runs with a TCO1279 Gaussian cubic octahedral grid (equivalent to approximately 9km horizontal resolution). Note that the CO_2, CH_4 and linear CO tracers are initialized with the GHG analysis (gqiq) for CO_2 and CH_4 and the CAMS operational analysis for CO.

- The greenhouse gas analysis experiment "**gqiq**" runs on a TCO399 grid (equivalent to around 25km) and 137 vertical levels and is available from January 2017. This experiment runs in delayed mode (4 days behind real time) and makes use of observations from TANSO-GOSAT (methane and CO_2) and MetOp-IASI (methane).

2.2 Other systems

2.2.1 BASCOE

The NRT analyses and forecasts of ozone and related species for the stratosphere, as delivered by the Belgian Assimilation System for Chemical ObsErvations (BASCOE) of BIRA-IASB (Lefever et al., 2014; Errera et al., 2008), are used as an independent model evaluation of the CAMS products. The NRT BASCOE product is the ozone analysis of Aura/MLS-SCI level 2 standard products, run in the following configuration (version 05.07):

- The following species are assimilated: O_3, H_2O, HNO_3, HCl, HOCl, N_2O and ClO.
- It lags by typically 4 days, due to latency time of 4 days for arrival of non-ozone data from Aura/MLS-SCI (i.e. the scientific offline Aura/MLS dataset).
- Global horizontal grid with a 3.75° longitude by 2.5° latitude resolution.
- Vertical grid is hybrid-pressure and consists in 86 levels extending from 0.01 hPa to the surface.
- Winds, temperature and surface pressure are interpolated in the ECMWF operational 6-hourly analyses.
- Time steps of 20 minutes, output every 3 hours

See the stratospheric ozone service at http://www.copernicus-stratosphere.eu/. It delivers graphical products dedicated to stratospheric composition and allows easy comparison between the results of o-suite, BASCOE and TM3DAM. The BASCOE data products (HDF4 files) are also distributed from this webpage. Other details and bibliographic references on BASCOE can be found at http://bascoe.oma.be/. A detailed change log for BASCOE can be found at http://www.copernicus-stratosphere.eu/4_NRT_products/3_Models_changelogs/BASCOE.php.

2.2.2 TM3DAM and the multi-sensor reanalysis

One of the MACC products was a 30-year reanalysis, near-real time analysis and 10-day forecast of ozone column amounts performed with the KNMI TM3DAM data assimilation system, the Multi-Sensor Reanalysis (MSR) system (van der A et al., 2010, 2013),
http://www.temis.nl/macc/index.php?link=o3_msr_intro.html.
The corresponding validation report can be found at
http://www.copernicus-atmosphere.eu/services/gac/global_verification/validation_reports/.

The NRT TM3DAM product used for the validation of the CAMS NRT streams is the ozone analysis of Envisat/SCIAMACHY (until April 2012), AURA/OMI, and MetOp-A/GOME-2, run in the following configuration:

- total O_3 columns are assimilated
- Global horizontal grid with a 3° longitude by 2° latitude resolution.
- Vertical grid is hybrid-pressure and consists in 44 levels extending from 0.1 hPa to 100 hPa.
- Dynamical fields from ECMWF operational 6-hourly analysis.

An update of the MSR (MSR-2) was presented in van der A et al. (2015), which extended the record to 43 years based on ERA-interim reanalysis meteo and with an improved resolution of 1x1 degree.

2.2.3 SDS-WAS multimodel ensemble

The World Meteorological Organization's Sand and Dust Storm Warning Advisory and Assessment System (WMO SDS-WAS) for Northern Africa, Middle East and Europe (NAMEE) Regional Center (http://sds-was.aemet.es/) has established a protocol to routinely exchange products from dust forecast models as the basis for both near-real-time and delayed common model evaluation. Currently, twelve regional and global models (see the complete list in the following link https://sds-was.aemet.es/forecast-products/forecast-evaluation/model-inter-comparison-and-forecast-evaluation/at_download/file) provides daily operational dust forecasts (i.e. dust optical depth, DOD, and dust surface concentration).

Different multi-model products are generated from the different prediction models. Two products describing centrality (multi-model median and mean) and two products describing spread (standard deviation and range of variation) are daily computed. In order to generate them, the model outputs are bi-linearly interpolated to a common grid mesh of 0.5º x 0.5º. The multimodel DOD (at 550 nm) Median from nine dust prediction models participating in the SDS-WAS Regional Center is used for the validation of the CAMS NRT streams.

2.3 CAMS products

An extended list of output products from the NRT stream o-suite are available as 3-hourly instantaneous values up to five forecast days. These are available from ECMWF (through ftp in grib2 and netcdf format, https://atmosphere.copernicus.eu/data).

2.4 Availability and timing of CAMS products

The availability statistics provided in Table 2.6 are computed for the end of the 5-day forecast run. The CAMS production KPI is defined as the percentage of cycles in which all the general data dissemination tasks are completed before the deadlines: 10 UTC for the 00:00 and 22 UTC for the 12:00 UTC run. This was in part based on requirements from the regional models. We note that at present most regional models can still provide their forecasts even if the global forecast is available a bit later. Note that since 21 June 2016 two CAMS forecasts are produced each day.

For the period December 2018 – February 2019, 98.85% of the forecasts were delivered on time. There were two delays.

Table 2.6: Timeliness of the o-suite from Dec 2014 to the end of May 2018. From June 2016 onwards CAMS has produced two forecasts per day.

Months	**On time, 10 & 22 utc**	**80th perc**	**90th perc**	**95th perc**
Dec-Feb '14-'15	97%	D+0, 19:43	D+0, 20:28	D+0, 21:13
Mar-May 2015	96%	D+0, 19:38	D+0, 21:03	D+0, 21:40
Jun-Aug 2015	95%	D+0, 20:24	D+0, 20:53	D+0, 21:54
Sept-Nov 2015	95%	D+0, 19:44	D+0, 20:55	D+0, 21:51
Dec-Feb '15-'16	100%	D+0, 18:39	D+0, 18:57	D+0, 19:43
Mar-May 2016	98%	D+0, 19:32	D+0, 19:47	D+0, 20:00
Jun-Aug 2016 (00 and 12 cycle)	100%	D+0, 08:53 D+0, 20:55	D+0, 09:04 D+0, 21:01	D+0, 09:18 D+0, 21:18
Sep-Nov 2016	98.9%	D+0, 08:44 D+0, 20:44	D+0, 08:51 D+0, 20:48	D+0, 08:52 D+0, 20:51
Dec 2016 - Feb 2017	99.4%	D+0, 09:02 D+0, 21:01	D+0, 09:11 D+0, 21:02	D+0, 09:18 D+0, 21:04
Mar-May 2017	100%	D+0, 09:08 D+0, 21:07	D+0, 09:14 D+0, 21:09	D+0, 09:19 D+0, 21:11
Jun-Aug 2017	100%	D+0, 09:05 D+0, 21:05	D+0, 09:07 D+0, 21:08	D+0, 9:09 D+0, 21:10
Sep-Nov 2017	100%	D+0, 09:02 D+0, 21:00	D+0, 09:05 D+0, 21:04	D+0, 9:09 D+0, 21:07
Dec 2017 - Feb 2018	98.33%	D+0, 08:55 D+0, 20:54	D+0, 08:59 D+0, 20:59	D+0, 09:01 D+0, 21:02
Mar-May 2018	98.9%	D+0, 09:00 D+0, 21:00	D+0, 09:06 D+0, 21:03	D+0, 09:08 D+0, 21:06
Jun-Aug 2018	100%	D+0, 09:11 D+0, 21:07	D+0, 09:14 D+0, 21:09	D+0, 09:20 D+0, 21:11
Sep-Nov 2018	100%	D+0, 09:05 D+0, 21:03	D+0, 09:09 D+0, 21:07	D+0, 09:13 D+0, 21:10
Dec 2018 - Feb 2019	98.85%	D+0, 09:03 D+0, 21:04	D+0, 09:06 D+0, 21:06	D+0, 09:08 D+0, 21:10

3. Tropospheric Ozone

3.1 Validation with sonde data in the free troposphere

Model profiles of the CAMS runs were compared to free tropospheric balloon sonde measurement data of 38 stations taken from the NDACC, WOUDC, NILU and SHADOZ databases for January 2013 to February 2019 (see Fig. 3.1.1 - 3.1.2). Towards the end of the period, the number of available soundings decreases, which implies that the evaluation results may become less representative. The figures contain the number of profiles in each month that are available for the evaluation. The methodology for model comparison against the observations is described in Douros et al., 2017. The free troposphere is defined as the altitude range between 750 and 200hPa in the tropics and between 750 and 300hPa elsewhere.

MNMBs for the o-suite are mostly within the range ±20%, for all months, in all zonal bands, except for the Tropics and Antarctica, where larger positive MNMBs up to ±45% appear, see Fig. 3.1.1.-3.1.4. During the last year (Feb 2018 to Feb 2019) MNMBs are ±10% over the Arctic and Northern Midlatitudes and up to 40% for Antarctica and the Tropics.

Over the Arctic, the o-suite mostly shows slightly positive MNMBs during summer and spring (MNMBs up to 10%), while during the winter season the MNMBs get negative (within -10%) see, Fig. 3.1.1.

Over the NH mid-latitudes MNMBs for the o-suite are on average close to zero all year round (maxima are -8% to +4%), which is generally a clear improvement compared to the control run, which shows larger negative MNMBs during the respective period.

Over the Tropics and over Antarctica, ozone mixing ratios are mostly overestimated by the o-suite (up to 34%) by the o-suite, see Fig. 3.1.2. The control run shows large negative MNMBs for Antarctica.

In the UTLS, ozone is overestimated by the o-suite over all regions. MNMBs range mostly within ±20%.

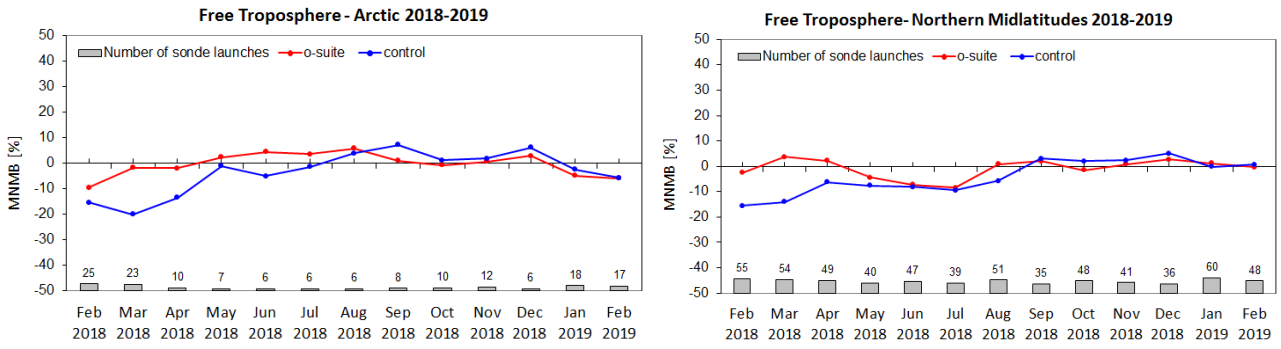

Figure 3.1.1: MNMBs (%) of ozone in the free troposphere (between 750 and 300 hPa) from the IFS model runs against aggregated sonde data over the Arctic (left) and the Northern mid latitudes (right). The numbers indicate the amount of individual number of sondes.

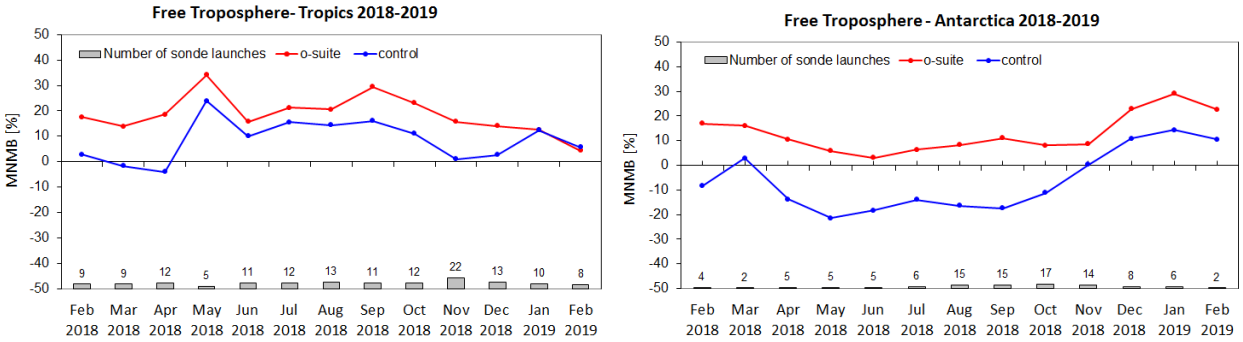

Figure 3.1.2: MNMBs (%) of ozone in the free troposphere (between 750 and 200hPa (Tropics) / 300hPa) from the IFS model runs against aggregated sonde data over the Tropics (left) and Antarctica (right). The numbers indicate the amount of individual number of sondes.

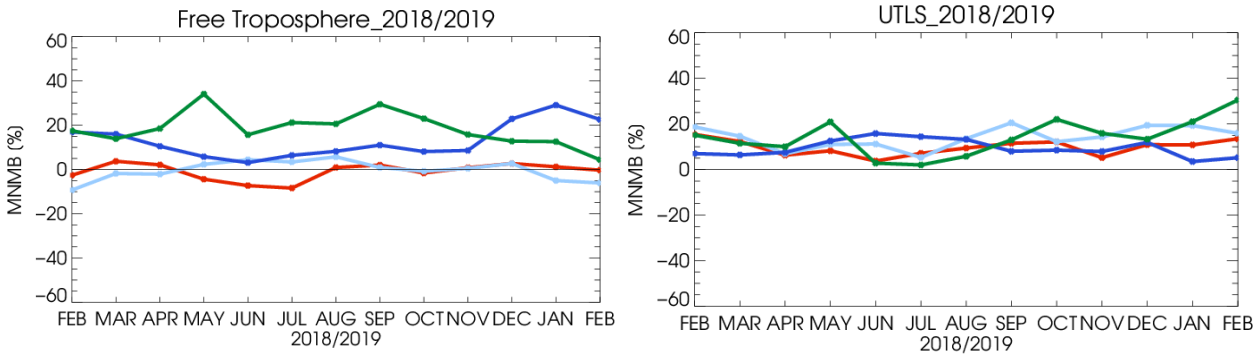

Figure 3.1.3: MNMBs (%) of ozone in the free troposphere (left, between 750 and 200hPa (Tropics) / 300hPa) and UTLS (right, between 300 and 100hPa (Tropics) / 60hPa) from the IFS model runs against aggregated sonde data over the Tropics (green) and Antarctica (blue), Arctic (light blue) and Northern Midlatitudes (red).

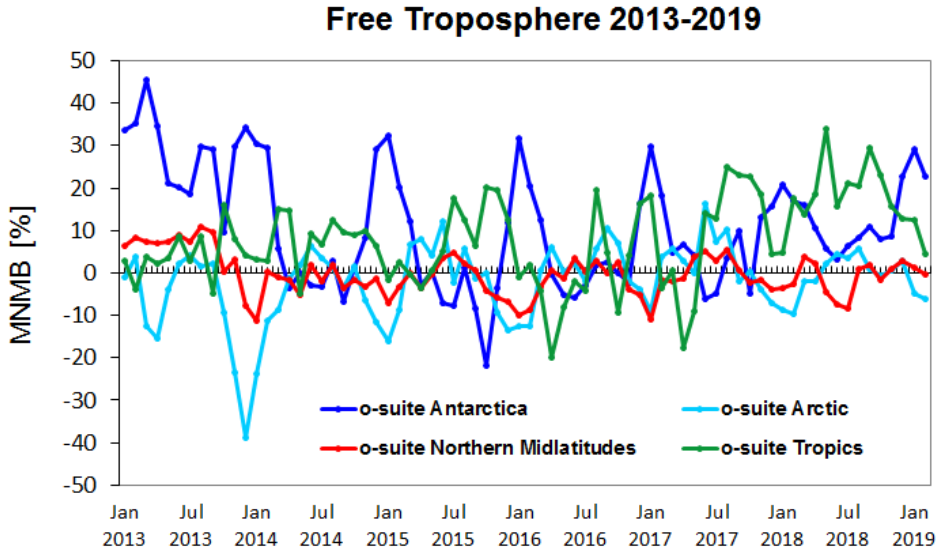

Figure 3.1.4: Time series of MNMB of ozone in the o-suite, compared against ozone sondes, averaged over different latitude bands. The free troposphere is defined here as the layer between 750 and 300 hPa.

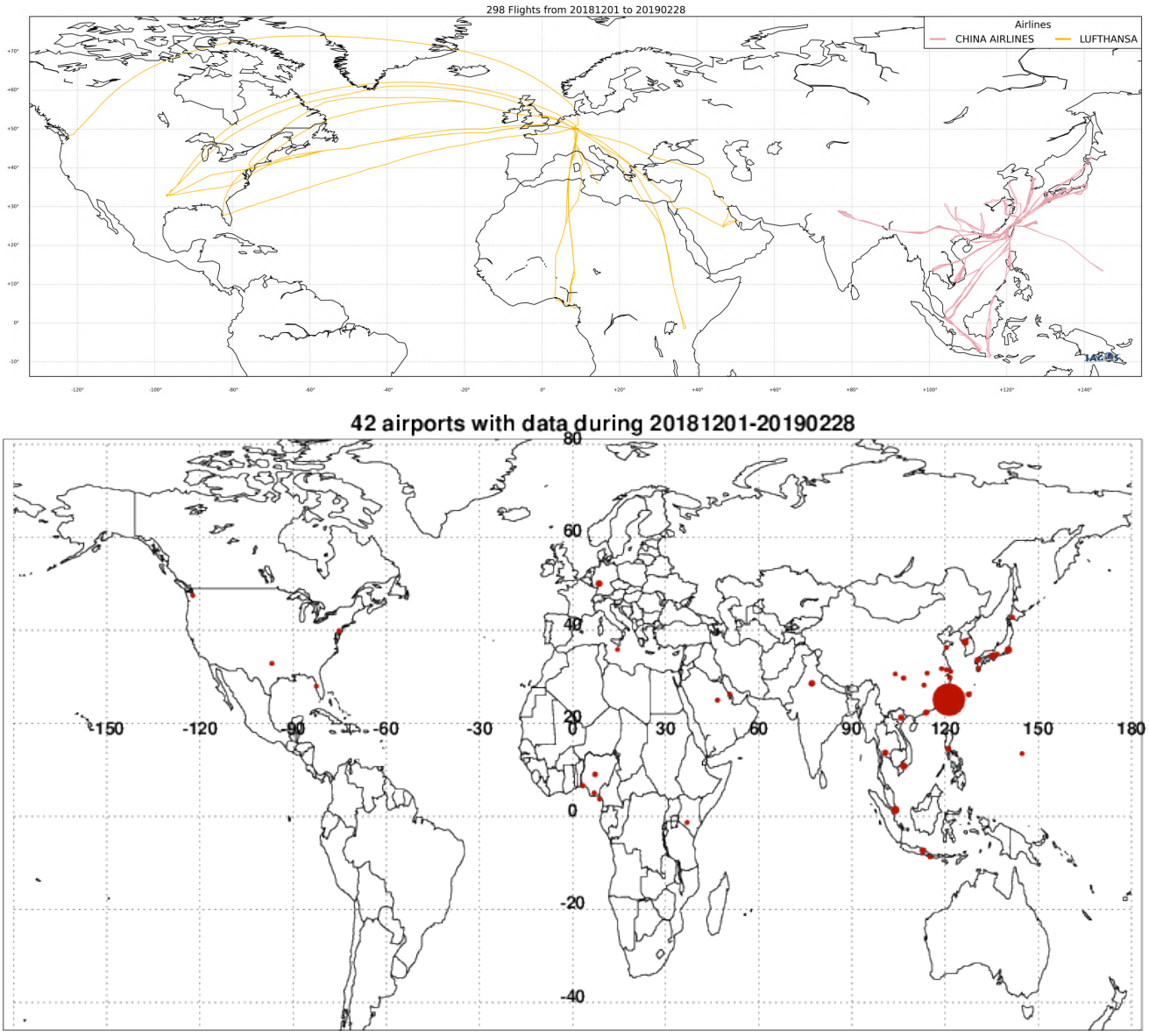

Figure 3.2.1. Map of the flights (top) and the visited airports (bottom) during the period December 2018 - February 2019, by the IAGOS-equipped aircraft. The size of the plotting circle represents the number of profiles available.

3.2 Ozone validation with IAGOS data

The daily profiles of ozone measured at airports around the world are shown on the CAMS website at http://www.iagos.fr/macc/nrt_day_profiles.php. For the period from December 2018 - February 2019, the data displayed on the web pages and in this report include only the data as validated by the instrument PI. The available flights and available airports are shown in Fig. 3.2.1 top and bottom respectively. Performance indicators have been calculated for different parts of the IAGOS operations.

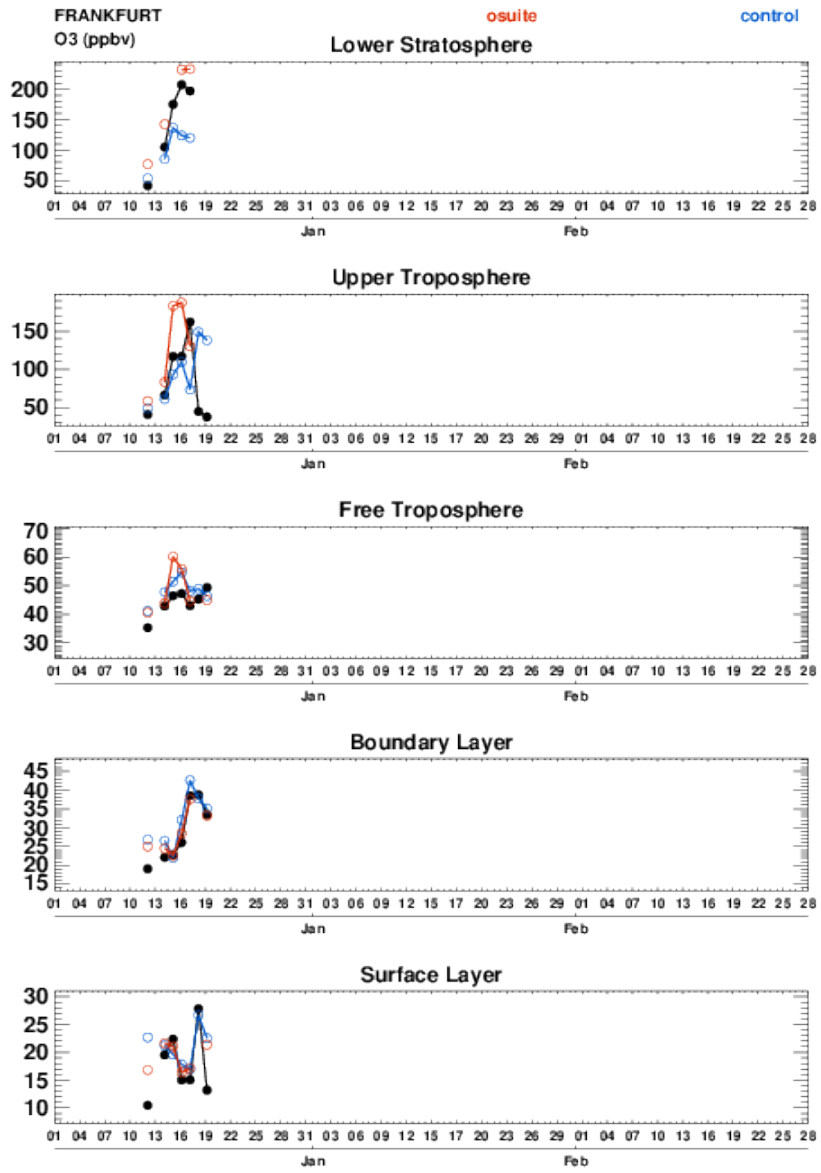

Figure 3.2.2. Time series of daily mean ozone over Frankfurt during DJF 2019 for 5 layers: Surface, Boundary layer, Free Troposphere, Upper Troposphere and Lower Stratosphere.

Six aircraft were operating during this period. With these aircrafts, operating fully over the three-month period, we can expect a total of about 1260 flights. The actual number of flights within the period was 298 (596 profiles) giving a performance of 23 %. These flights are shown in Fig. 3.2.1 (top). Nine percent (9%) of the operational flights had usable measurements of ozone and 3% of the flights had usable CO. Delivering these O_3 and CO data were two aircraft from Lufthansa operating from Frankfurt, one aircraft operated by Air France based in Paris, two from China Airlines based in Taipei and one from Hawaiian Airlines with flight operations from Honolulu. Fig. 3.2.1 (bottom) shows the available airports, with a plotting circle scaled to the highest number of flights at an airport.

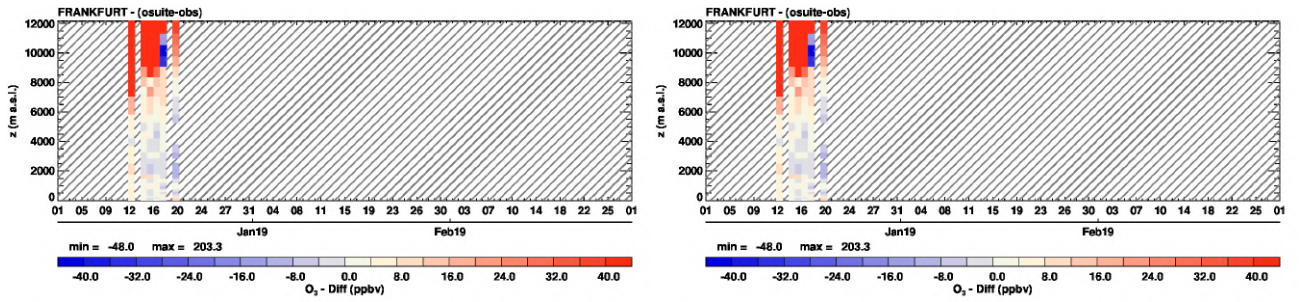

Figure 3.2.3 Time series of the absolute differences (model - observations) in daily profiles for ozone over Frankfurt during DJF 2019. Left panel correspond to o-suite and right panel to control run.

Europe

Fig. 3.2.2 presents ozone time series at Frankfurt during December 2018 – February 2019. In the UTLS region a few profiles show an overestimation of ozone by the o-suite and better results for the control run. Some examples of individual profiles are presented in Fig. 3.2.4.

Like for the period SON 2018 and as mentioned in the previous report, several issues explain the poor availability of data for the DJF 2019 period. Ozone sensors are working only on the two operating Lufthansa aircrafts, which explains the poor availability of ozone data. Moreover, due to transmission problems on one of these two packages, many profiles are not available, which also affects the availability of CO data. The other ozone instrument started having measurement problems, and a number of measurements could not be validated as Level 1. Therefore, there is only a small number of ozone profiles for this season, mainly at Frankfurt but also a few at the other airports visited by Lufthansa.

All the daily profiles at Frankfurt are presented in Fig. 3.2.4. All IAGOS profiles on this figure present low ozone in the lowest layers between 10 and 30 ppbv near the surface and less than 50 ppbv in the boundary layer and a nearly constant in the free troposphere. Both models provide results close to the observations from the surface to an altitude of about 6000 m, where the tropopause is found, except for day 19 which presents a nearly constant profile. The high ozone values related to the tropopause descent are reproduced by the models with in general a better agreement for control run.

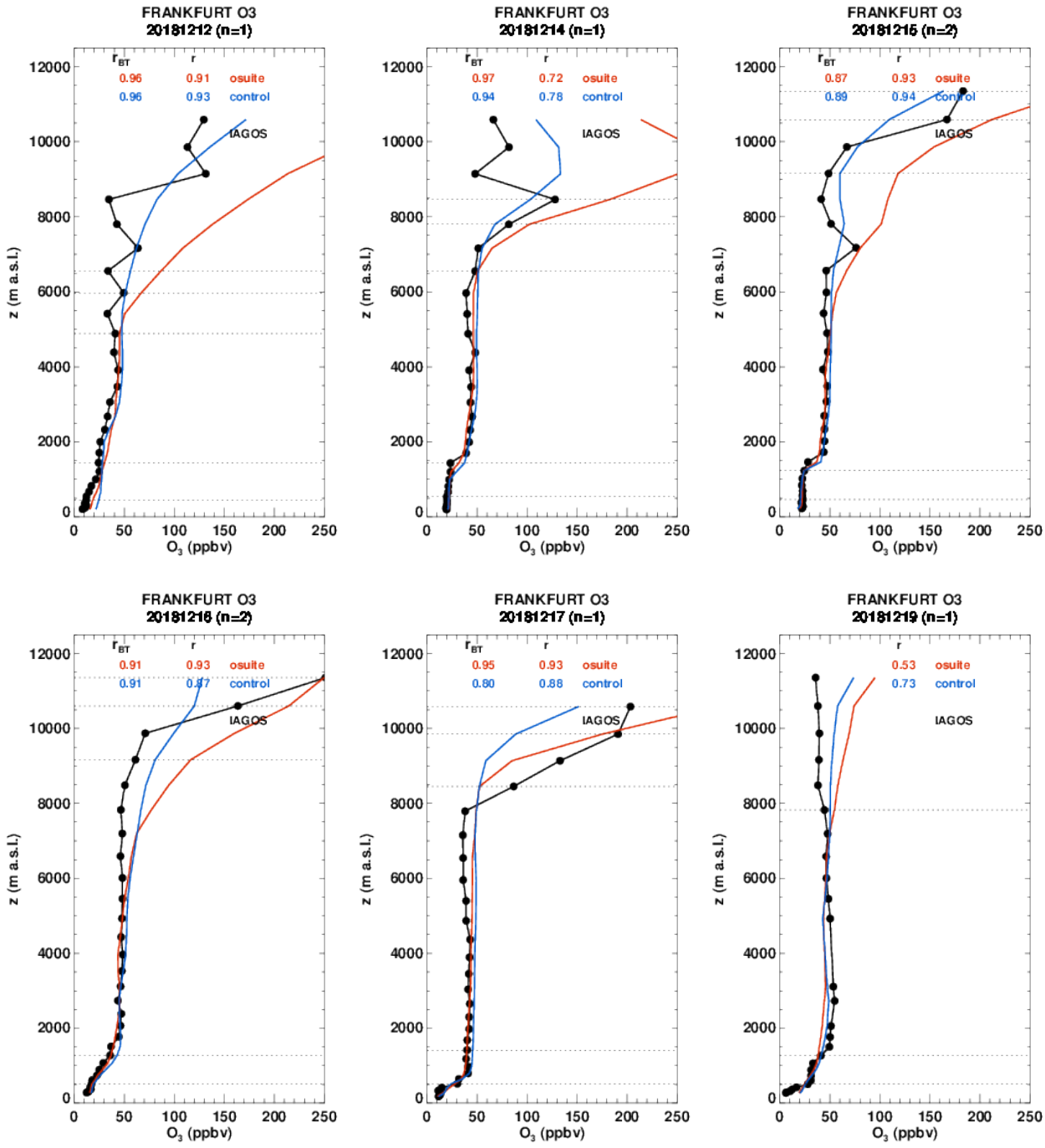

Figure 3.2.4 Daily profiles for ozone from IAGOS (black) and the two NRT runs (o-suite: red, control: blue) over Europe during DJF 2019.

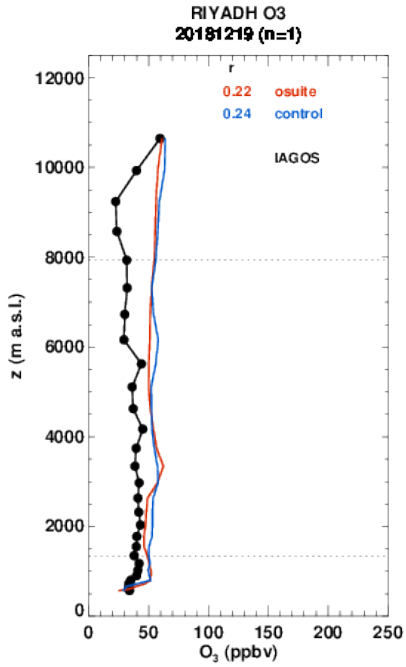

Figure 3.2.5 Daily profile for ozone from IAGOS (black) and the two NRT runs (o-suite: red, control: blue) over the Middle East during DJF 2019.

Middle East

On 19 December 2018, a profile is available at the airport of Riyadh (Fig. 3.2.5). This profile is nearly constant with values of ozone of about 40 ppbv. CAMS global and control also present a constant profile with a good agreement in the lowest layers and an overestimation of ozone values in the free troposphere and UTLS.

West Africa

IAGOS profiles are available at Nigerian airports in Abuja and Port Harcourt (Fig. 3.2.6). The profiles observed at Abuja on 14 and 16 December 2019 are nearly constant with ozone values in the range of 60 to 70 ppbv. These two profiles are overall well reproduced by both models. On day 14 and 16 December, IAGOS profiles at Port Harcourt present a maximum of ozone in the lower part of the free troposphere near 2000 m with about 70 ppbv. On day 16, the profile presents a complex shape with another maximum observed near 7000 m with about 50 ppbv. CAMS global and the associated control run behave similarly, with the occurrence of maxima in the boundary layer and in the mid-troposphere, which are located at different altitudes leading to under/overestimations of ozone values.

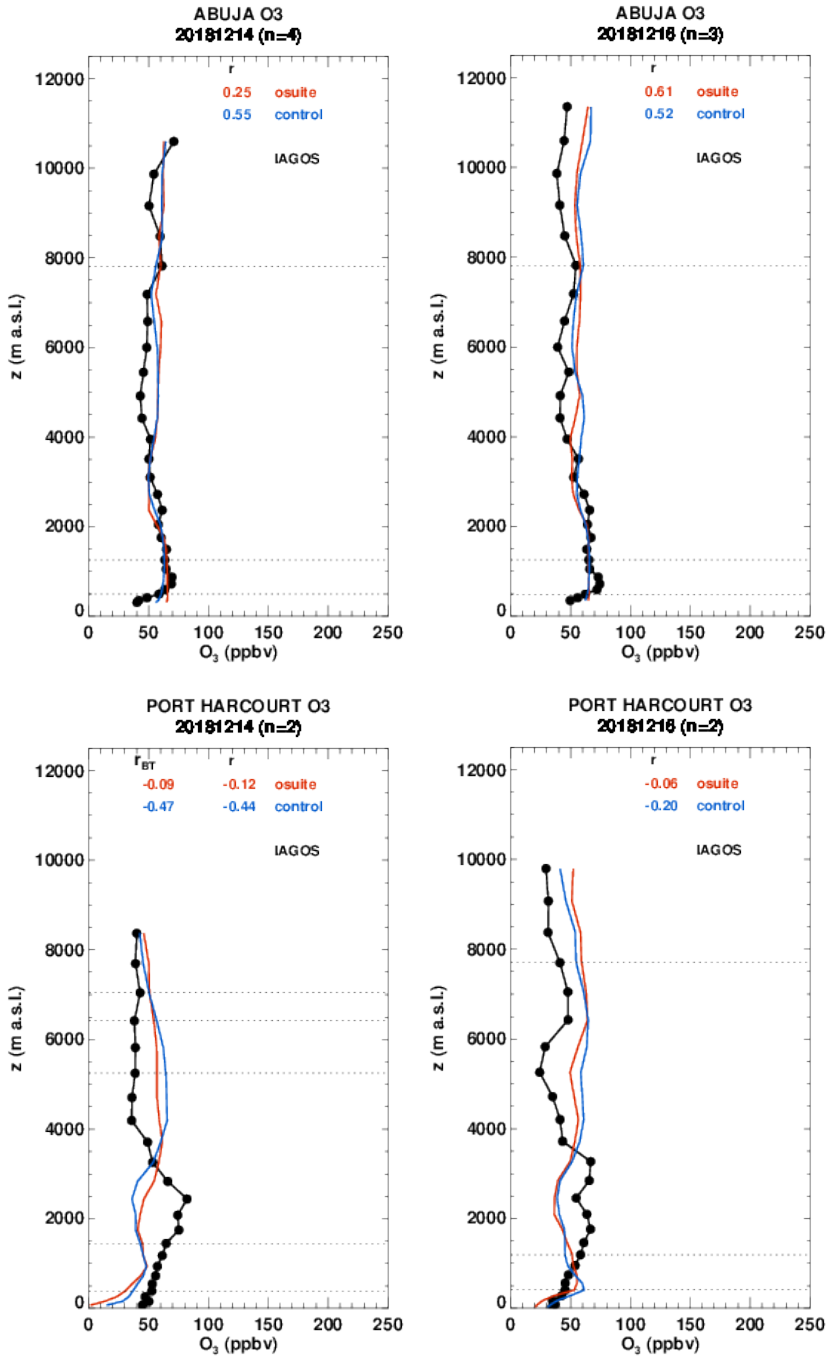

Figure 3.2.6 Daily profiles for ozone from IAGOS (black) and the two NRT runs (o-suite: red, control: blue) over West Africa during DJF 2019.

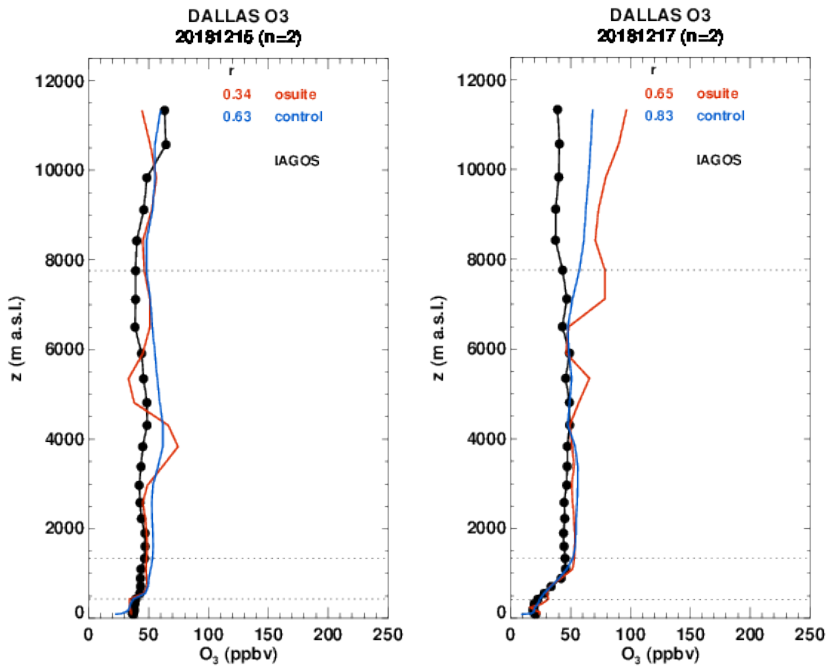

Figure 3.2.7 Daily profiles for ozone from IAGOS (black) and the two NRT runs (o-suite: red, control: blue) over North America during DJF 2019.

North America

Two IAGOS profiles are available at Dallas on 15 and 17 December. These profiles are nearly constant with ozone of about 40 ppbv, except in the lowest layers on day 17 where ozone values are even lower with 20 ppbv. The results of both runs are similar in the low troposphere, presenting a good agreement with the observations. On 15 December, CAMS global present a maximum in the free troposphere (80 ppbv near 4000 m), which is not present in the observations, while the control run agrees well with the observations. In the mid-troposphere up to the UTLS, the two runs overestimate ozone with a slightly better performance of the control run.

3.3 Validation with GAW and ESRL-GMD surface observations

For the Near Real Time (NRT) validation, 13 GAW stations and 14 ESRL stations are currently delivering O_3 surface concentrations in NRT, and the data are compared to model results. In the following, a seasonal evaluation of model performance for the 2 NRT runs (o-suite and control) has been carried out for the period from December to February 2019. The latest validation results based on GAW stations and based on ESRL observations can be found on the CAMS website, see section 1, table 1.2.

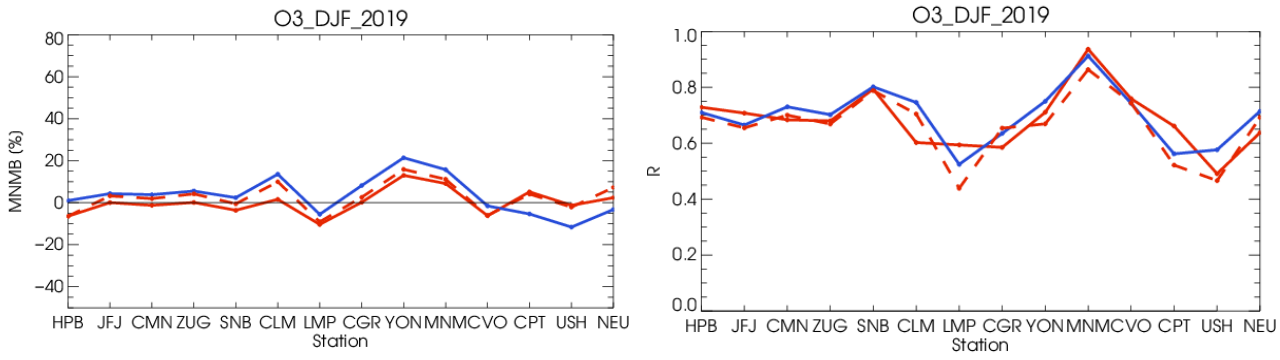

Figure 3.3.1: Modified normalized mean bias in % (left) and correlation coefficient (right) of the NRT model runs compared to observational GAW data in the period December 2018 to February 2019 (o-suite: solid red, D+2: red-dashed, and control: blue).

Modified normalized mean biases in % (left panel) and correlation coefficients (right panel) for different forecasts days (D+2, red-dashed and D+4, red- pointed) with respect to GAW and ESRL observations are shown in Figs. 3.3.1 and 3.3.2. It indicates that MNMBs for both o-suite and control run mostly remain stable up to D+4 (forecast run from 96h to 120h). Correlations between simulated and observed surface ozone values remain almost stable up to D+2 (forecast run from 48h to 72h), but then drop (correlations for D+4 are lower than correlations for D+2 and D+0), see Fig. 3.3.1 and 3.3.2, right graph).

A comparison of the seasonal-mean MNMB over Europe (Fig. 3.3.3) from December 2012 to present shows that the MNMB over European GAW stations is minimal during the winter season and tends to increase in other months. Also, on average the MNMB for the o-suite and control shows an improvement over the years. The temporal correlation is consistently better for the control run than for the o-suite, but the o-suite shows strong improvements recently. The GAW results are summarized in Figs 3.3.1 and 3.3.3.

Looking at different regions, for European stations (HPB, JFJ, ZUG, SNB, CMN, LMP, CLM, CGR), observed O_3 surface mixing ratios are very close to the observations. MNMBs are between -10% and 1% for the o-suite and between -5% and 13% for the control run, see Fig. 3.3.1. Correlations for European stations are between 0.58 and 0.79 for the o-suite and between 0.52 and 0.80 for the control run, see Fig. 3.3.1.

Over Arctic stations (EUK, BRW and SUM), the o-suite has almost zero bias at Eureka and overestimates surface ozone values by 7% at Summit and by 14% at Point Barrow. The control run has higher positive MNMBs than the o-suite for all 3 Arctic stations (MNMB control: 9% at Eureka, 12 at Summit and 24% at Point Barrow). Notable is that the o-suite runs reproduces better than the control the day to day surface ozone variability over the Arctic stations (R o-suite≈0.2 and R control≈0.1 at EUK, R o-suite≈0.75 and R control≈0.65 at SUM and R o-suite≈0.80 and R control≈0.75 at BRW).

For stations located in Asia (RYO, YON, MNM) both runs strongly overestimate O_3 mixing ratios with MNMBs between 9% and 13% for the o-suite and between 15% and 21% for the control run, see Fig 3.3.6. Correlation coefficients range between 0.71 and 0.93.

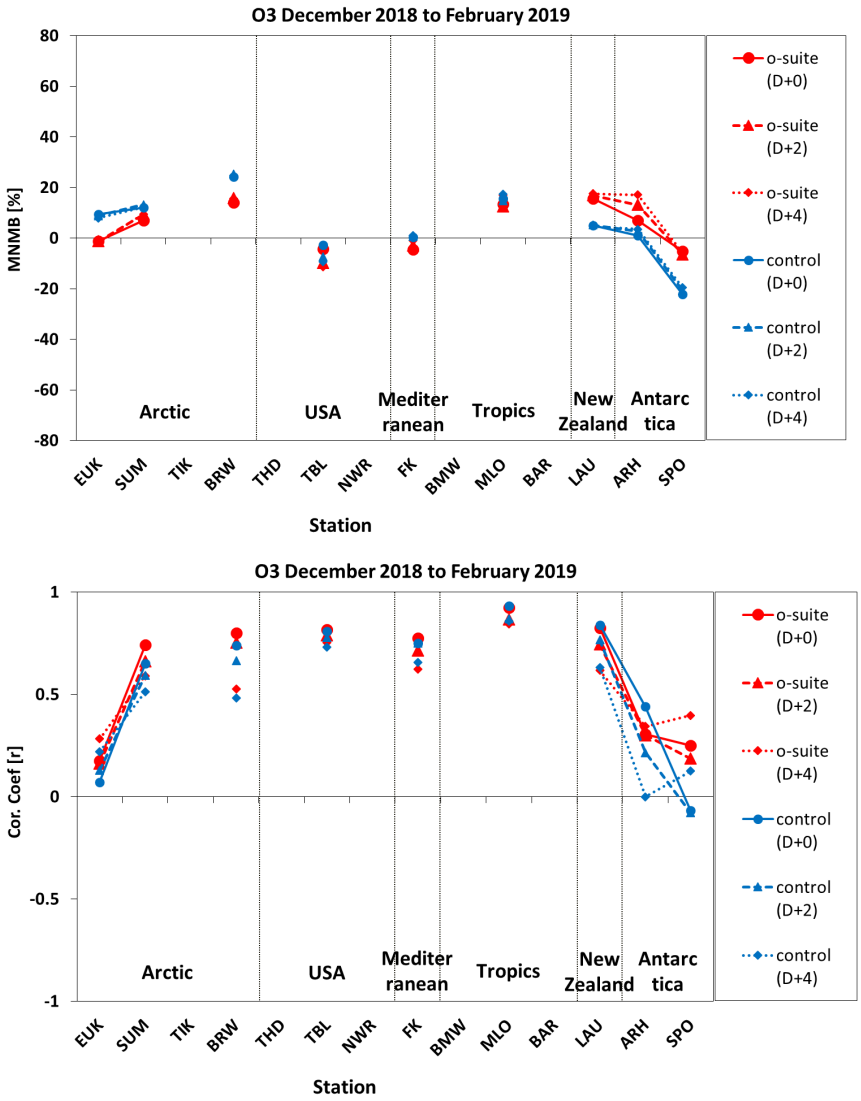

Figure 3.3.2: Modified normalized mean bias in % (left) and correlation coefficient (right) of the NRT forecast runs compared to observational ESRL data in the period December to February 2019. Circles correspond to D+0, triangles to D+2 and rhombs to D+4 metrics respectively.

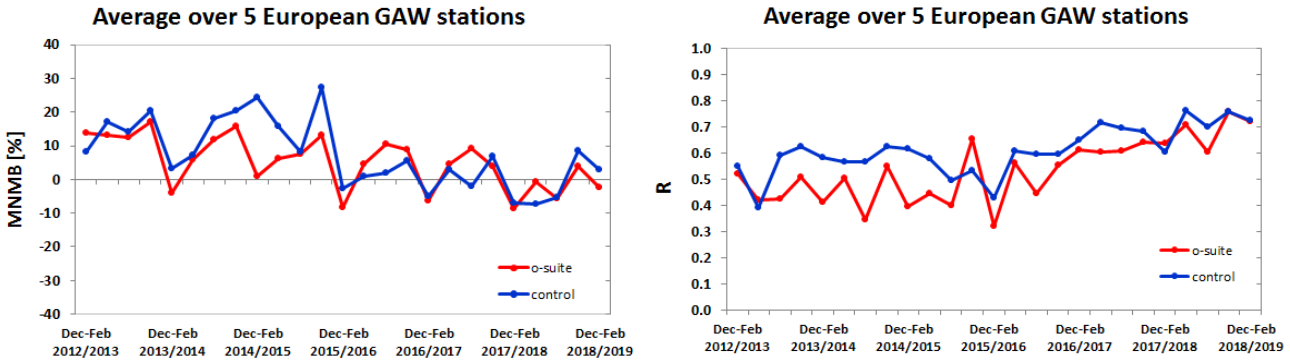

Figure 3.3.3: Long term (Dec. 2012 – February 2019) evolution of seasonal mean MNMB (left) and correlation (right), as averaged over 5 GAW stations in Europe, for o-suite (red) and control (blue).

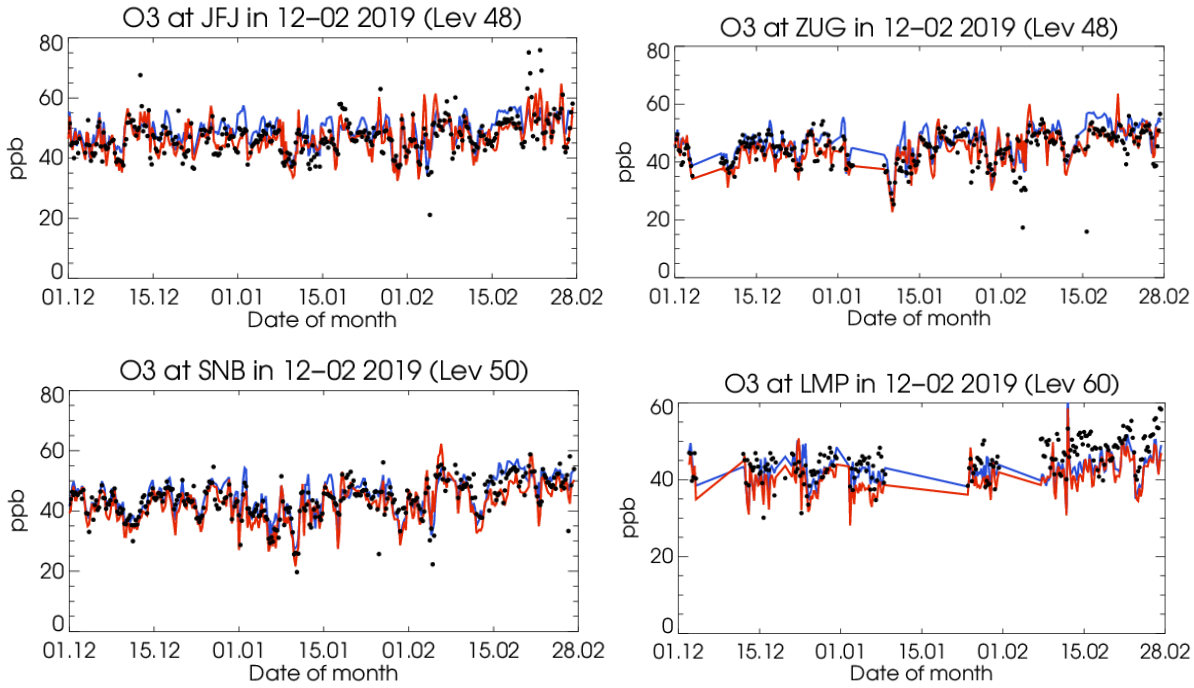

Figure 3.3.4: Time series for the o-suite (red) and control (blue) compared to GAW observations at Zugspitze (47.4°N, 11.9°E) (upper panel). Sonnblick (47.05°N, 12.96°E) and Lampedusa (35.52°N, 12.63°E) (lower panel).

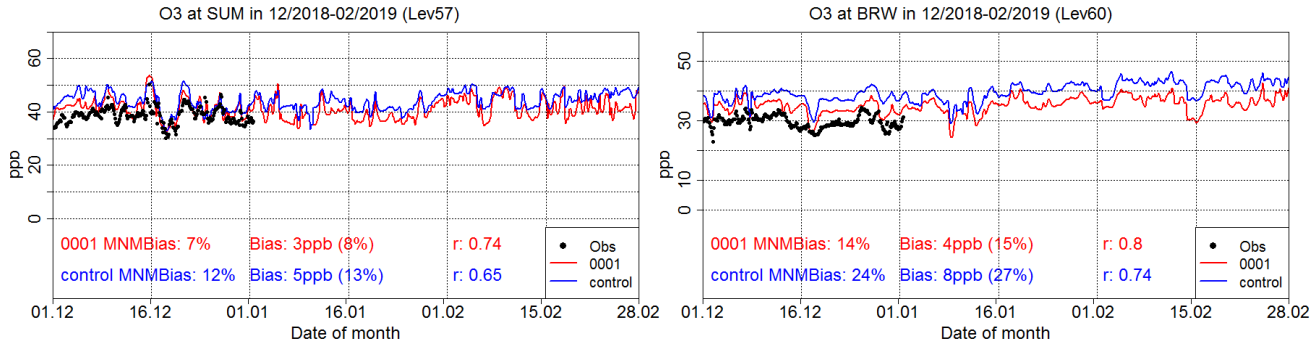

Figure 3.3.5: Time series for the o-suite (red) and control (blue) compared to ESRL observations at Summit, Greenland station (72.57°N, 38.48°W, left) and at Point Barrow, Alaska station (71.32°N, 156.51°W, right)

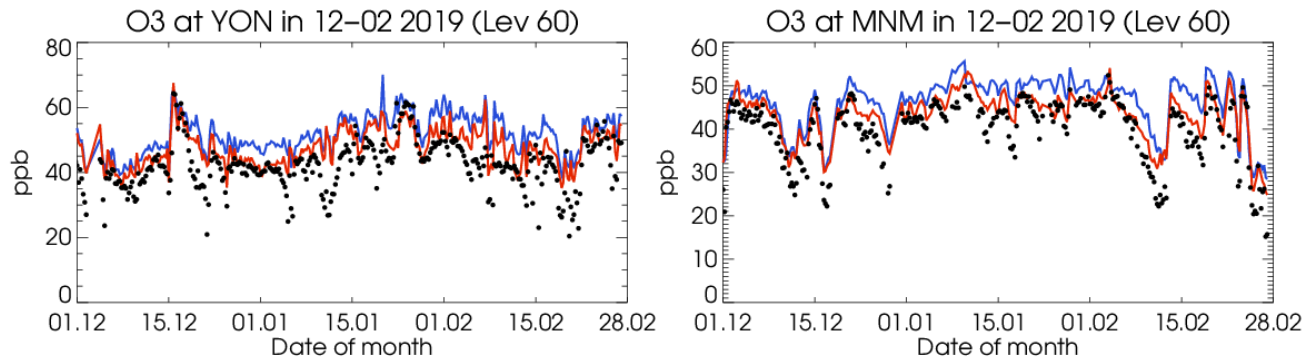

Figure 3.3.6: Time series for the o-suite (red) and control (blue) compared to GAW observations for Yonagunijima (24.47°N, 123.02°E) and Minamitorishima (24.29°N, 153.98°E).

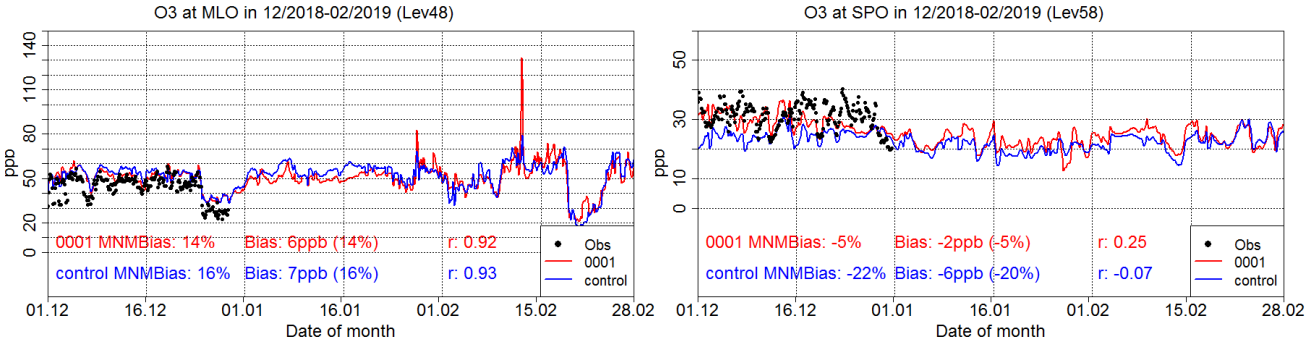

Figure 3.3.7: Time series for the o-suite (red) and control (blue) compared to ESRL observations (black dots) at Maouna Loa, Hawaii station (19.54°N, 155.58°W) and at South Pole, Antarctica station (90.00°S, 24.80°W).

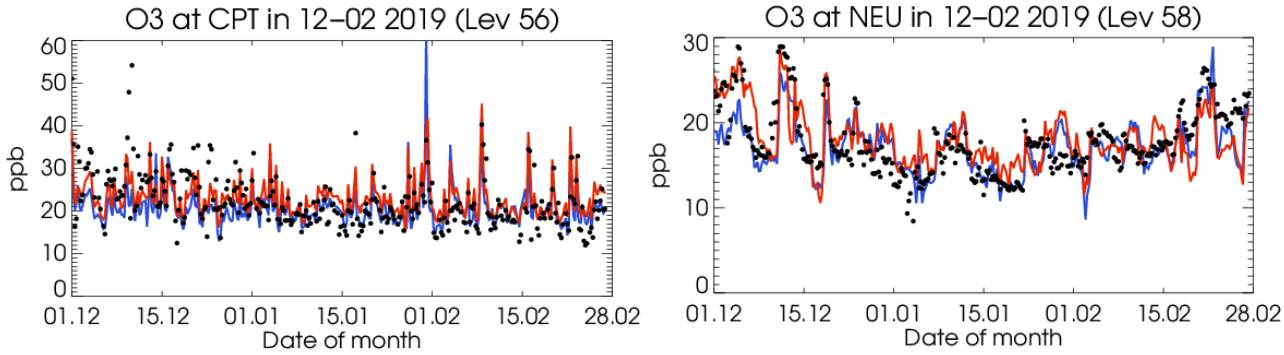

Figure 3.3.8: Time series for the o-suite (red) and control (blue) compared to GAW observations (black dots) at Cape Point (34.55°S, 18.48°W) and GAW observations at Neumayer (70.65°S, 8.25°W).

For TBL USA station, the observed ozone mixing ratios are slightly underestimated (MNMB≈-3%) by both the o-suite and the control run. Correlations between modelled and observed surface ozone values are 0.80 for both the o-suite and the control run.

The observed ozone mixing ratios are overestimated by both runs over Mauna Loa (MLO) station in the Tropics ($MNMB_{o\text{-}suite}$ and $MNMB_{control}$≈15%). Correlations between simulated and observed surface ozone are extremely high for both the o-suite and the control run over MLO station (R>0.9).

The O_3 mixing ratios of the southern hemispheric stations (CPT, USH) show MNMBs between -1 and 5% by the o-suite. The control run shows larger underestimations up to -11%, see Fig 3.3.8. Correlation coefficients range around 0.49 and 0.66. At Lauder (LDR) station in New Zealand the control run overestimates O_3 mixing ratios by 5% and the o-suite by 15%. Correlations between simulated and observed surface ozone values are 0.83 for both runs.

At Arrival Height (ARH) station in Antarctica the control run has almost zero bias while the o-suite overestimates O_3 mixing ratios by 7%. Finally, for South Pole station in Antarctica (SPO), the data assimilation almost corrects the negative offset in the control run (o-suite MNMBs= -5%, control MNMB= -20%), see Fig 3.1.3.7 (right panel).

For Neumayer station (NEU) the MNMB is 2% for the o-suite and -3% for the control run. Correlation coefficients are 0.63 for the o-suite and 0.71 for the control run, Fig. 3.3.8.

Table 3.4.1: Coordinates, elevation, corresponding model level (level 60 is the surface level), as well as validation scores (MNMBs and correlations for the period DJF 2018-2019) obtained with the 2 forecast runs (o-suite and control), for each one of the selected Mediterranean stations. MNMBs and correlations with blue denote stations where control run performs better while with red are denoted stations where o-suite performs better.

						Distance from the	MNMB		Cor. Coef	
Station Name	Stat_ID	Lon	Lat	Alt (m)	Level	shore (km)	o-suite	control	o-suite	control
Al Cornocales	ES1648A	-5.66	36.23	189	57	16	11.3	17.5	0.80	0.78
Caravaka	ES1882A	-1.87	38.12	1	60	73	-7.3	-0.6	0.53	0.48
Zarra	ES0012R	-1.10	39.08	885	56	70	-9.7	-2.8	0.88	0.87
VIillar Del Arzobispo	ES1671A	-0.83	39.71	430	60	48	-3.6	3.4	0.66	0.59
Cirat	ES1689A	-0.47	40.05	466	60	37	-20.5	-13.8	0.71	0.69
Bujaraloz	ES1400A	-0.15	41.51	327	60	60	-16.7	-9.4	0.59	0.58
Morella	ES1441A	-0.09	40.64	1150	53	51	8.3	13.0	0.79	0.78
Bc-La Senia	ES1754A	0.29	40.64	428	59	21	-23.1	-16.3	0.61	0.63
Ay-Gandesa	ES1379A	0.44	41.06	368	58	15	14.9	20.9	0.53	0.51
Ak-Pardines	ES1310A	2.21	42.31	1226	57	81	3.8	9.5	0.51	0.47
Hospital Joan March	ES1827A	2.69	39.68	172	57	3	NA	NA	NA	NA
Al-Agullana	ES1201A	2.84	42.39	214	60	25	-51.7	-44.4	0.69	0.67
Av-Begur	ES1311A	3.21	41.96	200	56	9	-7.3	-0.9	0.79	0.75
Plan Aups/Ste Baume	FR03027	5.73	43.34	675	54	21	3.7	8.2	0.63	0.57
Gharb	MT00007	14.20	36.07	114	57	31	-12.8	-8.5	0.69	0.70
Aliartos	GR0001R	23.11	38.37	110	59	18	NA	NA	NA	NA
NEO	-	21.67	37.00	50	60	2	NA	NA	NA	NA
Finokalia	GR0002R	25.67	35.32	250	57	4	-4.6	0.4	0.77	0.75
Agia Marina	CY0002R	33.06	35.04	532	55	14	4.5	7.5	0.82	0.82

3.4 Validation with AirBase observations in Mediterranean

The surface ozone validation analysis over the Mediterranean is based on an evaluation against station observations from the Airbase Network (http://acm.eionet.europa.eu/databases/airbase/). In addition, 1 station from the Department of Labour Inspection - Ministry of Labour and Social Insurance, of Cyprus (http://www.airquality.dli.mlsi.gov.cy/) is used in the validation analysis. For the validation analysis, stations in the Mediterranean located within about 100 km from the shoreline of the Mediterranean shore are used. Table 3.4.1 shows the names, coordinates, elevation and the MNMBs and correlations obtained with the 2 forecast runs (o-suite and control). It indicates that the variance explained by each station of both the o-suite and control is high and correlations are highly significant over Western, Central and Eastern Mediterranean. It should be noted that the o-suite run reproduces slightly better than the control run the surface ozone day-to-day variability over the majority of the Mediterranean stations (see Table 3.4.1).

In terms of biases, o-suite MNMBs vary between -20% and 15% depending on the stations over the Mediterranean shore of Spain. The control MNMBs are on average 6% higher than o-suite MNMBs. Over the stations Plan Aups/Ste Baume in France the o-suite overestimates surface ozone concentrations by 4% while over Gharb station in Malta O_3 is underestimated by -13%. Again, the control MNMBs are slightly higher by 4.5% than the o-suite MNMBs. Over Finokalia station in Crete the o-suite underestimates surface ozone by -4.5% while the control run has almost zero bias. Finally, over Agia Marina in Cyprus both, the o-suite and the control run overestimate surface ozone values by 4.5% and 7.5% respectively.

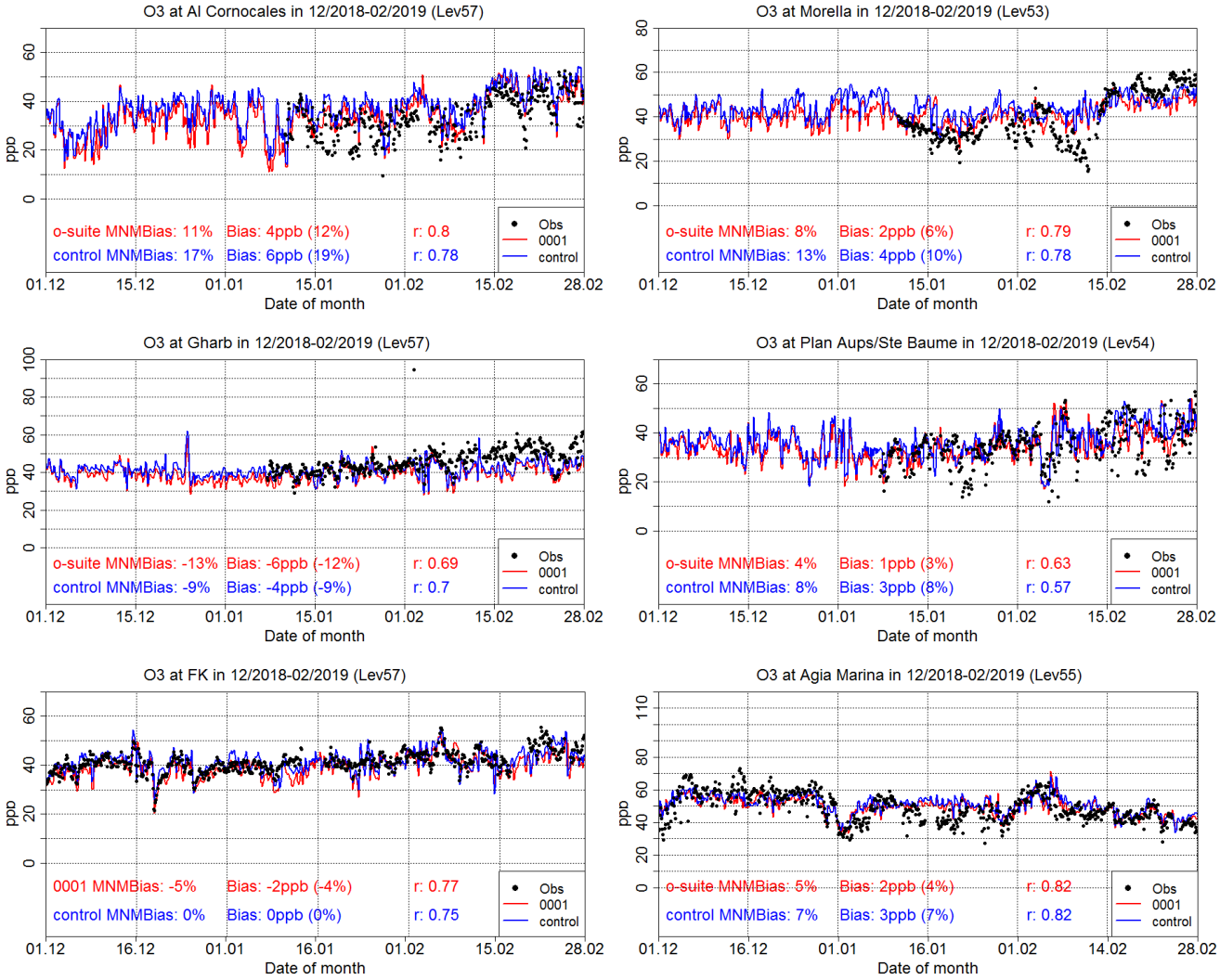

Figure 3.4.1: Time series for the o-suite (red) and Control (blue) compared to Airbase observations at Al Cornocales, Spain station (36.23°N, 5.66 °W, top left), at Morrela, Spain station (40.64°N, 0.09°W, top right), at Plan Aups/Ste Baume, France station (43.34°N, 5.73°E, center left), at Gharb, Malta station (36.07°N, 14.20°E, center right at Finokalia, Crete Greece station (35.32°N, 25.67°E, bottom left) and compared to observations provided by the Department of Labour Inspection - Ministry of Labour and Social Insurance of Cyprus) at Agia Marina, Cyprus station (35.04°N, 33.06 °E, low right).

The spatial distribution of MNMBs and the correlation coefficients of the o-suite over the Mediterranean are shown in 3.4.2, where it is evident that correlations over the entire Mediterranean from Gibraltar to Cyprus are highly significant. It is also evident that the CAMS NRT runs have a better performance over Central and Eastern Mediterranean compared to the Mediterranean shore of Spain in terms of biases.

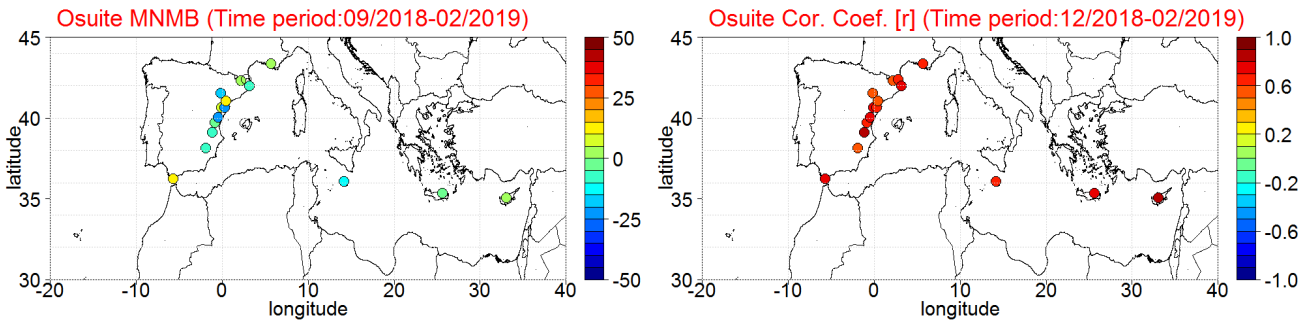

Figure 3.4.2: Spatial distribution of MNMB in % (left) and correlation coefficient (right) of the o-suite run compared to observational data during the period from 1 December 2018 to 28 February 2019.

3.5 Validation with IASOA surface observations

Model results were compared to surface O_3 observations from the Villum Research Station, Station Nord in north Greenland (81.6°N 16.7°W), Alert Nunavut, Canada (82.5°N 62.5°W), and Zeppelin Mountain, Svalbard (78.9°N 11.9°E) from the IASOA network, Fig. 3.5.1.

The data from Svalbard and VRS are covering the period from December 2014 to January 2019 and Data from Alert covers the period January 2016 – February 2019. Ozone depletion events in March – June in 2015 – 2018 are not captured by the model simulations during spring at any of the sites. These events are related to halogen chemistry reactions that are not represented in the model simulations. The simulations are on average in good agreement with the observations apart from the spring depletion events.

For the period December 2018 – February 2019 the measurements are not quality controlled. The bias is low with a tendency for underestimation for the o-suite for the three stations (-12% - -4%) and mainly overestimation (-2% - 9%) for the control run (Table 3.5.1). The negative bias in the winter period is seen to be a recurring event although the performance is improved compared to previous years (Fig. 3.5.1). The control run performs better than the o-suite in terms of the correlation; r = 0.64 – 0.70 for the o-suite compared to r = 0.67 – 0.74 for the control run.

Table 3.5.1. Normalised Mean Bias (NMB) and correlation coefficient (r) of the Control and the O-suite simulations for the sites Alert, Svalbard, and Villum Research Station (VRS) for the period December 2018 – February 2019.

		NMB	R
Alert	o-suite	-0.04	0.69
	control	0.09	0.73
Svalbard	o-suite	-0.12	0.64
	control	-0.01	0.67
VRS	o-suite	-0.06	0.70
	control	0.06	0.74

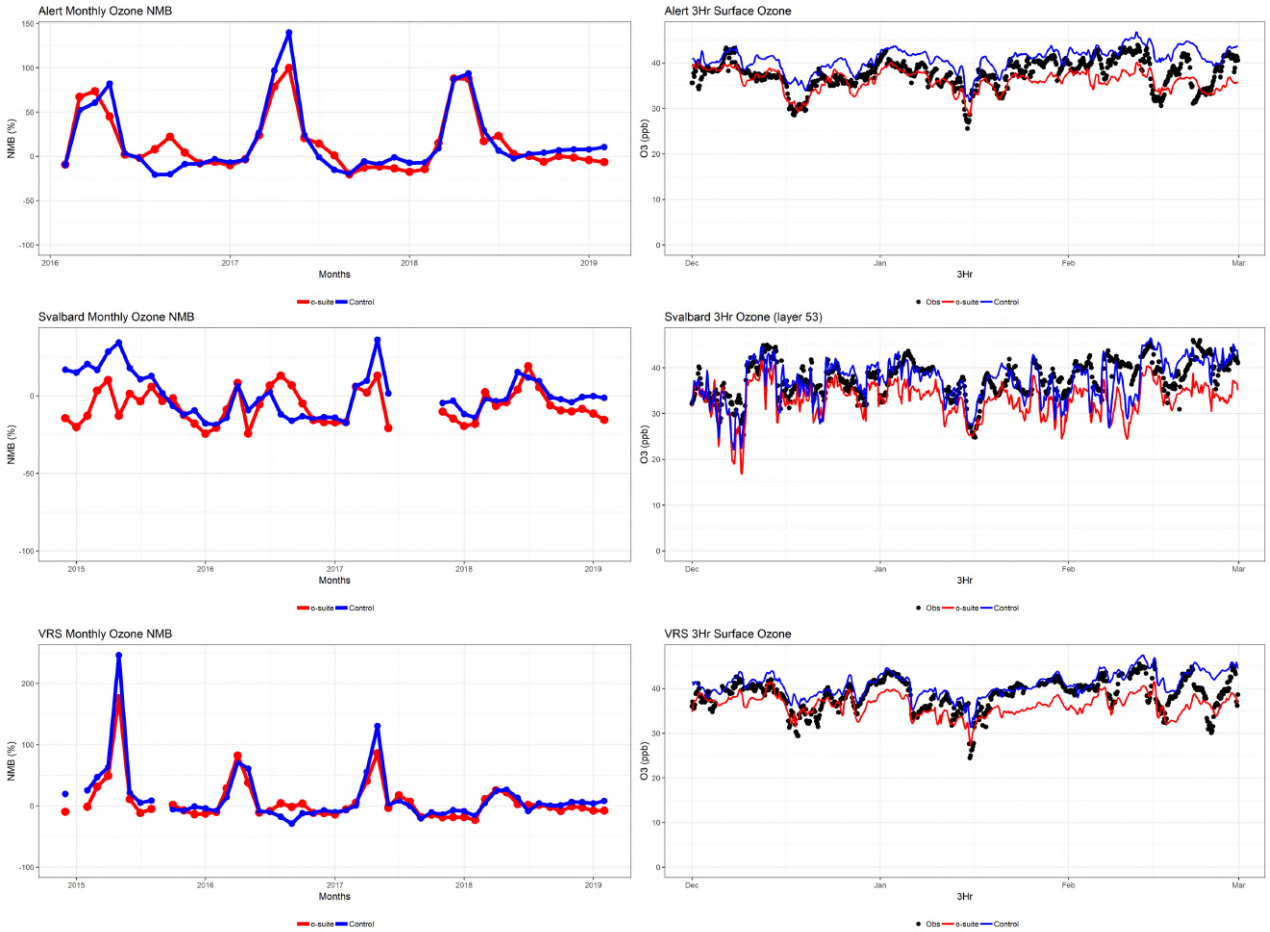

Figure 3.5.1: Time series for o-suite (red) and Control (blue) compared to observations (black dots) at Alert, Nunavut, Canada (Top row) Svalbard (second row), and the Villum Research Station, Station Nord, Greenland (bottom row) NMB for the full period (left) and concentrations for December 2018 – February 2019 (right).

3.6 Validation with IASI data

CAMS o-suite and control O_3 total column data are compared with IASI Metop-A version v20151001 satellite observations (Clerbaux et al., 2009). For the comparison with the IASI data, the vertically integrated model O_3 data were transformed using IASI averaging kernels (Rodgers, 2000).

The global distribution of the O_3 total column obtained from IASI, as well as the relative difference between the model runs and IASI, are shown in Fig. 3.6.1 for January 2019. In January 2019, IASI shows high O_3 over the northern mid-latitudes and relatively low values over the Northern Hemisphere low latitudes. The o-suite run captures the high as well as low O_3 values relatively well and is in good agreement with the observations, showing MNMBs within 5%. The high O_3 values over the north-eastern part of North America are underestimated by up to 20%. The control run is mainly negatively biased (up to 20% over the high southern latitudes). The low value band in the Northern hemispheric low latitudes is slightly overestimated (MNMBs within +5%).

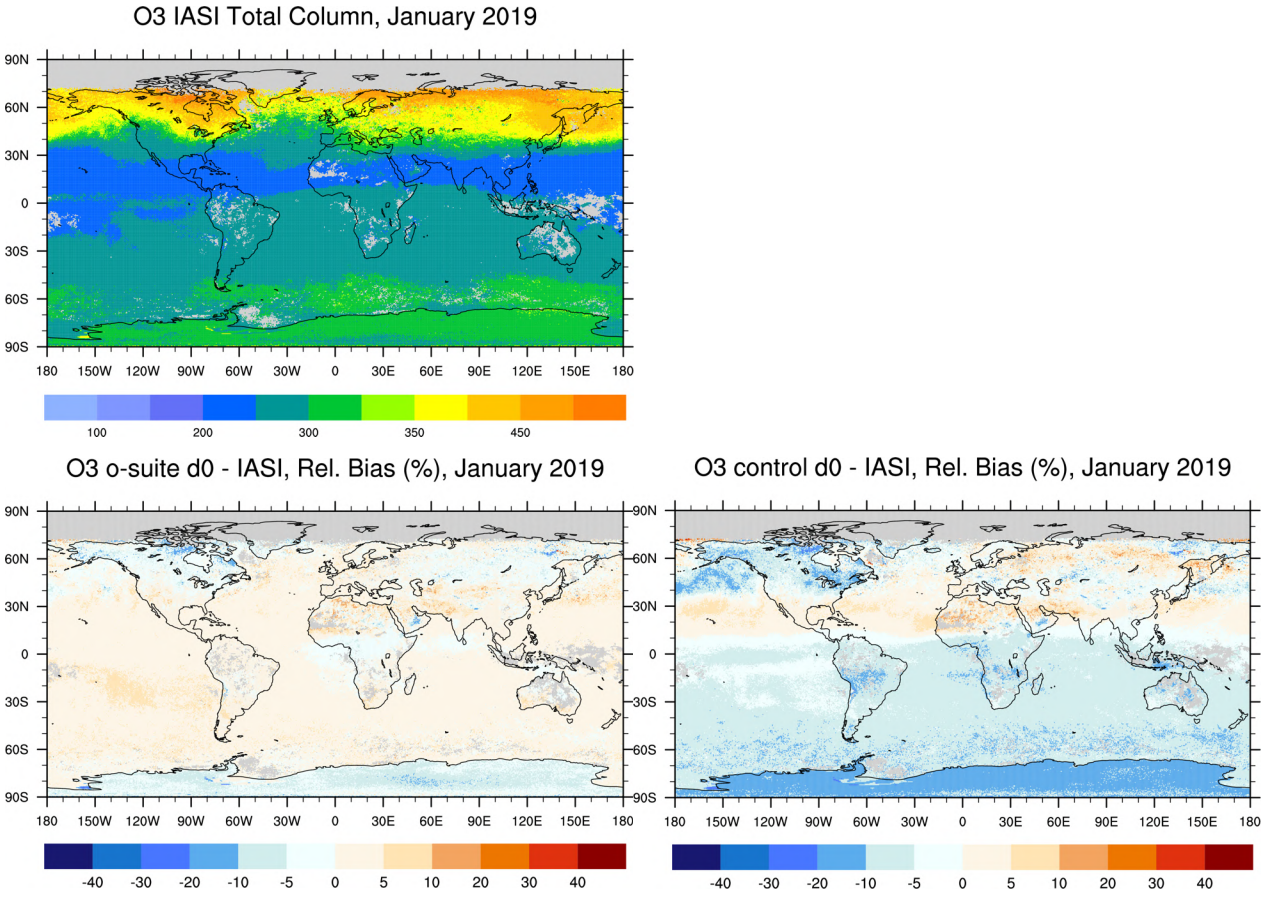

Figure 3.6.1: O_3 total column for IASI satellite observations (top) and relative difference between the model runs and IASI for January 2019: o-suite (lower left), control run (lower right). Grey colour indicates missing values.

4. Carbon monoxide

4.1 Validation with Global Atmosphere Watch (GAW) Surface Observations

For the Near-Real-Time (NRT) validation, 10 GAW stations have delivered CO surface mixing ratios in NRT and data is compared to model results as described in Eskes et al (2018) and is used for CAMS model evaluation for December 2018– February 2019. The latest validation results can be found on the CAMS website, see section 1.

For stations in the Northern Hemisphere, both runs mostly show slightly negative MNMBs. For the stations located in the Southern Hemisphere, both runs show a slight positive offset.

For most stations, the MNMBs and correlation coefficients indicate that the forecast remains stable for the D+2.

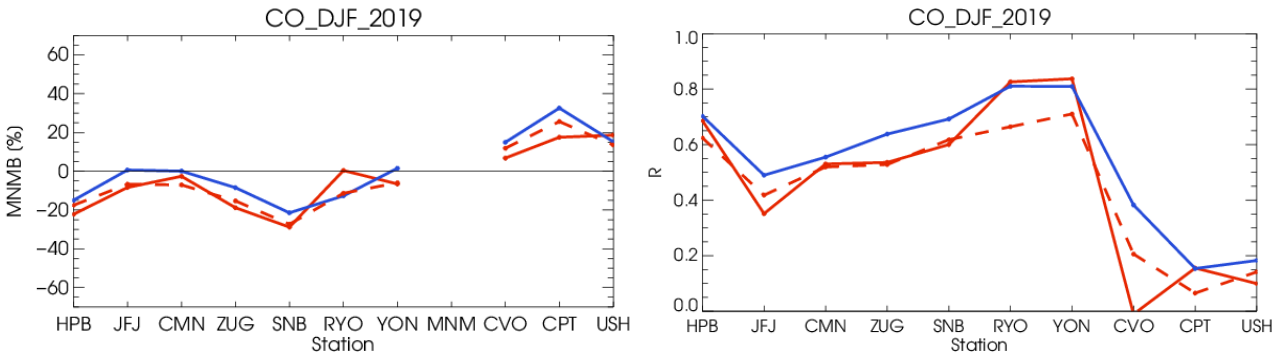

Figure 4.1.1: Modified normalized mean bias in % (left) and correlation coefficient (bottom right) of the NRT model runs compared to observational GAW data in the period December 2018 to February 2019 (o-suite: solid red, D+2: red-dashed, and control: blue).

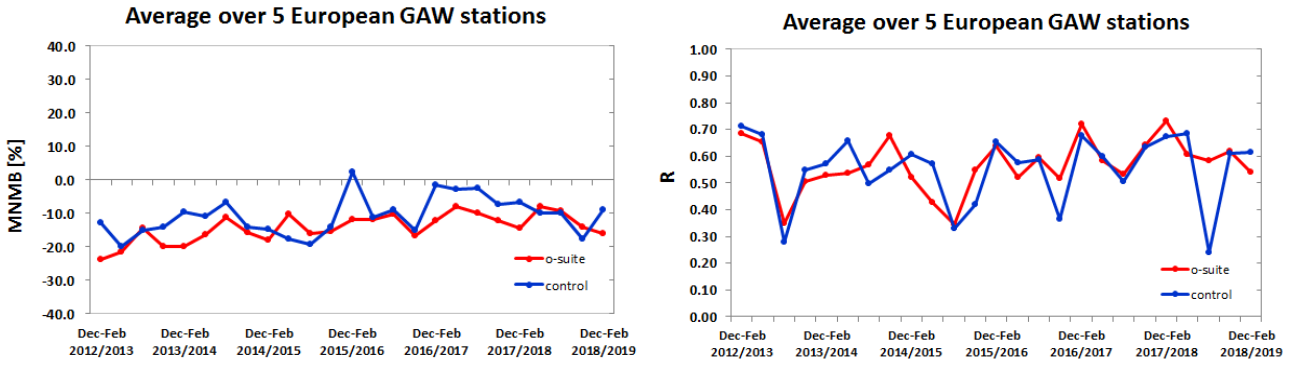

Figure 4.1.2: Long term (Dec. 2012 – February 2019) evolution of seasonal mean MNMB (left) and correlation (right), as averaged over 5 GAW stations in Europe, for o-suite (red) and control (blue).

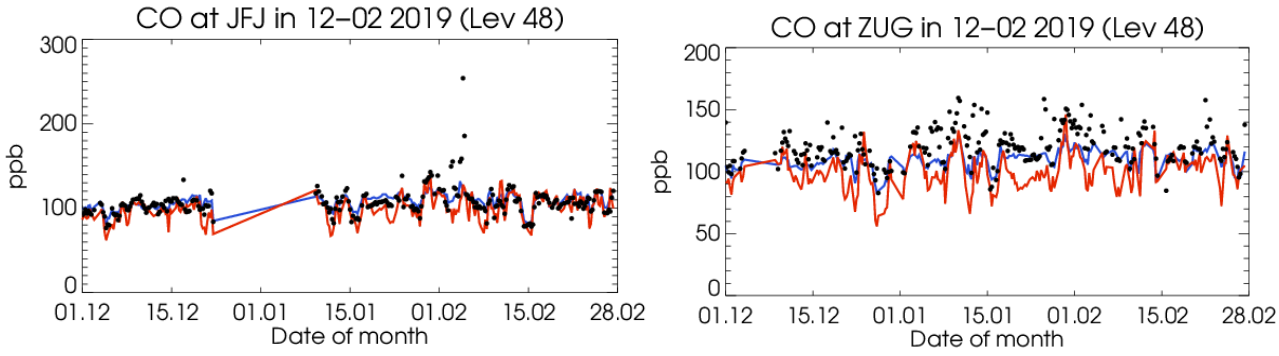

Figure 4.1.3: Time series for the o-suite (red) and control (blue) compared to GAW observations at Jungfraujoch (46.55°N, 7.99°E) and Zugspitze (47.4°N, 10.9°E)

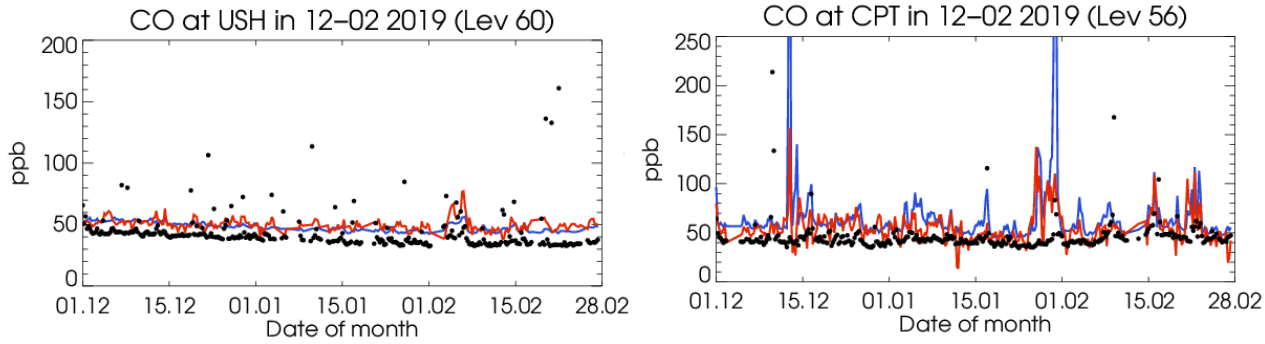

Figure 4.1.4: Time series for the o-suite (red) and control (blue) compared to GAW observations at Ushuaia (-54.85°N, -68.32°W) and Cape Point (34.35°S, 18.5°E).

A comparison of the seasonal-mean MNMB over Europe (Fig. 4.1.2) from December 2012 to present shows a slowly improving MNMB from about -20% in 2013 to about -10% for more recent periods. Temporal correlation remains relatively constant at r=0.6 on average, except for the quarter JJA in 2018, where the correlation of the control run drops to 0.24.

For European stations, the o-suite shows an underestimation of observed CO mixing ratios, with MNMBs between -2% and -28%. The control shows slightly higher CO mixing ratios for European stations with MNMBs between -22% and 0%. Correlation coefficients are between 0.35 and 0.68 for the o-suite and between 0.48 and 0.70 for the control run.

For stations in Asia (RYO, YON, MNM) both runs show a good correspondence with the observations with MNMBs between 0 and -12%, see Fig. 4.1.5. Correlation coefficients range between 0.80 and 0.83.

For the two stations in the Southern Mid-latitudes (CPT and USH) the models shows an overestimation of CO with MNMBs between 15% and 32% (control) and around 18% (o-suite). The control run shows large CO peaks in December and February that are not present in the observations and that are reduced by the data assimilation (Fig.4.1.4.)

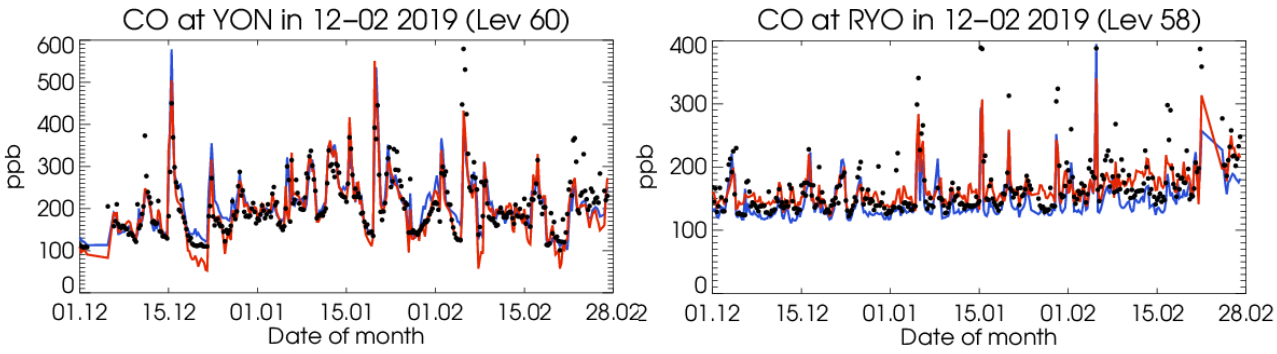

Figure 4.1.5: Time series for the o-suite (red) and control (blue) compared to GAW observations for Yonagunijima (24.47°N, 132.02°E) and Ryori (39.03°N, 141.82°E).

4.2 Validation with IAGOS Data

Due to issues on most CO sensors, no IAGOS profiles for CO are available for the period DJF 2019.

4.3 Validation against FTIR observations from the NDACC network

In this section, we compare the CO profiles of the CAMS models with available FTIR measurements at stations within the NDACC network. These ground-based remote-sensing instruments are sensitive to the CO abundance in the troposphere and lower stratosphere, i.e. between the surface and up to 20 km altitude. Tropospheric CO columns are validated. A description of the instruments and applied methodologies can be found at http://nors.aeronomie.be.

Figure 4.3.1 show that the o-suite tropospheric columns of CO agree well. All biases for the o-suite analysis and 1d forecast are within the measurement uncertainty. For the NH mid-latitude stations, the bias becomes slightly negative (<-5%) since JJA 2018 compared to the reporting period, which is related to a trend and seasonal cycle observed in the relative differences, see Fig. 4.3.2. For the SH, the bias changes sign but remains within the 5% range.

For all stations in the southern hemisphere, the control run overestimates the CO with MBs up to 20%.

The Taylor diagrams in Figure 4.3.3 provide information on the correlation of all three models under consideration with the FTIR time series. Leaving out the sites with few measurements, the assimilation has a positive effect on the correlation coefficient. Looking at the correlation values for the period 2018 DJF, the o-suite 1-day forecast (averaged correlation for all sites is 0.86) is comparable to the o-suite analysis (averaged correlation for all sites is 0.83) and higher than the control run (averaged correlation of 0.77). The number of measurements in this period is limited because the majority of the sites are situated in the NH. The variability of the measured columns is comparable to the variability of the corresponding model columns (approximately by a factor of 0.9).

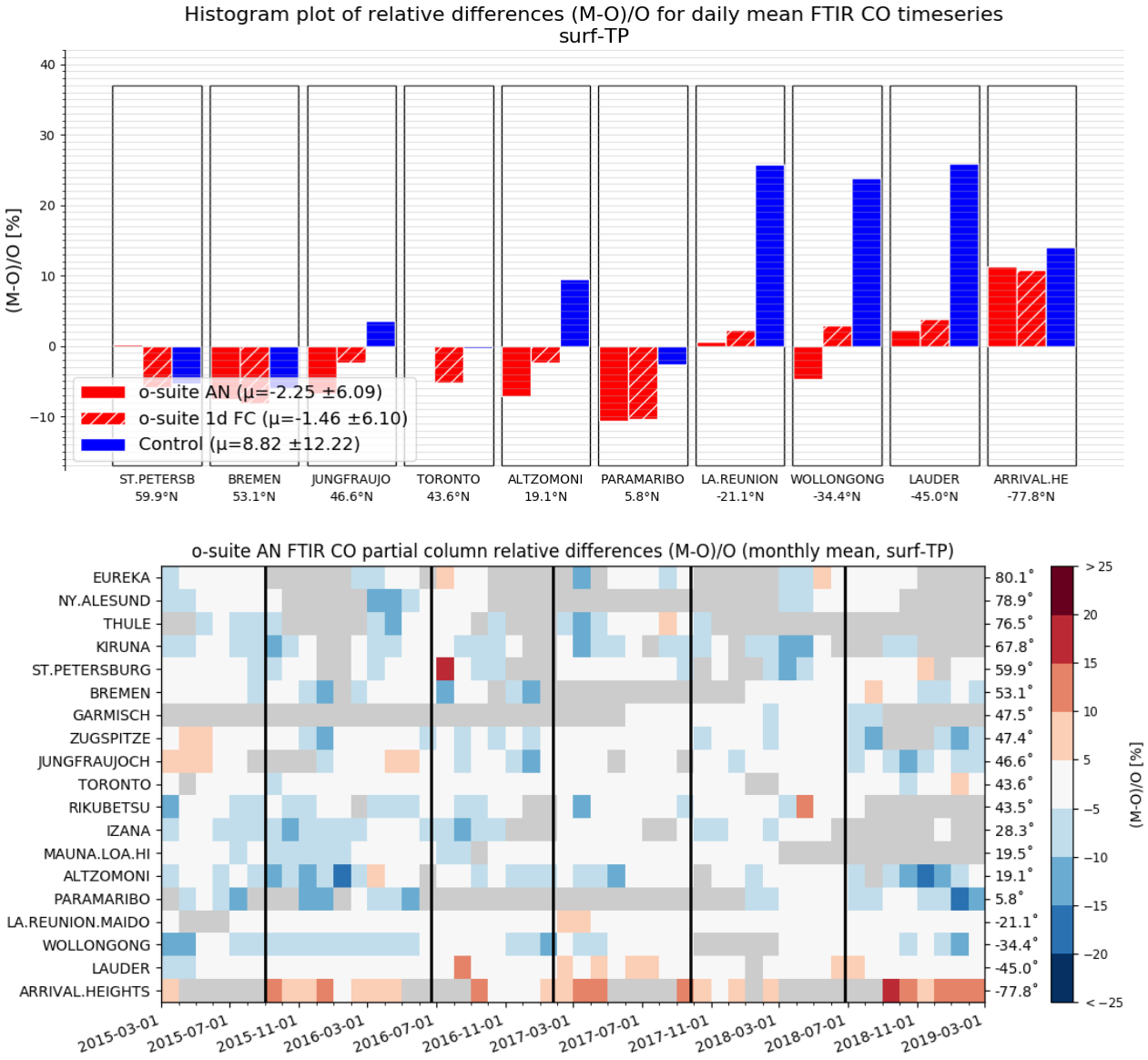

Figure 4.3.1: Seasonal relative mean bias for tropospheric CO columns (MB, %) against NDACC FTIR data for the considered period 2018 DJF (top) and monthly mean biases for a longer time period (bottom, model upgrades are indicated in black vertical lines).The overall uncertainty for the CO measurements is approximately 5% and the o-suite analysis averaged bias for all stations is -2.25% for DJF. Stations are sorted with decreasing latitude (northern to southern hemisphere).

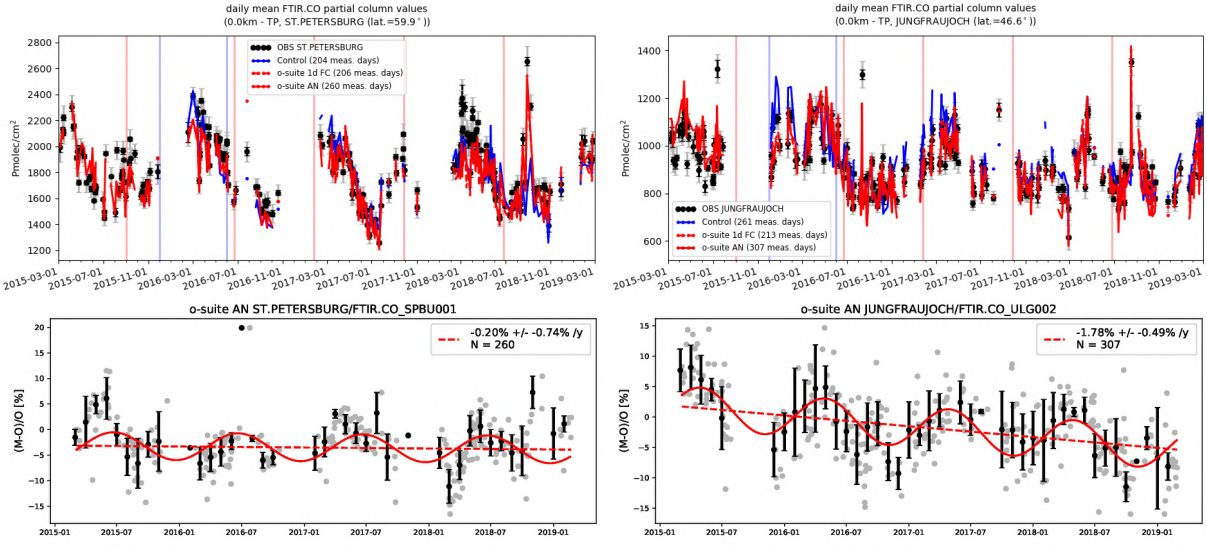

Figure 4.3.2: Top: daily mean values of tropospheric CO columns by the o-suite (AN and 1d FC, red) and the Control run (blue) compared to NDACC FTIR data at St Petersburg and Jungfraujoch for the period March 2015-February 2019. The CAMS upgrades are indicated by the vertical lines. The bottom row contains a linear fit and seasonal cycle fit through the relative differences for the o-suite AN. An underestimation is observed during the local autumn/winter months.

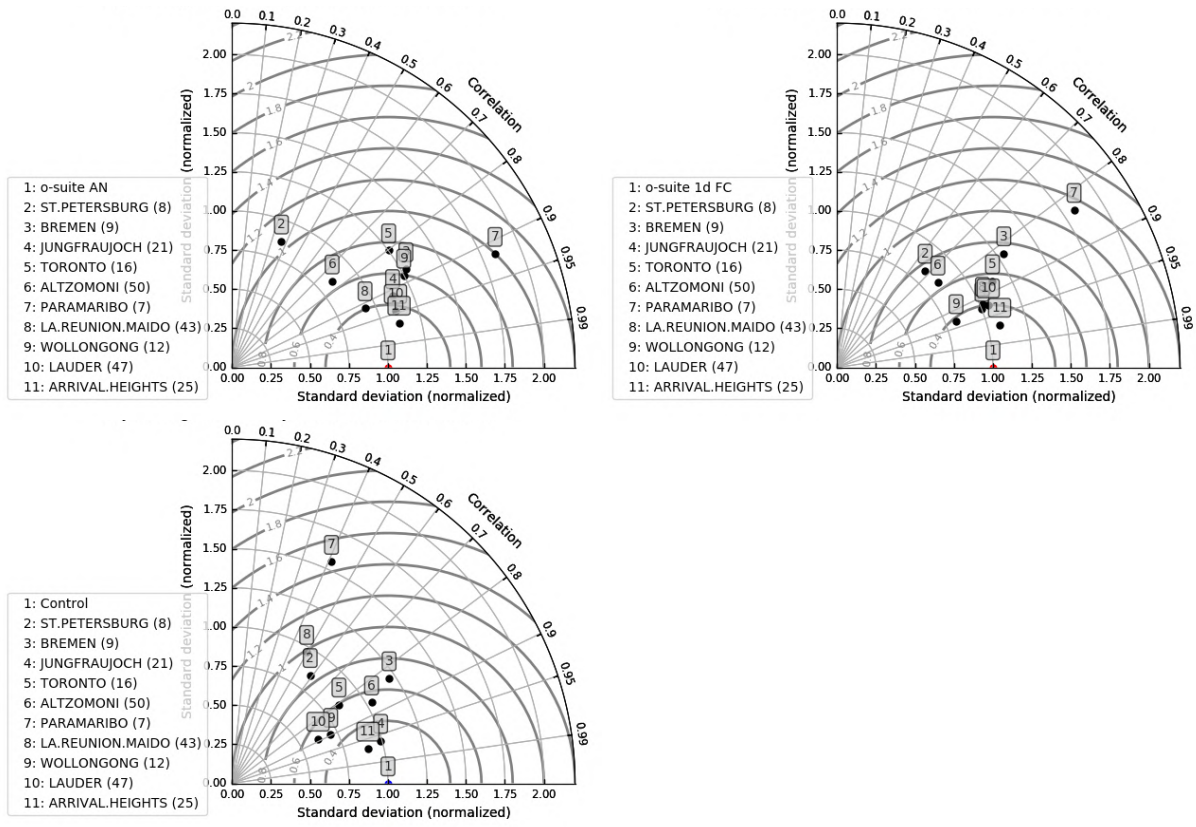

Figure 4.3.3: Taylor diagrams relating the standard deviations for the model /GB time series of daily tropospheric CO column data and their correlation. All time-series are normalized such that the standard deviation of the model is 1. The control run has higher variability in the CO columns compared to the FTIR variability.

4.4 Validation against FTIR observations from the TCCON network

CO column averaged mole fractions of the CAMS models are compared with data from the Total Carbon Column Observing Network (TCCON). For the validation column averaged mole fractions of CO (denoted as XCO) are used. Column averaged mole fractions provide different information content than the in-situ measurements and are therefore complementary to the in-situ data. Only measurements within 2.5h around local noon have been used for the comparison. The reason is that at high solar zenith angles the comparisons worsen due to the averaging kernels.

In this section, we compare column averaged mole fractions of CO of the CAMS models with TCCON retrievals. Data from the following TCCON sites has been used: Izana (Blumenstock et al., 2017), Reunion (De Mazière et al., 2017), Bialystok (Deutscher et al., 2017), Manaus (Dubey et al., 2017), Four Corners (Dubey et al., 2017), Ascension (Feist et al., 2017), Anmeyondo (Goo et al., 2017), Darwin (Griffith et al., 2017), Wollongong (Griffith et al., 2017), Karlsruhe (Hase et al., 2017), Edwards (Iraci et al., 2017), Indianapolis (Iraci et al., 2017), Saga (Kawakami et al., 2017), Sodankyla (Kivi et al., 2017), Hefei (Liu et al., 2018), Tsukuba (Morino et al., 2017), Burgos (Morino et al., 2018), Rikubetsu (Morino et al., 2017), Bremen (Notholt et al., 2017), Spitsbergen (Notholt et al., 2017), Lauder (Sherlock et al., 2017, Pollard et al., 2019), Eureka (Strong et al., 2018), Garmisch (Sussmann et al., 2017), Zugspitze (Sussmann et al., 2018), Paris (Te et al., 2017), Orleans (Warneke et al., 2017), Park Falls (Wennberg et al., 2017), Caltech (Wennberg et al., 2017), Lamont (Wennberg et al., 2017), Jet Propulsion Laboratory (Wennberg et al., 2017), East Trout Lake (Wunch et al., 2017)

For the validation of the models in December, January and February only data from Edwards, Orleans, Karlsruhe and Izana is available (Fig. 4.4.1). For Edwards, Karlsruhe and Izana, data is only available for December. Since Edwards and Karlsruhe only have one measurement day in December these data are not used in this report.

The reason for the changing availability of TCCON data is the following: The requirement for TCCON data to become public is 1 year after the measurement. Some TCCON groups make their data earlier available. In the previous CAMS-84 project only data from Bialystok, Orleans and Reunion was timely available for the validation of the CAMS models. The Bialystok site has stopped operation and the instrument is currently being transported to Cyprus. Reunion had technical problems and is currently not operational. It is likely that for future reports fast data will become available again for these three sites. During the first year of the current CAMS-84 project data was timely available from several TCCON sites. The reason was that during the first year after the launch of the Sentinel 5 precursor (S5p) several sites received funding to make TCCON data timely available for the validation of the S5p CH4 and CO retrievals. Several non-European TCCON partners contributed to this effort. It is likely that for the next report more data become available since the TCCON PIs usually do the data processing before the annual TCCON meeting (May 20-24, 2019) to discuss the measurements from the previous year. However, it is very likely that for future reports after the next report available data is limited to the TCCON sites at Cyprus, Orleans and Reunion.

The comparisons at Izana and Orleans (Fig 4.4.2 and 4.4.3) show that all models capture the seasonality and the differences during the reporting period (Dec 2018, Jan, Feb 2019) are less than 10 ppb for all models at Izana and less than 5 ppb at Orleans.

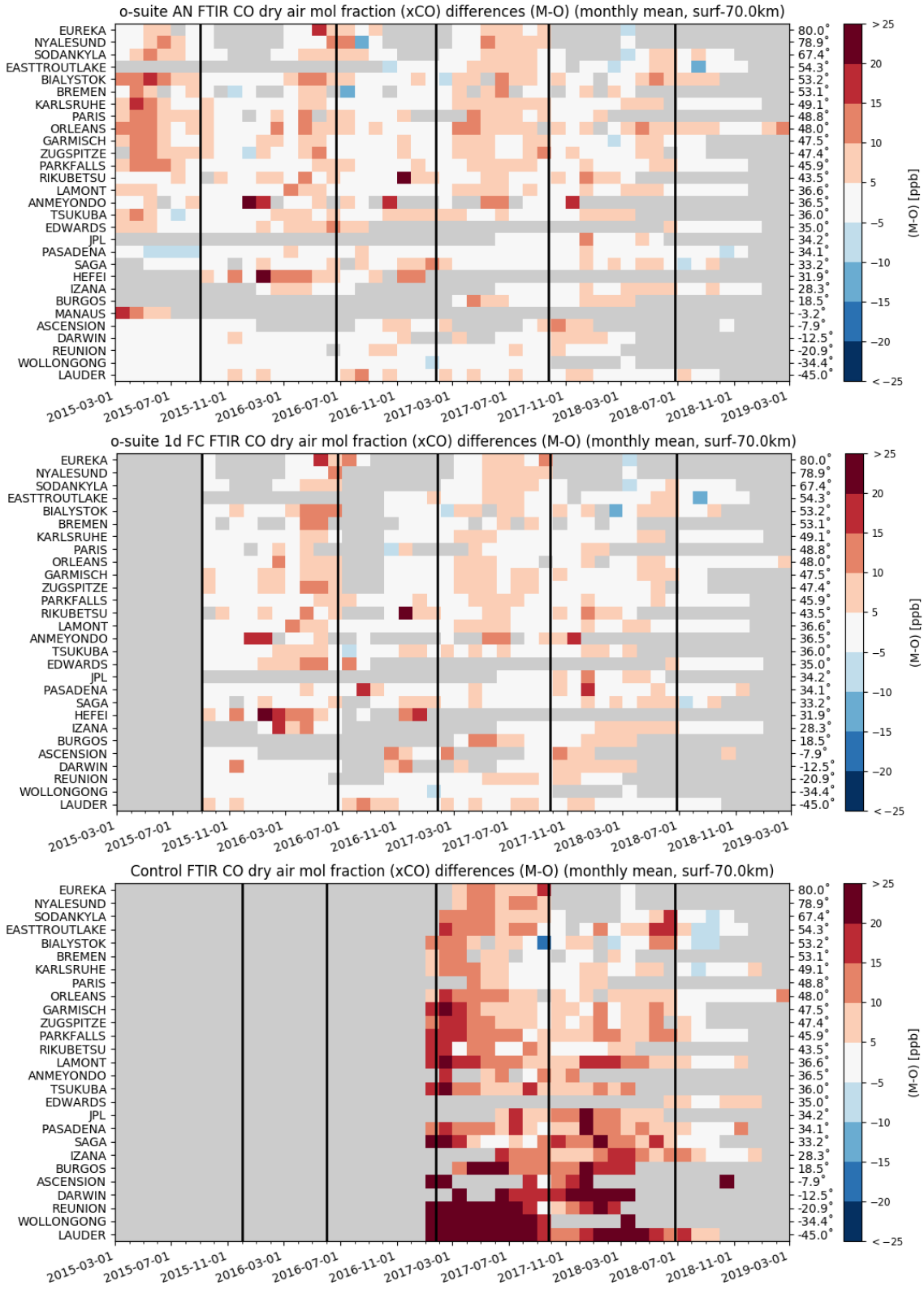

Figure 4.4.1: Monthly differences against TCCON FTIR CO observations for the period March 2015 - February 2019, for the o-suite analysis (top), o-suite 1-day forecast (middle) and control run (bottom). The stations are sorted by latitude (northern to southern hemisphere).

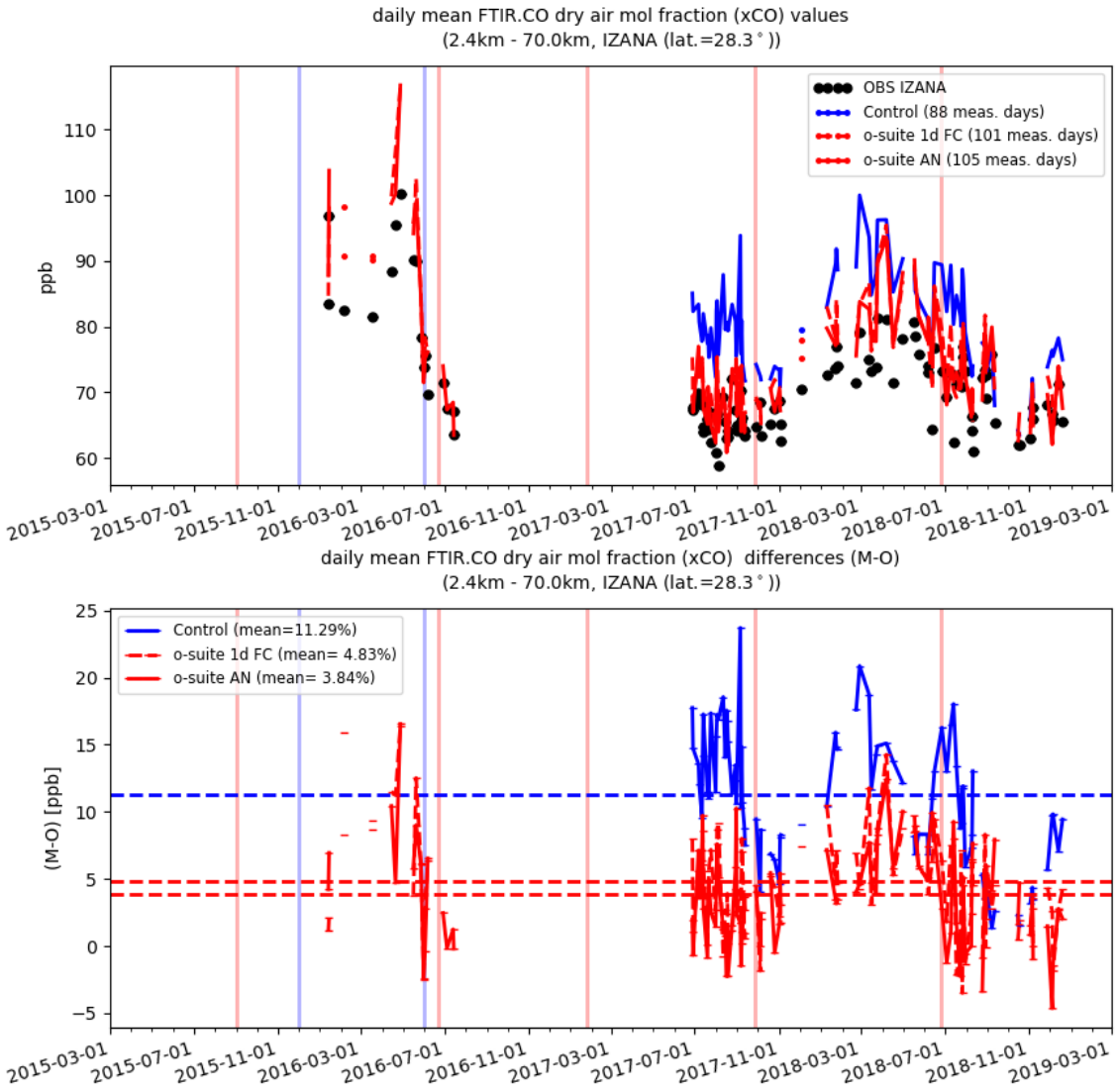

Figure 4.4.2: Comparison of the CAMS CO results with TCCON CO at Izana, for the period March 2015 to February 2019. Blue: control run; red solid: o-suite analysis; red dashed: o-suite 1-day forecast.

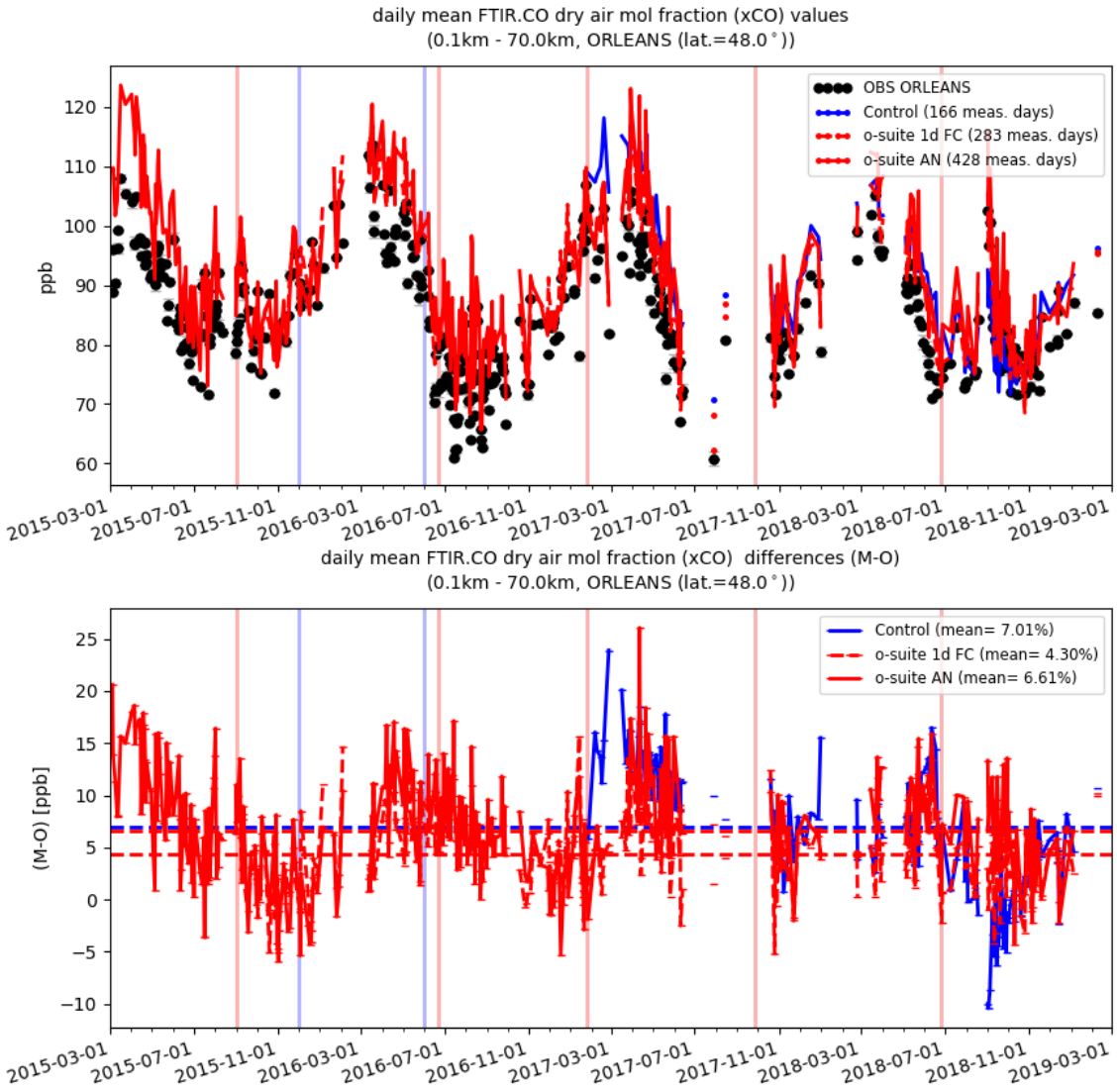

Figure 4.4.3: Comparison of the CO model data with TCCON CO at Orleans, for the period March 2015 to February 2019. Blue: control run; red solid: o-suite analysis; red dashed: o-suite 1-day forecast.

4.5 Evaluation with MOPITT and IASI data

In this section, modeled CO total columns are compared to MOPITT versions 6 and 7 (thermal infrared radiances) (Emmons et. al., 2009, Deeter et al., 2010) and IASI satellite retrievals (Clerbaux et al., 2009). Figure 4.5.1 shows the global distribution of CO total columns retrieved from MOPITT V7 (top left) and IASI (top right) and the relative biases of the model runs with respect to MOPITT V7 for January 2019.

In January 2019, both, MOPITT and IASI show high CO values over the biomass burning areas in Central Africa and over the East of China and part of Indochina. The IASI observations show somewhat higher values than MOPITT especially over the above-mentioned regions with high CO emissions. The modeled CO geographical distribution and magnitude of values show that the model performs reasonably well. The relative difference between the model runs and MOPITT shows that, the o-suite performs better than the control run without data assimilation, with some regional

biases by about ±10% (except over the biomass burning areas). Both runs have a positive bias over biomass burning areas in Central Africa and South America and partly over Asia that amounts up to about 20% for the o-suite run and up to 40% for the control run (also over Indonesia). The control run in general overestimates the satellite observations over the Southern Hemisphere by about 20-30 % and over the ocean in the Northern Hemisphere by about 10-20%. The o-suite has a negative bias over Patagonia and over some sparse parts of the North African and Asian regions up to 20%. Both runs show a growing positive bias on the 4th forecast day over the fire active areas in North America and Africa and over India and Indonesia (up to 30% for the o-suite and up to 50% for the control run), and strong bias can be seen especially over Eastern China (up to 50%). A growing negative bias can be seen in the o-suite over North Africa (up to 20%).

Figure 4.5.2 shows time series of CO total column for MOPITT V6 and V7, IASI and the model runs over the eight selected regions. For the comparison with MOPITT, the modelled CO concentrations were transformed using MOPITT V7 averaging kernels (Deeter, 2004). Both, MOPITT and IASI CO total columns are assimilated in the o-suite run, while a bias correction scheme is applied to IASI data to bring it in line with MOPITT. MOPITT and IASI CO total columns show a relatively similar variability over different regions. IASI CO values are lower than MOPITT over most regions with some seasonal exceptions till the year 2016. Since then IASI and MOPITT are more consistent with each other over Europe, the US and East Asia. Significant difference between MOPITT and IASI are observed over the Alaskan and Siberian fire regions in winter seasons, with IASI CO total column values lower up to 30%. In North and South Africa, deviations become larger since 2016 with IASI values being higher than MOPITT by up to 20%. The modelled seasonality of CO total columns is in relatively good agreement with the retrievals. In general, the comparison between the o-suite and control run shows that the assimilation of satellite CO has a more positive, pronounced impact on model results over East and South Asia, South Africa, and since the end of 2016, over the US in winter and spring seasons, and smaller impact over the other regions. Since June 2016, the o-suite shows very good agreement with the satellite retrievals over Europe and the US with biases less than 5%. In late summer and early autumn of 2018 over Europe, the control run has larger negative biases compared to the satellite data then early in 2018 and the two previous autumn seasons.

A general reduction of CO emissions from the year 2015 to the year 2018 can be seen over Europe, the US and East Asian regions. The East Asian region shows a decrease in the seasonal maximum compared to previous winters.

The modified normalized mean bias (MNMB) of the model runs compared to MOPITT V7 (Fig. 4.5.3) allows quantifying the impact of the assimilation on the model performance. The o-suite model run shows negative biases over Europe, the US and Alaskan fire regions with some seasonal exceptions. The control run shows a systematic positive bias up to 20% over South Asia in November-December 2014, 2015, 2016, and 2017. Over southern Africa the control run overestimates satellite retrieved values by up to 25% in winter and spring 2015, 2016, and 2017. In general, the o-suite is within +/-10% in all regions, while the control run shows larger biases over East and South Asia and North and South Africa, as well as stronger seasonal cycles.

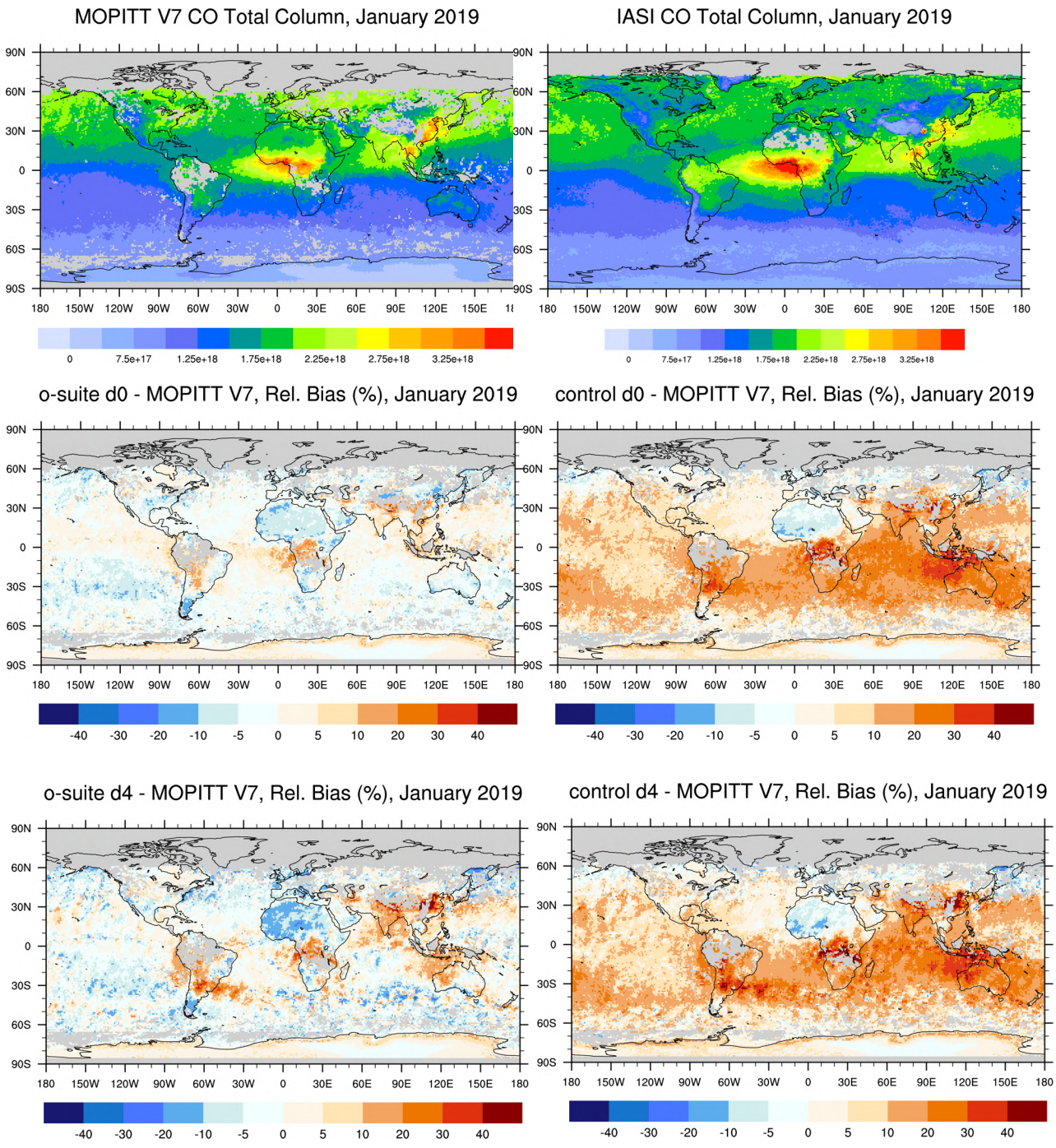

Fig. 4.5.1: CO total columns for MOPITT V7 (top left) and IASI (top right) satellite retrievals and relative difference between the model runs and MOPITT for January 2019: o-suite (middle left), control run (middle right), o-suite 4th forecast day (bottom left), o-suite 4th forecast day (bottom right). Grey colour indicates missing values.

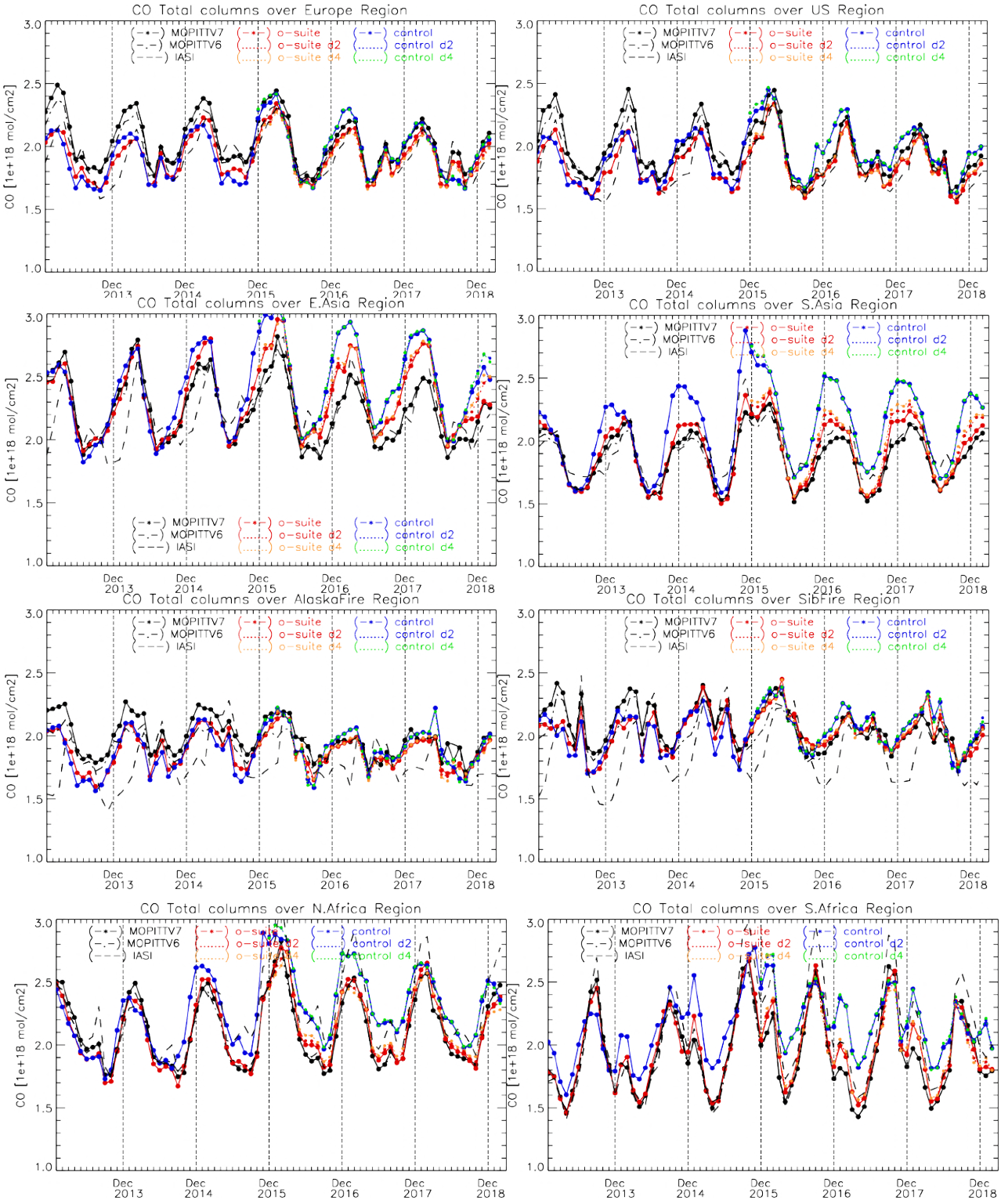

Fig. 4.5.2: Time series of CO total columns for satellite retrievals MOPITT V6 and V7, IASI (black) and the model runs over the selected regions: o-suite (red, solid), control (blue, solid), o-suite 2nd forecast day (red, dotted), o-suite 4th forecast day (orange, dotted), control 2nd forecast day (blue, dotted), control 4th forecast day (green, dotted). Period: January 2013 to February 2019.

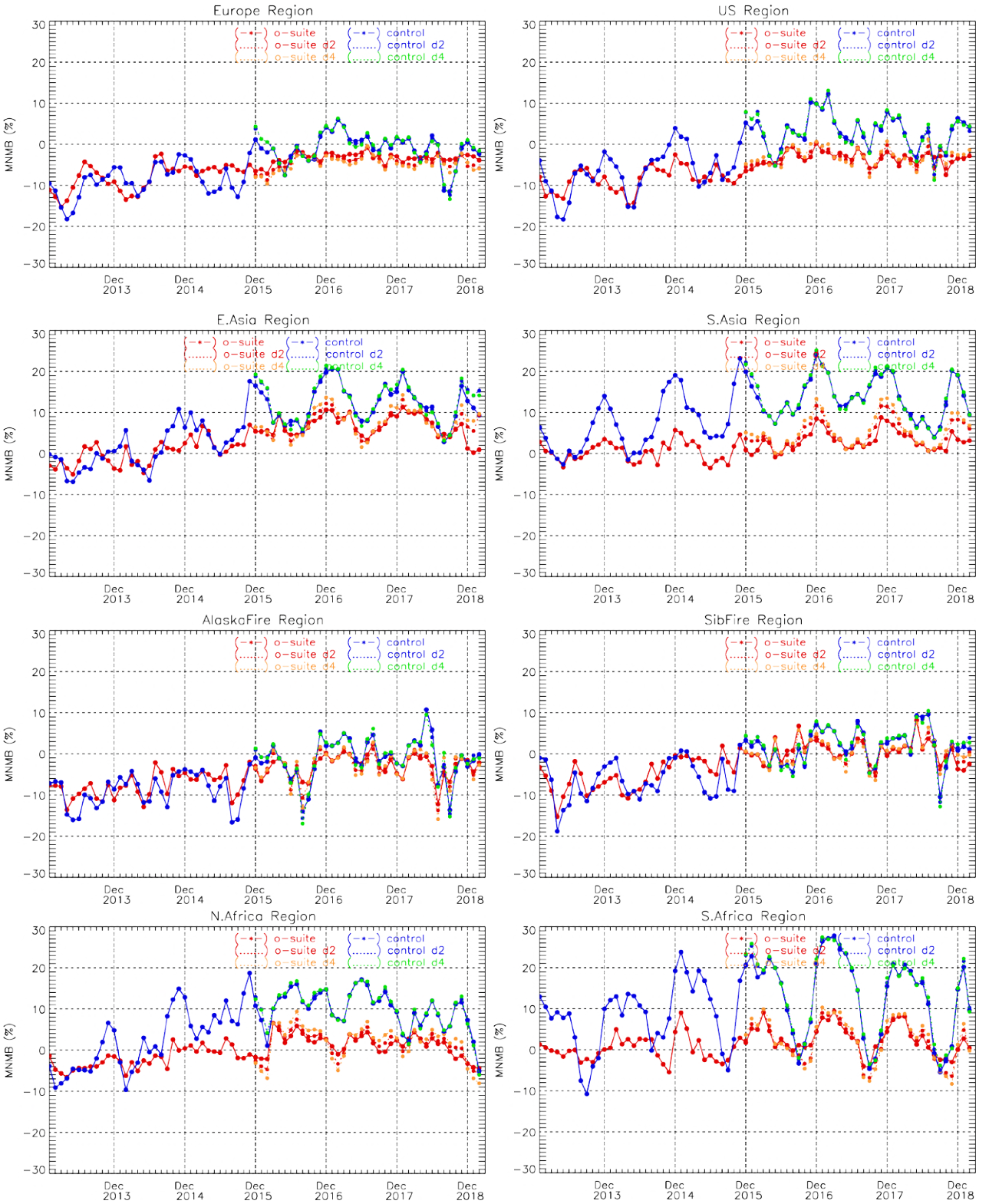

Fig. 4.5.3: Timeseries of modified normalized mean bias (%) for CO total columns from the model simulations vs MOPITT V7 retrievals over selected regions. O-suite (red, solid), control run (blue, solid), o-suite 2nd forecast day (red, dotted), o-suite 4th forecast day (orange, dotted), control 2nd forecast day (blue, dotted), control 4th forecast day (green, dotted). Period: January 2013 to February 2019.

East Asian region shows good improvements indicating high agreement with satellite data. The o-suite bias in DJF is almost 0, whereas it is about 10% during the last two winters and more than 5% in 2018 in general. The bias in the control run is also reduced from 20% during the previous winters to about 10 % in the current winter. In the other side, the biases for the 2nd and 4th forecast days are increased relative to analysis and count more than 5 % positive bias, especially for o-suite (about 10% in February 2019). The o-suite bias is also reduced compared to previous winters in South Asian region. The positive biases for the 2nd and 4th forecast days are slightly higher compared to previous winters (relative to analysis) and count about 5%. In the North African region, the bias changes the sign form positive in previous years to negative in DJF 2019 (-5%). The growing negative biases for the 2nd and 4th forecast days are about 5 and about 8% respectively. The o-suite bias in the South African region is reduced compared to the previous winters from about 8% to 2%.

5. Tropospheric nitrogen dioxide

5.1 Evaluation against GOME-2 retrievals

In this section, model columns of tropospheric NO_2 are compared to SCIAMACHY/Envisat NO_2 satellite retrievals (IUP-UB v0.7) [Richter et al., 2005] for model data before April 2012, and to GOME-2/MetOp-A NO_2 satellite retrievals (IUP-UB v1.0) [Richter et al., 2011] for more recent simulations. This satellite data provides excellent coverage in space and time and very good statistics. However, only integrated tropospheric columns are available, and the satellite data is always taken at the same local time, roughly 10:00 LT for SCIAMACHY and 09:30 LT for GOME-2, and at clear sky only. Therefore, model data are vertically integrated, interpolated in time and then sampled to match the satellite data. GOME-2 data were gridded to model resolution (i.e. 0.4° deg x 0.4° deg). Model data were treated with the same reference sector subtraction approach as the satellite data. Uncertainties in NO_2 satellite retrievals are large and depend on the region and season. Winter values in mid and high latitudes are usually associated with larger error margins. As a rough estimate, systematic uncertainties in regions with significant pollution are on the order of 20% – 30%.

Figure 5.1.1 shows global maps of GOME-2 and model monthly mean tropospheric NO_2 columns as well as differences between retrievals and simulations for January 2019 as an example of the maps for winter 2018/2019. The overall spatial distribution and magnitude of tropospheric NO_2 is well reproduced by both model runs, indicating that emission patterns and NO_x photochemistry are reasonably represented. Some differences are apparent between observations and simulations, with generally larger shipping signals simulated by the models. For example, shipping signals are much more pronounced in model simulations to the south of India. Emissions over Europe and especially the pollution hotspots around the Benelux countries are underestimated. However, other local maxima of values observed over anthropogenic emission hotspots in East Asia (e.g. over the heavily populated Sichuan Basin; 30°N, 105°E), India and others such as Teheran, Mecca, around Lebanon/Israel and Moscow are regularly overestimated.

Closer inspection of the seasonal variation of tropospheric NO_2 in some selected regions (Fig. 5.1.2) reveals significant differences between the models and points to some simulation problems. Over regions where anthropogenic emissions are major contributors to NO_x emissions, models catch the shape of the satellite time series rather well. However, over East-Asia absolute values and seasonality were strongly underestimated before 2014 by all model runs (most likely due to an underestimation of anthropogenic emissions) for all seasons apart from summertime minima, with the o-suite showing the best results since an upgrade in July 2012. As wintertime NO_2 column retrievals decreased since 2014, model simulated wintertime maxima are in better agreement with the satellite retrieved ones for recent years. However, the observed NO_2 decrease is not reproduced by the simulations and therefore the better agreement for more recent years cannot be attributed to model improvements. Moreover, summertime model minima increased in 2015 compared to previous years, which is in contrast to the satellite retrievals, so that the simulated values for the summers since 2015 are about 50% larger than satellite retrieved ones. The observed July and August means of 2018 over East-Asia are a bit lower compared to previous years, but it is still

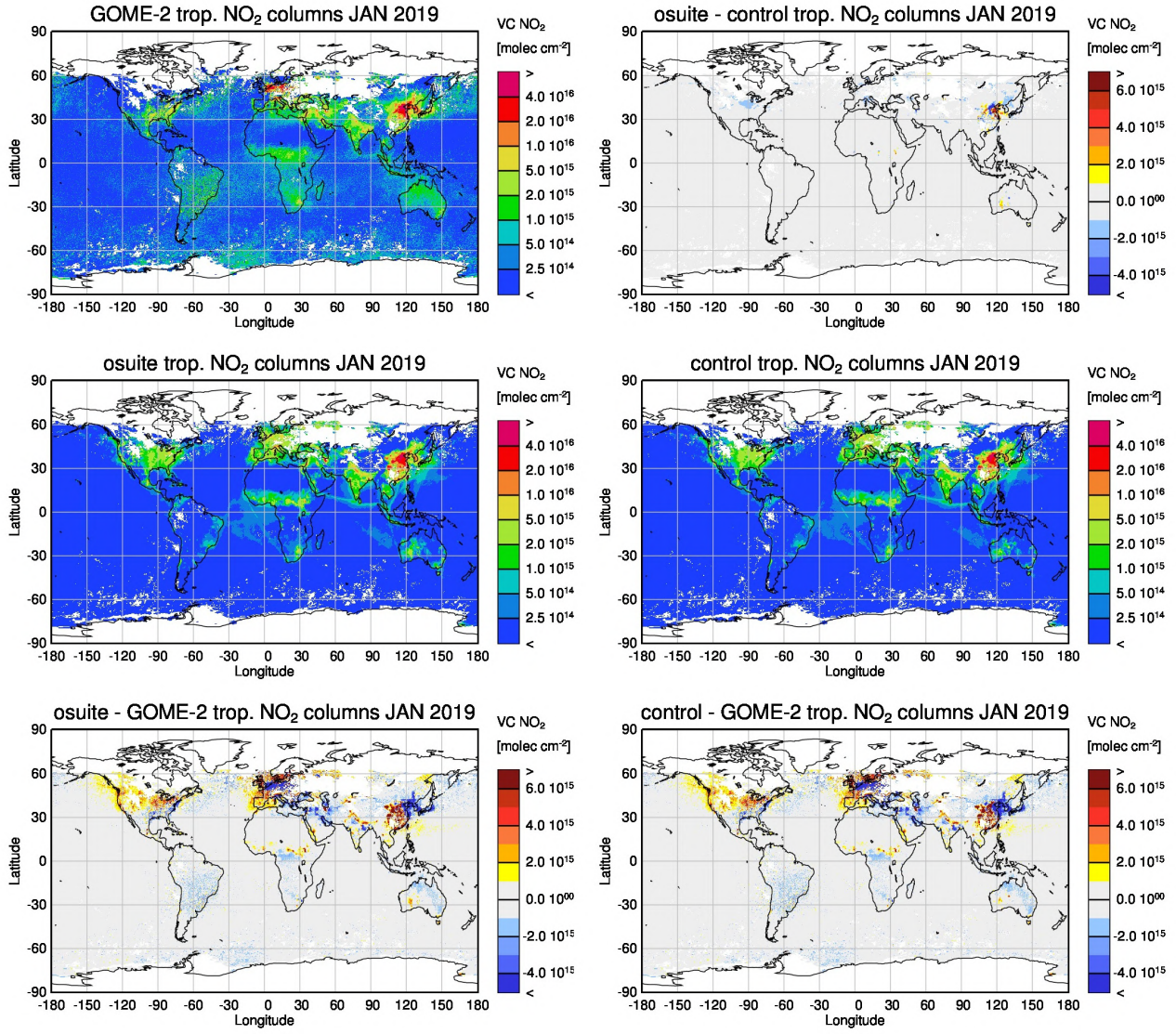

Figure 5.1.1: Global map comparisons of satellite retrieved, and model simulated tropospheric NO2 columns [molec cm-2] for January 2019. The top row shows monthly mean tropospheric NO2 columns retrieved by GOME-2 as well as the difference between o-suite and control, the second row shows the corresponding tropospheric NO2 columns for model simulated averages. The third row shows differences of monthly means between models and GOME-2. GOME-2 data were gridded to model resolution (i.e. 0.4° deg x 0.4° deg). Model data were treated with the same reference sector subtraction approach as the satellite data.

unclear yet if this trend continues over the next summers. The sharp decrease observed by GOME-2 for February 2019 is not reproduced by the simulations. As for East-Asia, a decrease in satellite retrieved values also occurred in 2015 over Europe where a peak is usually found around January, which was, as a result, only slightly underestimated by the models for January 2015. The underestimation of tropospheric NO_2 columns over Europe may be caused to some extent by a change of emission inventories in 2012. However, the situation changed over the previous three winter periods, for which GOME-2 shows (compared to previous years) a strong increase in January peak values, combined with a decrease in values for December and February that is not reproduced

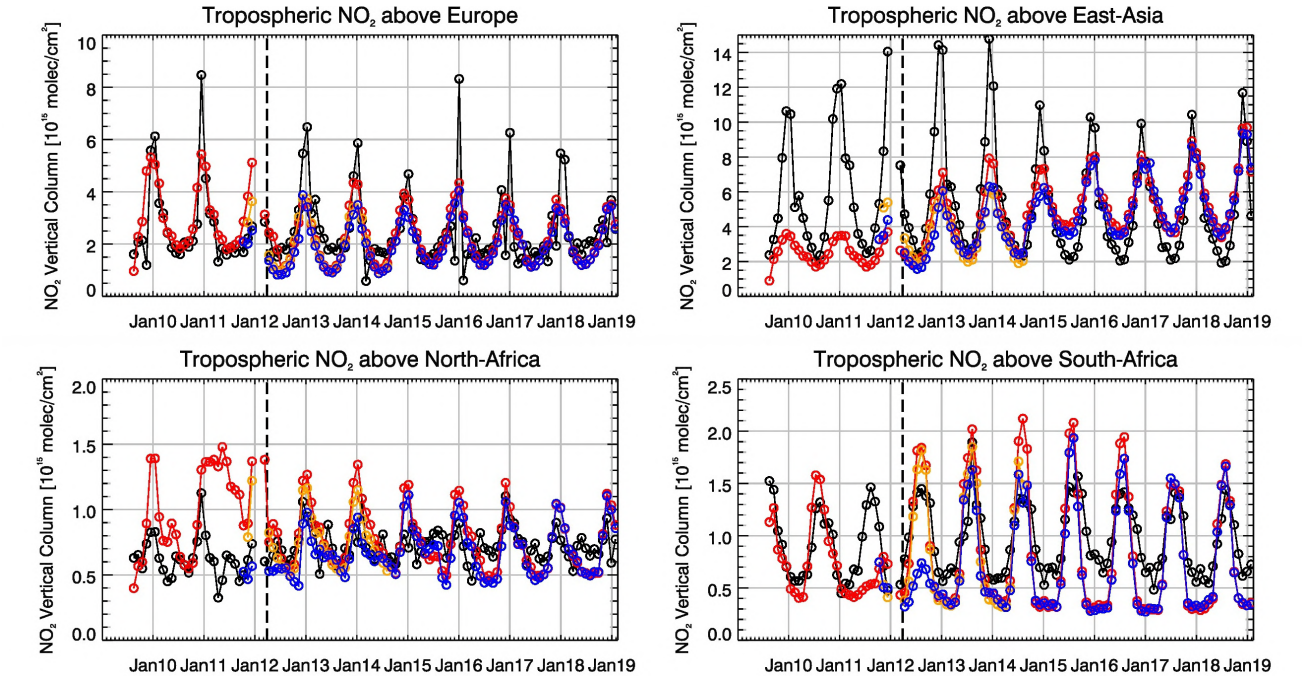

Figure 5.1.2: Time series of average tropospheric NO_2 columns [10^{15} molec cm^{-2}] from SCIAMACHY (up to March 2012, black) and GOME-2 (from April 2012 onwards, black) compared to model results (red - osuite, blue - MACC_fncrt_TM5/MACC_CIFS_TM5/control, orange - MACC_fcnrt_MOZ) for different regions (see Annex 2 for definition of regions). The upper panels represent regions dominated by anthropogenic emissions, and the lower panels represent those dominated by biomass burning. The blue line shows MACC_fcnrt_TM5 from November 2011 to November 2012, MACC_CIFS_TM5 results from December 2012 to August 2014 and control results from September 2014 onwards (the model run without data assimilation is termed control since Sep 2014). Vertical dashed black lines mark the change from SCIAMACHY to GOME-2 based comparisons in April 2012.

by the models. It is not clear if the GOME-2 observations are realistic here, although a first inspection of daily GOME-2 satellite images did not point to problems regarding the retrieval. The retrievals show the same pattern as the simulations however for winter 2018/2019.

Over regions where biomass burning is the major contributor to NO_x emissions, seasonality and amplitude of model columns are determined by fire emissions. The seasonality for the two regions in Africa was simulated reasonably well for 2010 and after October 2011. In the time period in between, a bug in reading fire emissions lead to simulation errors for all MOZART runs. Over North-Africa, the o-suite shows improved results since an update in July 2012 and the change to IFS-CB05 in September 2014. However, tropospheric NO_2 columns around December are still overestimated by the models. Summertime NO_2 columns over North-Africa are underestimated compared to the satellite data from 2015 onwards. The models (especially the o-suite) generally overestimate the seasonal cycle for South-Africa, particularly for 2014 -2016 with an overestimation of the seasonal maximum which usually occurs around August (e.g. by a factor of 1.4 larger compared to GOME-2 retrievals in 2016). However, August maxima are in better agreement since the upgrade of the o-suite in 2017, but minima during SH summer remain underestimated.

More NO_2 evaluation plots can be found on the CAMS website, see table 1.2.

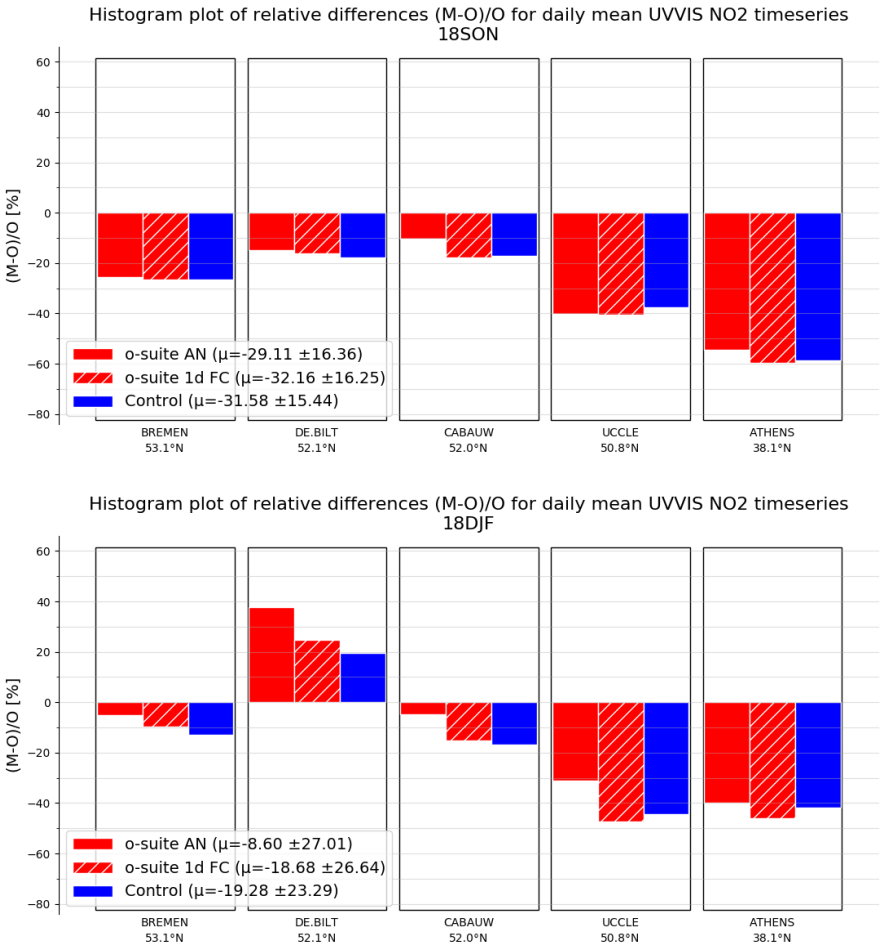

Figure 5.2.1: Table diagram showing the seasonal bias for September-November 2018 (top) and December-February 2019 (bottom) for five stations, sorted by latitude.

5.2 Evaluation against ground-based DOAS observations

In this section, we compare the NO_2 columns of the CAMS models with UVVIS DOAS profile measurements at Uccle and column data from the other stations.[1] This ground-based, remote-sensing instrument is sensitive to the NO_2 abundance in the lower troposphere, up to 1km altitude with an estimated uncertainty of 8%. Tropospheric NO_2 profiles and columns are validated (up to 3.5km or 10km). A description of the instruments and applied methodologies is the same for all DOAS OFFAXIS measurements, see http://nors.aeronomie.be. It is important to mention here that the model partial column values are calculated from the smoothed model profiles. This guarantees that the model levels where the measurement is not sensitive do not contribute to the observed bias. We should mention that the measurement data is still catalogued as rapid delivery and not in the consolidated NDACC database.

[1] No contribution from Xianghe, Reunion and OHP due to instrument failure.

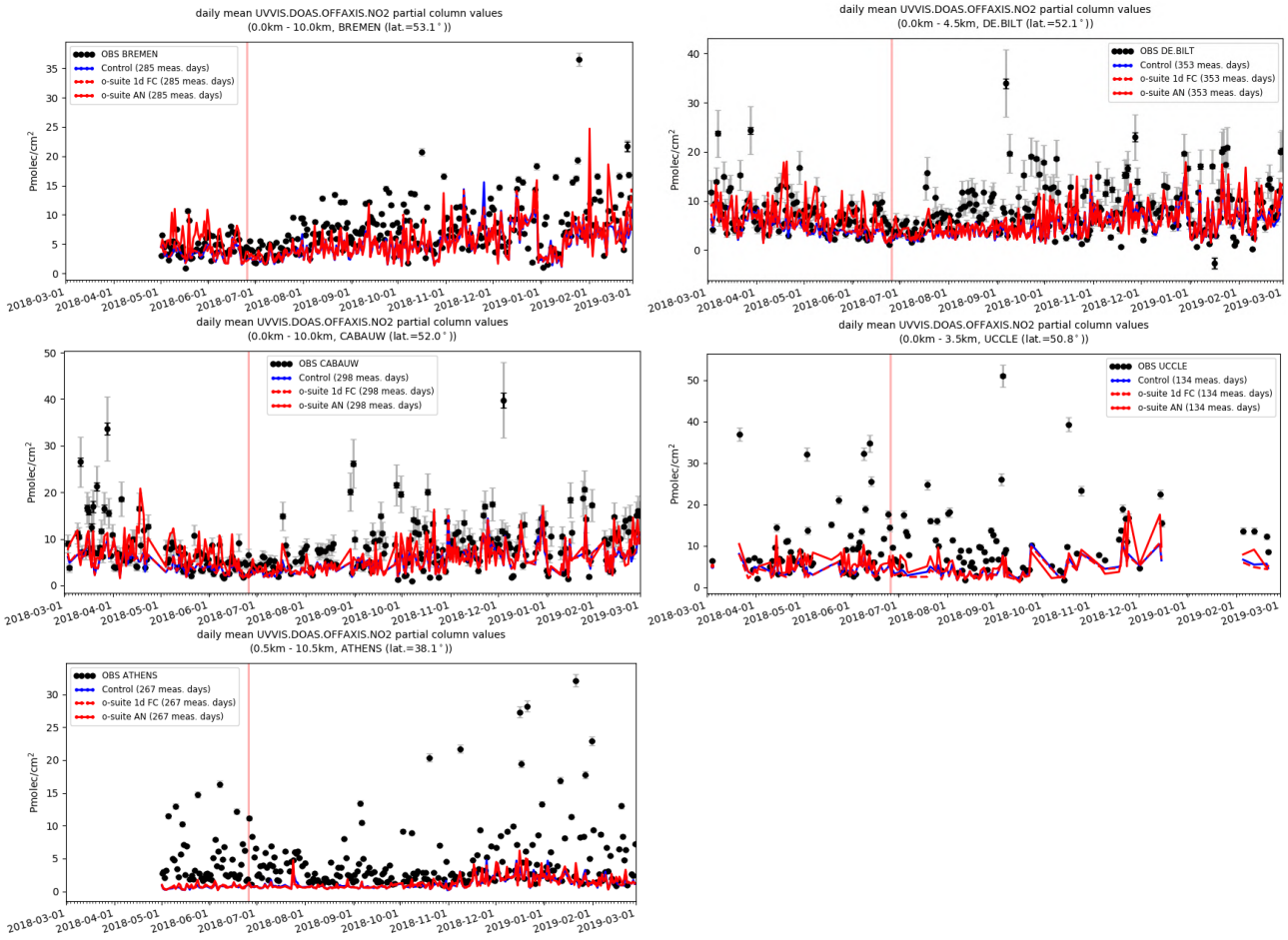

Figure 5.2.2: Time series of NO_2 partial columns at the five different sites Bremen (Germany), De Bilt (Netherlands), Cabauw (Netherlands), Uccle (Belgium) and Athens (Greece). For all sites except Athens, background concentrations are well captured by the model. The o-suite and control run show little difference.

Fig. 5.2.1 shows the biases for the latest validation periods Sept-Nov 2018 and Dec-Feb 2019 at the different sites. At the urban sites at Uccle and Athens a strong underestimation is observed. For the other sites (Bremen, De Bilt and Cabauw) the o-suite AN is able to capture only few of the high pollution events. The corresponding time series are shown in Fig. 5.2.2.

6. Formaldehyde

6.1 Validation against satellite data

In this section, simulations of tropospheric formaldehyde are compared to SCIAMACHY/Envisat HCHO satellite retrievals (IUP-UB v1.0) [Wittrock et al., 2006] for model data before April 2012 and to GOME-2/MetOp-A HCHO data (IUP-UB v1.0) [Vrekoussis et al., 2010] afterwards. As the retrieval is performed in the UV part of the spectrum where less light is available and the HCHO absorption signal is smaller than that of NO_2, the uncertainty of monthly mean HCHO columns is relatively large (20% – 40%) and both noise and systematic offsets have an influence on the results. However, absolute values and seasonality are retrieved more accurately over HCHO hotspots.

In Figure 6.1.1, monthly mean satellite HCHO columns are compared to model results for January 2019. The magnitude of oceanic and continental background values and the overall spatial distribution are well represented by the o-suite and control. The models overestimate values over regions in Australia and Central Africa which could be due to fire or biogenic emissions.

Time series in Fig. 6.1.2 highlight three cases:

East-Asia and the Eastern US, where HCHO is dominated by biogenic emissions. Model results and measurements generally agree rather well. However, all model runs underestimate the yearly cycle over East-Asia since 2012. In contrast to MOZART runs, MACC_CIFS_TM5 overestimated satellite values for the Eastern US since the middle of 2013. However, the newer IFS-CB05 runs perform well for Eastern US since 2015. For recent years and both regions, there is virtually no difference between the most recent o-suite run with IFS-CB05 chemistry and the corresponding control run without data assimilation. The variability or “ups and downs” in HCHO columns observed by GOME-2 since December 2014 is due to the lack of data (caused by instrument degradation) for these regions during winter in the Northern Hemisphere, leading to e.g. the negative values in the GOME-2 time series for Eastern US since December 2015. Summertime maxima are still underestimated over East-Asia despite of the higher resolution of the model runs since 2016.

North-Africa, where biomass burning as well as biogenic sources largely contribute to HCHO and its precursors. Satellite observations over North-Africa are generally slightly overestimated by IFS-CB05 chemistry model runs since 2014 and also the latest higher resolution model versions since July 2016.

Indonesia, where HCHO is also dominated by biogenic sources and biomass burning. Old MOZART based model versions generally overestimated satellite values here (by a factor of 3 – 4 in the second half of 2010) and failed to reproduce the observed seasonality. This may be due to the use of fire emissions including El Nino years, which experience much larger fire activities. MOZART simulations and observations agreed much better since late 2012. IFS-CB05 runs agree very well with satellite retrieved ones for December 2014 to August 2015. For September and October 2015, satellite retrieved HCHO columns show a pronounced maximum. 2015 was a strong El Nino year, which caused droughts and higher fire activity in Indonesia. As for previous

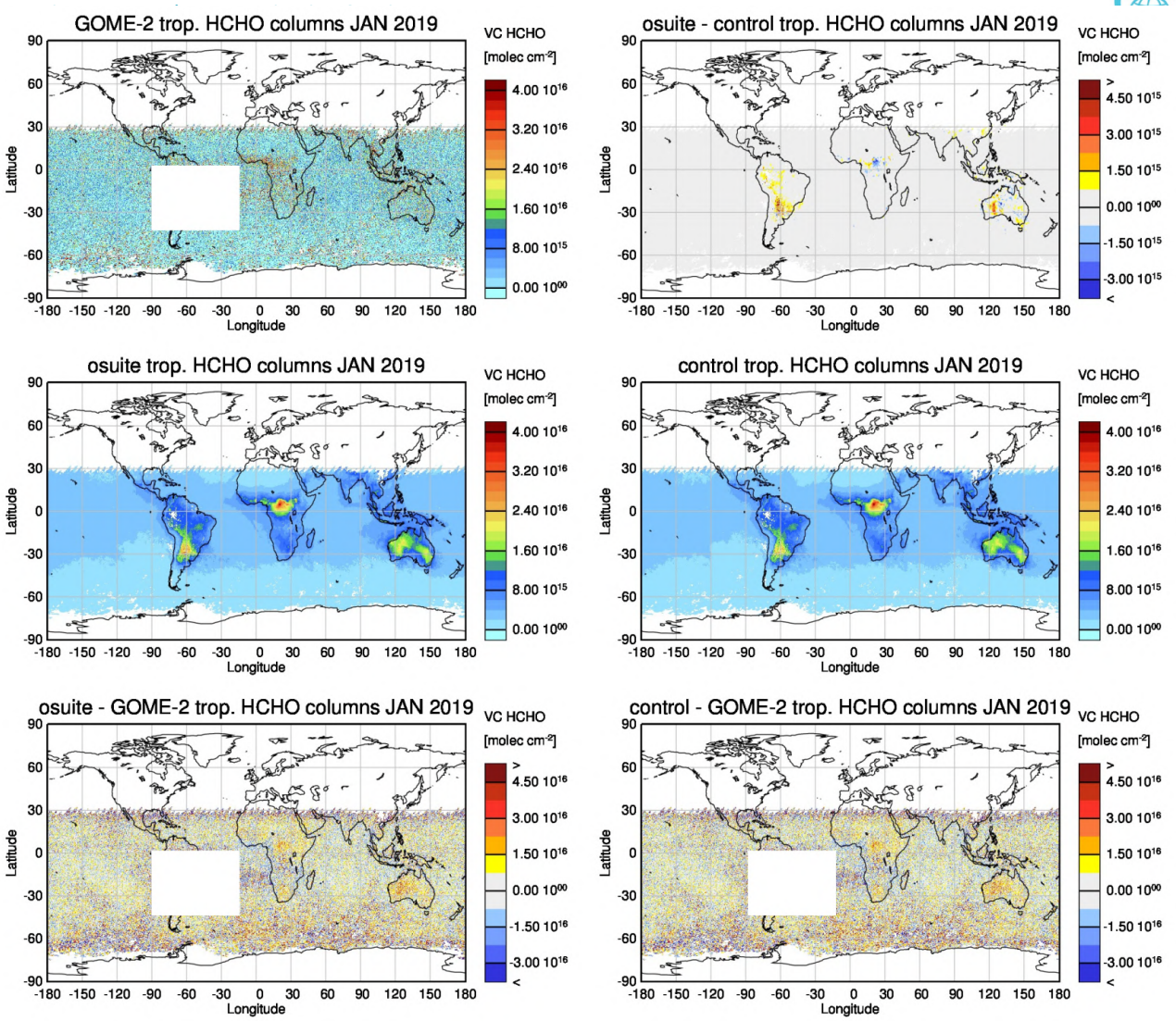

Figure 6.1.1: Global map comparisons of satellite retrieved and model simulated tropospheric HCHO columns [molec cm-2] for January 2019. The top row shows monthly mean tropospheric HCHO columns retrieved by GOME-2, the second row shows the same but for model simulated averages. The third row shows differences of monthly means between models and GOME-2. GOME-2 data were gridded to model resolution (i.e. 0.4° deg x 0.4° deg). Model data were treated with the same reference sector subtraction approach as the satellite data. Satellite retrieved values in the region of the South Atlantic anomaly are not valid and therefore masked out (white boxes in all images except those which show model results only).

El Nino years, fire emissions used by IFS-CB05 seem to be largely overestimated, resulting in model simulated HCHO columns which are almost twice as large as those retrieved by GOME-2. Further investigations (see previous reports) show that this is not caused by cloud flagging applied to the satellite and model data. The recent higher resolution runs in general overestimate values over Indonesia as well. There is mainly little variation from one month to another in both, satellite observations and model simulations since middle of 2016, the decrease in retrieved HCHO columns for Dec 17/ Jan 18 and an increase in May 2018 is not reproduced by the simulations.

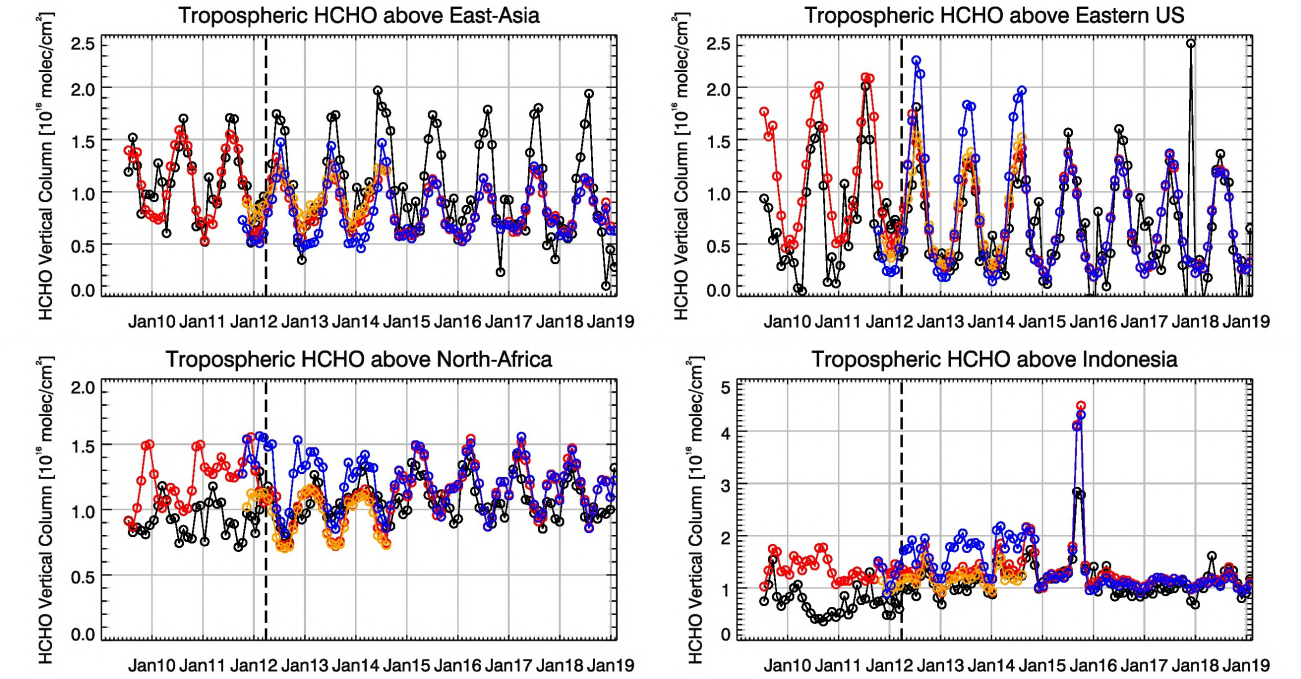

Figure 6.1.2: Time series of average tropospheric HCHO columns [10^{16} molec cm^{-2}] from SCIAMACHY (up to March 2012, black) and GOME-2 (from April 2012 onwards, black) compared to model results (red - osuite, blue - MACC_fncrt_TM5/MACC_CIFS_TM5/control, orange - MACC_fcnrt_MOZ) for different regions. The blue line shows MACC_fcnrt_TM5 from November 2011 to November 2012, MACC_CIFS_TM5 results from December 2012 to August 2014 and control results from September 2014 onwards (the model run without data assimilation is termed control since Sep 2014). The regions differ from those used for NO_2 to better focus on HCHO hotspots: East-Asia (25-40°N, 110-125°E), Eastern US (30-40°N, 75-90°W), Northern Africa (0-15°N, 15°W-25°E) and Indonesia (5°S-5°N, 100-120°E). Negative satellite retrieved values over Eastern US are due to a lack of data (caused by instrument degradation) during Northern Hemisphere winter months for this region. Vertical dashed black lines mark the change from SCIAMACHY to GOME-2 based comparisons in April 2012.

For details on the HCHO evaluation: http://www.doas-bremen.de/macc/macc_veri_iup_home.html

6.2 Evaluation against ground-based DOAS observations

In this section, we compare the H_2CO columns of the CAMS models with UVVIS DOAS measurements at Uccle, Cabauw and De Bilt.[2] These ground-based, remote-sensing instruments are sensitive to the HCHO abundance in the lower troposphere. Tropospheric HCHO profiles and columns are validated (up to 3.5km (Uccle) or 10km (Cabauw and De Bilt)). A description of the instruments and applied methodologies is the same as for the MWR O_3 and FTIR O_3 and CO validations see http://nors.aeronomie.be. It is important to mention here that the model partial column values are calculated for the smoothed model profiles. This guarantees that the model levels where the measurement is not sensitive do not contribute to the observed bias. We should mention that the measurement data is catalogued as rapid delivery and not in the consolidated NDACC database.

[2] No contribution from Reunion, Xianghe and OHP due to instrument failure.

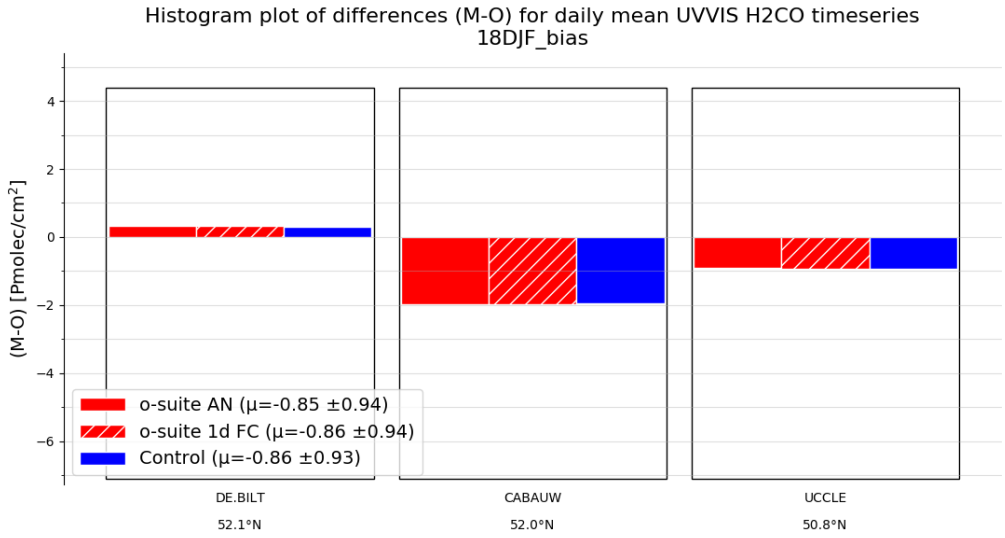

Figure 6.2.1: Table diagram showing the seasonal absolute bias DJF for three stations, sorted by latitude.

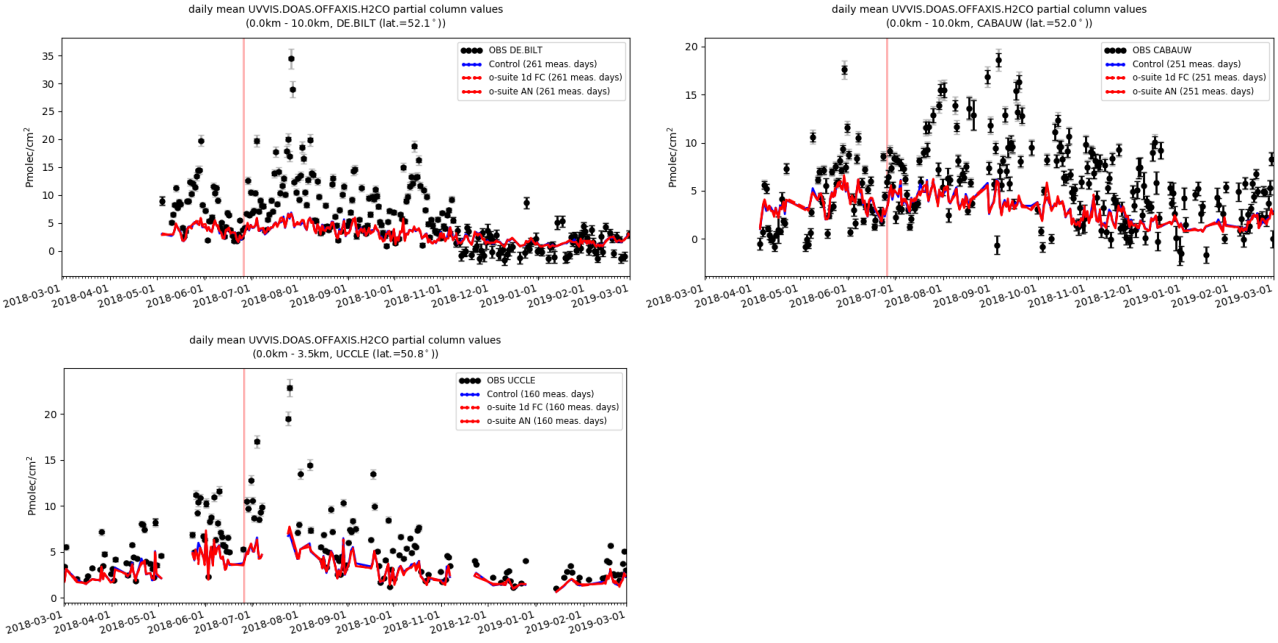

Figure 6.2.2: Time series of H_2CO partial columns at the five different sites. All models underestimate the H2CO concentrations, except at De Bilt, where the model overestimates during the winter months.

Fig. 6.2.1 shows the absolute biases Dec 2018 – Feb 2019 at the different sites and indicates nearly vanishing bias for the different sites. At Cabauw and De Bilt the underestimation has decreased during the SON period and during November 2018 the bias has changed sign (Fig 6.2.2): the HCHO abundance decreased due to less production and this seasonal variation is not fully captured by the model. From Fig. 6.2.1 and 6.2.2 we see little difference between the o-suite and the control run. Although the background column values are well captured by the models, the high emission events are not.

7. Aerosol

7.1 Global comparisons with Aeronet and EMEP

The comparison of the CAMS simulation of time series of aerosol optical depth can be found for all Aeronet stations at: http://aerocom.met.no/cams-aerocom-evaluation/

More detailed evaluation including scores, maps, scatterplots, bias maps and histograms illustrating the performance of the aerosol simulation in the IFS system are made available through the AeroCom web interface. The model run can be compared here to e.g. the CAMS interim reanalysis and other models, such as the AeroCom Median model.

Correlation, based on daily aerosol optical depth and NRT Aeronet observations, has been rather stable recently. The o-suite forecast at +3 days shows only slightly lower correlation. See figure S3.

Part of the month-to-month variation in correlation is due to the varying quality and coverage of the Aeronet network. This has been improved by the version 3 from Aeronet. We use therefore version 3 level 1.5 for all global comparison to Aeronet.

The performance of the o-suite model exhibits some seasonal variation in AOD depending on region (Fig. 7.1.1). Noteworthy is the persistent AOD overestimation over North America (Fig. 7.1.1-bottom), but also a long-term trend to overestimation in East Asia. The latitudinal display of model and Aeronet AOD in the period investigated here (Fig. 7.1.2) shows a specific positive bias against Aeronet in the Southern Hemisphere.

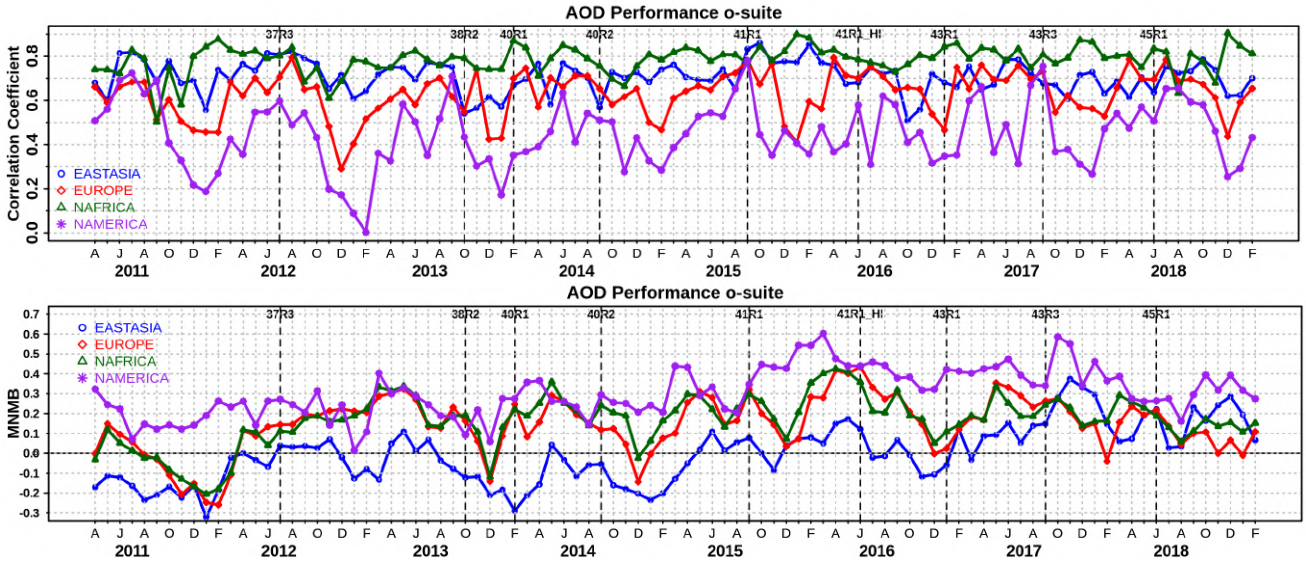

Figure 7.1.1. (top) Correlation coefficient and (bottom) modified normalized mean bias (MNMB) in AOD, since 2011, based on daily AOD comparison (Aeronet V3 level 1.5 data) in four world regions [East-Asia (blue); Europe (red); North Africa (green); North America (purple)] for the o-suite.

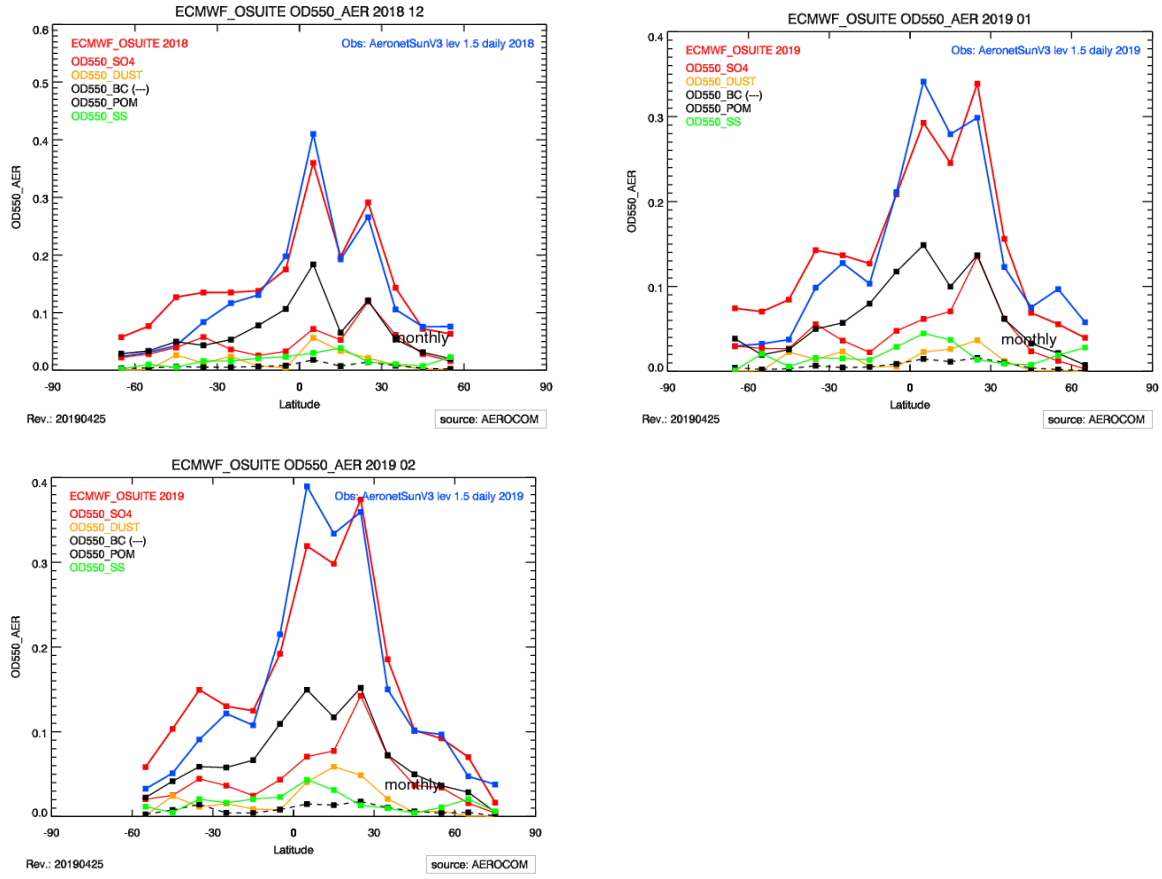

Figure 7.1.2. Aerosol optical depth of o-suite (red) compared to latitudinally aggregated Aeronet V3 level 1.5 data (blue) for the three months covered by this report.

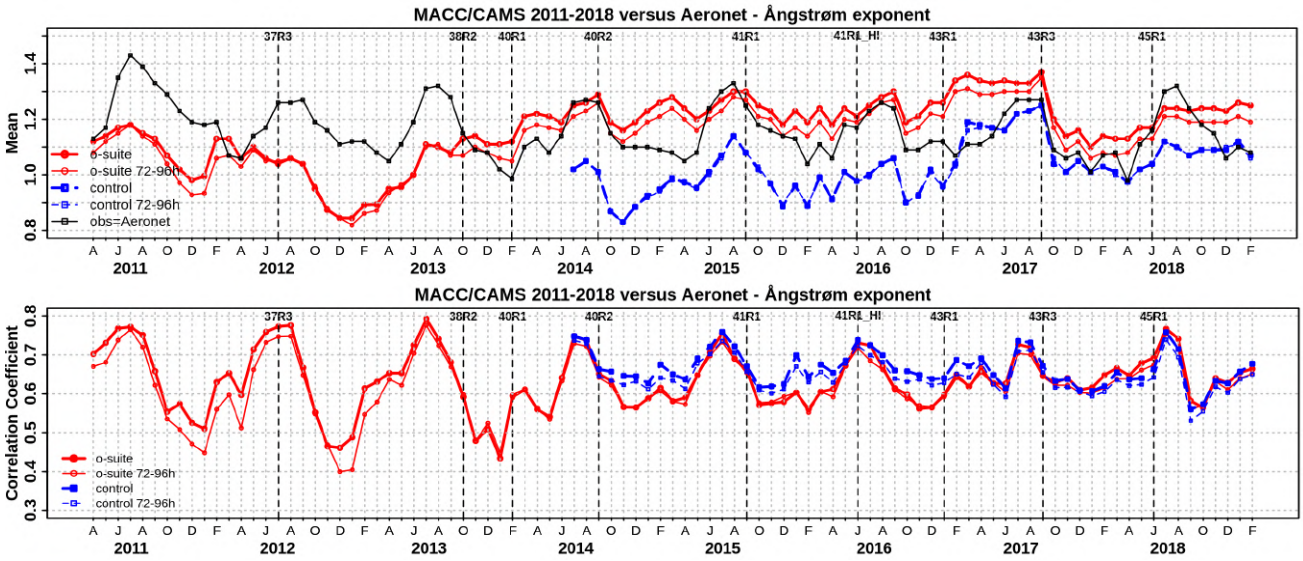

Figure 7.1.3. a) (top) Evolution of mean Ångström exponent in o-suite and control at Aeronet sites (Aeronet V3 level 1.5 data), based on matching monthly mean values. o-suite (thick red curve); o-suite at last forecast day (light red curve); control (blue dashed curve); control at last forecast day (light blue dashed curve). b) (bottom) Correlation using daily matching Ångström exponent.

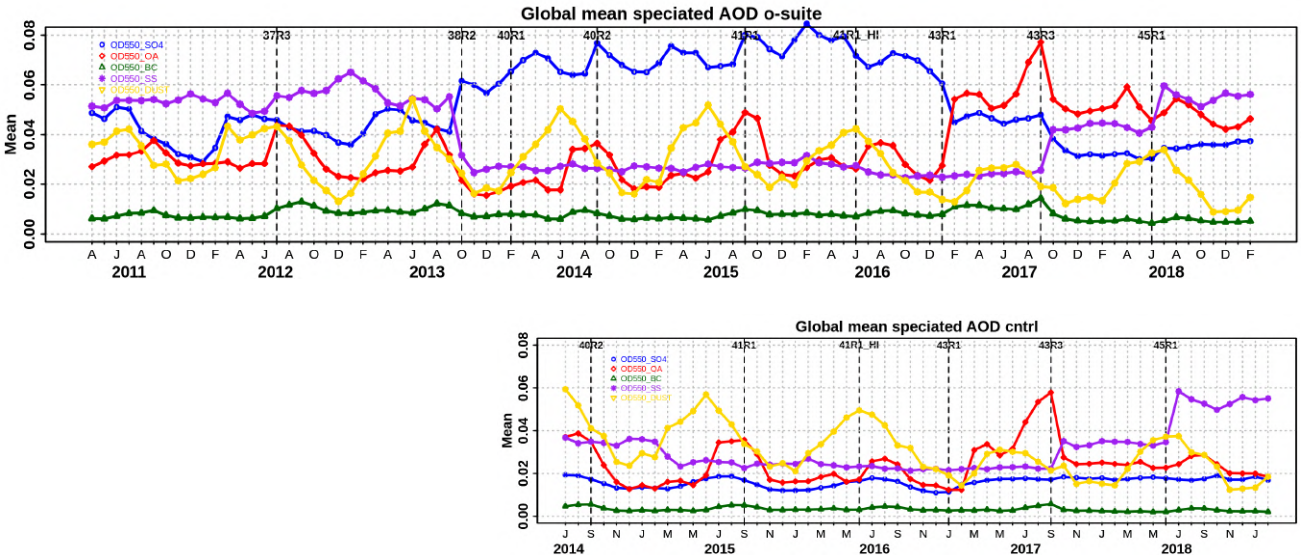

Figure 7.1.4. Evolution of the aerosol components of total AOD@550nm [OD550_SO4 = sulphate(blue); OD550_OA = organics(red); OD550_BC = black carbon(green); OD550_SS = sea salt(purple); OD550_DUST = dust(yellow)] in o-suite and control simulation.

o-suite				
	Mean SON 2018 0-24h	Change wrt to first day on day 4	Mean DJF 2018/19 0-24h	Change wrt to first day on day 4
AOD@550	0.158	-14%	0.153	-15%
BC-OD@550	0.005	-19%	0.005	-24%
Dust-OD@550	0.015	13%	0.011	13%
OA-OD@550	0.048	-24%	0.044	-28%
SO4-OD@550	0.035	-22%	0.037	-23%
SS-OD@550	0.053	-6%	0.056	-6%

Table 7.1.1. Mean global total and speciated AOD in the o-suite for the last two periods covered by the VAL report and change after 3 forecast days.

The simulated aerosol size distribution may be validated to first order using the wavelength dependent variation in AOD, computed as Ångström exponent, with higher Ångström exponents indicative of smaller particles. We find in DJF 2018/19 a small bias (Figure 7.1.3-a). Temporal and spatial variability is difficult to capture, but correlation from all daily data is lower than for AOD (Figure 7.1.3-b and S3). Figure 7.1.4 shows that the Sep 2017 and Jun 2018 model changes are responsible for a shift in Ångström exponent. More organic matter seems to shift the size distribution to smaller sizes. The model upgrade in Feb 2017 with a bugfix for sea salt and improved parameterisations for SO4 lead to sea salt increased with 45% while sulphate further decreased a bit. Sea salt has increased further due to a new sea salt emission scheme implemented in the latest model upgrade and is back to earlier 2011-2013 levels.

The o-suite uses data assimilation to obtain an analysis of the aerosol field. In the forecast period, however, a-priori model parameterisations and emissions (except fire emissions, which are kept in

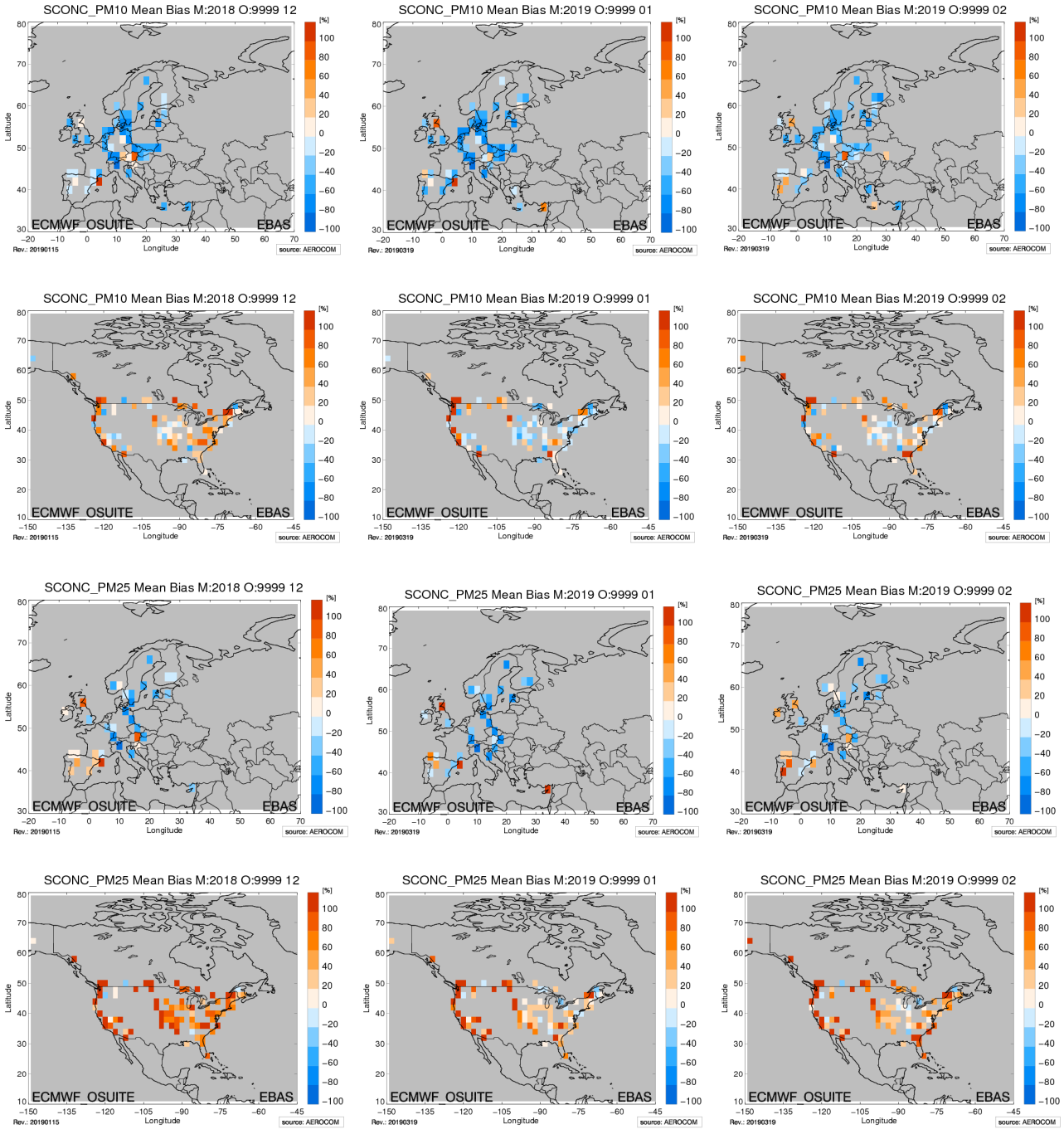

Figure 7.1.5. Bias [%] map of monthly mean PM10 and PM2.5 concentrations at EMEP (Europe, first and third row) and IMPROVE sites (North America, second and fourth row) for December 2018 (left column), January (middle) and February 2019 (right); simulated o-suite versus EMEP/IMPROVE derived climatological average (2000-2009).

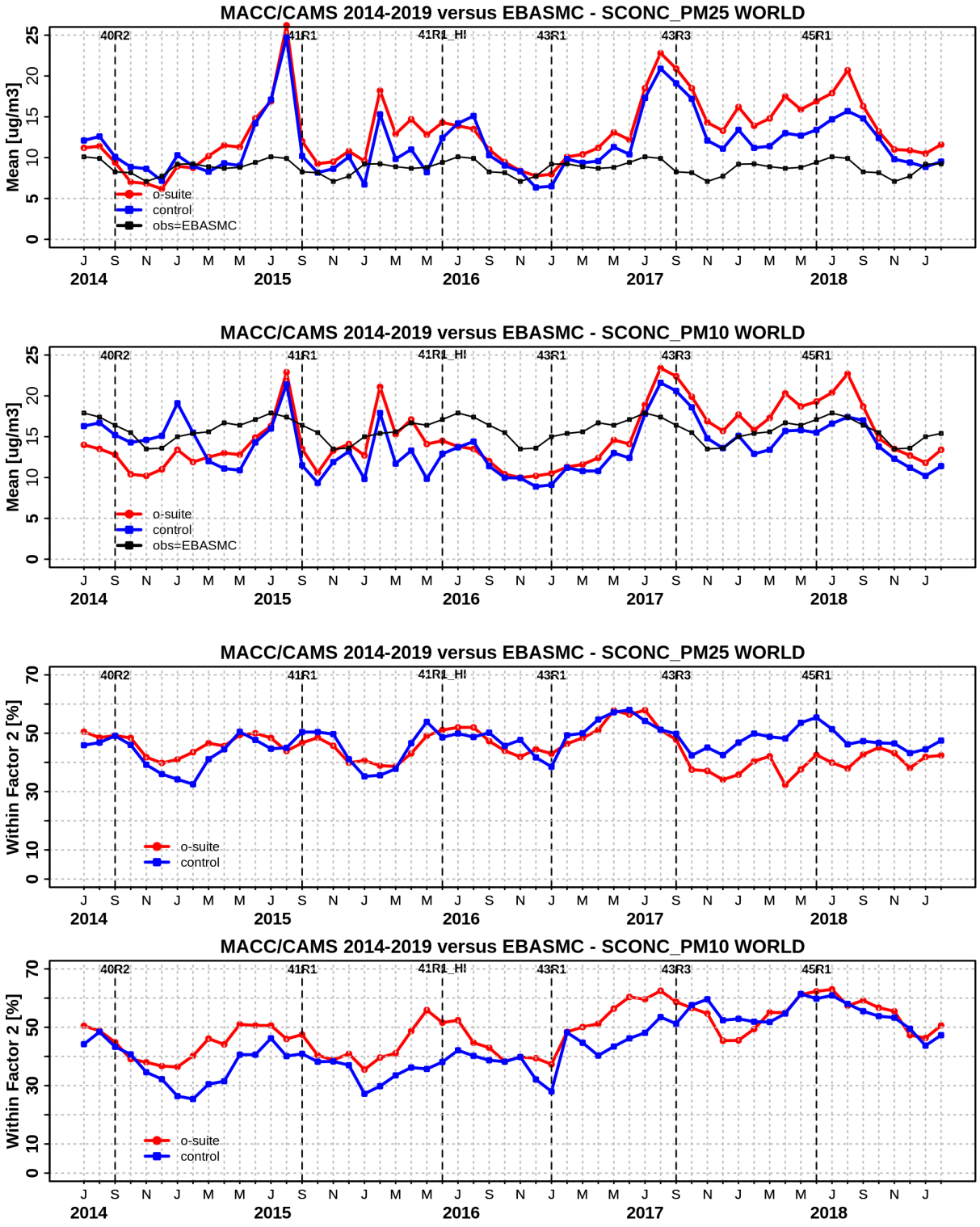

Figure 7.1.6. Temporal evolution of monthly mean average PM25 and PM 10 concentrations at EMEP (Europe) and IMPROVE sites (North America) and data fraction within a factor 2 of observed; ca 160 sites, observed data averaged from data available in EBAS from 2000-2009.

the forecast equal to the latest GFAS emission values) determine increasingly the aerosol fields. The performance of the day three forecasted AOD fields as compared to the first guess is shown in Figure S3 in the summary of this report. Table 7.1.1 shows an average global decrease in total aerosol optical depth during the first four forecast days, dominated by sulphate and organics. The control run with no assimilation shows significant less AOD (-15% compared to o-suite, see figure S3). All this supports the conclusion that either a-priori IFS aerosol and aerosol precursor sources are too small, or sinks are too effective in the IFS model.

Surface concentration of particulate matter below 10 µm (PM10) and below 2.5 µm (PM25) from the o-suite experiment have been validated against data from 160 background IMPROVE and EMEP stations. A climatological average has been constructed from data in the period 2000-2009 as available in the EBAS database hold at NILU. The data availability is not the same at all stations, and sometimes covers only a few years.

A negative MNMB bias of PM10 in Europe and an overestimate in North America PM2.5 appears (Fig. 7.1.5), consistent with the AOD bias in the two regions. Figure 7.1.6 shows the evolution of mean observed and simulated PM10 and PM2.5. The biggest change appeared in July 2017 with the bias of o-suite now becoming positive overall. Shown is also the statistics of being within factor 2, a more robust metrics for a comparison to climatological data. This statistical indicator has clearly improved over time, indicating best PM10 and PM25 performance in summer months for the o-suite. O-suite is also better most of the times than the control simulation for PM10. For PM25 the difference is less clear, but since September 2017 (upgrade to 43R3) the control is performing better than the o-suite.

7.2 Dust forecast model inter-comparison: Validation of DOD against AERONET, and comparisons with Multi-model Median from SDS-WAS

The 72-hour forecasts (on a 3-hourly basis) dust aerosol optical depth (DOD) from CAMS o-suite and control have been validated for the period 1 December 2018 – 28 February 2018 against AERONET direct-sun cloud-screened observations, MODIS/Terra and Aqua Collection 6.1 Level 3 (1º x 1º) and SDS-WAS Multi-model Median DOD. The SDS-WAS Multi-model Median DOD is obtained from (currently) twelve dust prediction models participating in the Sand and Dust Storm Warning Advisory and Assessment System (SDS-WAS) Regional Center for Northern Africa, Middle East and Europe (http://sds-was.aemet.es/).

For this winter period, satellites detected the presence of biomass burning from Savanah fires (see MODIS in Figure 7.2.1) and showed that major dust activity in Northern Africa is concentrated in the Bodélé Basin (Sahara) and south-eastern Arabia Peninsula. In North Africa, both CAMS experiments can simulate the main areas of dust activity in comparison with MODIS (see Figure 7.2.1) although the o-suite and control show lower season values (seasonal DOD up to 0.3). The o-suite shows lower values in the Sahara region than control and the SDS-WAS multi-median product, in particular over the Bodélé. Neither the CAMS experiments, nor the SDS-WAS multi-model product are capturing the maximum AOD values observed in the Arabian Peninsula and the Red Sea, indicating missing dust emissions in all the model experiments.

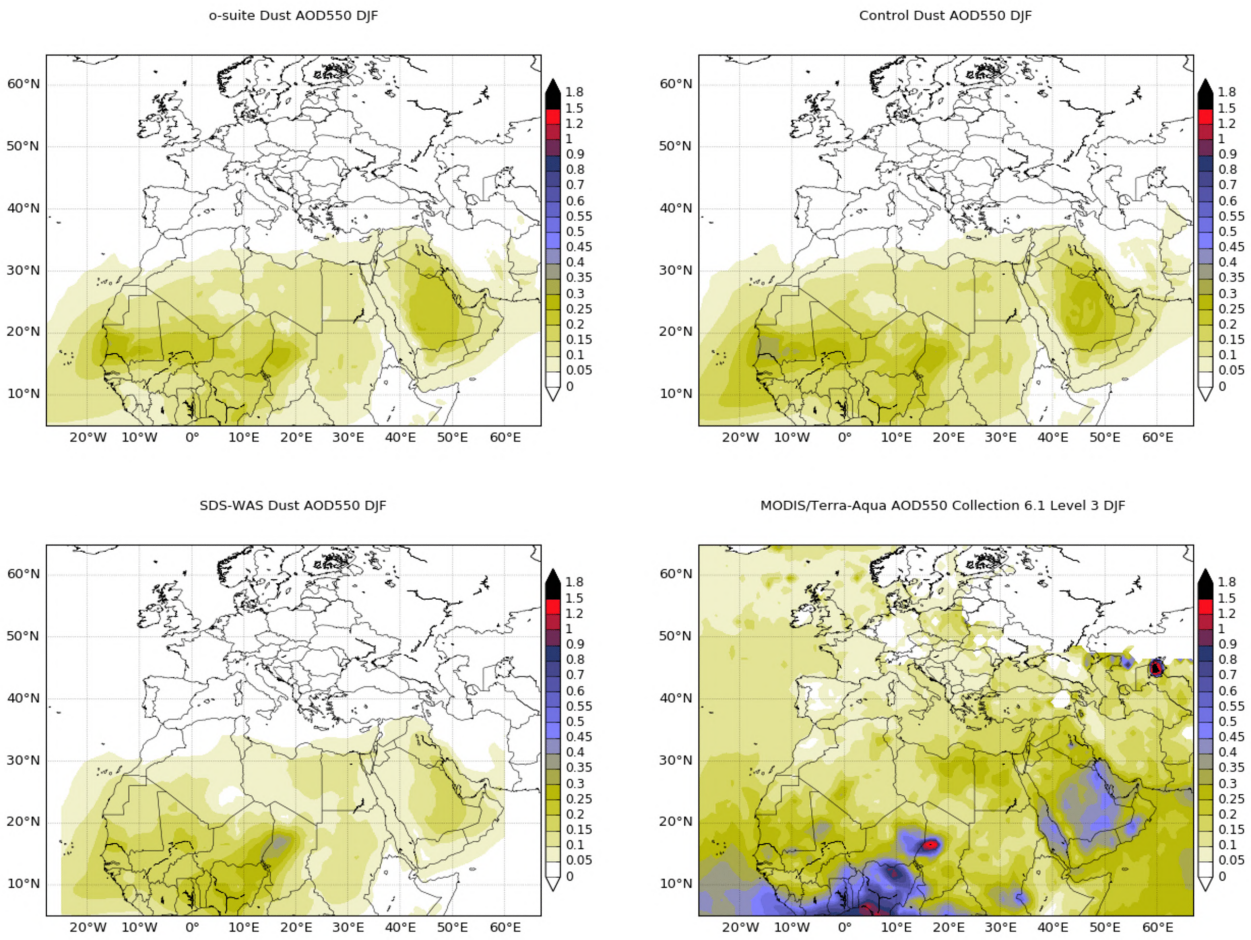

Figure 7.2.1: Averaged DOD 24h forecast from o-suite (top left) and control (top right), DOD of the multi-model SDS-WAS Median product (bottom left) as well as AOD from MODIS/Terra-Aqua Collection 6.1 Level 3 combined Dark target and Deep Blue product (bottom right) for the study period.

For December to February, the o-suite reproduces the daily variability of AERONET observations with a correlation coefficient of 0.74, averaged over all the AERONET sites, in comparison to 0.65 for the control experiment. These results are slightly lower than those obtained by the SDS-WAS Multi-model product (0.78). In terms of MB, both CAMS experiments (o-suite and control) as well as the SDS-WAS Multi-model underestimate the AERONET observations resulting in a MB of -0.05 for control , -0.07 for o-suite and -0.06 the SDS-WAS multi-model. The Middle East region (see Mezaira in Figure 7.2.3. and Table 7.2.1) region shows the best results in the AERONET comparison in terms of correlation. The o-suite can reproduce the daily variability with correlation coefficient of 0.86 and MB of -0.11.

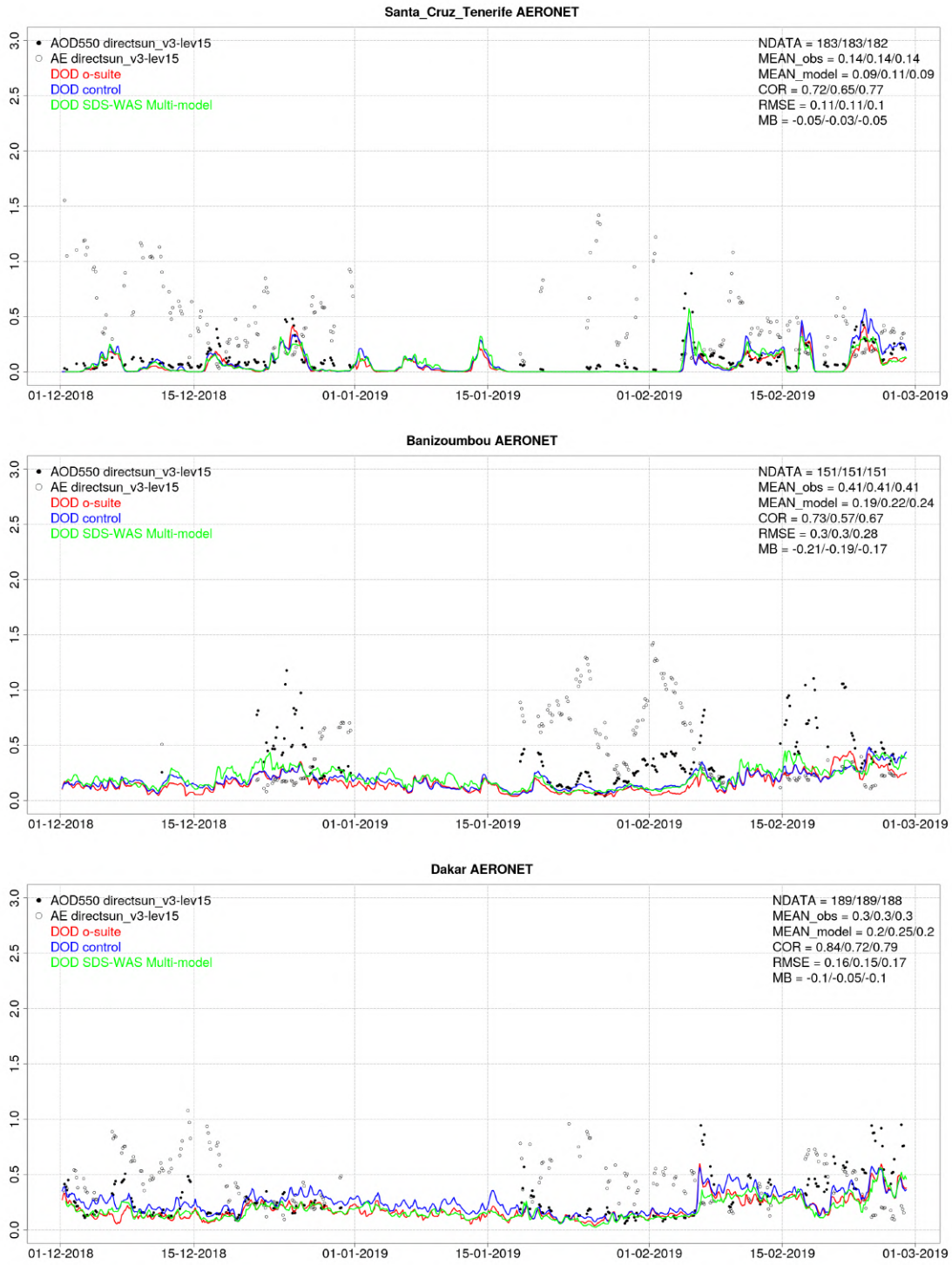

Figure 7.2.2: Timeseries of AOD from AERONET (black dots), DOD o-suite (red line), DOD control (blue line) and DOD Multimodel SDS-WAS Median (green line) for the study period over Tunis Carthage (North Western Magrebh), Banizoumbou (Sahel) and Dakar (Tropical North Atlantic). Skill scores per each individual site and model (o—suite/control/SDS-WAS Multi-model) are shown in the upper right corner (NDATA: available 3-hourly values used for the calculations, MEAN observations, MEAN model, COR, RMSE, MB).

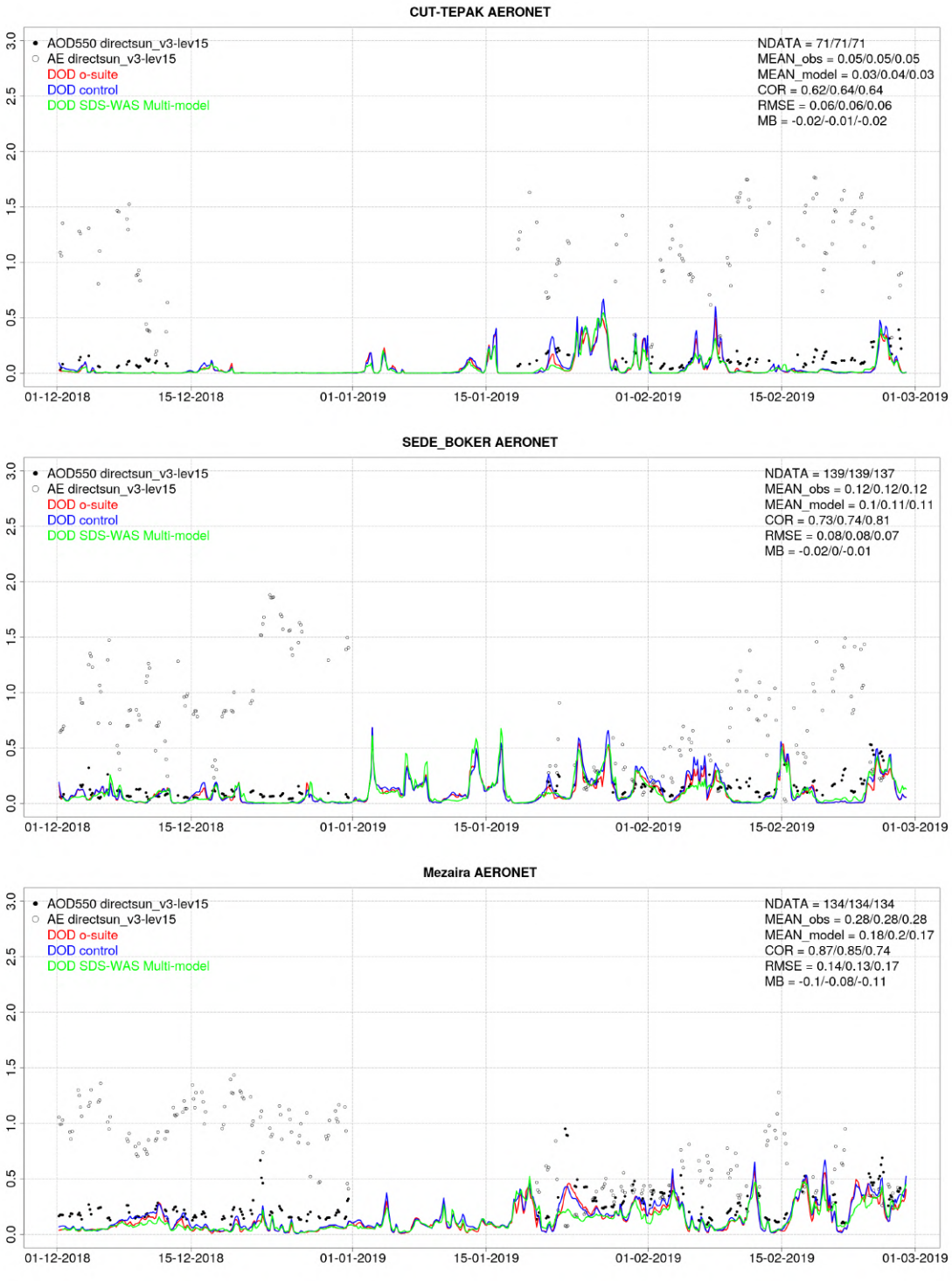

Figure 7.2.3: Timeseries of AOD from AERONET (black dots), DOD o-suite (red line), DOD control (blue line) and DOD Multimodel SDS-WAS Median (green line) for the study period over CUT-TEPAK and SEDE BOKER (Eastern Mediterranean) and Mezaira (Middle East). Skill scores per each individual site and model (o—suite/control/ SDS-WAS Multi-model) are shown in the upper right corner (NDATA: available 3-hourly values used for the calculations, MEAN observations, MEAN model, COR, RMSE, MB).

Table 7.2.1: Skill scores (MB, FGE, RMSE and r) of 24h forecasts for CAMS o-suite, CAMS control and SDS-WAS Multi-model Median for the study period, and the number of data (NDATA) used. Dust AOD (DOD) from AERONET is the reference.

		control				o-suite DOD				SDS-WAS Median DOD			
	NDATA	**MB**	**FGE**	**RMSE**	**r**	**MB**	**FGE**	**RMSE**	**r**	**MB**	**FGE**	**RMSE**	**r**
Sahara	197	0.04	0.55	0.11	0.67	0.02	0.45	0.10	0.75	-0.01	-0.10	0.10	0.73
Sahel	658	-0.28	-0.34	0.51	0.45	-0.31	-0.51	0.50	0.69	-0.27	-0.38	0.47	0.73
Tropical North Atlantic	98	-0.04	-0.33	0.09	0.81	-0.08	-0.58	0.11	0.82	-0.10	-0.67	0.13	0.83
Subtropical North Atlantic	283	0.01	0.09	0.12	0.49	-0.01	-0.05	0.11	0.55	0.00	0.01	0.11	0.55
North Western Maghreb	76	-0.09	-0.09	0.22	0.65	-0.12	-0.29	0.24	0.58	-0.13	-0.19	0.24	0.61
Western Iberian Peninsula	303	-0.03	0.08	0.07	0.71	-0.04	-0.01	0.07	0.76	-0.05	-0.02	0.08	0.68
Iberian Peninsula	427	-0.01	1.04	0.07	0.73	-0.03	0.95	0.06	0.73	-0.03	0.94	0.07	0.86
Western Mediterranean	1062	-0.01	1.05	0.05	0.69	-0.02	1.00	0.05	0.76	-0.02	1.02	0.05	0.73
Central Mediterranean	705	-0.02	0.76	0.06	0.40	-0.02	0.75	0.06	0.39	-0.02	0.81	0.06	0.39
Eastern Mediterranean	676	-0.01	0.82	0.08	0.78	-0.02	0.76	0.08	0.76	-0.02	0.77	0.08	0.78
Eastern Sahara	-	-	-	-	-	-	-	-	-	-	-	-	-
Middle East	143	-0.08	-0.11	0.14	0.84	-0.11	-0.20	0.15	0.86	-0.12	-0.18	0.18	0.73
All sites	**4628**	**-0.05**	**0.55**	**0.21**	**0.65**	**-0.07**	**0.46**	**0.20**	**0.74**	**-0.06**	**0.48**	**0.20**	**0.78**

Over the Sahara both CAMS experiments show closer results with a correlation coefficient of 0.67 for control and 0.75 for o-suite although o-suite shows a slightly higher overestimation (MB of 0.02) than the control experiment which tends to overestimate the AERONET observations (MB of 0.04). The o-suite presents better results than the SDS-WAS Median Multi-model that shows a correlation coefficient of 0.73 for the Sahara, although it underestimates the observations with an MB of -0.10. In the Sahel (see Banizoumbou in Figure 7.2.2 and Table 7.2.1), the o-suite shows a strong underestimations (MB of -0.31, slightly higher than control with MB of -0.28) although the o-suite better reproduces the observed daily variability (with a correlation value of 0.69 for o-suite in comparison of for control that has a correlation of 0.45). The underestimations observed in o-suite in the Sahel are also spread to the Tropical North Atlantic (MB of -0.08 for o-suite) in agreement with the underestimation also observed in the comparison with MODIS (Figure 7.2.1). In the Tropical North Atlantic region (see Dakar in Figure 7.2.2), the o-suite presents similar correlation coefficient (0.82) as the control experiment (0.81). In the North-Western Maghreb, the CAMS experiments show underestimations (MB of -0.09 for control and -0.12 for o-suite) in comparison with the AERONET observations and correlation coefficients of 0.58 for o-suite and 0.65 for control which are close to the results of the SDS-WAS Median Multi-model (0.61). This is associated to the low AOD values observed and the number of observations during this season when there are more clouds.

Table 7.2.2: Skill scores (MB, FGE, RMSE and r) of 48h and 72h forecasts for CAMS o-suite and CAMS control for the study period, and the number of data (NDATA) used. Dust AOD (DOD) from AERONET is the reference.

		48h control				48h o-suite				72h control				72h o-suite			
	NDATA	**MB**	**FGE**	**RMSE**	**r**	**MB**	**FGE**	**RMSE**	**r**	**MB**	**FGE**	**RMSE**	**R**	**MB**	**FGE**	**RMSE**	**r**
Sahara	194	0.03	0.54	0.11	0.60	0.02	0.48	0.11	0.63	0.03	0.50	0.11	0.66	0.02	0.45	0.11	0.68
Sahel	654	-0.28	-0.34	0.51	0.45	-0.30	-0.46	0.51	0.60	-0.28	-0.34	0.51	0.44	-0.30	-0.43	0.52	0.52
Tropical North Atlantic	94	-0.04	-0.33	0.09	0.82	-0.08	-0.52	0.11	0.81	-0.05	-0.34	0.09	0.83	-0.07	-0.51	0.11	0.81
Subtropical North Atlantic	279	0.01	0.09	0.12	0.49	-0.01	0.00	0.11	0.53	0.02	0.09	0.13	0.49	0.00	0.03	0.12	0.50
North Western Maghreb	75	-0.09	-0.12	0.22	0.65	-0.11	-0.25	0.24	0.60	-0.08	-0.06	0.20	0.73	-0.10	-0.15	0.22	0.68
Western Iberian Peninsula	301	-0.03	0.09	0.07	0.73	-0.05	0.00	0.07	0.78	-0.03	0.09	0.07	0.69	-0.04	0.01	0.07	0.68
Iberian Peninsula	427	-0.01	1.04	0.06	0.80	-0.02	0.96	0.06	0.73	-0.01	1.07	0.07	0.78	-0.02	1.00	0.06	0.74
Western Mediterranean	1052	-0.01	1.06	0.05	0.63	-0.02	1.03	0.05	0.66	-0.01	1.05	0.06	0.55	-0.02	1.02	0.06	0.53
Central Mediterranean	698	-0.02	0.77	0.06	0.40	-0.02	0.75	0.06	0.39	-0.02	0.79	0.06	0.38	-0.02	0.77	0.06	0.37
Eastern Mediterranean	667	-0.01	0.82	0.08	0.79	-0.02	0.78	0.08	0.78	-0.01	0.83	0.09	0.77	-0.01	0.80	0.09	0.76
Eastern Sahara	-	-	-	-	-	-	-	-	-	-	-	-	-	-	-	-	-
Middle East	143	-0.09	-0.13	0.14	0.84	-0.11	-0.19	0.15	0.84	-0.09	-0.14	0.16	0.76	-0.10	-0.17	0.16	0.81
All sites	**4584**	**-0.05**	**0.55**	**0.21**	**0.65**	**-0.06**	**0.49**	**0.21**	**0.70**	**-0.05**	**0.55**	**0.21**	**0.64**	**-0.06**	**0.50**	**0.21**	**0.67**

In the Middle East (see Table 7.2.1 and the Mezaira AERONET site in Figure 7.2.3), o-suite better reproduces the daily variability than control (with correlation coefficient of 0.86 for o-suite and 0.84 for control) and the SDS-WAS Multi-model presents lower correlations (0.73). Underestimations are observed in both CAMS experiments (MB of -0.05 for control and -0.07 for o-suite).

The CAMS o-suite model results are better than control over sub-Tropical North Atlantic region, characterized by long-range transport, with correlation values from 0.55 for control to 0.49 for o-suite (see Table 7.2.1). Both CAMS models present high correlations between 0.69 and 0.73 and slight underestimations (MB between -0.01 and -0.04) over the Iberian Peninsula and the Mediterranean. In the Central Mediterranean, both CAMS experiments present lower performances with correlation coefficients of 0.40 for control and 0.39 for o-suite. These results are similar to the SDS-WAS Multi-model product (0.39) and are associated to the low AOD values observed during this season in the Mediterranean.

The comparison of 1 to 3-day forecasts (see Table 7.2.2) shows that the prediction is stable during the 3-days forecasts with correlation coefficients of 0.74 (0.65), 0.70 (0.65), and 0.67 (0.64) respectively for 24, 48 and 72h forecasts for all the sites for o-suite (control). In North Western Maghreb, the correlation coefficient (r) for control increases from 0.65 to 0.73 in going from the 48h to 72h forecast. These scores are better than in the case of the o-suite that presents correlation coefficient (r) of 0.60 at 48h to 0.68 at 72h.

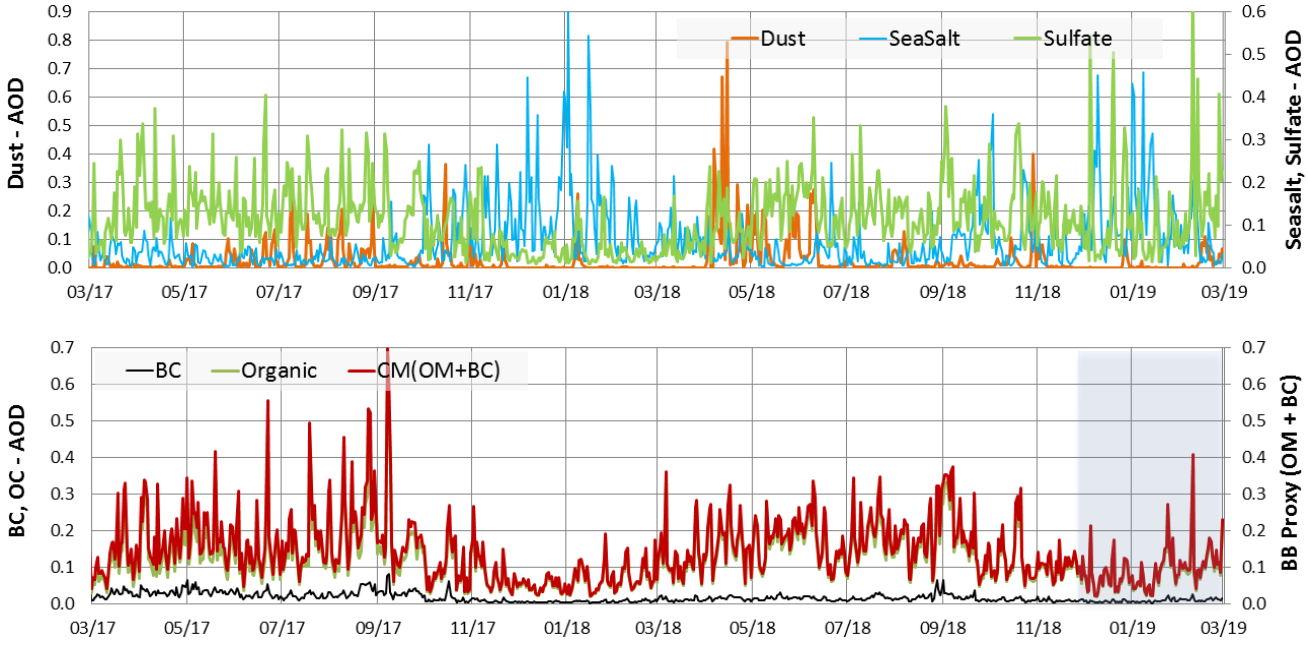

Figure 7.3.1: Maximum daily AOD over Germany for aerosols included in the IFS model from 03/2017 - 02/2019: sea salt (blue), dust (orange), sulphate (light green), black carbon (BC, black), organic matter (green), proxy for 'biomass burning' (as OC+BC - red). Note the different y-axes for the aerosol species.

7.3 Backscatter profiles

The technical specifications of the data sources, the evaluated parameters and the methods are described in Eskes et al. (2018). In this section, the temporal and vertical variation of the backscatter coefficient (BSC) profiles are evaluated, showing the statistics including bias, correlation, and standard deviation of the o-suite and control run versus ceilometers. These scores are summarized in Taylor plots.

Period Overview

The model aerosol optical depth (AOD) and ceilometer overviews exhibit periods with significant aerosol plumes over Germany. Figure 7.3.1 shows the maximum AOD over Germany, separately for contributions of mineral dust (SD), sea salt (SS), carbonaceous matter (CM), black (BC) and organic carbon (OC), as well as sulphate (SU). Weak SD events, e.g. 15-18 Feb 2019 and several days with elevated sulfate and sea salt stick out. All components follow their usual seasonality.

Mean profiles

Model BSC in the PBL are on average lower than observed (Fig. 7.3.2, 7.3.3). The annual variation of the PBL height is rudimentary reproduced but is strongly smoothed. While enhanced emissions of organic matter (OM) have been introduced in Jan 2017, and parametrizations of SO_2/SO_4 conversion/deposition were improved, nitrate and ammonia are still missing in the current model version, which contribute roughly 10-30% of aerosol mass (as NO_3NH_4 or $(NH_4)_2SO_4$) in the rural central European PBL. (According to pers. communication - S. Remy/Z. Kipling - nitrates and ammonium are ready in the current model and possibly get activated in the next cycle). Technically,

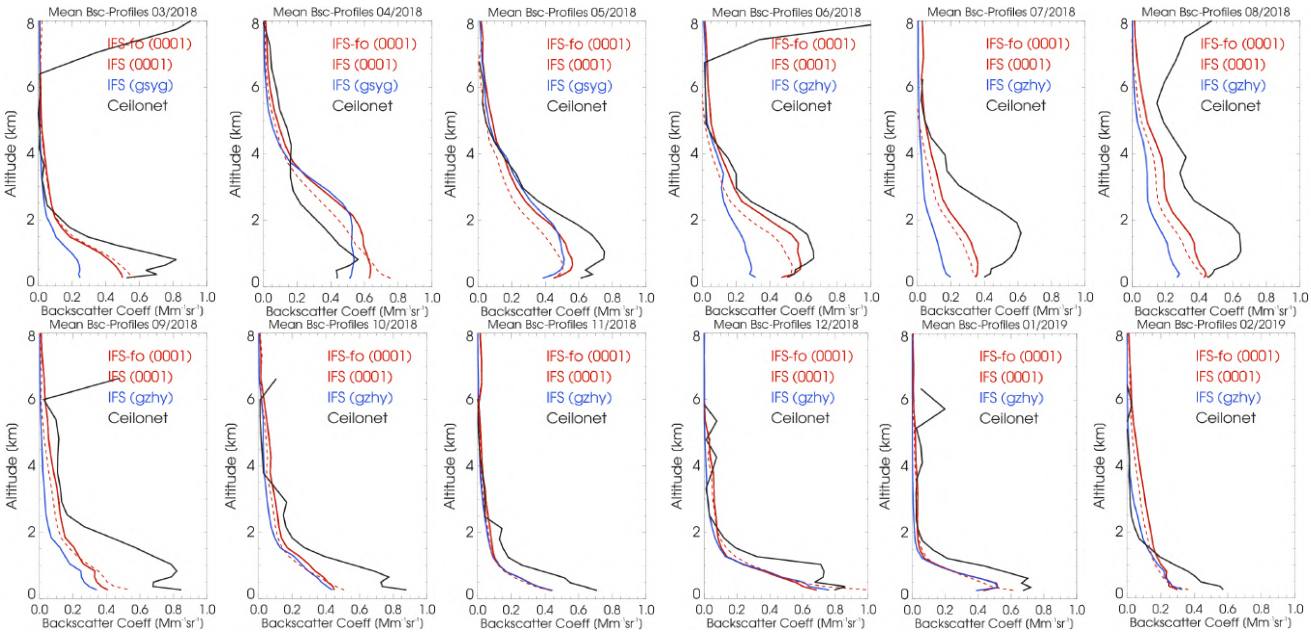

Figure 7.3.2: Monthly mean profiles of backscatter coefficients from o-suite (red), control run (blue), and ceilometers (black) combined from 21 German stations in Mar 2018 to Feb 2019. The profiles are partly contaminated by remaining cloud artefacts.

this could be compensated by assimilating observational data for the o-suite, but without profile information this results in a vertical redistribution with a positive bias in the free troposphere, a too smooth transition at the PBL top (Fig. 7.3.2) and a negative bias in the PBL. Thus, the assimilation increases aerosol loads in the o-suite relative to the control but does not introduce a realistic step at the top of the PBL to lower values in the free troposphere (FT) evident in the ceilometer profiles. Therefore, the amplitude of the vertical profile of the model compared to observations (reference), coded in the standard deviation in the Taylor plots, is too low.

Secondly, our forward operator (including mass-to-volume conversion) presently uses particle densities of the pure materials, not taking into account that dry atmospheric particles are often porous (sponge-like, even fractal) with entrapped air owing to coagulation and variable internal mixing, and thus exhibit reduced bulk density. A high-biased particle density results in low-biased equivalent volume, and a corresponding underestimation of optical properties, because these depend strongly on the particle size. Density reductions for accumulation mode particles, composed of hydrophilic and hydrophobic materials may be as high as a factor 1.5 (~1.3 for surface). Thirdly, the capping transport barrier at the PBL top is less effective in the model, diluting high PBL concentrations with clean FT air. On average, however, the PBL height seems reasonable (this has been discussed in an earlier report).

The reason for the difference between mean model profiles calculated from DWD's forward operator DWD-fo and those retrieved from the MARS archive (IFS-fo implemented in the IFS) is still investigated. Higher backscatter is calculated by the DWD-fo in summer (04-08) while it is small in autumn and winter. (Note, this is corrected as against the last report because there the molecular fraction had not been subtracted from the IFS-fo profiles.) In dust-dominated periods (e.g. 07-13 Apr 19), profiles from both fo are consistent. IFS-fo often, but not always, yields higher BSC during

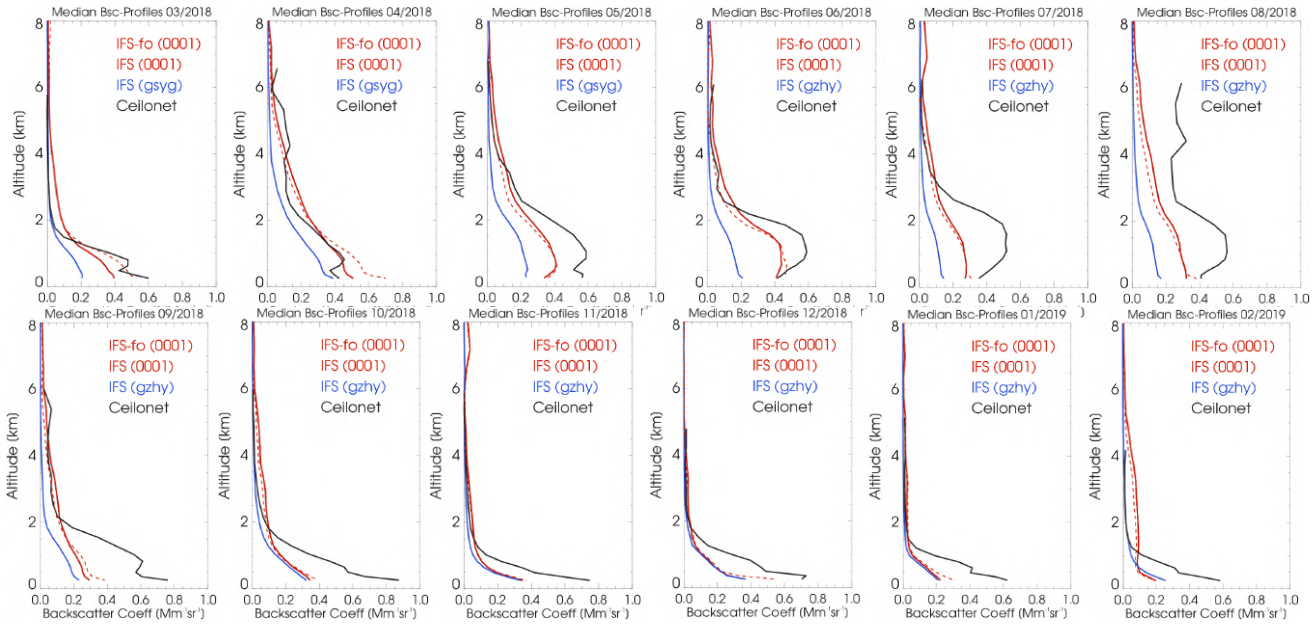

Figure 7.3.3: Monthly median profiles of backscatter coefficients from o-suite (red), control run (blue), and ceilometers (black) combined from 21 German stations in Mar 2018 to Feb 2019. The profiles are partly contaminated by remaining cloud artefacts.

sea-salt/organic cases. This points to humidity-dependent hygroscopic growth as a possible contribution, but we have to check why the clean free troposphere is equally affected as the boundary layer and calculating the profiles with overall high (90%) relative humidity by the DWD-fo has little effect. In many cases, the IFS-fo profiles are smoother which contributes to lower monthly average BSC at altitudes with strong layers like around 1-3 km in April. This issue remains under investigation.

Taylor Plots (Fig. 7.3.4)

The average coefficient of correlation between modelled and observed vertical backscatter profiles clusters around r = 0.4-0.6. The absolute standard deviation (SD) are normalized to the SD of observations per day, as reference value at SD ≡ 1.0. The better performance of the o-suite (red dots) compared to the control run (blue dots) in terms of SD, observed during summer, becomes less marked during autumn and vanishes in winter. There is a very large day-to-day and also a seasonal variation of the performance. Individual cases suggest that the large spread and the high bias, observed on many days in winter (Dec, Jan) is due to layers with high sea-salt concentrations.

Summary

Backscatter coefficients are low-biased in the planetary boundary layer (PBL). As before, possible reasons are missing of ammonia and nitrate in the model (foreseen to be activated soon), assumption of too high particle densities (for pure compact materials) in the mass to backscatter conversion, and the lack of vertical transport barrier at the top of the PBL, causing dilution with free troposphere air. Against this, free troposphere (FT) background backscatter coefficients are biased high, probably due to the assimilation re-distributing between PBL and FT. The BSC bias on a specific level thus depends on its relative position w.r.t. the BLH. Generally, monthly average vertical

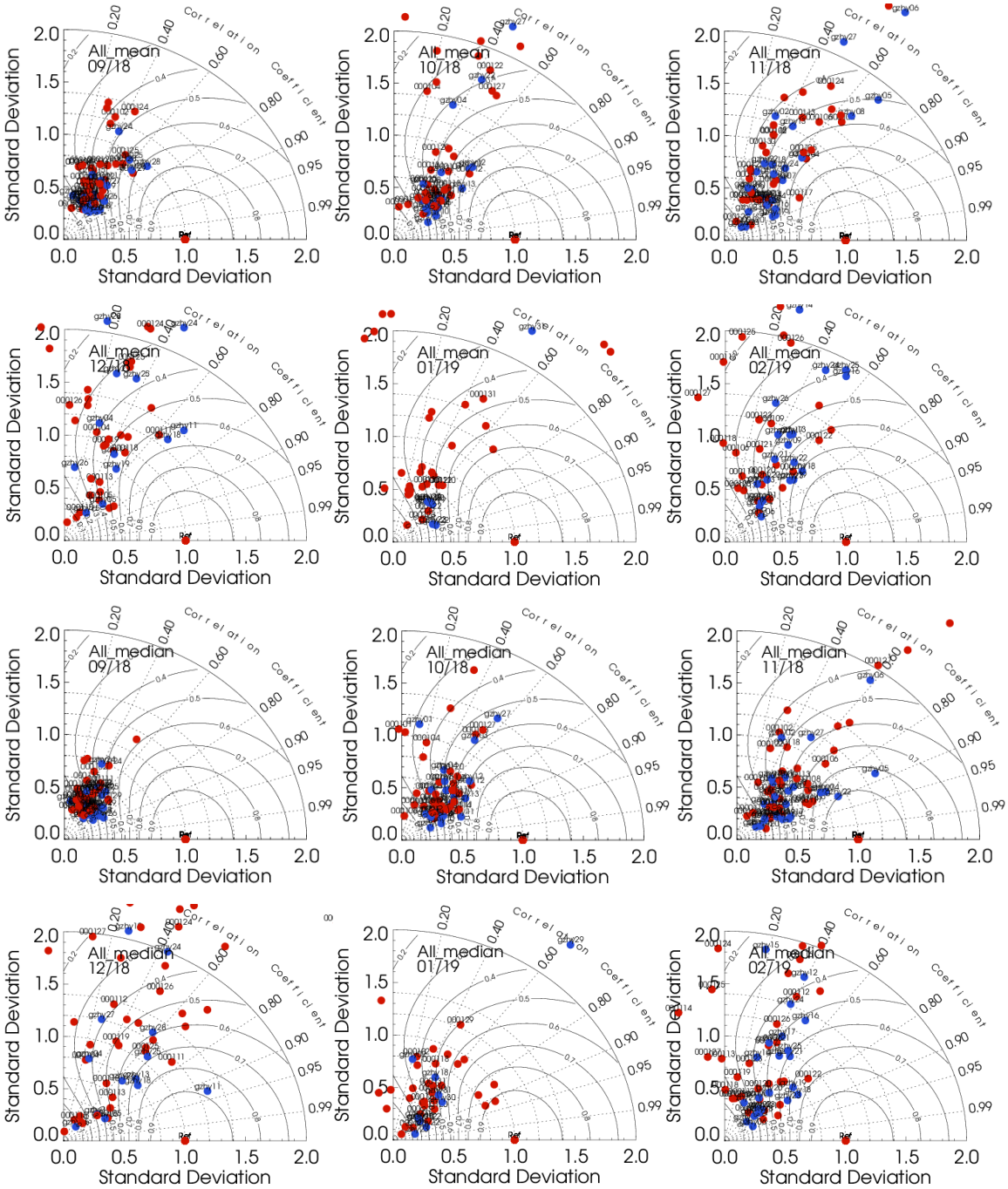

Fig. 7.3.4: Taylor polar plots with daily average standard deviation of vertical profiles vs correlation coefficient, averaged over 21 German ceilometer sites for Sept 2018 – Feb 2019. O-suite red, control blue. Top: mean values, Bottom: median values.

backscatter profiles to some extent follow the annual cycle of the observations, but they are smoother. The reason for the discrepancy between results with two different forward operators is yet not resolved. The summary monthly Taylor plots over 21 German stations indicate that daily averages of Pearson correlation coefficients cluster around 0.4-0.6, too large variability in winter, often due to overestimated layers of sea-salt and that this causes a less consistent day-to-day performance in winter as compared to summer.

7.4 Aerosol validation over the Mediterranean

Three-hourly aerosol optical depth (AOD) and surface concentration (PM10 and PM2.5) from the CAMS o-suite and control experiment have been validated for the period 1 September 2018 to 30 November 2018 against AERONET direct-sun cloud-screened observations.

Aerosol optical depth

The CAMS o-suite can reproduce the daily variability of AERONET observations. In the Western, Central and Eastern Mediterranean, the correlation coefficient increases from 0.66, 0.32 and 0.50, to 0.68, 0.48 and 0.55 respectively, for control and o-suite during autumn (see the correlation coefficient by sites in Figure 7.4.1). Underestimations observed in the Mediterranean Basin in control (MB of -0.02, -0.02 and 0 for Western, Central and Eastern Mediterranean regions respectively) are corrected in o-suite introducing overestimations in the Basin (MB of 0.01, 0.02 and 0.03 for Western, Central and Eastern Mediterranean regions respectively), particularly in Tunesia as it is shown in Figure 7.4.1. The dust activity was low during the entire season and the most important events were observed in the Eastern Mediterranean (see Figure 7.4.2).

Surface aerosol concentrations

For winter, PM10 and PM2.5 results of CAMS o-suite and control show similar skill scores in comparison with EIONET-Airbase observations (see Figure 7.4.3). The CAMS forecast tends to overestimate the PM10 and PM2.5 EIONET-Airbase observations in north-western Mediterranean sites (see Figure 7.4.3 and Figure 7.4.4), but meanwhile tends to underestimate the PM10 and PM2.5 observed values at Spanish sites.

Overestimations at north-western Mediterranean sites are linked to the overestimation of the CAMS model in mid-January and end-February (see Venaco in Corsica in Figure 7.4.5 in which control and o-suite experiments show concentration above 50 $\mu g/m^3$).

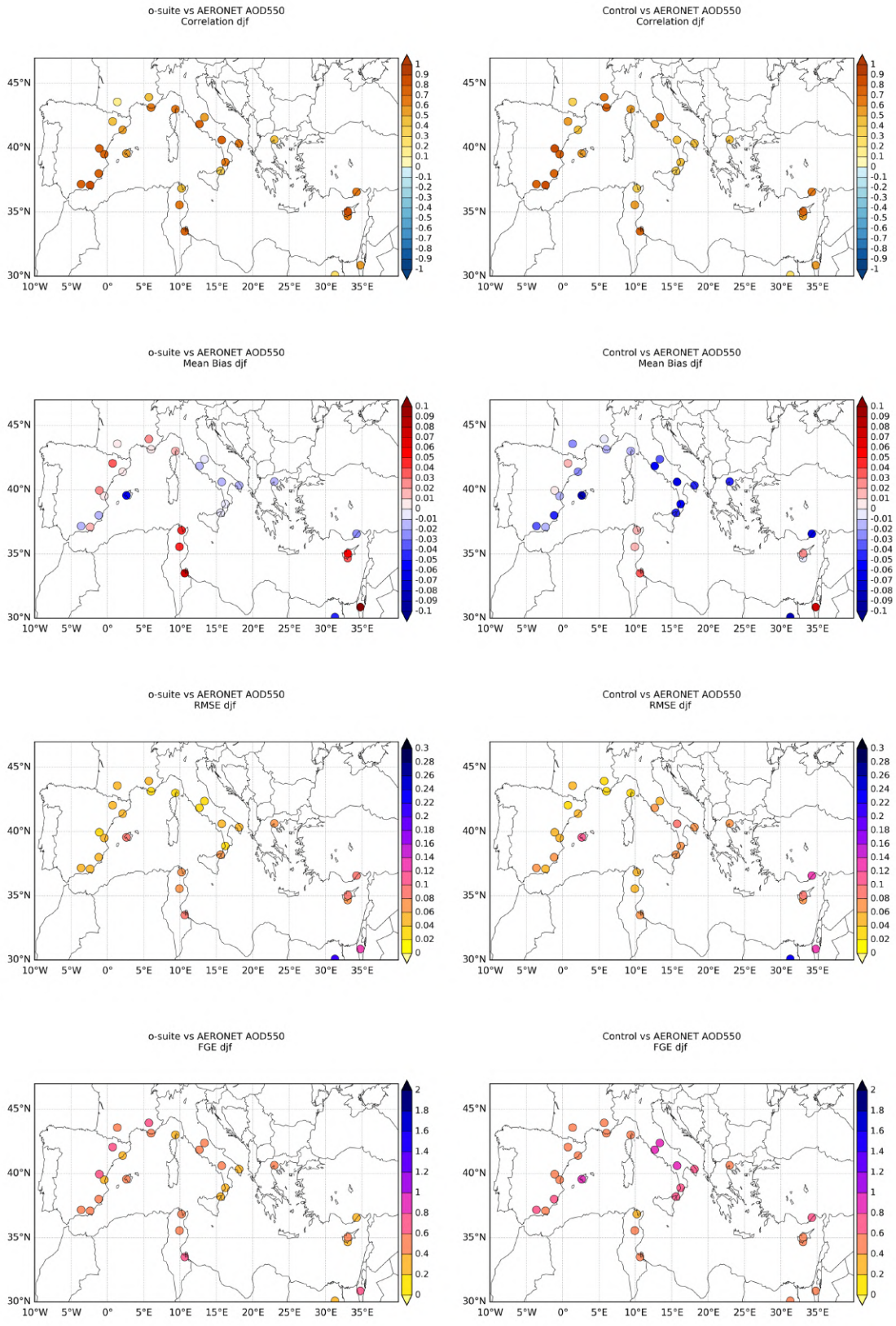

Figure 7.4.1: Skill scores (correlation coefficient, MB, RMSE and FGE) for 24-hour forecasts of CAMS o-suite and control for the study period. AOD from AERONET is the reference.

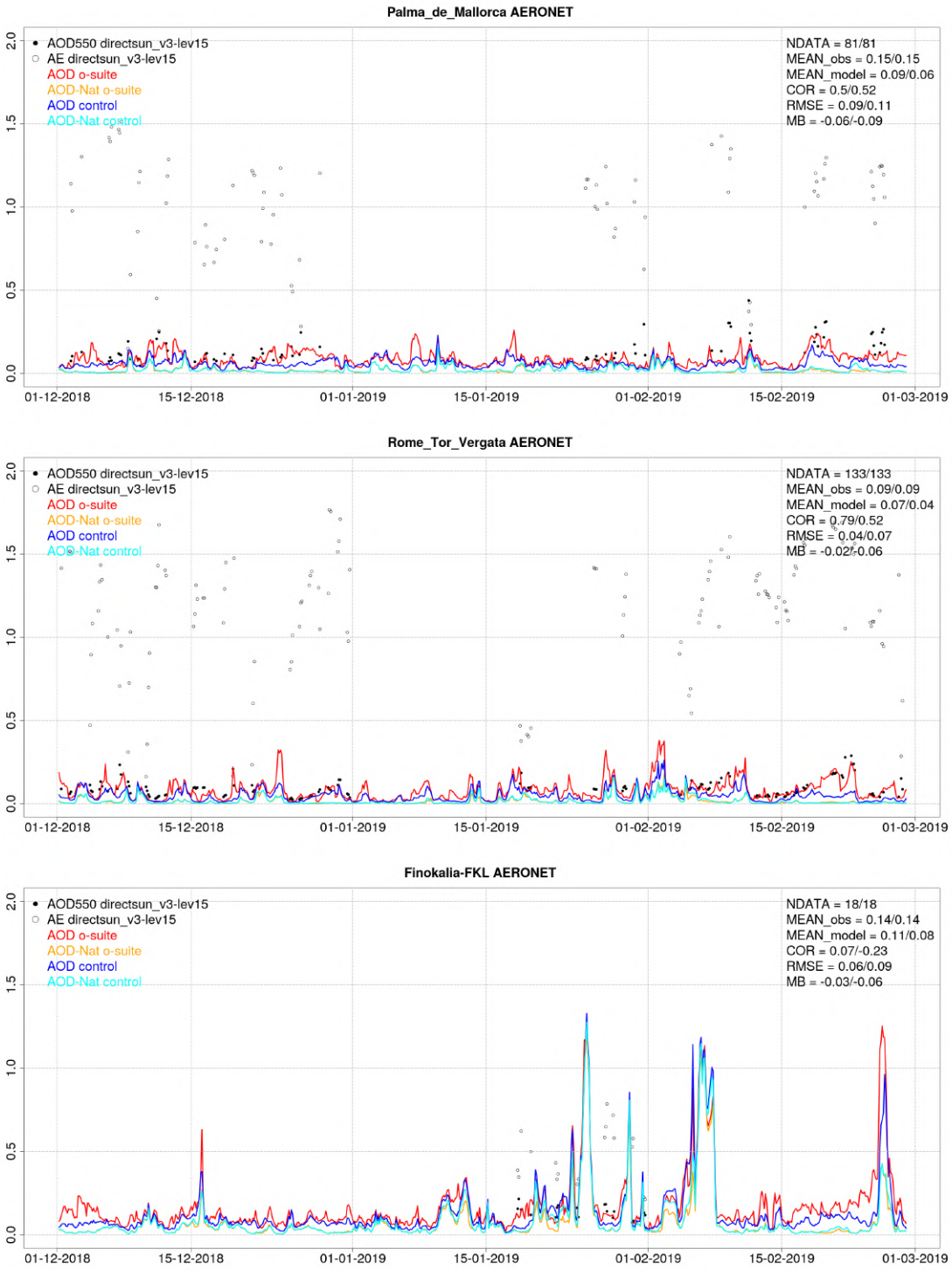

Figure 7.4.2: AOD from AERONET (black dot), AOD o-suite (red line), AOD control (blue line), AOD-Nat o-suite (orange line), AOD-Nat control (cyan line), for the study period over Palma de Mallorca (Balearic Islands, Spain), Messina (Italy) and IMS-METU-ERDEMLI (Israel). AOD-Nat corresponds to the natural aerosol optical depth that includes dust and sea-salt. Skill scores per each individual site and model (o—suite/control) are shown in the upper right corner (NDATA: available 3-hourly values used for the calculations, MEAN observations, MEAN_model, COR, RMSE, MB).

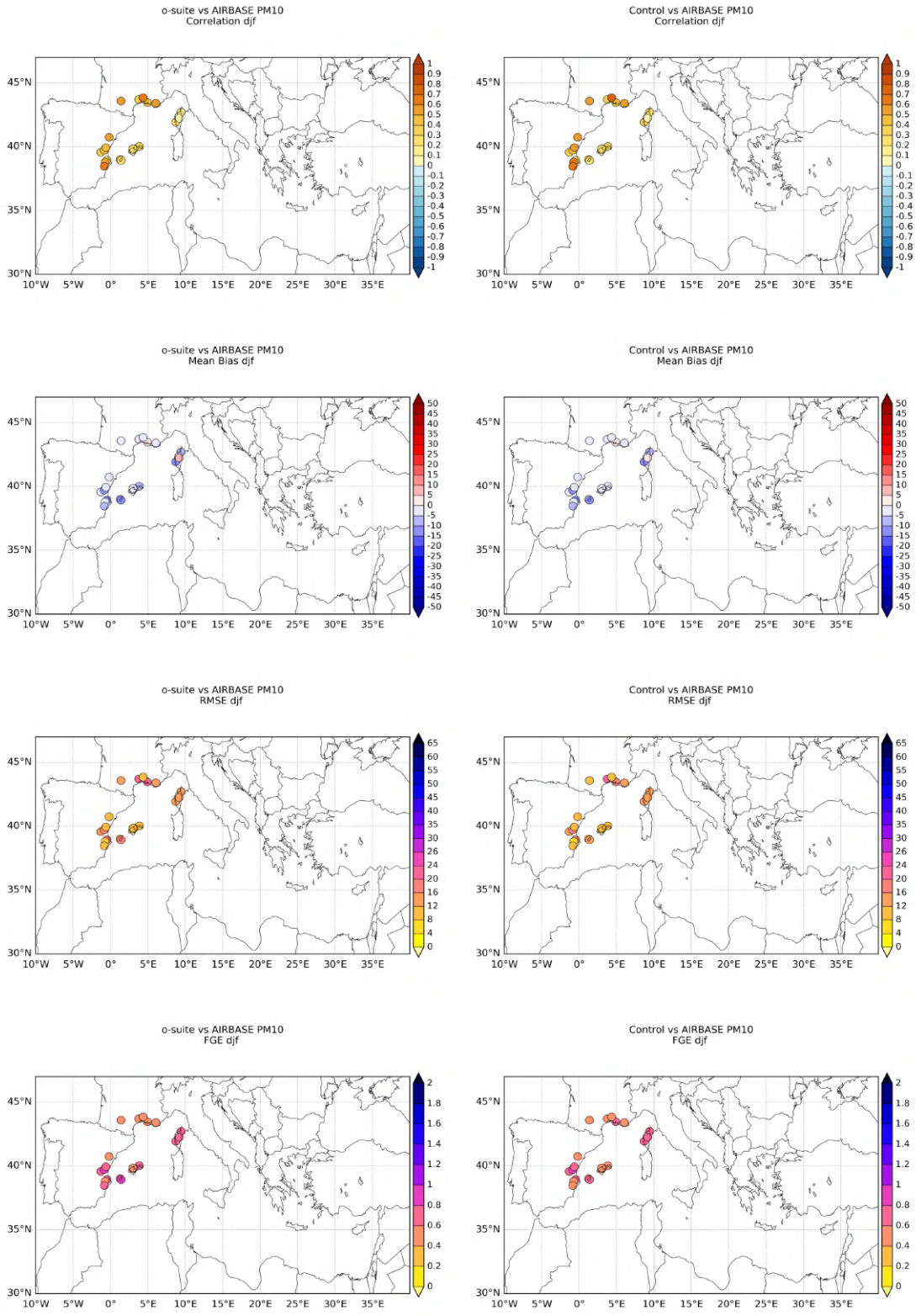

Figure 7.4.3: Skill scores (correlation coefficient, MB, RMSE and FGE) for 24-hour forecasts of CAMS o-suite and control for the study period. PM10 from EIONET are the reference. Only background suburban and rural available stations are displayed.

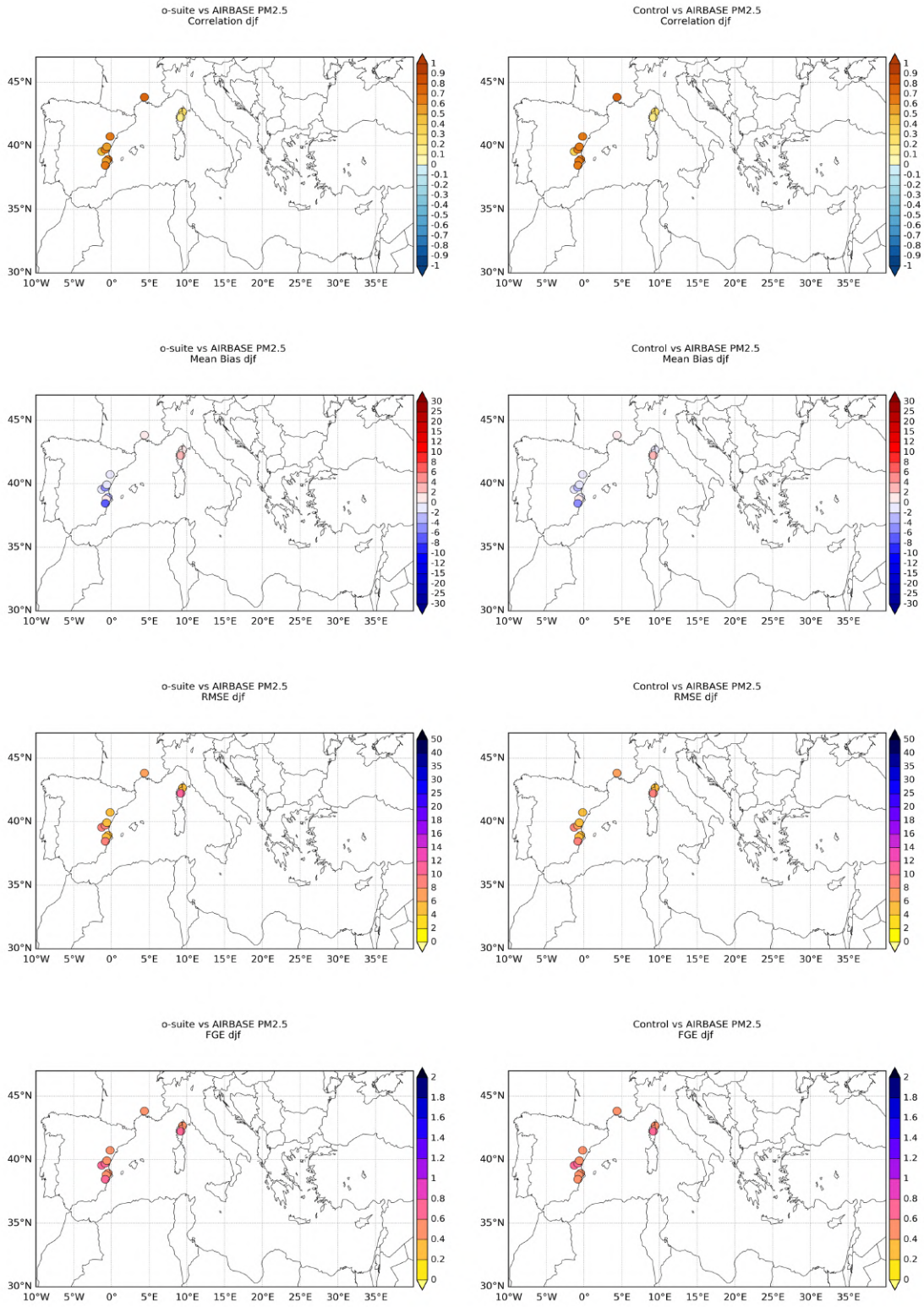

Figure 7.4.4: Skill scores (correlation coefficient, MB, RMSE and FGE) for 24-hour forecasts of CAMS o-suite and control for the study period. PM2.5 from EIONET are the reference. Only background suburban and rural available stations are displayed.

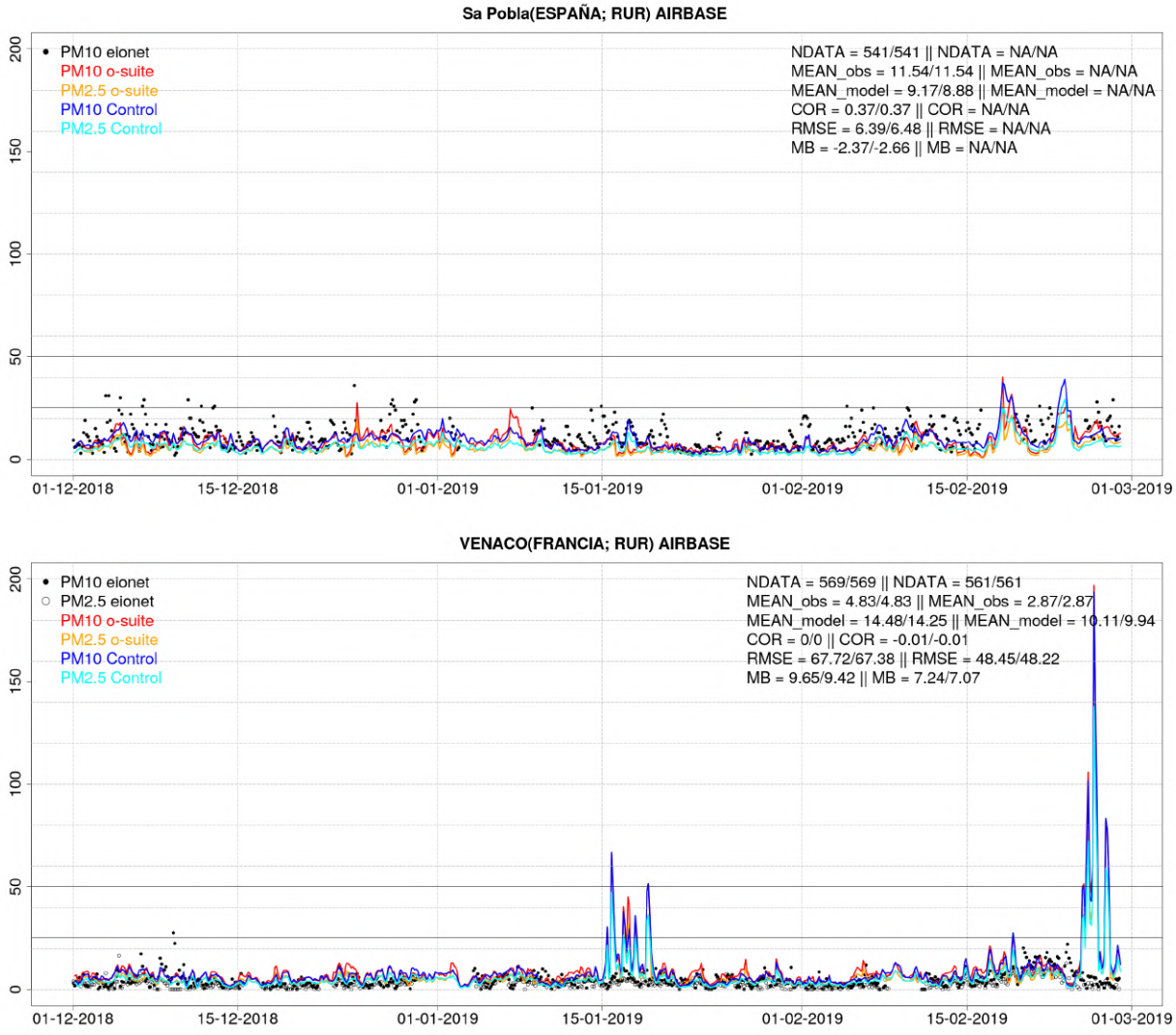

Figure 7.4.5: PM10 and PM2.5 Airbase observations (black and grey dots, respectively), PM10 and PM2.5 o-suite (red and orange lines, respectively) and PM10 and PM2.5 control (blue and cyan lines, respectively) for the study period over Can Llompart (Balearic Islands, Spain) and Venaco (Corse, France).

8. Stratosphere

8.1 Validation against ozone sondes

In this section, we present the results of the stratospheric ozone evaluation against ozone soundings from the NDACC, WOUDC, NILU and SHADOZ databases. The sondes have a precision of 3-5% (~10% in the troposphere for Brewer Mast) and an uncertainty of 5-10%. For further details see Cammas et al. (2009), Deshler et al. (2008) and Smit et al (2007). Model profiles of the o-suite are compared to balloon sondes measurement data of 44 stations for the period January 2013 to February 2019 (please note that towards the end of the validation period fewer soundings are available). As C-IFS-CB05 stratospheric composition products beyond O_3 in the o-suite is not useful we provide only a very limited evaluation of the control experiment. A description of the applied methodologies and a map with the sounding stations can be found in Eskes et al. (2016). The o-suite shows MNMBs within the range ±12%, for all regions and months (some exceptions with MNMBs of up to ±18% for single months in the high latitude regions). Figure 8.1.1. shows the results for the past year, and Figure 8.1.2 for the past 6 years.

Fig. 8.1.3 compares the averaged profiles in each region during January 2019. The vertical distribution of stratospheric ozone is quite well represented for all regions by the o-suite, with little overestimation in all latitude bands (MNMBs between -1 to 10% for DJF 2019).

The control run shows a strong overestimation of stratospheric ozone in the upper stratosphere, and an underestimation between 40hPa (Arctic 60 hPa) and 300 hPa in the Arctic and the Northern Midlatitudes. In the Tropics, the underestimation is between 80 and 30 hPa. The Antarctic profile shows a strong underestimation between 40 and 150 hPa. Above, O_3 partial pressures are overestimated.

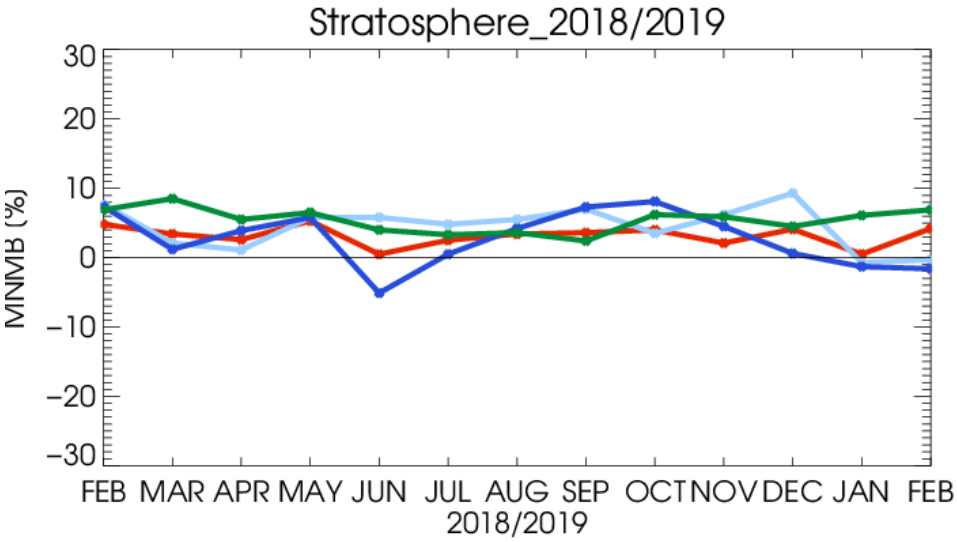

Figure 8.1.1: MNMBs (%) of ozone in the stratosphere from the o-suite against aggregated sonde data in the Arctic (light blue), Antarctic (dark blue) northern midlatitudes (red) and tropics (green). Period February 2018 to February 2019. The stratosphere is defined as the altitude region between 60 and 10 hPa in the tropics and between 90 and 10 hPa elsewhere.

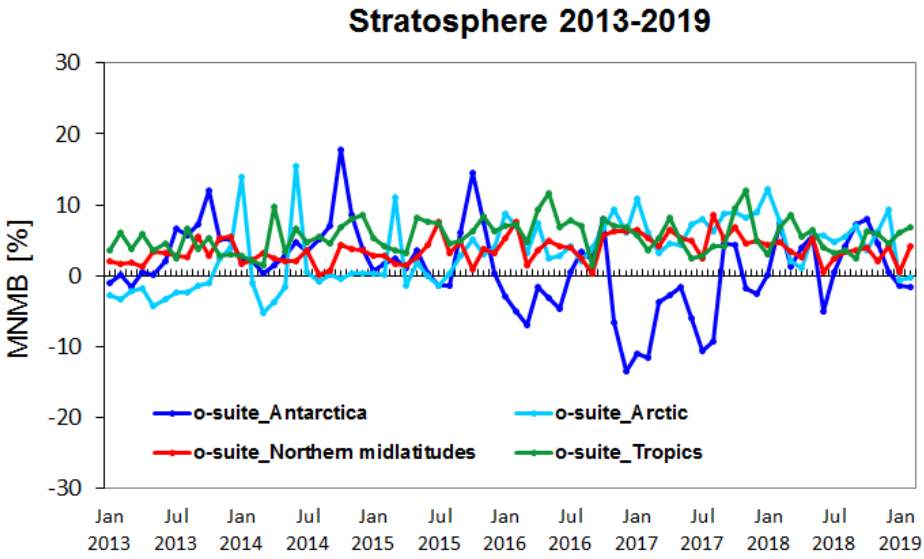

Figure 8.1.2: Same as Fig. 8.1.1, but for the extended time period January 2013 to February 2019.

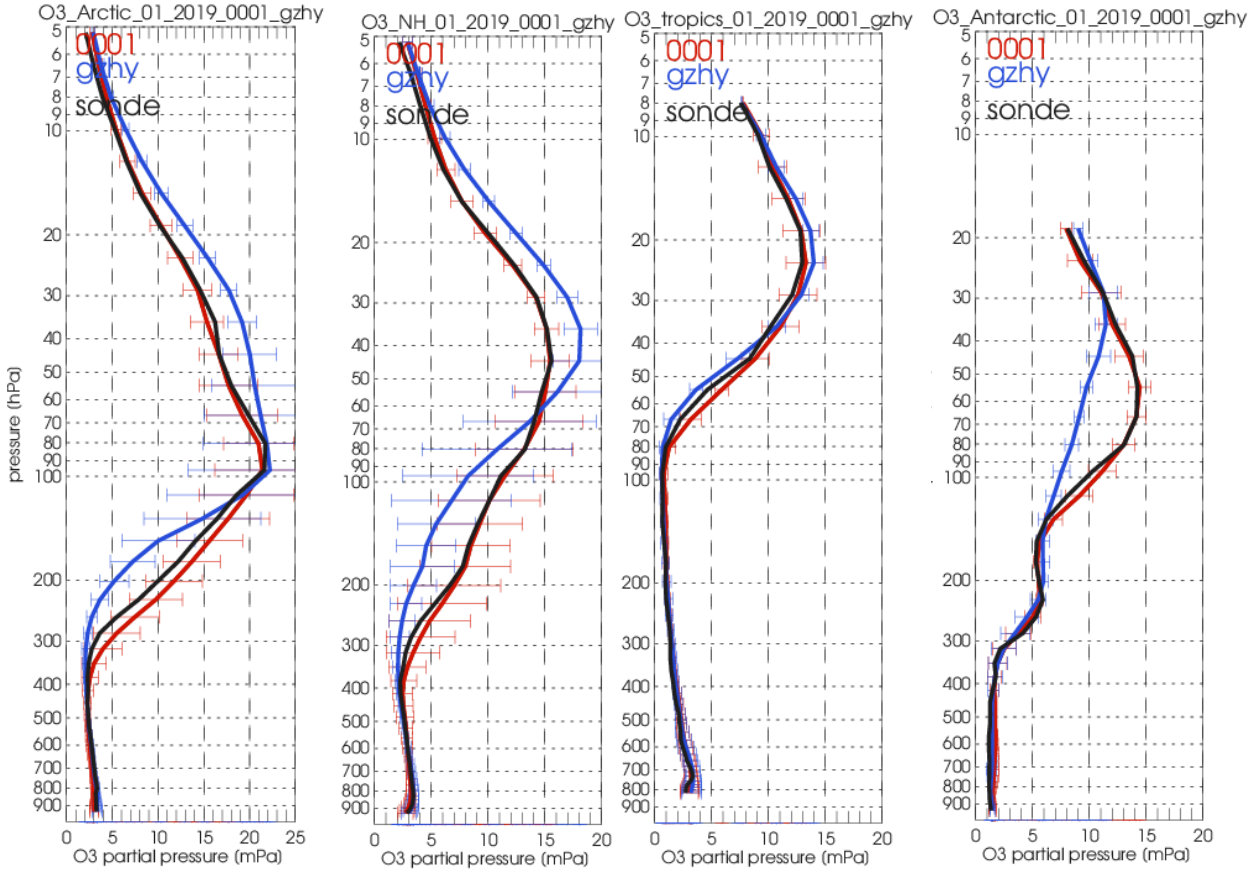

Figure 8.1.3. Comparison between mean O_3 profiles (units: mPa) of o-suite (red), and control (blue) in comparison with observed O_3 sonde profiles (black) for January 2019 for the various latitude bands: Arctic, NH-mid latitudes, Tropics and Antarctic.

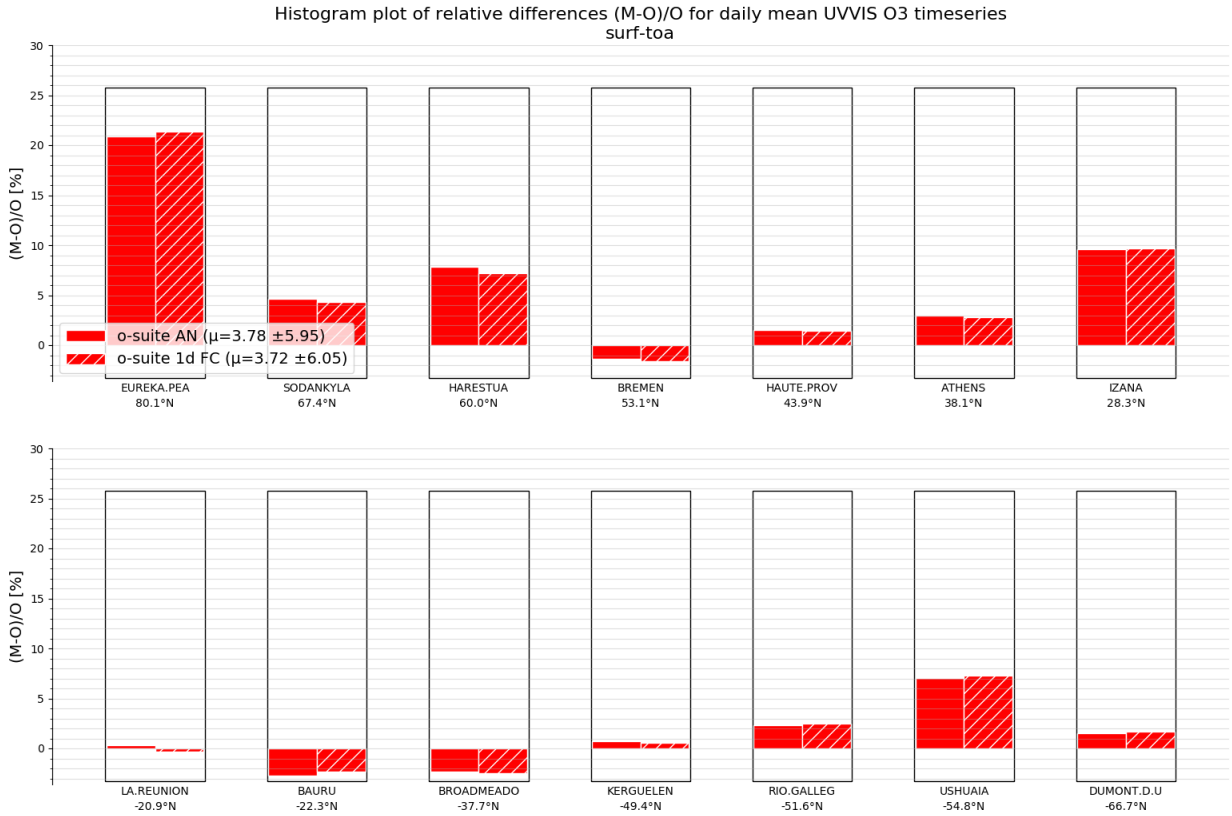

Figure 8.2.1 Relative biases during quarter DJF 2019 for 14 UVVIS stations measuring stratospheric ozone columns with ZENITH measurement geometry (stations sorted with decreasing latitude). The overall relative bias is positive for all latitudes and within the typical measurement uncertainty of 5% for most of the sites.

8.2 Validation against observations from the NDACC network

UVVIS and FTIR stratospheric columns

Since the start of the CAMS27 project, the number of UVVIS Zenith ozone measurements have increased on NDACC. Currently fifteen sites provided data in the recent quarter allowing for a representative picture on the latitude dependence of the model data.

The systematic uncertainty of the UVVIS measurements is typically 5%, hence the relative biases for most sites for both the AN and 1d FC of the o-suite are very close to each other and within the uncertainty ranges, see Figure 8.2.1. The averaged bias for the 16 UVVIS sites is 4.5% and the averaged correlation is 0.93.

The correlations between the sites and the model are presented in the Taylor diagrams in Figure 8.2.2. Again, the o-suite AN and 1d FC perform very similarly in correlation coefficients.

Figure 8.2.3 depicts the FTIR stratospheric columns showing a discontinuity in the o-suite 1d FC model for the tropical sites (Mauna Loa, Altzomoni and Reunion) in the June 2016 model update.

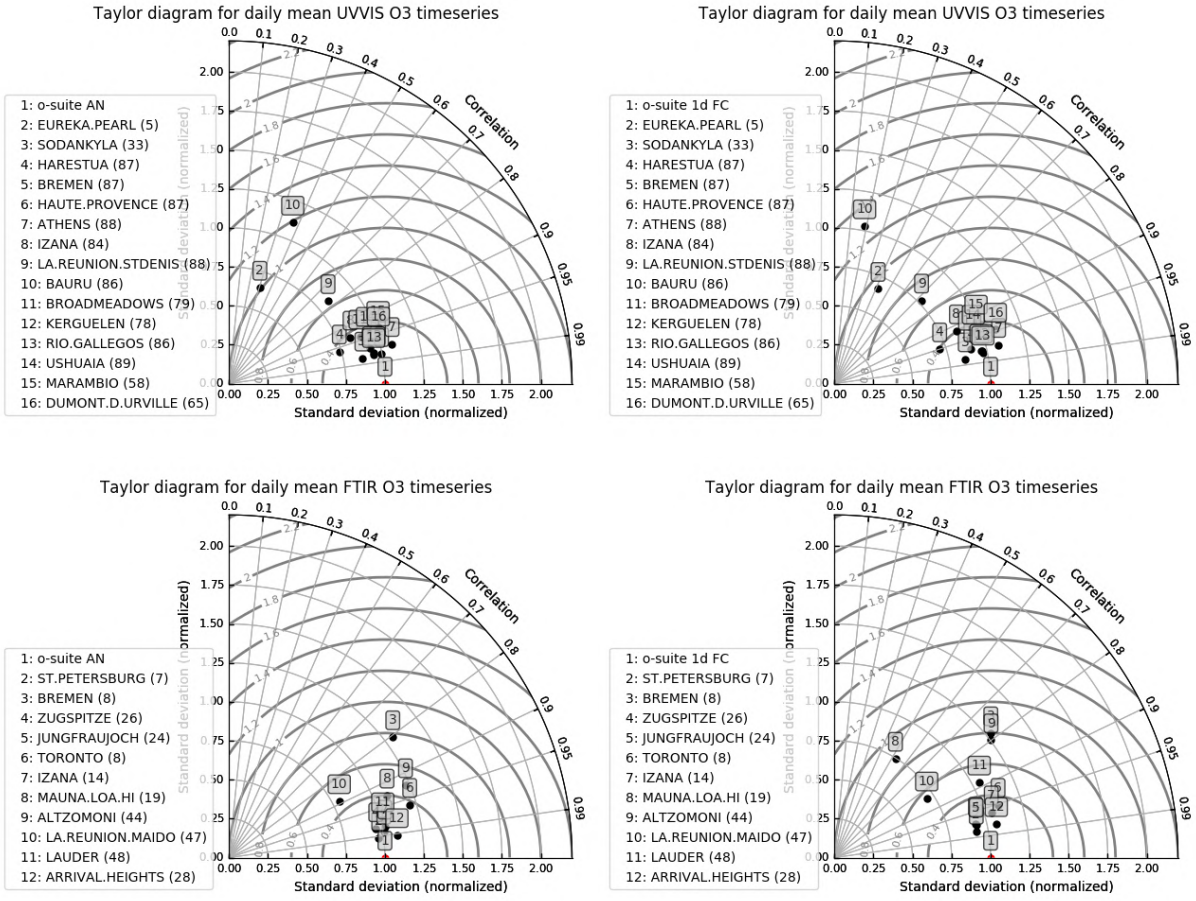

Figure 8.2.2 Taylor diagrams relating the standard deviations for the model and GB stratospheric column time series and their correlation for the time period DJF 2019. All time series are normalized such that the std of the model is 1. The performance for the osuiteAN is slightly better (averaged correlation is 0.95 for FTIR and 0.86 for UVVIS) compared to the 1d FC (averaged correlation is 0.88 for FTIR and 0.85 for UVVIS).

Profile comparison using LIDAR and MWR

In this section we present a comparison between the CAMS o-suite and control run models against MWR and LIDAR observations from the NDACC network. A detailed description of the instruments and applied methodologies for all NDACC instruments can be found at http://nors.aeronomie.be. MWR (microwave) at Ny Alesund (79°N, 12°E, Arctic station) and Bern (47°N, 7°E, northern midlatitude station). LIDAR at Observatoire Haute Provence (OHP), France (43°N, 5.7°E, altitude 650m) and Hohenpeissenberg, Germany (47°N, 11°E, altitude 1km)

Figure 8.2.3 shows that at Ny Alesund the o-suite overestimates the stratospheric ozone concentration with more than 10% during SON/DJF/MAM and the bias vanishes during summer JJA (the instrument is down since July 2018). Between the model upgrades from September 2015 and January 2017 the relative bias at Bern vanishes (i.e. is comparable to the measurement uncertainty). In Figure 8.2.3 a discontinuity is observed for the mesospheric ozone column measured by the MWR at Bern at the Jan 2017 update which is due to an underestimation of the upper stratospheric ozone column (see Figure 8.2.4).

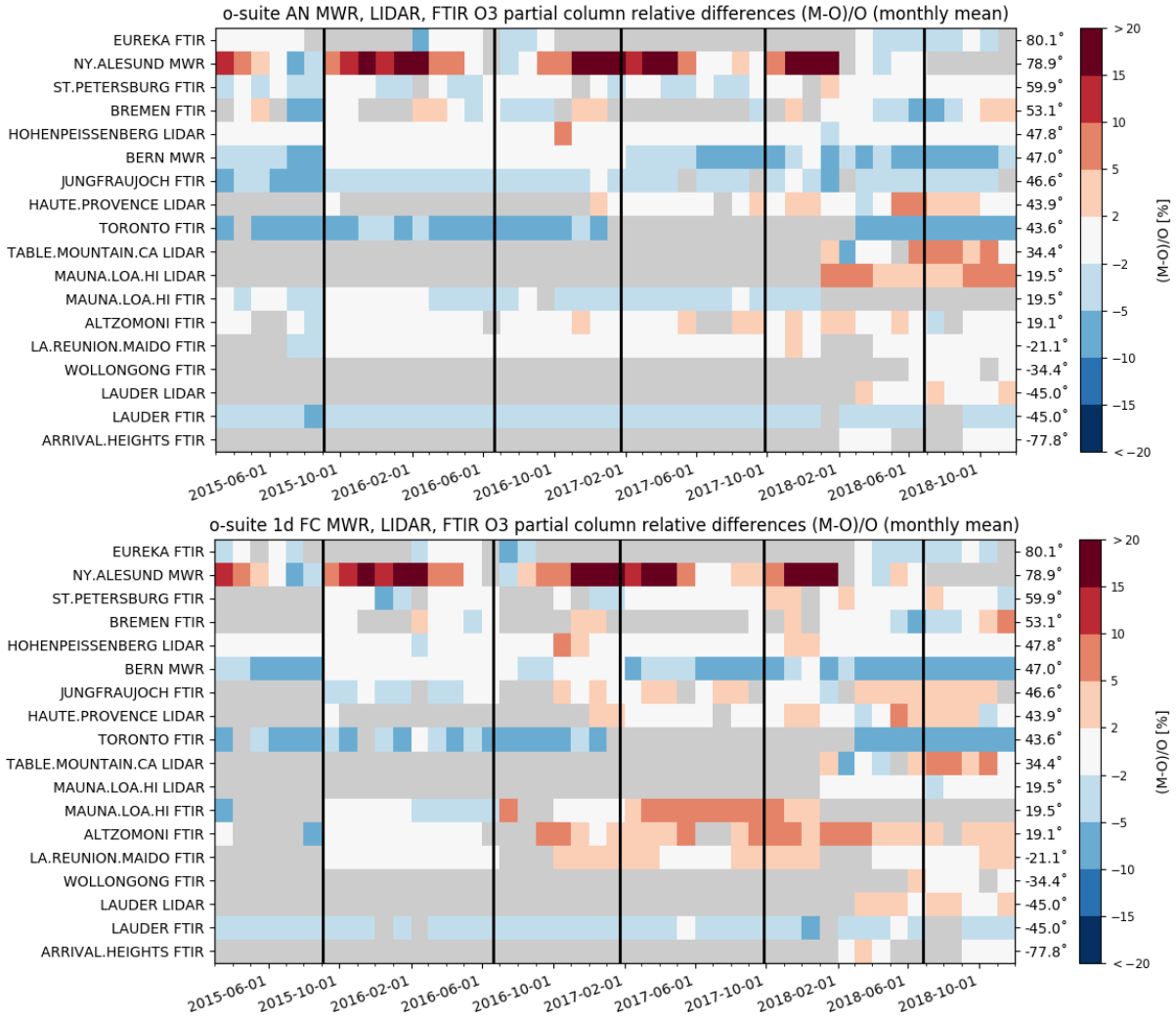

Figure 8.2.3 Time series of monthly mean relative differences for stratospheric columns (FTIR and LIDAR) and mesospheric (MWR) columns along with model cycle updates (black vertical lines) (o-suite AN top, o-suite 1d FC bottom). The stratospheric FTIR columns at St Peterburg, Jungfraujoch, Altzomoni and La Reunion show a slight positive trend in the relative differences, which is probably introduced by model updates.

In MAM-JJA 2015-2018, both MWR stations observe a significant (i.e. comparable to the measurement uncertainty) overestimation of the upper stratospheric/mesospheric ozone content, and the converse is seen during autumn and winter SON-DJF, underestimating up to -30% at Ny Alesund, see also Figure 8.2.4.

At OHP and Hohenpeissenberg (LIDAR), the o-suite slightly overestimates the observed ozone (<10%) between 25km and 35km. The uncertainty on the LIDAR concentration increases with altitude and above 35km the observed differences are comparable to the measurement uncertainty (>10%, see http://nors.aeronomie.be/projectdir/PDF/NORS_D4.2_DUG.pdf)

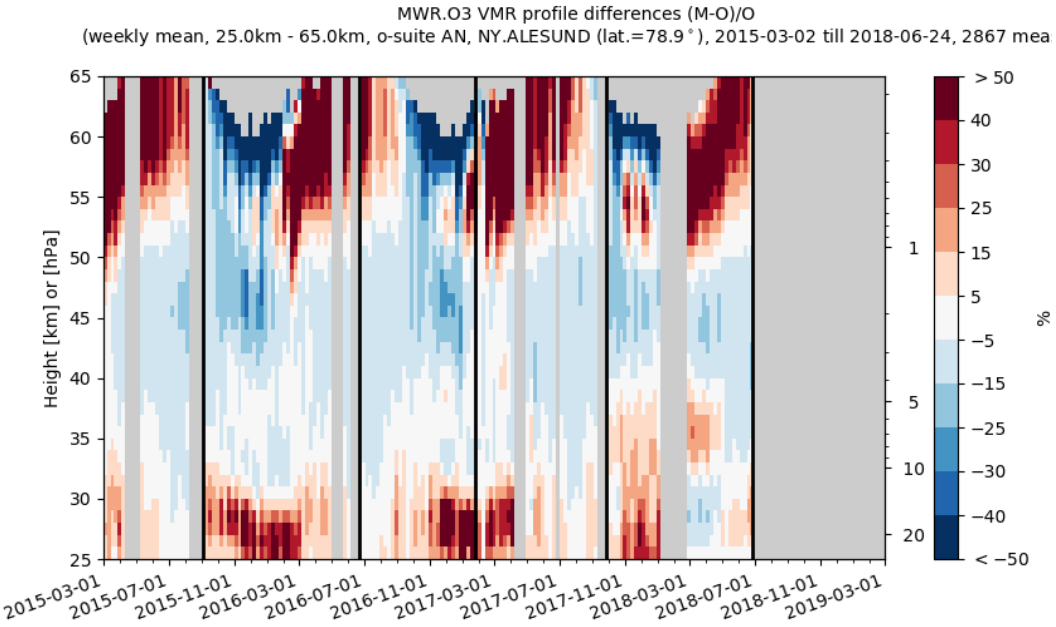
MWR.O3 VMR profile differences (M-O)/O
(weekly mean, 25.0km - 65.0km, o-suite AN, NY.ALESUND (lat.=78.9°), 2015-03-02 till 2018-06-24, 2867 mea
Height [km] or [hPa]
65
60
55
50
45
40
35
30
25
1
5
10
20
> 50
40
30
25
15
5
−5
−15
−25
−30
−40
< −50
%
2015-03-01
2015-07-01
2015-11-01
2016-03-01
2016-07-01
2016-11-01
2017-03-01
2017-07-01
2017-11-01
2018-03-01
2018-07-01
2018-11-01
2019-03-01

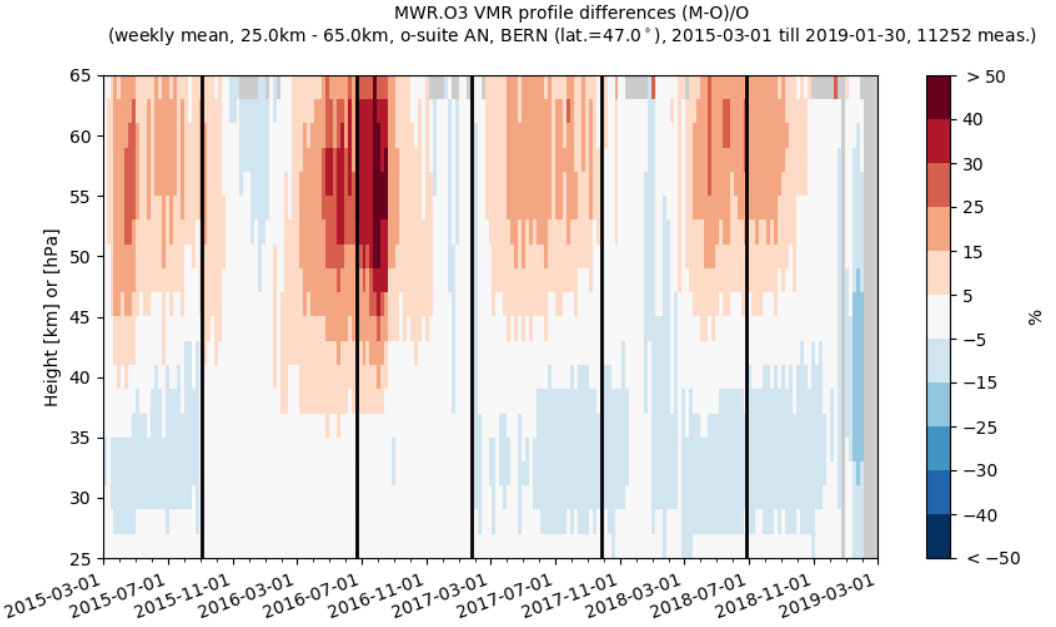
MWR.O3 VMR profile differences (M-O)/O
(weekly mean, 25.0km - 65.0km, o-suite AN, BERN (lat.=47.0°), 2015-03-01 till 2019-01-30, 11252 meas.)
Height [km] or [hPa]
65
60
55
50
45
40
35
30
25
> 50
40
30
25
15
5
−5
−15
−25
−30
−40
< −50
%
2015-03-01
2015-07-01
2015-11-01
2016-03-01
2016-07-01
2016-11-01
2017-03-01
2017-07-01
2017-11-01
2018-03-01
2018-07-01
2018-11-01
2019-03-01

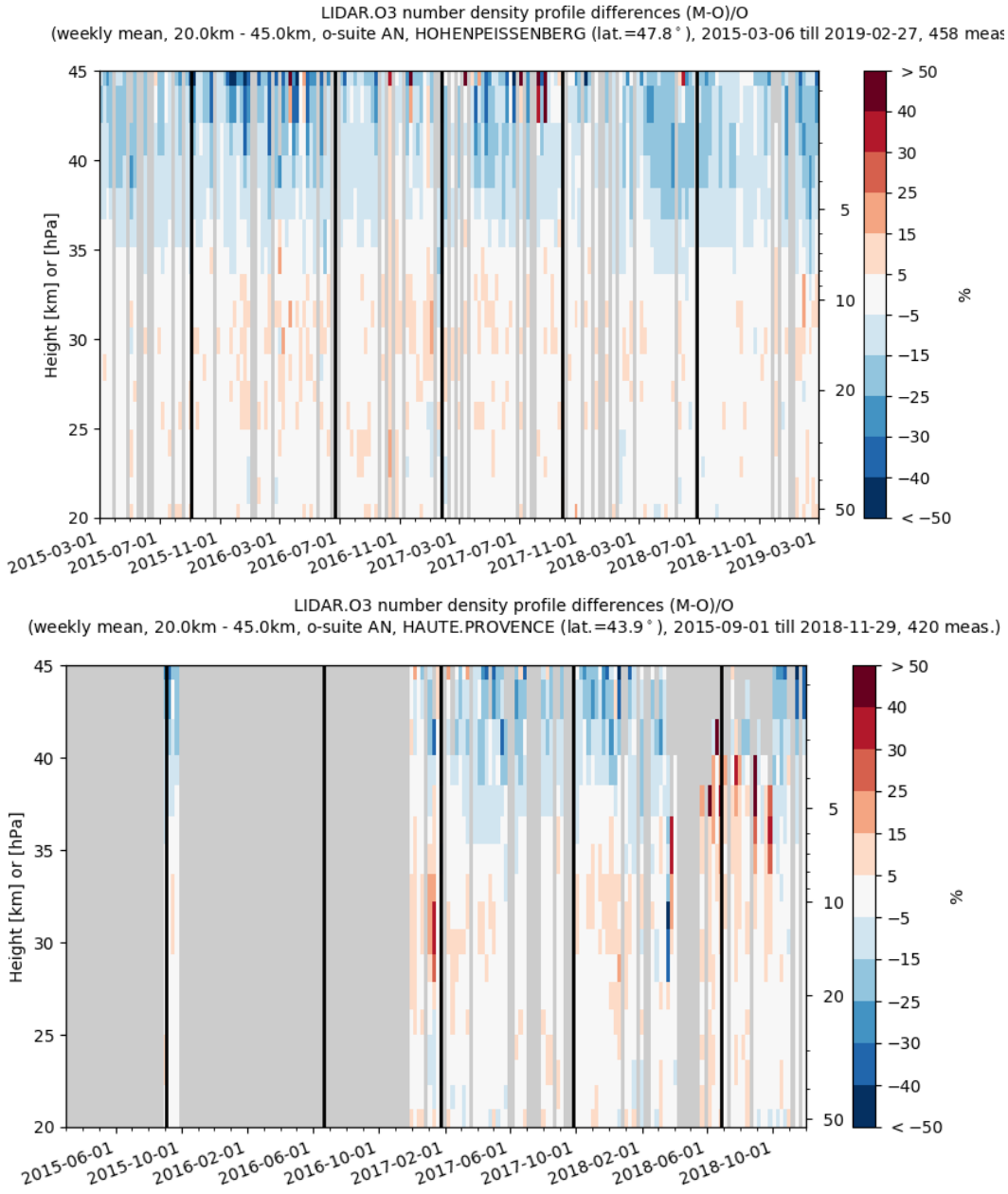

Figure 8.2.4: Comparison of the weekly mean profile bias between the O_3 mixing ratios of o-suite and the NDACC station at Ny Alesund, Bern, Hohenpeissenberg and OHP. For the LIDAR stations, the measurement uncertainty above 35km is comparable to the observed profile bias.

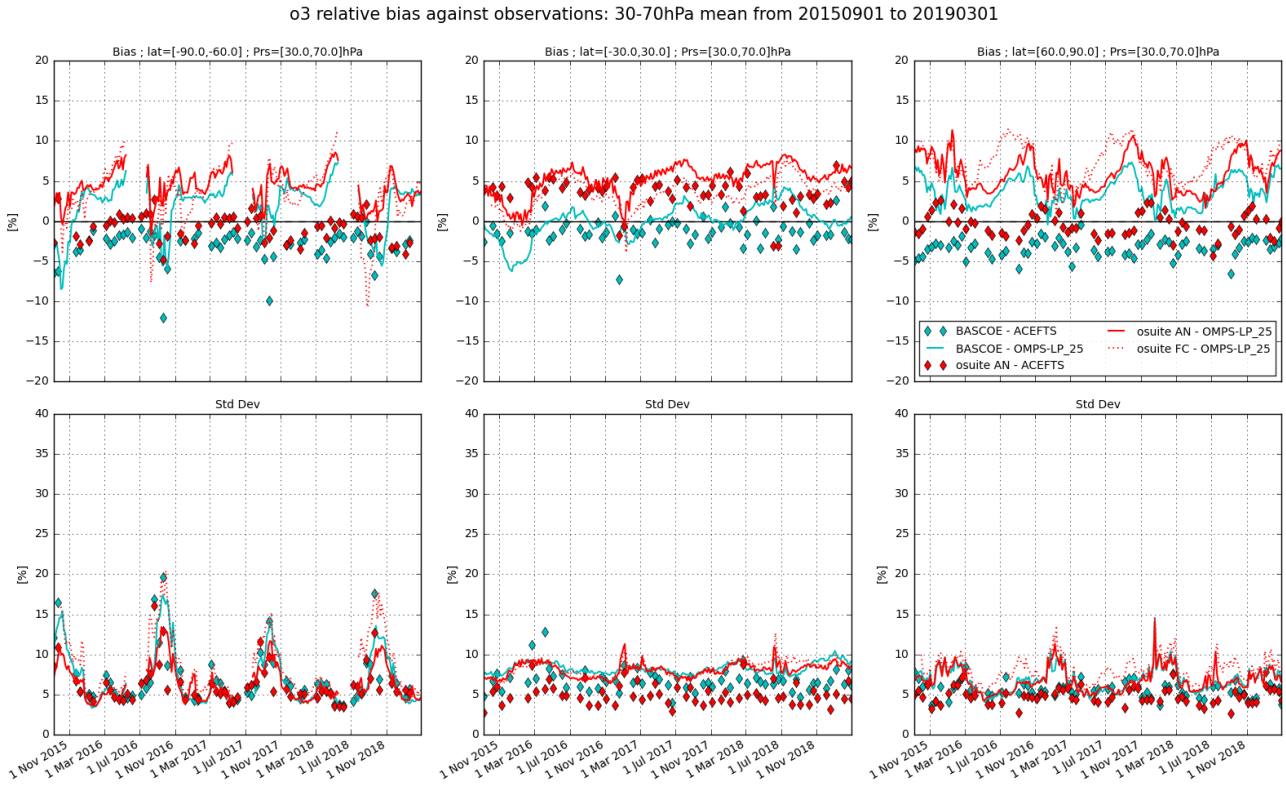

Figure 8.3.1: Time series comparing models to observations for the period 2015-09-01 to 2019-03-01 in the middle stratosphere (30-70hPa averages): o-suite analyses vs OMPS-LP (red, solid), o-suite forecasts 4th day vs OMPS-LP (red, dotted), o-suite analyses vs ACE-FTS (red markers), BASCOE vs OMPS-LP (cyan, solid) and BASCOE vs ACE-FTS(cyan markers). Top row, normalized mean bias (model-obs)/obs (%); bottom row, standard deviation of relative differences (%).

8.3 Comparison with dedicated systems and with observations by limb-scanning satellites

This section compares the output of the o-suite for the last period with observations by limb-scanning satellite instruments, using the methodology described by Lefever et al. (2015). We also include the comparisons for the o-suite 4th day forecasts (96h to 120h) of stratospheric ozone. These forecasts are represented by dotted lines in the figures.

All datasets are averaged over all longitudes and over the three most interesting latitude bands for stratospheric ozone: Antarctic (90°S-60°S), Tropics (30°S-30°N) and Arctic (60°N-90°N). In order to provide global coverage, the two mid-latitude bands (60°S-90°S and 60°N-90°N) are also included in some comparisons with satellite observations.

In this section, we use on one hand the version 2.5 of OMPS-LP (i.e. the Limb Profiler) and the version 3.6 of ACE-FTS. For reference, we include also the BASCOE analyses which are very constrained by the AURA MLS offline profiles.

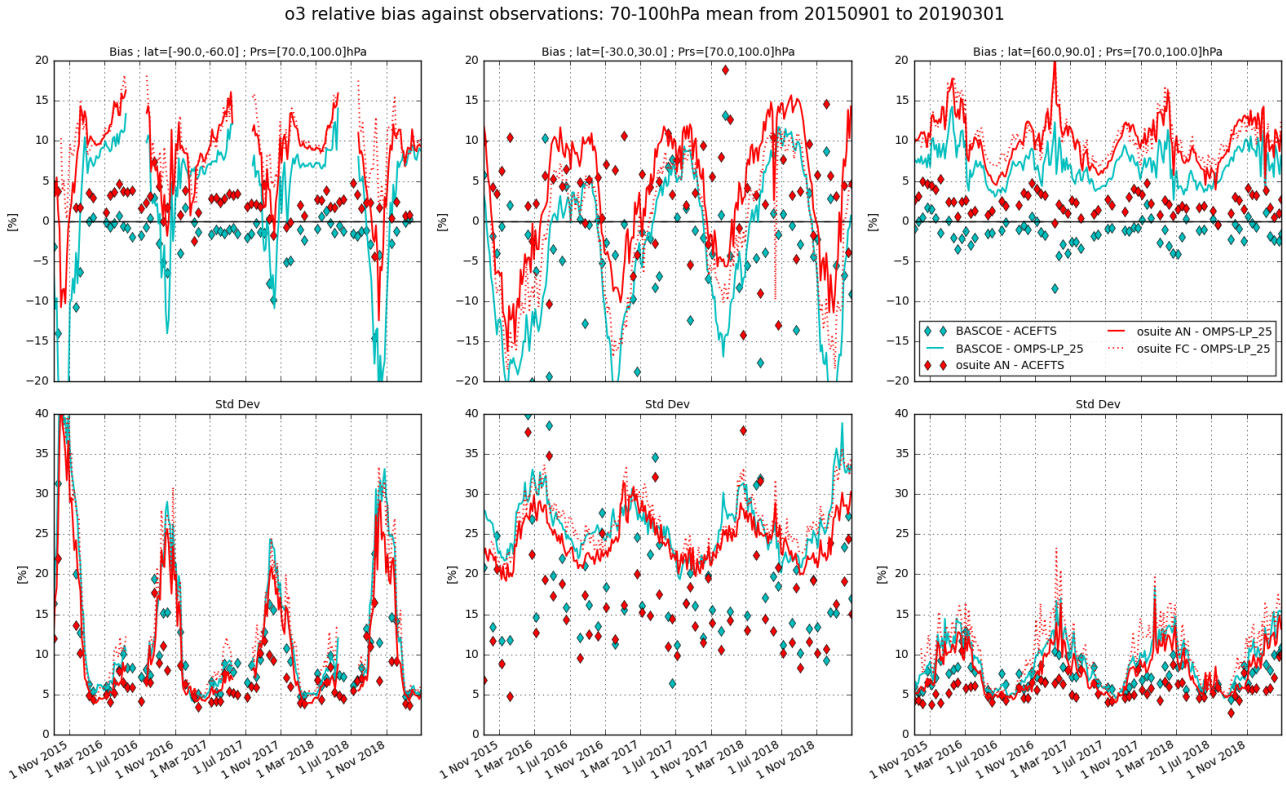

Figure 8.3.2: Time series comparing models to observations for the period 2015-09-01 to 2019-03-01 in the lower stratosphere (70-100hPa averages): o-suite analyses vs OMPS-LP (red, solid), o-suite forecasts 4th day vs OMPS-LP (red, dotted), o-suite analyses vs ACE-FTS (red markers), BASCOE vs OMPS-LP (cyan,solid) and BASCOE vs ACE-FTS(cyan markers). Top row, normalized mean bias (model-obs)/obs (%);bottom row, standard deviation of relative differences (%).

Figure 8.3.1 and Figure 8.3.2 present, in the upper row, the timeseries over the last 42 months of the bias of the o-suite against the two satellite measurements for respectively two regions of the lower stratosphere and UTLS (30-70hPa and 70-100hPa); the bottom row of the figures shows the standard deviation of the differences and can be used to evaluate the random error in the analyses.

Compared to OMPS-LP in the 30hPa to 70hPa region, there is a systematic overestimation by the o-suite: up to 8% in the South polar region and in the tropics and up to 12% in the North polar region. Compared to OMPS-LP in the 70hPa to 100hPa region, the North polar bias increases up to 20% at various periods, while the variability of the bias is much stronger in the South polar region; the tropics exhibits a strong seasonal variation for the bias, with a high variability indicated by the standard deviation.

The agreement with ACE-FTS is much better: the bias is generally within ±5%, except in the tropics for 70hPa to 100hPa region, where the standard deviations indicate less reliable results.

The bias of BASCOE against the satellite observations for the considered regions is systematically lower, but follows a similar evolution as the o-suite.

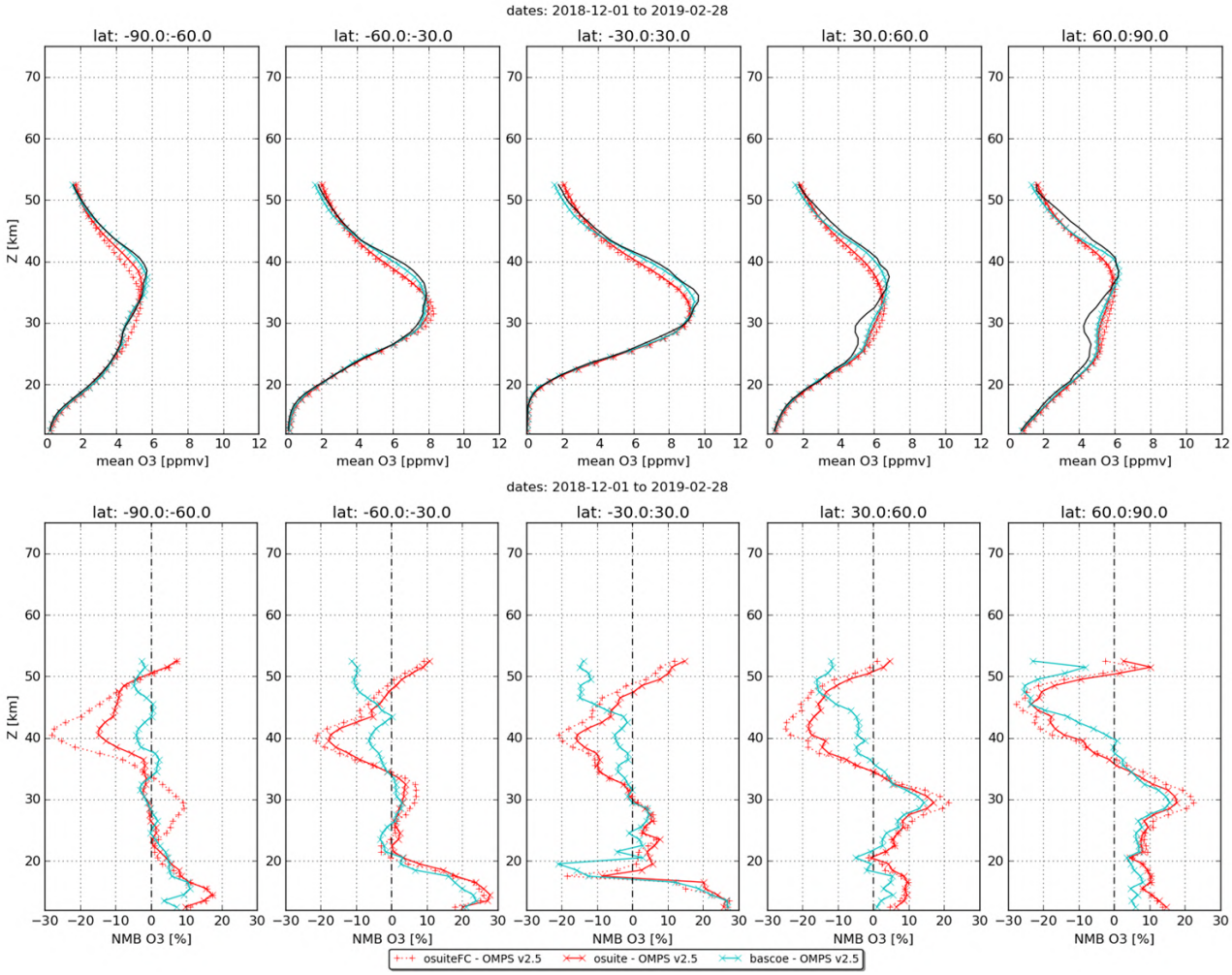

Figure 8.3.3: Mean value (top) and normalized mean bias (bottom) of the ozone profile between o-suite analyses (red, solid), o-suite forecasts 4th day (red, dotted) and BASCOE (cyan line) with OMPS-LP v2.5 observations for the period December 2018 to February 2019.

Figure 8.3.3 and Figure 8.3.4 display vertical profiles of the relative biases between the o-suite or BASCOE and the satellite measurements. The difference is averaged over the most recent 3-month period considered in this validation report, i.e. June to August 2018.

The OMPS-LP profiles are much more irregular than the ACEFTS or MLS profiles, but the relative bias between o-suite and OMPS-LP is mostly within ±10% between 20km and 35km.

The negative bias above 35km is confirmed by the ACEFTS profiles, otherwise there is a good agreement in the middle and lower stratosphere.

It must be noted that the different instruments have a variety of spatial and temporal coverage: for a 3 month period and over the latitude bands considered, OMPS and Aura MLS (not shown) provide daily data with more than 40000 valid profiles, while ACE-FTS provides around 300 profiles in the polar region and 90 profiles in the tropics.

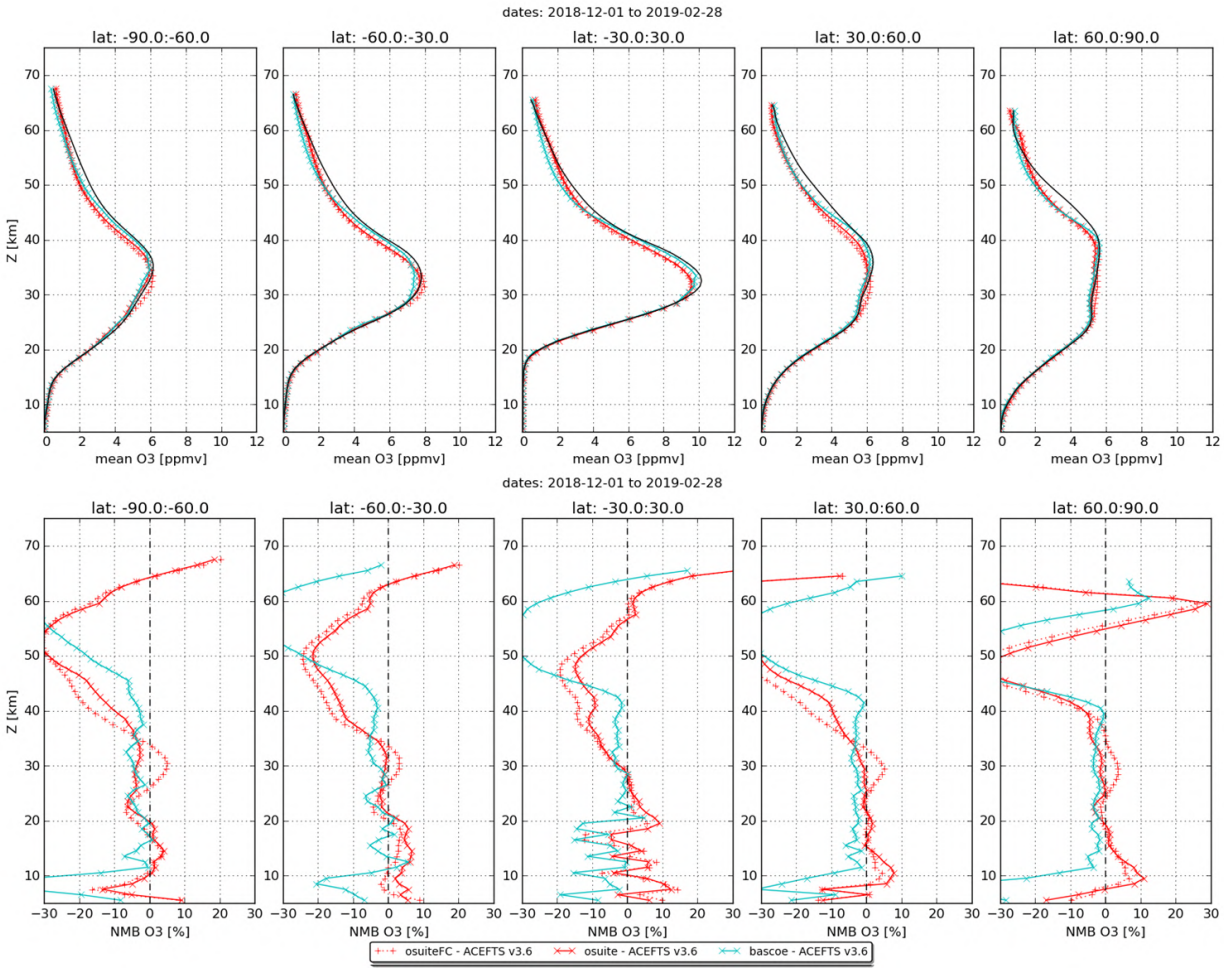

Figure 8.3.4: Mean value (top) and normalized mean bias (bottom) of the ozone profile between o-suite analyses (red, solid), o-suite forecasts 4th day (red, dotted) and BASCOE (cyan line) with ACE-FTS observations for the period December 2018 to February 2019.

8.4 Stratospheric NO_2

The CAMS model uses a tropospheric chemistry scheme in combination with a parameterization for stratospheric ozone. Stratospheric ozone is also well constrained by satellite observations. Therefore, the only useful product in the stratosphere is ozone, and all other compounds, including NO_2, should not be used, as demonstrated by the validation results presented here.

In this section, nitrogen dioxide from SCIAMACHY/Envisat satellite retrievals (IUP-UB v0.7) and GOME-2/MetOp-A satellite retrievals (IUP-UB v1.0) are compared to modelled stratospheric NO_2 columns. Monthly mean stratospheric NO_2 columns from SCIAMACHY and GOME-2 have relatively small errors on the order of 20% in the tropics and in mid-latitudes in summer and even lower errors at mid-latitudes in winter. As the time resolution of the saved model files is rather coarse and NO_x photochemistry in the stratosphere has a large impact on the NO_2 columns at low sun, some uncertainty is introduced by the time interpolation at high latitudes in winter.

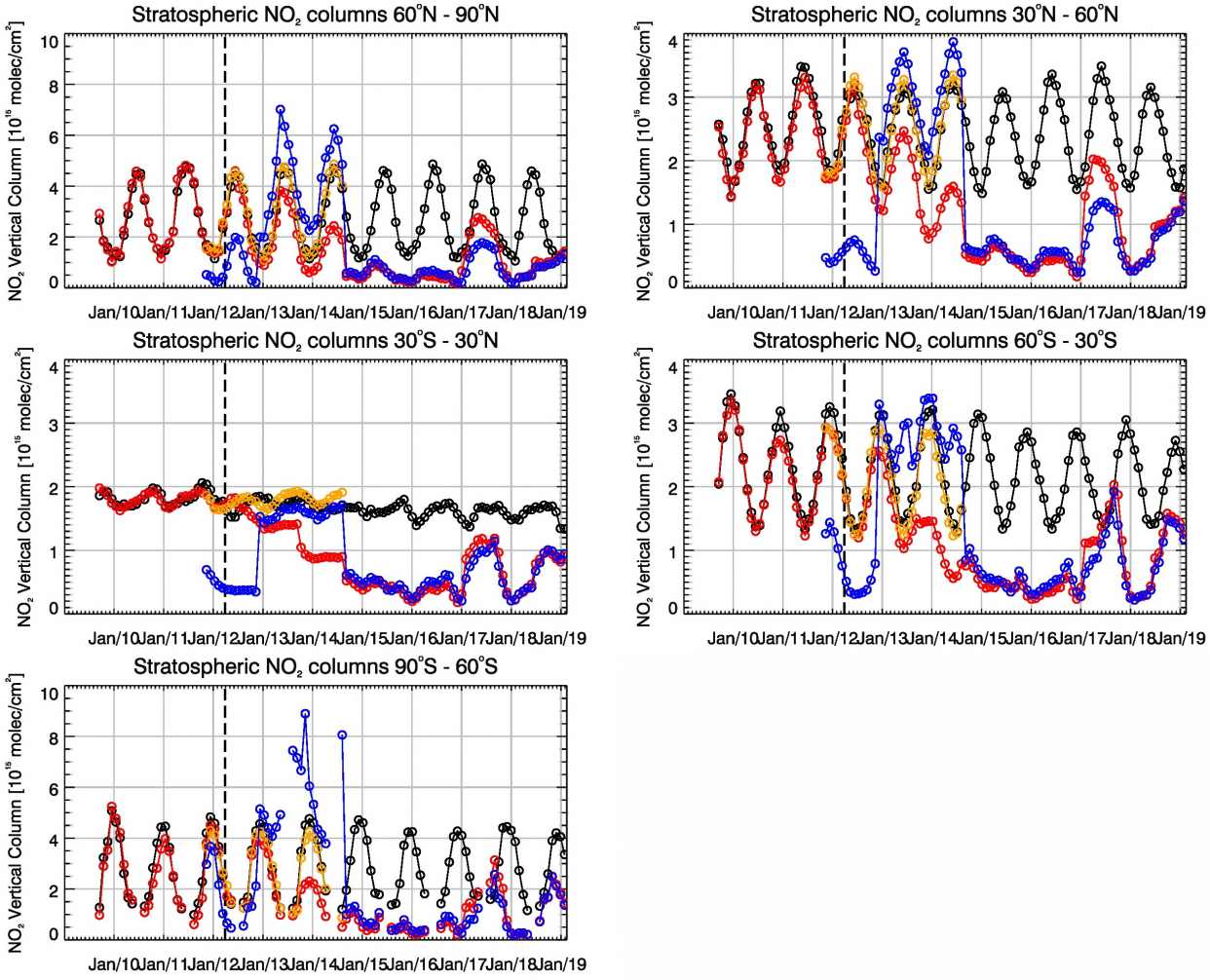

Figure 8.4.1: Time series of average stratospheric NO2 columns [10^{15} molec cm-2] from SCIAMACHY (up to March 2012) and GOME-2 (from April 2012, black) compared to model results (red: osuite, blue: MACC fcnrt TM5/MACC CIFS TM5/control, orange: MACC fcnrt MOZ) for different latitude bands. See text for details. The blue line shows MACC_fcnrt_TM5 from November 2011 to November 2012, MACC_CIFS_TM5 results from December 2012 until August 2014 and control results from September 2014 onwards (the model run without data assimilation is termed control since Sep 2014). The vertical dashed black lines mark the change from SCIAMACHY to GOME-2 based comparisons in April 2012.

As shown in Figure 8.4.1, amplitude and seasonality of satellite stratospheric NO_2 columns are poorly modelled with CB05-based chemistry runs including the more recent versions of the o-suite. The significant differences between observations and CB05 chemistry runs, i.e. a strong underestimation of satellite retrievals by models, can be explained by the missing stratospheric chemistry for these model versions. The only constraint on stratospheric NO_x is implicitly made by fixing the HNO_3/O_3 ratio at the 10 hPa level. This assumption, in combination with the changing model settings for stratospheric O_3 for control compared to MACC_CIFS_TM5, may explain some of the jumps we see in stratospheric NO_2. In any of these runs the stratospheric NO_2 is poorly constrained. It clearly indicates that stratospheric NO_2 in the latest versions of the o-suite is not a useful product and should be disregarded. However, model simulated values increased with an upgrade of the o-suite in February 2017, so that simulations are closer to the satellite observations

for 2017 only, especially for northern hemisphere latitude bands where seasonality seems to have been reproduced (in contrast to the Southern Hemisphere) by the o-suite apart from the pronounced underestimation. O-suite values are larger than the control in 2017 at all latitude bands. The better agreement found for 2017 did not continue in 2018 and values decreased to the magnitude of 2015-2016 runs at all latitude bands, followed however by a recent increase (development to be seen with the next reports).

Comparison of the o-suite from July 2012 until August 2014 with the other model runs and satellite observations shows that the previous version of the o-suite stratospheric NO_2 columns had a systematic low bias relative to those from MACC_fcnrt_MOZ and satellite observations for all latitude bands. For example, o-suite values are a factor of 2 smaller than satellite values between 60°S to 90°S for October 2013. Best performance was achieved with the MOZART chemistry experiments without data assimilation (MACC_fcnrt_MOZ, running until September 2014), especially northwards of 30°S. Details on the NO_2 evaluation can be found at: http://www.doas-bremen.de/macc/macc_veri_iup_home.html.

9. Validation results for greenhouse gases

This section describes the NRT validation of the pre-operational, high resolution forecast of CO_2 and CH_4 from 1st Mars 2018 to 1st Mars 2019 based on observations from 17 surface stations, located in Western Europe; 15 TCCON stations measuring XCO_2 and XCH_4 total columns, and 13 NDACC stations measuring partial and total CH_4 columns. We compare the observations to the high-resolution forecast experiments (*gqpe/gznv, Tco1279L137; 9x9 km*), coupled to the analysis experiment (*gqiq/gwx3, Tco399L137, 25x25 km*). The *gqpe* forecast experiment is using the IFS model cycle CY43R1, and has been officially implemented on 1st Nov. 2017. The *gznv*/*gwx3* experiments, based on IFS CY45R1, are used from 1st December 2018 on. This new experiment benefits from a couple of bug fixes in the modelled biogenic fluxes which should result in an improved seasonal cycle in the northern hemisphere and some degradation in the tropics.

9.1 CH4 and CO2 validation against ICOS observations

The CO_2 and CH_4 simulations from the analysis and high-resolution forecast have been compared to the 17 ICOS stations. The near–real time data processing of the in-situ measurements is ensured by the Atmospheric Thematic Center (Hazan *et al.*, 2016). Among the 17 stations we can distinguish three sites located on top of mountains (PUY, JFJ, CMN), two background sites (PAL, ZEP) and 12 tall towers. For the later we consider only in this report the highest sampling level which is at least at 100m above the ground.

For CO_2 the correlation coefficients are higher than 0.8 for all sites except one at Ispra, located in the Po valley, and poorly represented by the model due to the complex orography (Figure 9.1.1). The synoptic scale variability is overestimated at almost all stations except one (CMN). The best correlation coefficients are obtained for the background stations PAL, ZEP and JFJ. For CH_4, there is not much difference in the correlation coefficients between the background sites and the tall towers, which are close to 0.8 with two exceptions at Monte Cimone and Ispra where correlations are below 0.6. Overall, we notice a small degradation of the CH_4 correlations with the high-resolution forecast experiment compared to the analysis (Figure 9.1.1). This is particularly true at the Trainou tall tower. In this case several spikes are wrongly simulated by the models in summer, and their amplitude is getting worse with the high-resolution forecast. This is probably due to the vicinity of hot spot emissions in Paris area, either mislocated or overestimated in the emission inventory, whose influence is amplified when using higher resolution.

Figure 9.1.2 shows the time varying biases (observations minus model), averaged on a weekly basis, for all ICOS stations. There is not much differences between the high-resolution forecast and the analysis runs. The CO_2 biases display clear seasonal cycles (±10 ppm) at most sites with negative biases in Summer/Autumn, and positive biases in Winter/Spring. One example is detailed on Figure 9.1.3 for the Norunda tall tower located in Sweden. At this stage it is too early to evaluate the improvement expected from the new experiments, used since December 2018. For CH_4 we observe a clear latitudinal gradient in the biases. At the Scandinavian sites the model overestimates (up to 50 ppb) the observations all along the year. The example of Norunda (Figure 9.1.3) clearly shows that the CH_4 spikes are systematically too high in the model runs, which could indicate that the

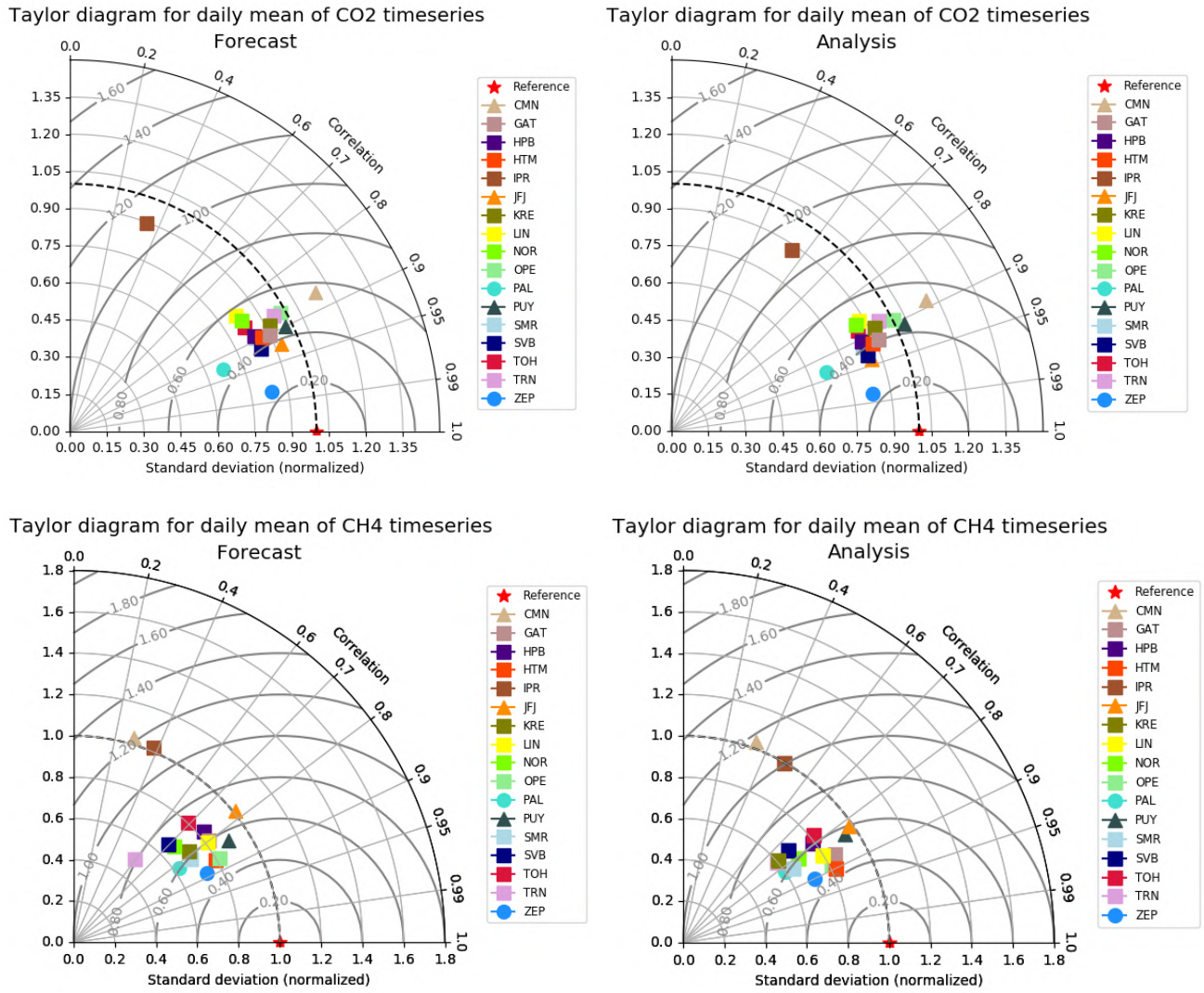

Figure 9.1.1: Taylor diagrams relating the standard deviations for the model and time series of CO_2 (above) and CH_4 (below) mole fractions and their correlation. The normalized standard deviation is calculated as the ratio observed SD / modelled SD (SD values lower than one mean an overestimation of the variability by the model). The left panels show the high-resolution forecast, and the right panels the analysis.

wetland emissions are overestimated. For sites located at lower latitudes, the bias is generally lower, and is getting negative in Summer/Autumn. It is even systematically negative at the mountain sites PUY and JFJ.

We have done an evaluation of the model performance based on a composite of all European stations (Figure 9.1.4). Overall this composite comparison highlights the seasonal cycle of the CO_2 bias, and an overestimation of CH_4 concentrations. For CO_2, the model overestimation is maximal in Spring 2018 (May-June). For several sites, like Norunda (Figure 9.1.3), this maximum corresponds to a large mismatch resulting from the heatwave that hit North Europe in 2018. It should also be noted that the correlation coefficients are significantly lower from April to September, during the growing season of the vegetation when the biospheric fluxes are maximum. The overestimation of the CO_2

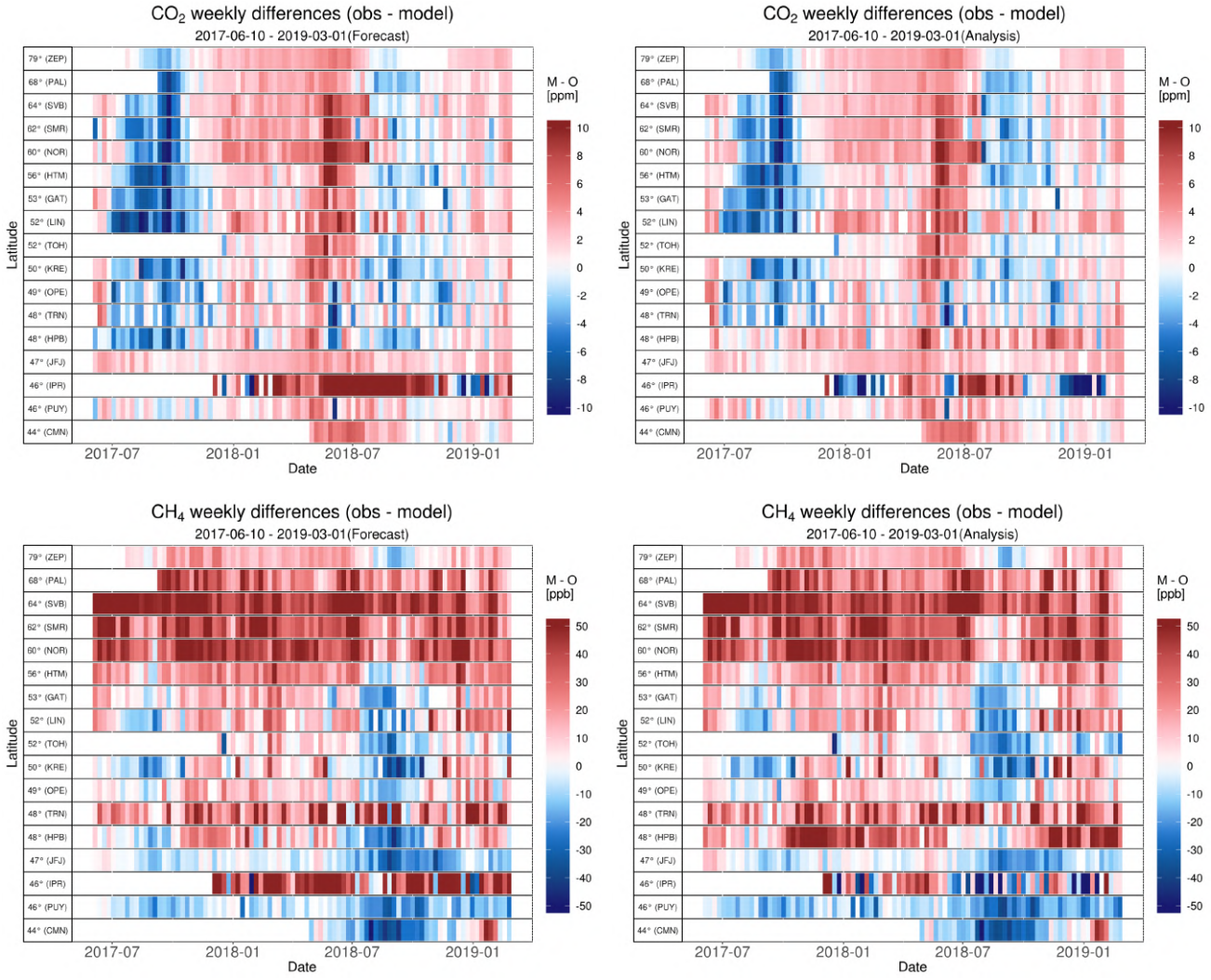

Figure 9.1.2: Mosaic plot of CO2 (above, in ppm) and CH4 (below, in ppb) biases of the CAMS products (left: high resolution forecast, right: analysis run) compared to surface station observations. Each vertical coloured line represents a weekly mean.

seasonal amplitude by ±1% was already described in previous reports and is expected to decrease with the new experiments. For CH_4 we observe positive biases between 10 and 20 ppb for most of the year, getting closer to zero in summertime.

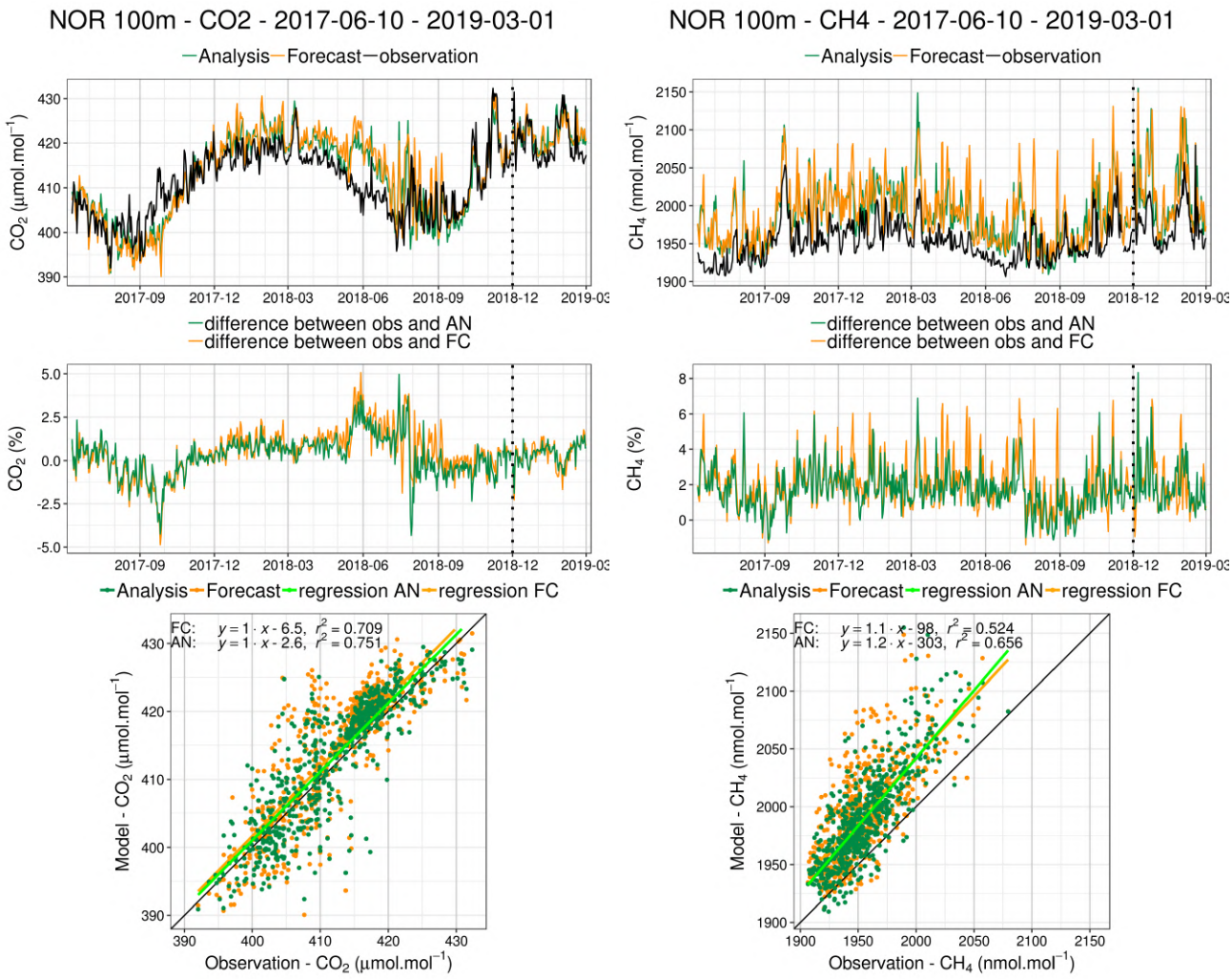

Figure 9.1.3: Comparison of CO2 (left) and CH4 (right) daily means observed (black) with the analysis run (green) and the high-resolution forecast (orange) at the Norunda tall tower. Middle: differences of the observations minus the simulations. Below: Linear fit between observations and simulations.

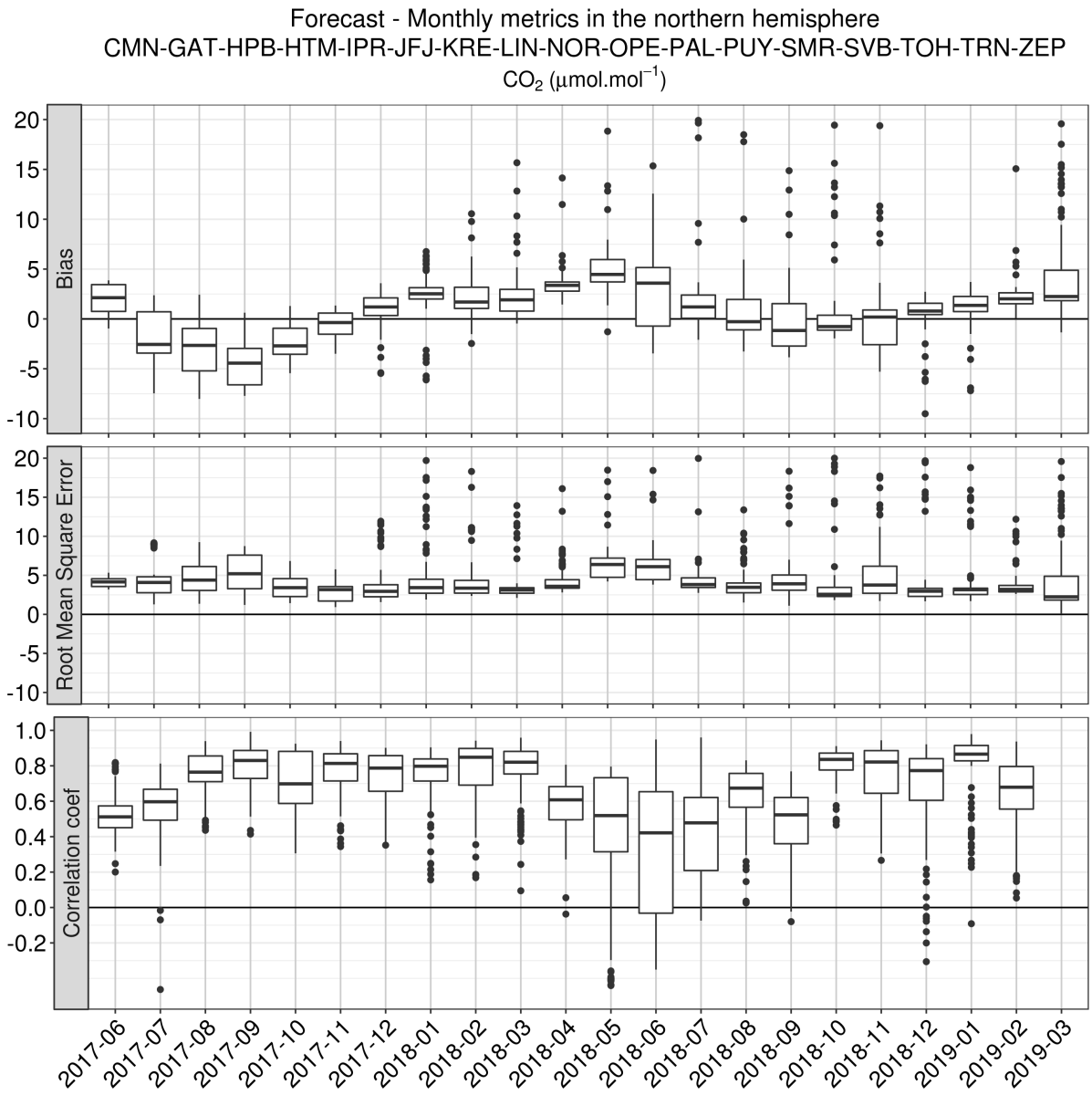

Figure 9.1.4a: Monthly statistics (bias, RMSE, correlation coefficients) of the analysis experiment compared to CO2 surface measurements at ICOS sites. The results obtained for all European sites (see the list of sites in the title) are averaged.

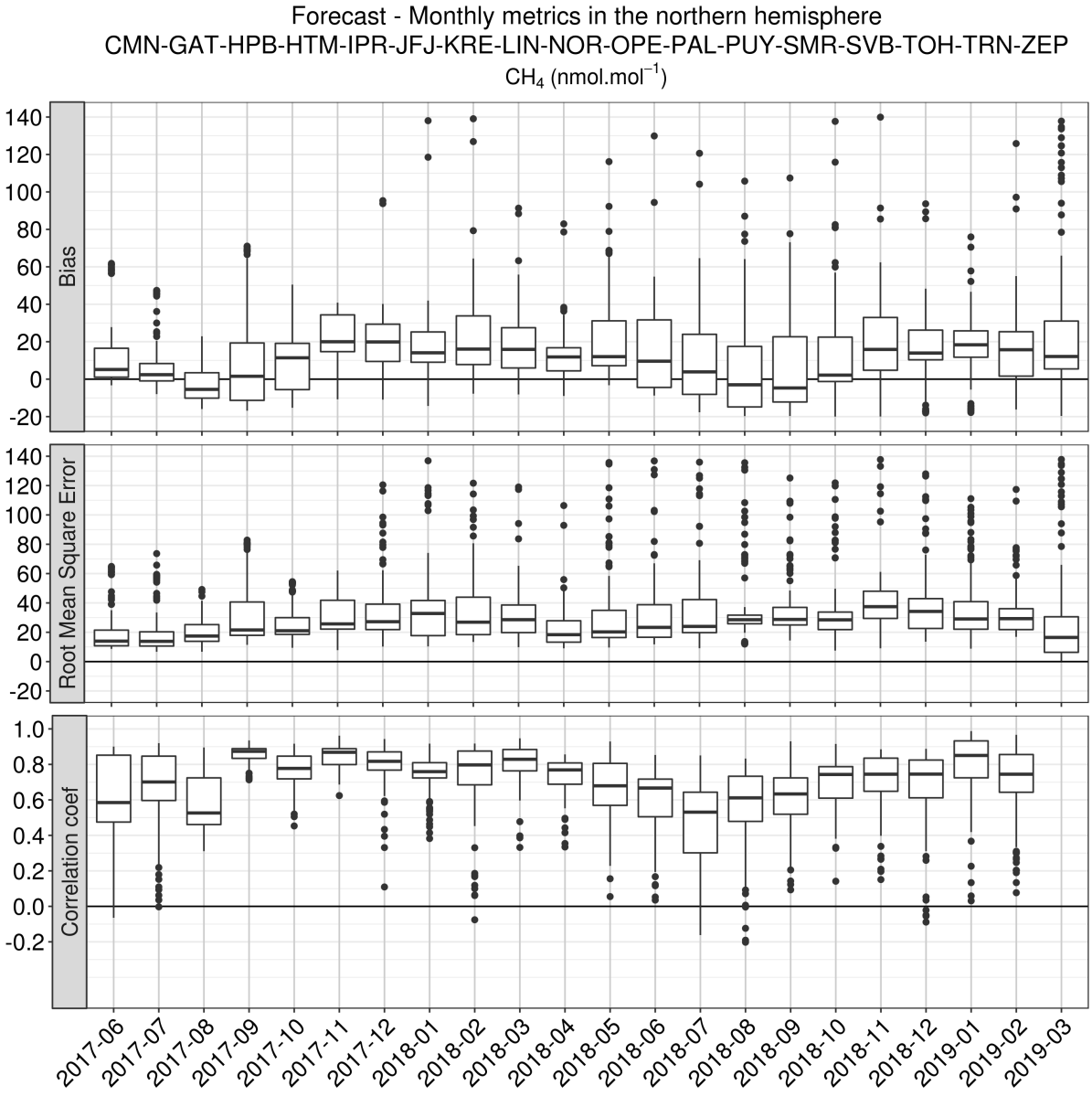

Figure 9.1.4b: Same as Figure 9.1.3a for CH4.

9.2 CH_4 and CO_2 validation against TCCON observations

For the validation column averaged mole fractions of CO_2 and CH_4 (denoted as XCO_2 and XCH_4) from the Total Carbon Column Observing Network (TCCON) are used. Column averaged mole fractions provide different information than the in situ measurements and are therefore complementary to the in situ data. For example, if models suffer from problems in vertical transport, the combination of TCCON and surface in situ measurements will provide a means to detect this.

The validation routines used for TCCON data are the same as used for the NDACC network and are documented in Langerock et al. (2015). The routines have been adapted to use the TCCON data format. Only measurements within 2.5h around local noon have been used for the comparison.

In this section, we compare column averaged mole fractions of CO_2 and CH_4 of the CAMS products with TCCON retrievals. Data from the following TCCON sites has been used: Izana (Blumenstock et al., 2017), Reunion (De Mazière et al., 2017), Bialystok (Deutscher et al., 2017), Manaus (Dubey et al., 2017), Four Corners (Dubey et al., 2017), Ascension (Feist et al., 2017), Anmeyondo (Goo et al., 2017), Darwin (Griffith et al., 2017), Wollongong (Griffith et al., 2017), Karlsruhe (Hase et al., 2017), Edwards (Iraci et al., 2017), Indianapolis (Iraci et al., 2017), Saga (Kawakami et al., 2017), Sodankyla (Kivi et al., 2017), Hefei (Liu et al., 2018), Tsukuba (Morino et al., 2017), Burgos (Morino et al., 2018), Rikubetsu (Morino et al., 2017), Bremen (Notholt et al., 2017), Spitsbergen (Notholt et al., 2017), Lauder (Sherlock et al., 2017, Pollard et al., 2019), Eureka (Strong et al., 2018), Garmisch (Sussmann et al., 2017), Zugspitze (Sussmann et al., 2018), Paris (Te et al., 2017), Orleans (Warneke et al., 2017), Park Falls (Wennberg et al., 2017), Caltech (Wennberg et al., 2017), Lamont (Wennberg et al., 2017), Jet Propulsion Laboratory (Wennberg et al., 2017), East Trout Lake (Wunch et al., 2017)

For the validation of the products in December, January and February only data from Edwards, Orleans, Karlsruhe and Izana is available. For Edwards, Karlsruhe and Izana data is only available for December. Since Edwards and Karlsruhe only have one measurement day in December these data are not used in this report.

The reason for the changing availability of TCCON data is the following: The requirement for TCCON data to become public is 1 year after the measurement. Some TCCON groups make their data earlier available. In the previous CAMS84 project only data from Bialystok, Orleans and Reunion was timely available for the validation of the CAMS products. The Bialystok site has stopped operation and the instrument is currently being transported to Cyprus. Reunion had technical problems and is therefore not operational. It is likely that for future reports fast data will become available again for these three sites. During the first year of the current CAMS84 project data was timely available from several TCCON sites. The reason was that during the first year after the launch of the Sentinel 5 precursor (S5p) several sites received funding to make TCCON data timely available for the validation of the S5p CH4 and CO retrievals. Several non-European TCCON partners contributed to this effort. It is likely that for the next report more data become available since the TCCON PIs usually do the data processing before the annual TCCON meeting (May 20-24, 2019) to discuss the measurements from the previous year. However, it is very likely that for future reports only data from Cyprus, Orleans and Reunion will be available.

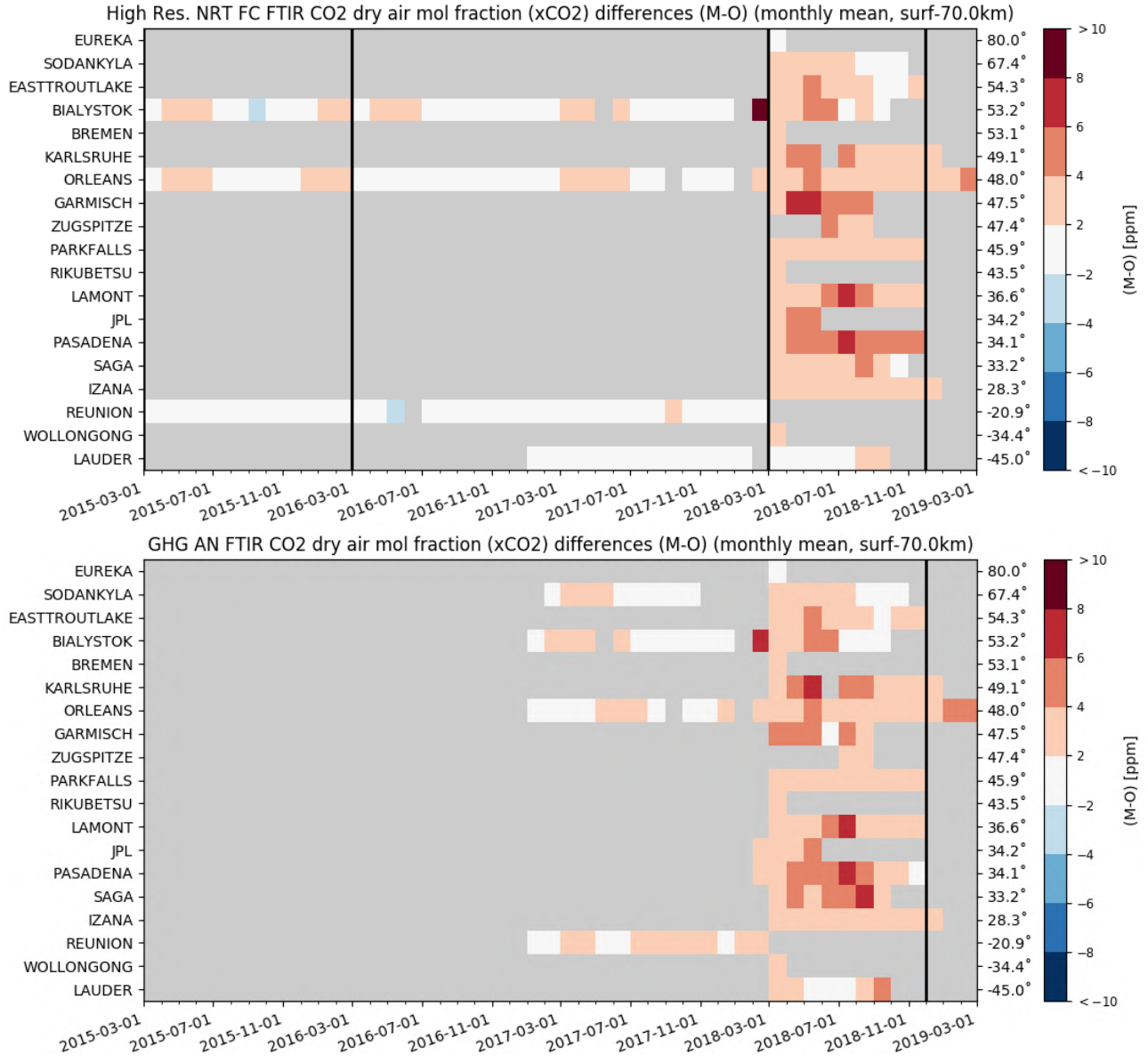

Figure 9.2.1: Monthly differences for the last 2 years (upper plot: high res NRT, lower plot: GHG AN). The stations are sorted by latitude (northern to southern hemisphere).

Carbon dioxide (CO_2)

Figure 9.2.1 shows the data for the last 2 years. Most of the data has been discussed in the previous reports. The only new data for the period of interest is from Orleans and Izana. The data from these two stations (Fig 9.2.3 and 9.2.4) show that the model data continues to overestimate the CO_2 for these two stations. The comparison at Orleans shows that the overestimation is significantly higher than in previous years.

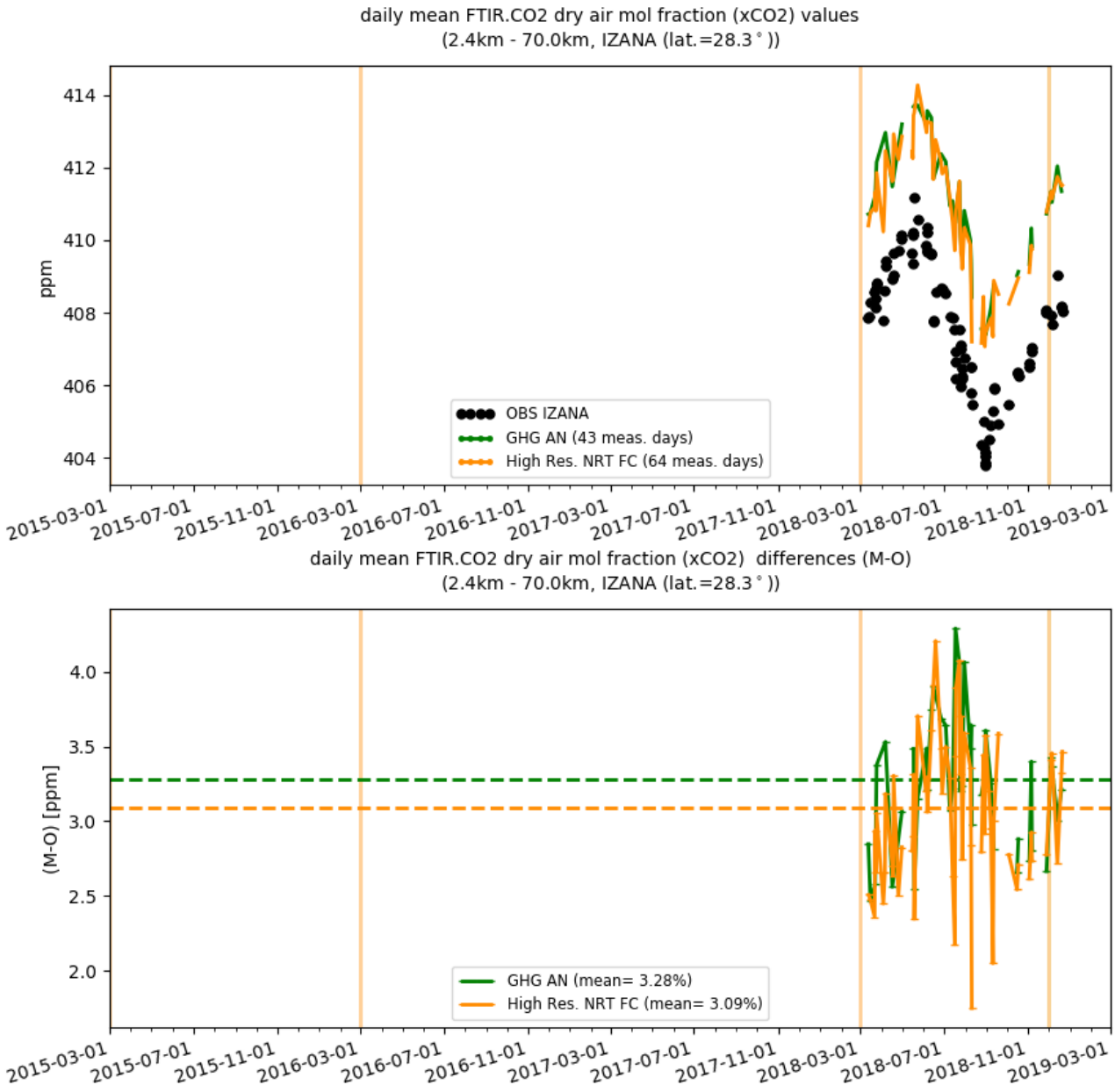

Figure 9.2.3: Comparison of the CO_2 model data with TCCON CO_2 at Izana.

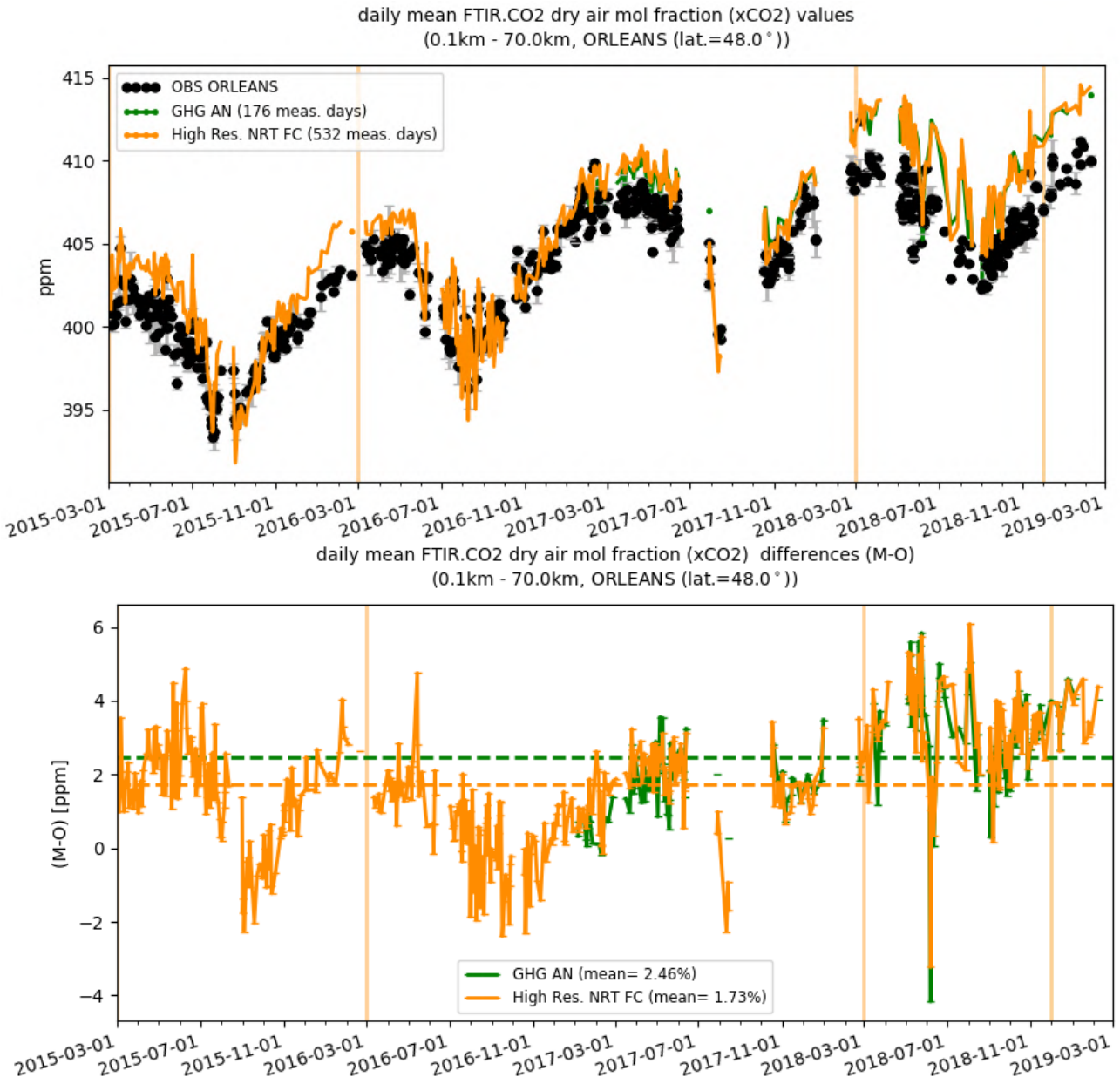

Figure 9.2.4: Comparison of the CO_2 model data with TCCON CO_2 at Orleans.

Methane (CH_4)

Figure 9.2.5 shows the data for the last 2 years. Most of the data has been discussed in the previous reports. The only new data for the period of interest is from Orleans and Izana. The data from these two stations (Fig 9.2.6 and 9.2.7) show that the model slightly underestimates the CH_4 by less than 1% for these two stations in Dec, Jan, Feb.

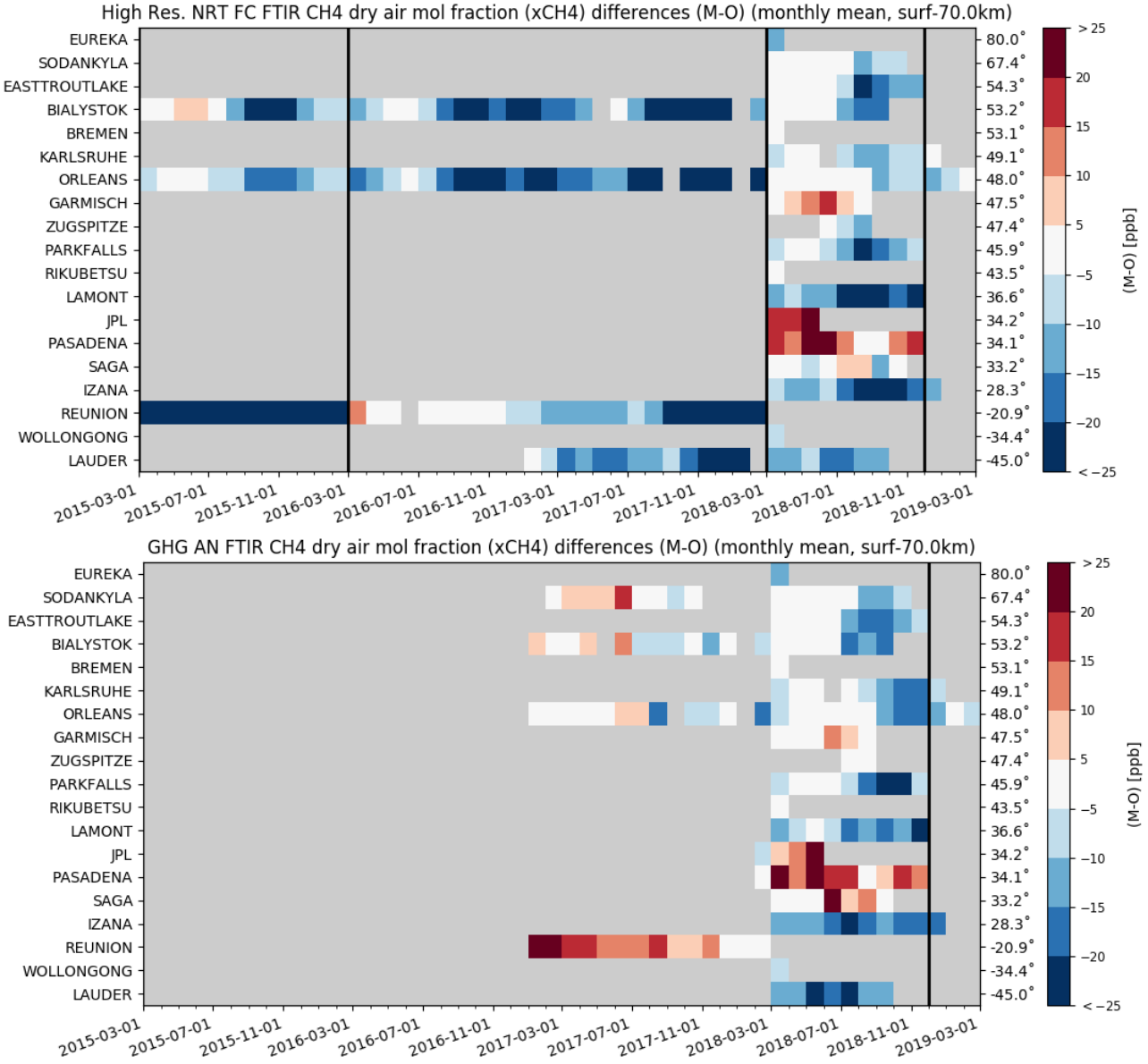

Figure 9.2.5: Monthly differences for the last 2 years (upper plot: high res NRT, lower plot: GHG AN). The stations are sorted by latitude (northern to southern hemisphere).

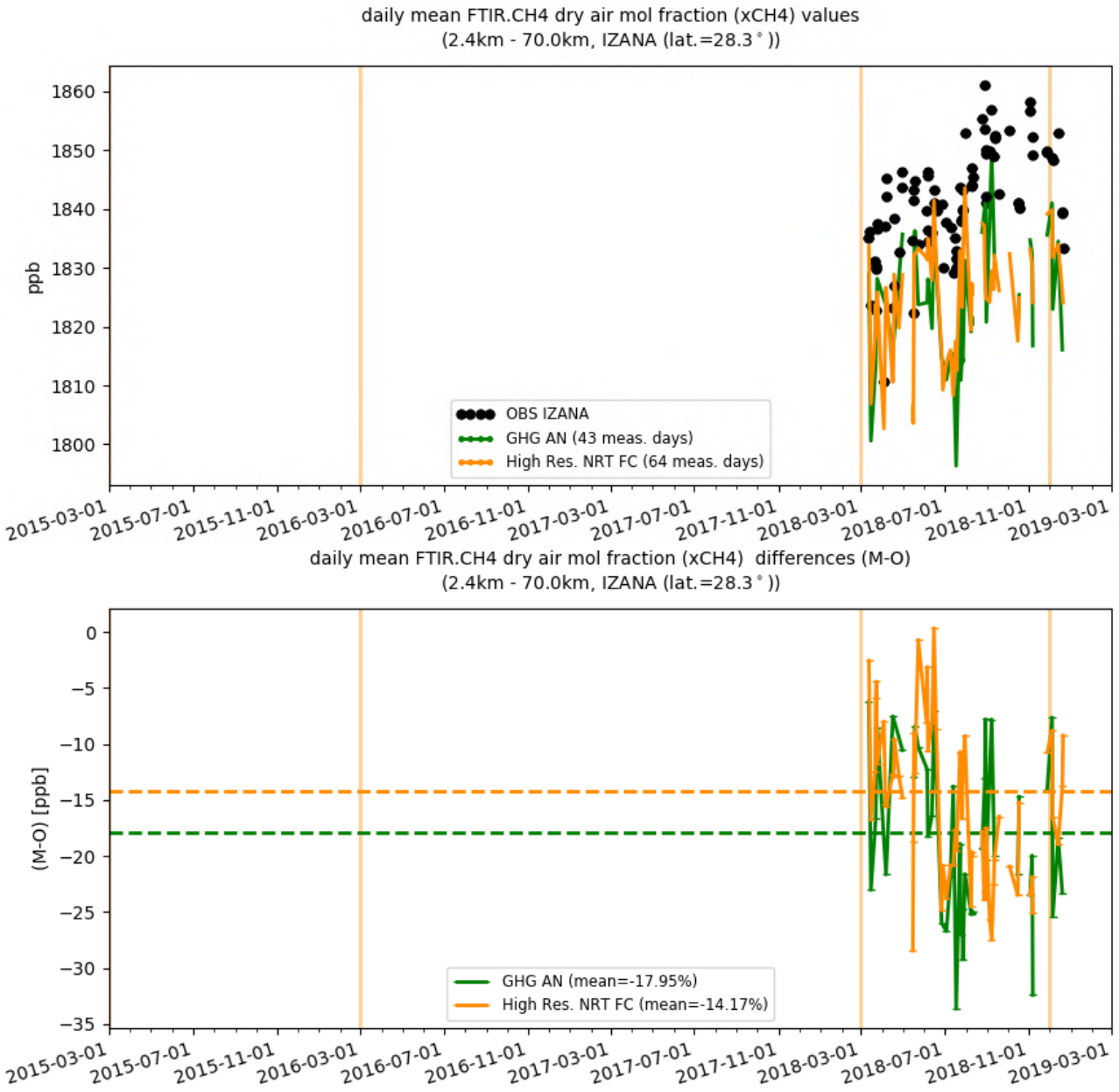

Figure 9.2.6: Comparison of the CAMS CH_4 forecast and analysis data with TCCON CH_4 column observations at Izana.

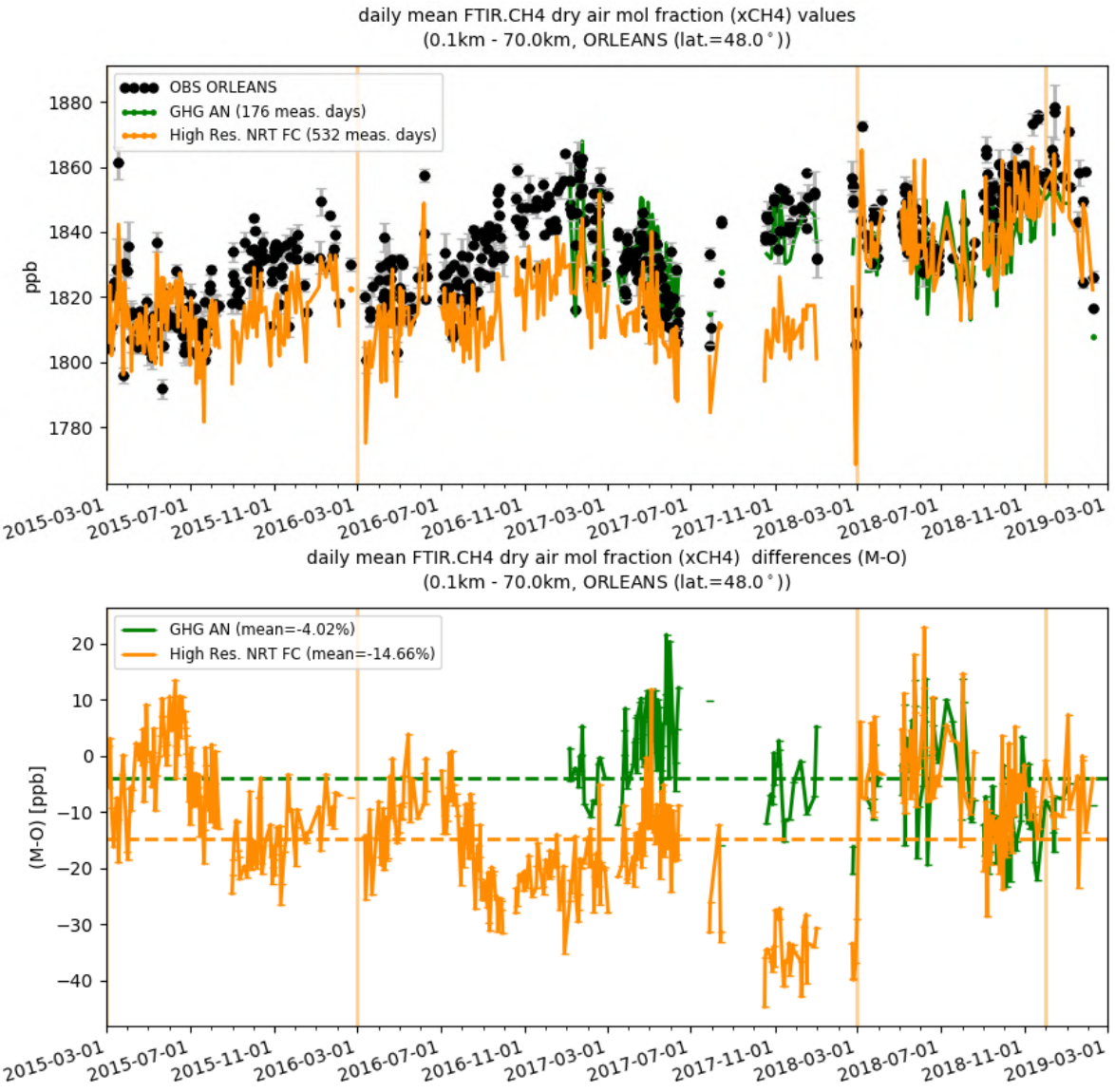

Figure 9.2.7: Comparison of the CAMS CH_4 forecast and analysis data with TCCON CH_4 column observations at Orleans.

9.3 Validation against FTIR observations from the NDACC network

In this section, we compare the CH_4 profiles of the CAMS GHG products with FTIR measurements at different FTIR stations within the NDACC network. These ground-based, remote-sensing instruments are sensitive to the CH_4 abundance in the troposphere and lower stratosphere, i.e. between the surface and up to 25 km altitude. Tropospheric and stratospheric CH_4 columns are calculated from the FTIR profile data and used to validate corresponding columns obtained from the model data. A description of the instruments and applied methodologies can be found at http://nors.aeronomie.be. The typical uncertainty on the FTIR tropospheric column is 3.5%, while the uncertainty on the stratospheric column is 7.5%, adding together to a 4% uncertainty on the total column. The systematic uncertainty is large for the NDACC methane product mostly due to higher spectroscopic uncertainties.

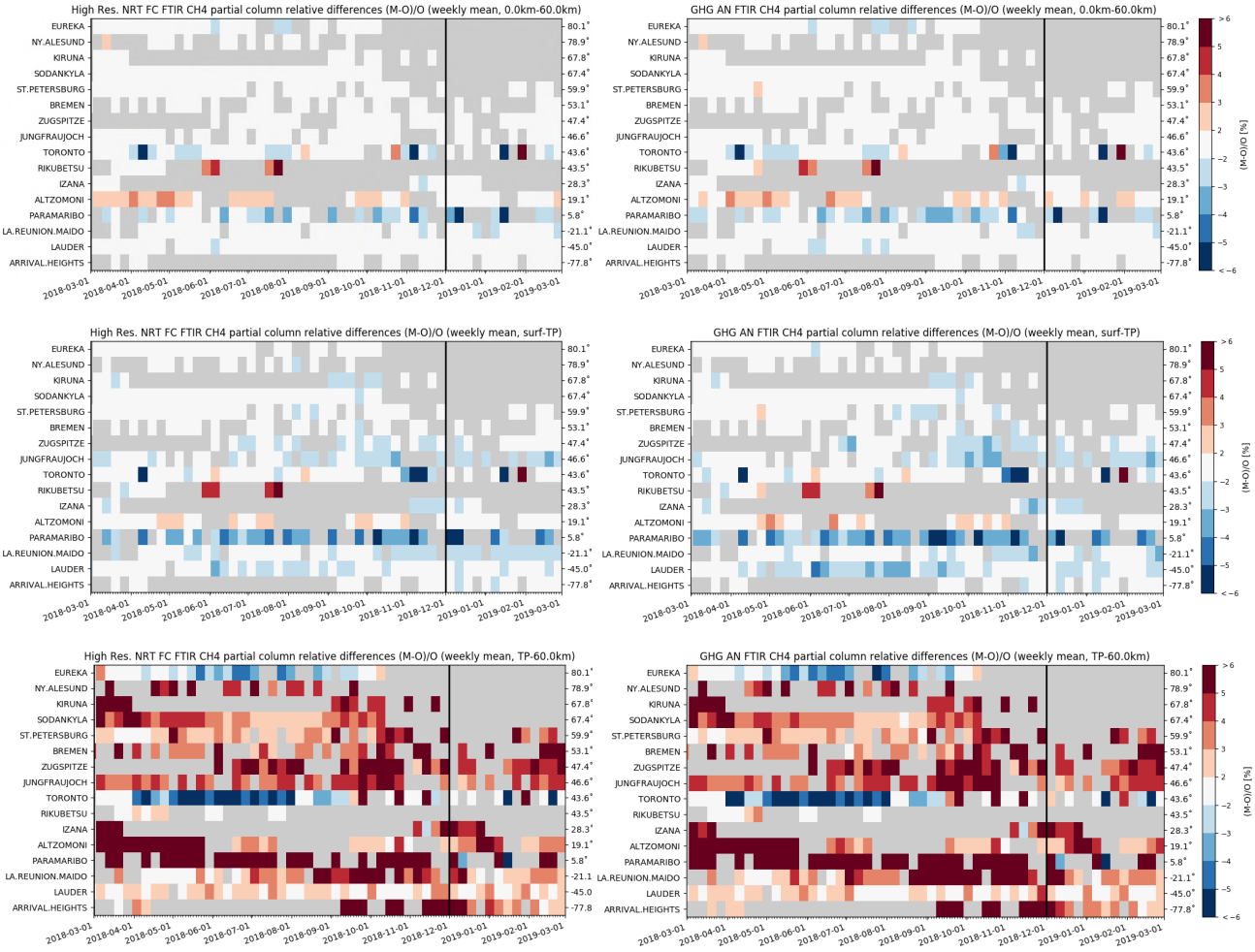

Figure 9.3.1: Weekly mean relative bias against NDACC-FTIR for total (top row), tropospheric (middle row) and stratospheric CH_4 columns (bottom row) for the period March 2018 – February 2019 for the high-resolution forecast (left) and the analysis (right). The mid latitude stations at Rikubetsu and Altzomoni show a strong overestimation for both CAMS products of the CH_4 column. The overall uncertainty for the CH_4 total column measurements is approximately 4%.

Figure 9.3.1 shows that the tropospheric columns of CH_4 agree well and only small differences appear between the analysis and the high-resolution model.

At some sites a seasonal change is observed in either the tropospheric or stratospheric concentrations. Due to the short time period, it is unclear if this is a recurring seasonal dependent model performance. In Figure 3.9.2 the tropospheric and stratospheric relative difference time series are plotted at Eureka and St. Petersburg.

Figure 9.3.3 shows Taylor diagrams for the DJF time period and for a selected number of sites (many high latitude stations are not measuring during DJF): some stations have limited observations and should be treated with care. Assimilation has a small effect on the correlation coefficients for most sites; at Reunion and Altzomoni, the analysis has worse correlation.

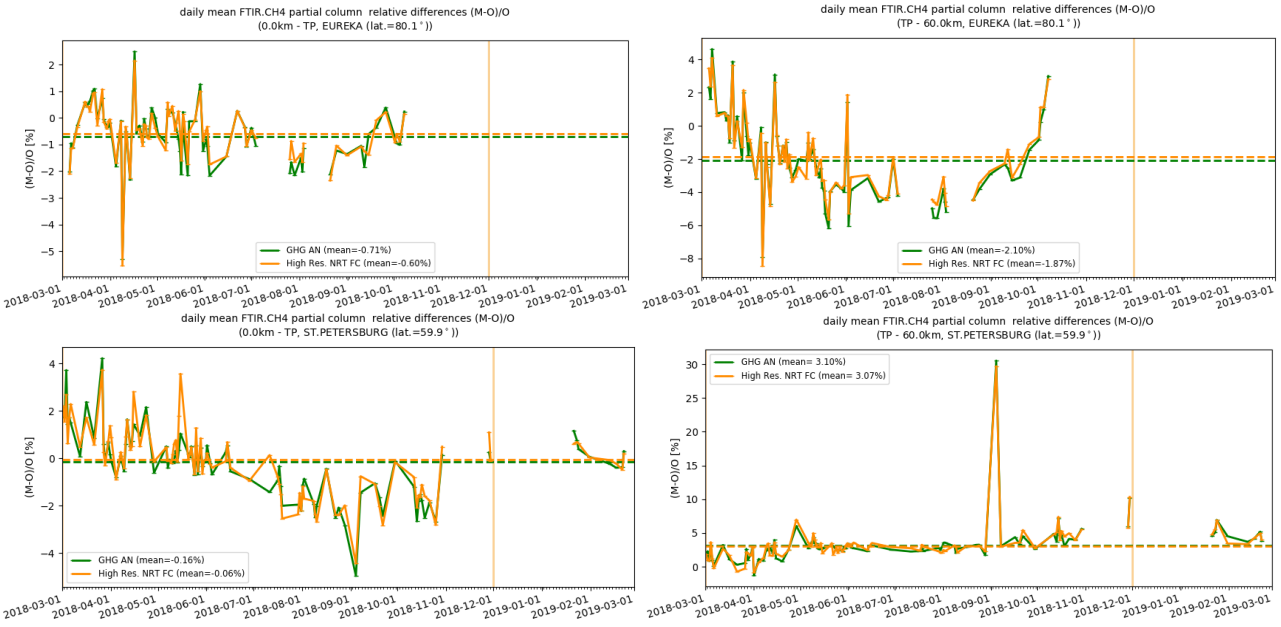

Figure 9.3.2: Daily mean of relative differences for tropospheric CH_4 columns (left) and stratospheric CH4 columns (right) at Eureka (top) and St Petersburg (bottom). The performance at Eureka changes from a positive bias in March-April for the stratospheric column to a negative bias in July-September, while at St Petersburg the tropospheric column performs worse during June-October.

Note that the NDACC methane plots (Fig. 9.3.1) show relative differences (in %) of total columns, while the TCCON mosaic plots (Fig. 9.2.5) are absolute differences of column averaged methane values. The chosen color scale and the range covered by the 'white' color is important to compare the two plots (NDACC / TCCON). For the NDACC data white means within 2%, while for the TCCON data white means within 5ppb or ±0.25%. The underestimation of -0.5% in the TCCON plot is within the white range in the NDACC plot. The chosen color scales reflect the measurement uncertainty, which is smaller for TCCON.

The stratospheric contribution to the total column is roughly about 20%, so a 5% bias in the stratosphere becomes a 1% bias on the total column, which is within the 'white' of the NDACC mosaic total column plot.

Comparison of ICOS methane surface concentrations with TCCON/NDACC remote sensing:
Generally, the surface observations in Europe indicate a positive bias in methane, while the European TCCON sites indicate a slight negative bias. NDACC shows for the troposphere a null (Zugpitze and Bremen) or slightly negative bias (Jungfraujoch). At this latter site surface measurements also show a negative bias. The positive bias in the stratosphere leads to a total column with a bias close to zero. At Trainou/Orléans surface measurements shows positive bias, and TCCON finds a total column with small negative bias. It is mostly at the Scandinavian sites that surface observations show a positive bias. In order to understand these differences between in-situ and column observations there is a need for profile observations, e.g. from AirCore balloon measurements.

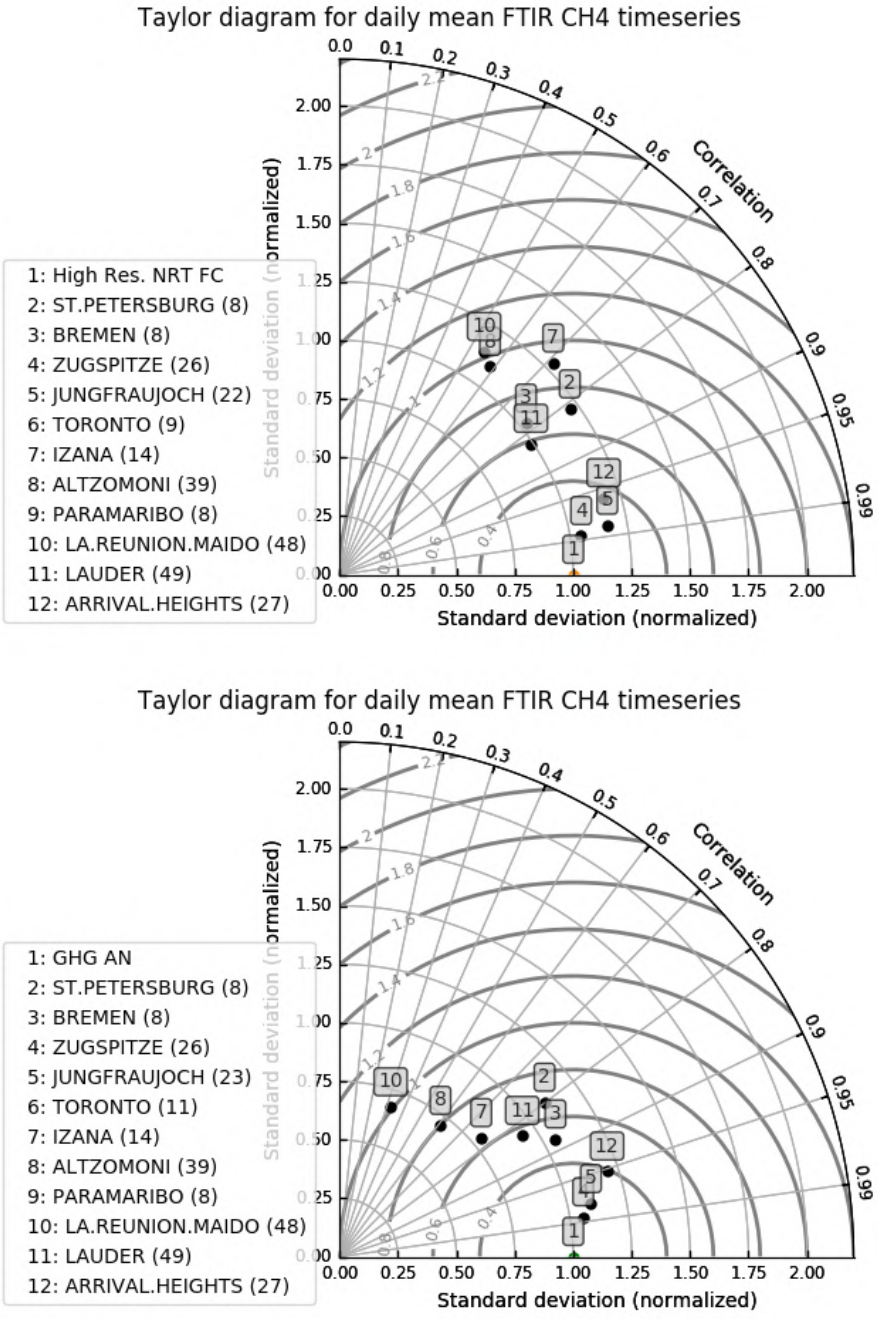

Figure 9.3.3: Taylor diagrams relating the standard deviations for the model /GB time series of total CH_4 column data and their correlation for the period 2018 DJF (the stations with a limited number of measurements are left out). All time-series are normalized such that the std of the model is 1. The correlation for the analysis time series is larger for most sites. For Altzomoni and Reunion (Maido) the assimilation decreases the ratio of the standard deviations of both time series significantly: the analysis methane columns are more variable compared to the high-resolution forecast.

10. Event studies

10.1 Dusty Eastern Mediterranean: 24-27 January 2019

In second half of January 2019, Saharan dust was heading for the central and eastern Mediterranean including Greece, Turkey and Cyprus. MODIS satellite detected the dust outbreak over the Central and Eastern Mediterranean Basin (see Figure 10.1.1). The event was nicely tracked by the AERONET sun photometers in the Eastern Mediterranean (see Figure 7.4.2).

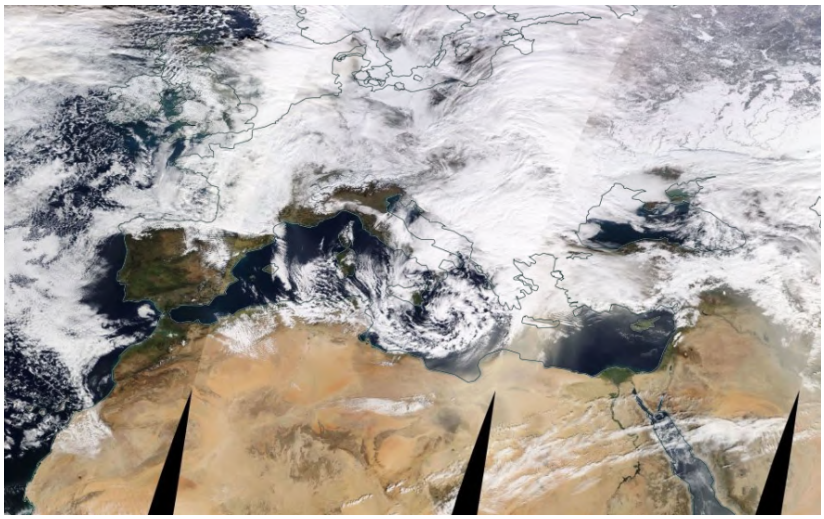

Figure 10.1.1: Daily composite of NASA MODIS/Terra on 25th January 2019 over the Central-Eastern Mediterranean.

The CAMS AOD from the o-suite did timely reproduce the spatial distribution of the dust plume as shown the comparison with MODIS/Aqua AOD comparison (see Figure 10.1.2) despite the fact that the event was associated with a high cloud coverage over the Mediterranean and Europe. The comparison with the satellite data shows how the model predicts a large band of dust with AOD up to 1.2 over Libya and Crete, consistent with the observations on 25th January but extending into the cloudy region over Europe where observations are not available from MODIS. On 26th January, the o-suite predicts AOD values over 1 in a very limited area over Cyprus, while MODIS shows a broader extension. During this event, the ratio of DOD/AOD for o-suite is close to 1 over Libya and Cyprus, indicating that the model was able to identify the source of mineral dust emissions. This in contrast to the Middle East where the ratio DOD/AOD is much smaller than 1.

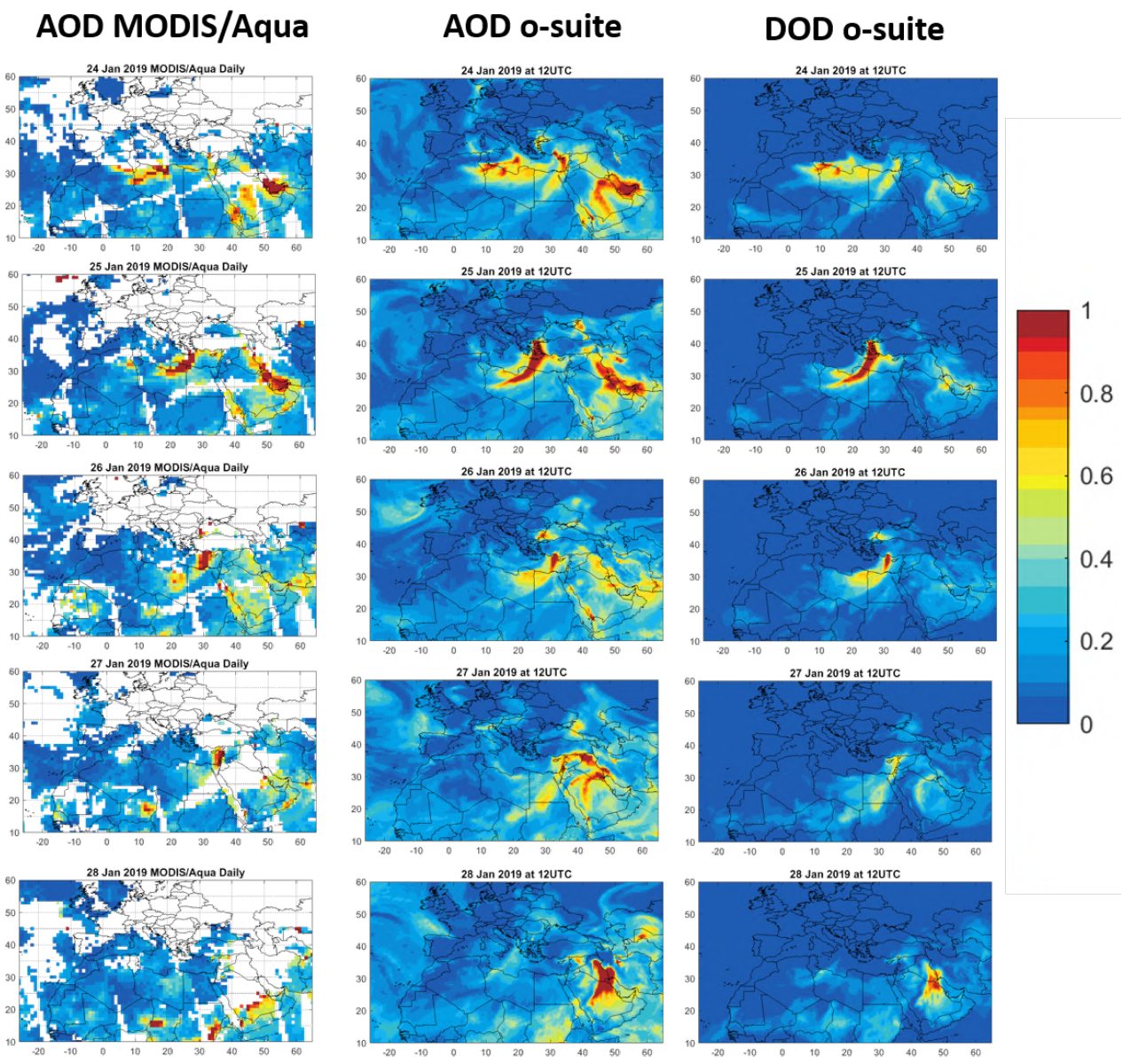

Figure 10.1.2. AOD from MODIS/Aqua Collection 6.1 Daily Level 3 product as well as AOD and DOD at 12UTC from o-suite (central and left columns) for 24-28 January 2019.

11. References

Agusti-Panareda, A., Monitoring upgrades of analysis/forecast system, MACC-III Deliverable D44.04, June 2015.

Bergamaschi, P., Frankenberg, C., Meirink, J. F., Krol, M., Villani, M. G., Houweling, S., Dentener, F., Dlugokencky, E. J., Miller, J. B., Gatti, L. V., Engel, A., and Levin, I.: Inverse modeling of global and regional CH4 emissions using SCIAMACHY satellite retrievals, J. Geophys. Res., 114, D22301, doi:10.1029/2009JD012287, 2009.

Benedetti, A., J.-J. Morcrette, O. Boucher, A. Dethof, R. J. Engelen, M. Fisher, H. Flentjes, N. Huneeus, L. Jones, J. W. Kaiser, S. Kinne, A. Mangold, M. Razinger, A. J. Simmons, M. Suttie, and the GEMS-AER team: Aerosol analysis and forecast in the ECMWF Integrated Forecast System. Part II : Data assimilation, J. Geophys. Res., 114, D13205, doi:10.1029/2008JD011115, 2009.

Boussetta, S., Balsamo, G., Beljaars, A., Agusti-Panareda, A., Calvet, J.-C., Jacobs, C., van den Hurk, B., Viterbo, P., Lafont, S., Dutra, E., Jarlan, L., Balzarolo, M., Papale, D., and van der Werf, G.: Natural carbon dioxide exchanges in the ECMWF Integrated Forecasting System: implementation and offline validation, J. Geophys. Res.-Atmos., 118, 1–24, doi: 10.1002/jgrd.50488, 2013.

Braathen, WMO Arctic Ozone Bulletin No 1/2016, DOI:10.13140/RG.2.1.4929.6403, 2016.

Cammas, J.P., Brioude J., Chaboureau J.-P., Duron J., Mari C., Mascart P., Nédélec P., Smit H., Pätz H.-W., Volz-Thomas A., Stohl A., and Fromm M., Injection in the lower stratosphere of biomass fire emissions followed by long-range transport: a MOZAIC case study. Atmos. Chem. Phys., 9, 5829-5846, 2009

Cariolle, D. and Teyssèdre, H.: A revised linear ozone photochemistry parameterization for use in transport and general circulation models: multi-annual simulations, Atmos. Chem. Phys., 7, 2183-2196, doi:10.5194/acp-7-2183-2007, 2007.

Dee, D. P. and S. Uppala, Variational bias correction of satellite radiance data in the ERA-Interim reanalysis. Quart. J. Roy. Meteor. Soc.,135, 1830-1841, 2009.

Deeter, M. N., Emmons, L. K., Edwards, D. P., Gille, J. C., and Drummond, J. R.: Vertical resolution and information content of CO profiles retrieved by MOPITT, Geophys. Res. Lett., 31, L15112, doi:10.1029/2004GL020235, 2004.

Deeter, M. N., et al. (2010), The MOPITT version 4 CO product: Algorithm enhancements, validation, and long-term stability, J. Geophys. Res., 115, D07306, doi:10.1029/2009JD013005.

Dentener, F., et al., 2006: Emissions of primary aerosol and precursor gases in the years 2000 and 1750 prescribed data-sets for AeroCom, Atmos. Chem. Phys., 6, 4321 – 4344.

Deshler, T., J.L. Mercer, H.G.J. Smit, R. Stubi, G. Levrat, B.J. Johnson, S.J. Oltmans, R. Kivi, A.M. Thompson, J. Witte, J. Davies, F.J. Schmidlin, G. Brothers, T. Sasaki (2008) Atmospheric comparison of electrochemical cell ozonesondes from different maufacturers, and with different cathode solution strengths: The Balloon Experiment on Standards for Ozonsondes. J. Geophys. Res.113, D04307, doi:10.1029/2007JD008975

Dupuy, E., et al.: Validation of ozone measurements from the Atmospheric Chemistry Experiment (ACE), Atmos. Chem. Phys., 9, 287-343, doi:10.5194/acp-9-287-2009, 2009.

Elbern, H., Schwinger, J., Botchorishvili, R.: Chemical state estimation for the middle atmosphere by four-dimensional variational data assimilation: System configuration. Journal of Geophysical Research (Atmospheres) 115, 6302, 2010.

Emmons, L. K., D. P. Edwards, M. N. Deeter, J. C. Gille, T. Campos, P. Nédélec, P. Novelli, and G. Sachse, Measurements of Pollution In The Troposphere (MOPITT) validation through 2006 Atmos. Chem. Phys., 9, 1795-1803, 2009

Errera, Q., Daerden, F., Chabrillat, S., Lambert, J. C., Lahoz, W. A., Viscardy, S., Bonjean, S., and Fonteyn, D., 4D-Var Assimilation of MIPAS chemical observations: ozone and nitrogen dioxide analyses, Atmos. Chem. Phys., 8, 6169-6187, 2008.

Errera, Q. and Ménard, R.: Technical Note: Spectral representation of spatial correlations in variational assimilation with grid point models and application to the belgian assimilation system for chemical observations (BASCOE), Atmos. Chem. Phys. Discuss., 12, 16763-16809, doi:10.5194/acpd-12-16763-2012, 2012.

Eskes, H.J., S. Basart, A. Benedictow, Y. Bennouna, A.-M. Blechschmidt, S. Chabrillat, Y. Christophe, E. Cuevas, J. Douros, H. Flentje, K. M. Hansen, J. Kapsomenakis, B. Langerock, M. Ramonet, A. Richter, M. Schulz, N. Sudarchikova, A. Wagner, T. Warneke, C. Zerefos, Observations characterisation and validation methods document, Copernicus Atmosphere Monitoring Service (CAMS) report, CAMS84_2015SC3_D.84.8.1.1-2018_observations_v3.pdf, October 2018 (2018a). Available from: http://atmosphere.copernicus.eu/user-support/validation/verification-global-services

Eskes, H. J., S. Basart, A. Benedictow, Y. Bennouna, A.-M. Blechschmidt, S. Chabrillat, Y. Christophe, H. Clark, E. Cuevas, K. M. Hansen, U. Im, J. Kapsomenakis, B. Langerock, K. Petersen, M. Schulz, A. Wagner, C. Zerefos, Upgrade verification note for the CAMS near-real time global atmospheric composition service, Copernicus Atmosphere Monitoring Service (CAMS) report, CAMS84_2015SC3_D84.3.1.5_201802_esuite_v1.pdf, February 2018 (2018b)

Eskes et al., Upgrade verification note for the CAMS near-real time global atmospheric composition service, Addendum July 2018, CAMS84_2015SC3_D84.3.1.5_201802_esuite_v1.pdf (2018c).

Flemming, J., Huijnen, V., Arteta, J., Bechtold, P., Beljaars, A., Blechschmidt, A.-M., Diamantakis, M., Engelen, R. J., Gaudel, A., Inness, A., Jones, L., Josse, B., Katragkou, E., Marecal, V., Peuch, V.-H., Richter, A., Schultz, M. G., Stein, O., and Tsikerdekis, A.: Tropospheric chemistry in the Integrated Forecasting System of ECMWF, Geosci. Model Dev., 8, 975-1003, doi:10.5194/gmd-8-975-2015, 2015.

Flemming, J., Benedetti, A., Inness, A., Engelen, R. J., Jones, L., Huijnen, V., Remy, S., Parrington, M., Suttie, M., Bozzo, A., Peuch, V.-H., Akritidis, D., and Katragkou, E.: The CAMS interim Reanalysis of Carbon Monoxide, Ozone and Aerosol for 2003–2015, Atmos. Chem. Phys., 17, 1945-1983, doi:10.5194/acp-17-1945-2017, 2017.

Franco, B., et al., Retrievals of formaldehyde from ground-based FTIR and MAX-DOAS observations at the Jungfraujoch station and comparisons with GEOS-Chem and IMAGES model simulations, Atmos. Meas. Tech., 8, 1733-1756, 2015

Gielen, C., Van Roozendael, M., Hendrick, F., Pinardi, G., Vlemmix, T., De Bock, V., De Backer, H., Fayt, C., Hermans, C., Gillotay, D., and Wang, P.: A simple and versatile cloud-screening method for MAX-DOAS retrievals, Atmos. Meas. Tech., 7, 3509-3527, doi:10.5194/amt-7-3509-2014, 2014.

Granier, C. et al.: Evolution of anthropogenic and biomass burning emissions of air pollutants at global and regional scales during the 1980–2010 period. Climatic Change (109), 2011

Holben, B. N., Eck, T. F., Slutsker, I., Tanré, D., Buis, J. P., Setzer, A., Vermote, E., Reagan, J. A., Kaufman, Y. J., Nakajima, T., Lavenu, F., Jankowiak, I., and Smirnov A.: AERONET – a federated instrument network and data archive for aerosol characterization, Remote Sens. Environ., 66, 1–16, 5529, 5533, 5537, 5544, 1998.

Hommel, R., Eichmann, K.-U., Aschmann, J., Bramstedt, K., Weber, M., von Savigny, C., Richter, A., Rozanov, A., Wittrock, F., Khosrawi, F., Bauer, R., and Burrows, J. P.: Chemical ozone loss and ozone mini-hole event

during the Arctic winter 2010/2011 as observed by SCIAMACHY and GOME-2, Atmos. Chem. Phys., 14, 3247-3276, doi:10.5194/acp-14-3247-2014, 2014.

Huijnen, V., et al.: The global chemistry transport model TM5: description and evaluation of the tropospheric chemistry version 3.0, Geosci. Model Dev., 3, 445-473, doi:10.5194/gmd-3-445-2010, 2010.

Inness, A., Blechschmidt, A.-M., Bouarar, I., Chabrillat, S., Crepulja, M., Engelen, R. J., Eskes, H., Flemming, J., Gaudel, A., Hendrick, F., Huijnen, V., Jones, L., Kapsomenakis, J., Katragkou, E., Keppens, A., Langerock, B., de Mazière, M., Melas, D., Parrington, M., Peuch, V. H., Razinger, M., Richter, A., Schultz, M. G., Suttie, M., Thouret, V., Vrekoussis, M., Wagner, A., and Zerefos, C.: Data assimilation of satellite-retrieved ozone, carbon monoxide and nitrogen dioxide with ECMWF's Composition-IFS, Atmos. Chem. Phys., 15, 5275-5303, doi:10.5194/acp-15-5275-2015, 2015.

Janssens-Maenhout, G., Dentener, F., Aardenne, J. V., Monni, S., Pagliari, V., Orlandini, L., Klimont, Z., Kurokawa, J., Akimoto, H., Ohara, T., Wankmueller, R., Battye, B., Grano, D., Zuber, A., and Keating, T.: EDGAR-HTAP: a Harmonized Gridded Air Pollution Emission Dataset Based on National Inventories, JRC68434, EUR report No EUR 25 299–2012, ISBN 978-92-79- 23122-0, ISSN 1831-9424, European Commission Publications Office, Ispra (Italy), 2012.

Jaross, G., Bhartia, P.K., Chen, G., Kowitt, M., Haken, M., Chen, Z., Xu, Ph., Warner, J., Kelly, T. : OMPS Limb Profiler instrument performance assessment, J. Geophys. Res. Atmos 119, 2169-8996, 2014.

Kaiser, J. W., Heil, A., Andreae, M. O., Benedetti, A., Chubarova, N., Jones, L., Morcrette, J.-J., Razinger, M., Schultz, M. G., Suttie, M., and van der Werf, G. R.: Biomass burning emissions estimated with a global fire assimilation system based on observed fire radiative power, Biogeosciences, 9, 527-554, doi:10.5194/bg-9-527-2012, 2012.

Kramarova, N. A., Nash, E. R., Newman, P. A., Bhartia, P. K., McPeters, R. D., Rault, D. F., Seftor, C. J., Xu, P. Q., and Labow, G. J.: Measuring the Antarctic ozone hole with the new Ozone Mapping and Profiler Suite (OMPS), Atmos. Chem. Phys., 14, 2353-2361, doi:10.5194/acp-14-2353-2014, 2014.

Lahoz, W. A., Errera, Q., Viscardy, S., and Manney G. L., The 2009 stratospheric major warming described from synergistic use of BASCOE water vapour analyses and MLS observations, Atmos. Chem. Phys. 11, 4689-4703, 2011

Lambert, A, et al., Aura Microwave Limb Sounder Version 3.4 Level-2 near real-time data user guide, http://disc.sci.gsfc.nasa.gov/Aura/data-holdings/MLS/documents/NRT-user-guide-v34.pdf

Langerock, B., De Mazière, M., Hendrick, F., Vigouroux, C., Desmet, F., Dils, B., and Niemeijer, S.: Description of algorithms for co-locating and comparing gridded model data with remote-sensing observations, Geosci. Model Dev., 8, 911-921, doi:10.5194/gmd-8-911-2015, 2015.

Lefever, K., van der A, R., Baier, F., Christophe, Y., Errera, Q., Eskes, H., Flemming, J., Inness, A., Jones, L., Lambert, J.-C., Langerock, B., Schultz, M. G., Stein, O., Wagner, A., and Chabrillat, S.: Copernicus stratospheric ozone service, 2009–2012: validation, system intercomparison and roles of input data sets, Atmos. Chem. Phys., 15, 2269-2293, doi:10.5194/acp-15-2269-2015, 2015.

Liu, Z., et al., Exploring the missing source of glyoxal (CHOCHO) over China, Geophys. Res. Lett., 39, L10812, doi: 10.1029/2012GL051645, 2012

Massart, S., Flemming, J., Cariolle, D., Jones, L., High resolution CO tracer forecasts, MACC-III Deliverable D22.04, May 2015, available from http://www.gmes-atmosphere.eu/documents/macciii/deliverables/grg

Morcrette, J.-J., O. Boucher, L. Jones, D. Salmond, P. Bechtold, A. Beljaars, A. Benedetti, A. Bonet, J. W. Kaiser, M. Razinger, M. Schulz, S. Serrar, A. J. Simmons, M. Sofiev, M. Suttie, A. M. Tompkins, and A. Untch: Aerosol

analysis and forecast in the ECMWF Integrated Forecast System. Part I: Forward modelling, J. Geophys. Res., 114, D06206, doi:10.1029/2008JD011235, 2009.

Richter, A., Burrows, J. P., Nüß, H., Granier, C, Niemeier, U.: Increase in tropospheric nitrogen dioxide over China observed from space, Nature, 437, 129-132, doi: 10.1038/nature04092, 2005

*Richter, A., Begoin, M., Hilboll, A., and Burrows, J. P.: An improved NO2 retrieval for the GOME-2 satellite instrument, Atmos. Meas. Tech. , **4**, 1147-1159, doi:10.5194/amt-4-1147-2011, 2011*

Sindelarova, K., Granier, C., Bouarar, I., Guenther, A., Tilmes, S., Stavrakou, T., Müller, J.-F., Kuhn, U., Stefani, P., and Knorr, W.: Global data set of biogenic VOC emissions calculated by the MEGAN model over the last 30 years, Atmos. Chem. Phys., 14, 9317-9341, doi:10.5194/acp-14-9317-2014, 2014.

Smit, H.G.J., W. Straeter, B.J. Johnson, S.J. Oltmans, J. Davies, D.W. Tarasick, B. Hoegger, R. Stubi, F.J. Schmidlin, T. Northam, A.M. Thompson, J.C. Witte, I. Boyd: Assessment of the performance of ECC-ozonesondes under quasi-flight conditions in the environmental simulation chamber: Insights from the Juelich Ozone Sonde Intercomparison Experiment (JOSIE), J. Geophys. Res. 112, D19306, doi:10.1029/2006JD007308, 2007.

Solomon, S., Haskins, J., Ivy, D. J. and Min, F.: Fundamental differences between Arctic and Antarctic ozone depletion, PNAS 2014 111 (17) 6220-6225, doi:10.1073/pnas.1319307111, 2014.

Stavrakou,T., First space-based derivation of the global atmospheric methanol fluxes, Atm. Chem. Phys., 11, 4873-4898, 2013.

Strahan, S.E., A.R. Douglass, and P.A. Newman, The contributions of chemistry and transport to low arctic ozone in March 2011 derived from Aura MLS observations, J. Geophys. Res. Atmos., 118, 1563–1576, doi:10.1002/jgrd.50181, 2013.

Taha, G.; Jaross, G. R.; Bhartia, P. K.: Validation of OMPS LP Ozone Profiles Version 2.0 with MLS, Ozone Sondes and Lidar Measurements, American Geophysical Union, Fall Meeting 2014, abstract #A33J-3322, 2014.

Taylor, K.E.: Summarizing multiple aspects of model performance in a single diagram. J.Geophys. Res., 106, 7183-7192, 2001.

van der A, R. J. , M. A. F. Allaart, and H. J. Eskes, Multi sensor reanalysis of total ozone, Atmos. Chem. Phys., 10, 11277–11294, doi:10.5194/acp-10-11277-2010, www.atmos- chem-phys.net/10/11277/2010/, 2010

van der A, R., M. Allaart, H. Eskes, K. Lefever, Validation report of the MACC 30-year multi-sensor reanalysis of ozone columns Period 1979-2008, MACC-II report, Jan 2013, MACCII_VAL_DEL_D_83.3_OzoneMSRv1_20130130.docx/pdf.

van der A, R. J., Allaart, M. A. F., and Eskes, H. J.: Extended and refined multi sensor reanalysis of total ozone for the period 1970–2012, Atmos. Meas. Tech., 8, 3021-3035, doi:10.5194/amt-8-3021-2015, 2015.

*Vrekoussis, M., Wittrock, F., Richter, A., and Burrows, J. P.: GOME-2 observations of oxygenated VOCs: what can we learn from the ratio glyoxal to formaldehyde on a global scale?, Atmos. Chem. Phys., **10**, 10145-10160, doi:10.5194/acp-10-10145-2010, 2010*

Wagner, A., M. Schulz, Y. Christophe, M. Ramonet, H.J. Eskes, S. Basart, A. Benedictow, Y. Bennouna, A.-M. Blechschmidt, S. Chabrillat, H. Clark, E. Cuevas, H. Flentje, K.M. Hansen, U. Im, J. Kapsomenakis, B. Langerock, A. Richter, N. Sudarchikova, V. Thouret, T. Warneke, C. Zerefos, Validation report of the CAMS near-real-time global atmospheric composition service: Period September-November 2018, Copernicus Atmosphere Monitoring Service (CAMS) report, CAMS84_2018SC1_D1.1.1_SON2018_v1.pdf, March 2019. Available from: http://atmosphere.copernicus.eu/user-support/validation/verification-global-services

Wennberg, P. O., Mui, W., Wunch, D., Kort, E. A., Blake, D. R., Atlas, E. L., Santoni, G. W., Wofsy, S. C., Diskin, G. S., Jeong, S., and Fischer, M. L.: On the sources of methane to the Los Angeles atmosphere, Environ. Sci. Technol., 46, 9282–9289, https://doi.org/10.1021/es301138y, 2012

Wittrock, F., A. Richter, H. Oetjen, J. P. Burrows, M. Kanakidou, S. Myriokefalitakis, R. Volkamer, S. Beirle, U. Platt, and T. Wagner, Simultaneous global observations of glyoxal and formaldehyde from space, Geophys. Res. Lett., 33, L16804, doi:10.1029/2006GL026310, 2006

WMO (2010), Guidelines for the Measurement of Atmospheric Carbon Monoxide, GAW Report No. 192, World Meteorological Organization, Geneva, Switzerland, 2010.

WMO (2013), Guidelines for the Continuous Measurements of Ozone in the Troposphere, GAW Report No. 209, World Meteorological Organization, Geneva, Switzerland, 2013.

Wunch, D., Wennberg, P. O., Toon, G. C., Keppel-Aleks, G., and Yavin, Y. G.: Emissions of greenhouse gases from a North American megacity, Geophys. Res. Lett., 36, 1–5, https://doi.org/10.1029/2009GL039825, 2009.

Annex 1: Acknowledgements

Listed below are the authors contributing to the sections in this report. The authors contributing to the model description are also provided, as well as acknowledgements to the validation datasets.

Tropospheric reactive gases reactive gases

Annette Wagner, MPG (editor, O3 sondes, GAW data)
Yasmine Bennouna, Valerie Thouret, CNRS-LA (IAGOS)
Harald Flentje, DWD (O3 sondes, GAW data)
Anne Blechschmidt and Andreas Richter, IUB Bremen (GOME-2 NO2, HCHO)
John Kapsomenakis, Christos Zerefos, AA (ESRL)
Natalia Sudarchikova, satellite IR observations (MPG)
Kaj Hansen, Ulas Im, AU (Arctic theme)
Bavo Langerock, BIRA (NDACC)

Tropospheric aerosol

Michael Schulz, MetNo (editor, Aerocom, Aeronet)
Anna Benedictow, Jan Griesfeller, MetNo (Aerocom, Aeronet)
Sara Basart, MTeresa Pay, Oriol Jorba, BSC-CNS (Aeronet, MODIS, AirBase, SDS-WAS NAMEE RC)
Emilio Cuevas, AEMET (Aeronet, MODIS, AirBase, SDS-WAS NAMEE RC)
Harald Flentje, DWD (Backscatter profiles)

Stratospheric reactive gases

Yves Christophe, BIRA (editor, model-satellite intercomparisons)
Simon Chabrillat, BIRA (model intercomparisons)
Annette Wagner, MPI-M (O_3 sondes)
Bavo Langerock, BIRA (NDACC FTIR, MWR, UVVIS DOAS, LIDAR)
Anne Blechschmidt and Andreas Richter, IUB-UB Bremen (SCIAMACHY/GOME-2 NO_2)

Greenhouse gases

Michel Ramonet, IPSL (ICOS)
Abdelhadi El-Yazidi and Leonard Rivier, LSCE (ICOS)
Thorsten Warneke, UBC (TCCON)
Bavo Langerock, BIRA (TCCON)

Reactive gases and aerosol modeling

Johannes Flemming (ECMWF), Antje Inness (ECMWF), Angela Benedetti (ECMWF), Sebastien Massart (ECMWF), Anna Agusti-Panareda (ECMWF), Johannes Kaiser (KCL/MPIC/ECMWF), Samuel Remy (LMD), Olivier Boucher (LMD), Vincent Huijnen (KNMI), Richard Engelen (ECMWF)

Acknowledgements for the validation datasets used

We wish to acknowledge the provision of NRT GAW observational data by: Institute of Atmospheric Sciences and Climate (ISAC) of the Italian National Research Council (CNR), South African Weather Service, National Centre for Atmospheric Science (NCAS, Cape Verde), National Air Pollution Monitoring Network (NABEL) (Federal Office for the Environment FOEN and Swiss Federal Laboratories for Materials Testing and Research EMPA), Atmospheric Environment Division Global Environment and Marine Department Japan Meteorological Agency, Chinese Academy of Meteorological Sciences (CAMS), Alfred Wegener Institut, Umweltbundesamt (Austria), National Meteorological Service (Argentina), Umweltbundesamt (UBA, Germany)

We are grateful to the numerous operators of the Aeronet network and to the central data processing facility at NASA Goddard Space Flight Center for providing the NRT sun photometer data, especially Ilya Slutker and Brent Holben for sending the data.

The authors thank to all researchers, data providers and collaborators of the World Meteorological Organization's Sand and Dust Storm Warning Advisory and Assessment System (WMO SDS-WAS) for Northern Africa, Middle East and Europe (NAMEE) Regional Node. Also special thank to Canary Government as well as AERONET, MODIS, U.K. Met Office MSG, MSG Eumetsat and EOSDIS World Viewer principal investigators and scientists for establishing and maintaining data used in the activities of the WMO SDS-WAS NAMEE Regional Center (http://sds-was.aemet.es/).

We wish to acknowledge the provision of ozone sonde data by the World Ozone and Ultraviolet Radiation Data Centre established at EC in Toronto (http://woudc.org), by the Data Host Facility of the Network for the Detection of Atmospheric Composition Change established at NOAA (http://ndacc.org), by the Norwegian Institute for Air Research and by the National Aeronautics and Space Administration (NASA).

We wish to thank the NDACC investigators for the provision of observations at Ny Alesund, Bern, Jungfraujoch, Izaña, Xianghe, Harestua, Reunion Maido, Uccle, Hohenpeissen, Mauna Loa, Lauder and Haute Provence.

The authors acknowledge the NOAA Earth System Research Laboratory (ESRL) Global Monitoring Division (GMD) for the provision of ground-based ozone concentrations.

The MOPITT CO data were obtained from the NASA Langley Research Center ASDC. We acknowledge the LATMOS IASI group for providing IASI CO data.

SCIAMACHY lv1 radiances were provided to IUP-UB by ESA through DLR/DFD.

GOME-2 lv1 radiances were provided to IUP-UB by EUMETSAT.

The authors acknowledge Environment and Climate Change Canada for the provision of Alert ozone data and Sara Crepinsek – NOAA for the provision of Tiksi ozone data. Surface ozone data from the Zeppelin Mountain, Svalbard are from www.luftkvalitet.info. Surface ozone data from the Villum Research Station, Station Nord (VRS) were financially supported by "The Danish Environmental Protection Agency" with means from the MIKA/DANCEA funds for Environmental Support to the Arctic Region. The Villum Foundation is acknowledged for the large grant making it possible to build VRS in North Greenland.

We acknowledge the National Aeronautics and Space Administration (NASA), USA for providing the OMPS limb sounder data (http://npp.gsfc.nasa.gov/omps.html) and the Aura-MLS offline data (http://mls.jpl.nasa.gov/index-eos-mls.php).

We thank the Canadian Space Agency and ACE science team for providing level 2 data retrieved from ACE-FTS on the Canadian satellite SCISAT-1.

The European Environment Information and Observation Network (Eionet) Air Quality portal provides details relevant for the reporting of air quality information from EU Member States and other EEA member and co-operating countries. This information is submitted according to Directives 2004/107/EC and 2008/50/EC of the European Parliament and of the Council.

We acknowledge the contribution of the ICOS Atmospheric Thematic Center (Lynn Hazan, Amara Abbaris, and Leonard Rivier) for the near real time data processing of surface CO_2 and CH_4 concentrations. The ICOS monitoring sites are maintained by the national networks: ICOS-Czech Rep. (Michal Marek, Katerina Komínková, Gabriela Vítková), ICOS-Finland (Olli Peltola, Janne Levula, Tuomas Laurila), ICOS-France (Michel Ramonet, Marc Delmotte, Sebastien Conil, Morgan Lopez, Victor Kazan, Aurélie Colomb, Jean Marc Pichon, Roxanne Jacob, Julie Helle, Olivier Laurent), ICOS-Germany (Matthias Lindauer, Dagmar Kubistin, Christian Plass-Duelmer, Dietmar Weyrauch, Marcus Schumacher), ICOS-Italy (Paolo Cristofanelli, Michela Maione, Francesco Apadula), ICOS-Norway (Cathrine Lund Myhre, Ove Hermansen), ICOS-Sweden (Jutta Holst, Michal Heliasz, Meelis Molder, Mikaell Ottosson Lofvenius, Anders Lindroth, Per Marklund), ICOS-Switzerland (Martin Steinbacher, Simon Wyss), European Commission, Joint Research Centre, Directorate for Energy, Transport and Climate (Peter Bergamaschi, Giovanni Manca).

The TCCON site at Orleans is operated by the University of Bremen and the RAMCES team at LSCE (Gif-sur-Yvette, France). The TCCON site at Bialystok is operated by the University of Bremen. Funding for the two sites was provided by the EU-project ICOS-INWIRE and the University of Bremen. The TCCON site at Réunion is operated by BIRA-IASB, in cooperation with UReunion and is funded by BELSPO in the framework of the Belgian ICOS program.

TCCON references:

Hazan, L., J. Tarniewicz, M. Ramonet, O. Laurent and A. Abbaris **(2016)**. *Automatic processing of atmospheric CO_2 and CH_4 mole fractions at the ICOS Atmosphere Thematic Centre*. Atmospheric Measurement Techniques 9(9): 4719-4736.

Blumenstock, T., F. Hase, M. Schneider, O. E. García, and E. Sepúlveda. 2017. "TCCON data from Izana (ES), Release GGG2014.R1." CaltechDATA. doi:10.14291/tccon.ggg2014.izana01.r1.

De Mazière, M., M. K. Sha, F. Desmet, C. Hermans, F. Scolas, N. Kumps, J.-M. Metzger, V. Duflot, and J.-P. Cammas. 2017. "TCCON data from Réunion Island (RE), Release GGG2014.R1." CaltechDATA. doi:10.14291/tccon.ggg2014.reunion01.r1.

Deutscher, N. M., J. Notholt, J. Messerschmidt, C. Weinzierl, T. Warneke, C. Petri, and P. Grupe. 2017. "TCCON data from Bialystok (PL), Release GGG2014.R1." CaltechDATA. doi:10.14291/tccon.ggg2014.bialystok01.r1/1183984.

Dubey, M. K., B. G. Henderson, D. Green, Z. T. Butterfield, G. Keppel-Aleks, N. T. Allen, J.-F. Blavier, C. M. Roehl, D. Wunch, and R. Lindenmaier. 2017. "TCCON data from Manaus (BR), Release GGG2014.R0." CaltechDATA. doi:10.14291/tccon.ggg2014.manaus01.r0/1149274.

Dubey, M. K., R. Lindenmaier, B. G. Henderson, D. Green, N. T. Allen, C. M. Roehl, J.-F. Blavier, et al. 2017. "TCCON data from Four Corners (US), Release GGG2014.R0." CaltechDATA. doi:10.14291/tccon.ggg2014.fourcorners01.r0/1149272.

Feist, D. G., S. G. Arnold, N. John, and M. C. Geibel. 2017. "TCCON data from Ascension Island (SH), Release GGG2014.R0." CaltechDATA. doi:10.14291/tccon.ggg2014.ascension01.r0/1149285.

Goo, T.-Y., Y.-S. Oh, and V. A. Velazco. 2017. "TCCON data from Anmeyondo (KR), Release GGG2014.R0." CaltechDATA. doi:10.14291/tccon.ggg2014.anmeyondo01.r0/1149284.

Griffith, D. W. T., N. M. Deutscher, V. A. Velazco, P. O. Wennberg, Y. Yavin, G. Keppel-Aleks, R. A. Washenfelder, et al. 2017. "TCCON data from Darwin (AU), Release GGG2014.R0." CaltechDATA. doi:10.14291/tccon.ggg2014.darwin01.r0/1149290.

Griffith, D. W. T., V. A. Velazco, N. M. Deutscher, C. Paton-Walsh, N. B. Jones, S. R. Wilson, R. C. Macatangay, G. C. Kettlewell, R. R. Buchholz, and M. O. Riggenbach. 2017. "TCCON data from Wollongong (AU), Release GGG2014.R0." CaltechDATA. doi:10.14291/tccon.ggg2014.wollongong01.r0/1149291.

Hase, F., T. Blumenstock, S. Dohe, J. Groß, and M.ä. Kiel. 2017. "TCCON data from Karlsruhe (DE), Release GGG2014.R1." CaltechDATA. doi:10.14291/tccon.ggg2014.karlsruhe01.r1/1182416.

Iraci, L. T., J. R. Podolske, P. W. Hillyard, C. Roehl, P. O. Wennberg, J.-F. Blavier, J. Landeros, et al. 2017. "TCCON data from Edwards (US), Release GGG2014.R1." CaltechDATA. doi:10.14291/tccon.ggg2014.edwards01.r1/1255068.

—. 2017. "TCCON data from Indianapolis (US), Release GGG2014.R1." CaltechDATA. doi:10.14291/tccon.ggg2014.indianapolis01.r1/1330094.

Kawakami, S., H. Ohyama, K. Arai, H. Okumura, C. Taura, T. Fukamachi, and M. Sakashita. 2017. "TCCON data from Saga (JP), Release GGG2014.R0." CaltechDATA. doi:10.14291/tccon.ggg2014.saga01.r0/1149283.

Kivi, R., P. Heikkinen, and E. Kyrö. 2017. "TCCON data from Sodankylä (FI), Release GGG2014.R0." CaltechDATA. doi:10.14291/tccon.ggg2014.sodankyla01.r0/1149280.

Liu, Cheng, Wei Wang, and Youwen Sun. 2018. "TCCON data from Hefei (PRC), Release GGG2014.R0." CaltechDATA. doi:10.14291/tccon.ggg2014.hefei01.r0.

Morino, I., N. Yokozeki, T. Matsuzaki, and M. Horikawa. 2017. "TCCON data from Rikubetsu (JP), Release GGG2014.R2." CaltechDATA. doi:10.14291/tccon.ggg2014.rikubetsu01.r2.

Morino, I., T. Matsuzaki, and M. Horikawa. 2017. "TCCON data from Tsukuba (JP), 125HR, Release GGG2014.R2." CaltechDATA. doi:10.14291/tccon.ggg2014.tsukuba02.r2.

Morino, Isamu, Voltaire A. Velazco, Akihiro Hori, Osamu Uchino, and David W. T. Griffith. 2018. "TCCON data from Burgos, Ilocos Norte (PH), Release GGG2014.R0." CaltechDATA. doi:10.14291/tccon.ggg2014.burgos01.r0.

Notholt, J., C. Petri, T. Warneke, N. M. Deutscher, M. Palm, M. Buschmann, C. Weinzierl, R. C. Macatangay, and P. Grupe. 2017. "TCCON data from Bremen (DE), Release GGG2014.R0." CaltechDATA. doi:10.14291/tccon.ggg2014.bremen01.r0/1149275.

Notholt, J., T. Warneke, C. Petri, N. M. Deutscher, C. Weinzierl, M. Palm, and M. Buschmann. 2017. "TCCON data from Ny Ålesund, Spitsbergen (NO), Release GGG2014.R0." CaltechDATA. doi:10.14291/tccon.ggg2014.nyalesund01.r0/1149278.

Pollard, David Frank, John Robinson, and Hisako Shiona. 2019. "TCCON data from Lauder (NZ), Release GGG2014.R0." CaltechDATA. doi:10.14291/tccon.ggg2014.lauder03.r0.

Sherlock, V., B. Connor, J. Robinson, H. Shiona, D. Smale, and D. F. Pollard. 2017. "TCCON data from Lauder (NZ), 120HR, Release GGG2014.R0." CaltechDATA. doi:10.14291/tccon.ggg2014.lauder01.r0/1149293.

—. 2017. "TCCON data from Lauder (NZ), 125HR, Release GGG2014.R0." CaltechDATA. doi:10.14291/tccon.ggg2014.lauder02.r0/1149298.

Strong, K., S. Roche, J. E. Franklin, J. Mendonca, E. Lutsch, D. Weaver, P. F. Fogal, J. R. Drummond, R. Batchelor, and R. Lindenmaier. 2018. "TCCON data from Eureka (CA), Release GGG2014.R3." CaltechDATA. doi:10.14291/tccon.ggg2014.eureka01.r3.

Sussmann, R., and M. Rettinger. 2017. "TCCON data from Garmisch (DE), Release GGG2014.R2." CaltechDATA. doi:10.14291/tccon.ggg2014.garmisch01.r2.

—. 2018. "TCCON data from Zugspitze (DE), Release GGG2014.R1." CaltechDATA. doi:10.14291/tccon.ggg2014.zugspitze01.r1.

Té, Y., P. Jeseck, and C. Janssen. 2017. "TCCON data from Paris (FR), Release GGG2014.R0." CaltechDATA. doi:10.14291/tccon.ggg2014.paris01.r0/1149279.

Warneke, T., J. Messerschmidt, J. Notholt, C. Weinzierl, N. M. Deutscher, C. Petri, and P. Grupe. 2017. "TCCON data from Orléans (FR), Release GGG2014.R0." CaltechDATA. doi:10.14291/tccon.ggg2014.orleans01.r0/1149276.

Wennberg, P. O., C. M. Roehl, D. Wunch, G. C. Toon, J.-F. Blavier, R. Washenfelder, G. Keppel-Aleks, N. T. Allen, and J. Ayers. 2017. "TCCON data from Park Falls (US), Release GGG2014.R1." CaltechDATA. doi:10.14291/tccon.ggg2014.parkfalls01.r1.

Wennberg, P. O., C. M. Roehl, J.-F. Blavier, D. Wunch, and N. T. Allen. 2017. "TCCON data from Jet Propulsion Laboratory (US), 2011, Release GGG2014.R1." CaltechDATA. doi:10.14291/tccon.ggg2014.jpl02.r1/1330096.

Wennberg, P. O., D. Wunch, C. M. Roehl, J.-F. Blavier, G. C. Toon, and N. T. Allen. 2017. "TCCON data from Caltech (US), Release GGG2014.R1." CaltechDATA. doi:10.14291/tccon.ggg2014.pasadena01.r1/1182415.

—. 2017. "TCCON data from Lamont (US), Release GGG2014.R1." CaltechDATA. doi:10.14291/tccon.ggg2014.lamont01.r1/1255070.

Wennberg, P. O., D. Wunch, Y. Yavin, G. C. Toon, J.-F. Blavier, N. T. Allen, and G. Keppel-Aleks. 2017. "TCCON data from Jet Propulsion Laboratory (US), 2007, Release GGG2014.R0." CaltechDATA. doi:10.14291/tccon.ggg2014.jpl01.r0/1149163.

Wunch, D., J. Mendonca, O. Colebatch, N. T. Allen, J.-F. Blavier, S. Roche, J. Hedelius, et al. 2017. "TCCON data from East Trout Lake, SK (CA), Release GGG2014.R1." CaltechDATA. doi:10.14291/tccon.ggg2014.easttroutlake01.r1.

Wunch, D., Toon, G. C., Sherlock, V., Deutscher, N. M., Liu, C., Feist, D. G., & Wennberg, P. O. (2015). The Total Carbon Column Observing Network's GGG2014 Data Version. Tech. rep., California Institute of Technology, Pasadena. doi:10.14291/tccon.ggg2014.documentation.R0/1221662

Copernicus Atmosphere Monitoring Service

ECMWF - Shinfield Park, Reading RG2 9AX, UK

Contact: info@copernicus-atmosphere.eu